NEAR-FIELD SEDIMENT RESUSPENSION MEASUREMENT AND MODELING FOR CUTTER SUCTION DREDGING OPERATIONS

A Dissertation

by

JOHN CHRISTOPHER HENRIKSEN

Submitted to the Office of Graduate Studies of
Texas A&M University
in partial fulfillment of the requirements for the degree of

DOCTOR OF PHILOSOPHY

December 2009

Major Subject: Ocean Engineering

NEAR-FIELD SEDIMENT RESUSPENSION MEASUREMENT AND MODELING FOR CUTTER SUCTION DREDGING OPERATIONS

A Dissertation

by

JOHN CHRISTOPHER HENRIKSEN

Submitted to the Office of Graduate Studies of
Texas A&M University
in partial fulfillment of the requirements for the degree of

DOCTOR OF PHILOSOPHY

Approved by:

Chair of Committee,	Robert E. Randall
Committee Members,	Billy L. Edge
	Scott Socolofsky
	Achim Stoessel
Head of Department,	David Rosowsky

December 2009

Major Subject: Ocean Engineering

ABSTRACT

Near-Field Sediment Resuspension Measurement and Modeling for Cutter Suction Dredging Operations. (December 2009)

John Christopher Henriksen, B.A.; B.S., University of Delaware,

M.S., Dartmouth College

Chair of Advisory Committee: Dr. Robert E. Randall

The sediment resuspension and turbidity created during dredging operations is both an economical and environmental issue. The movement of sediment plumes created from dredging operations has been predicted with numerical modeling, however, these far-field models need a “source term” or near-field model as input. Although data from field tests have been used to create near-field models that predict the amount of material suspended in the water column, these results are skewed due to limitations such as non-uniform sediment distributions, water currents, and water quality issues. Laboratory investigations have obtained data for turbidity during dredging operations, but these results do not take advantage of the most contemporary testing methods.

The purpose of this dissertation is to provide an estimation of turbidity created during a cutter suction dredging operation. This estimation was facilited by the development of resuspension measurement and data acquisition techniques in a laboratory setting. Near-field turbidity measurements around the cutter head were measured in the Haynes Coastal Engineering Laboratory at Texas A&M University. The

laboratory contains a dredge/tow tank that is ideal for conducting dredging research. A dredge carriage is located in the dredge/tow tank and is composed of a carriage, cradle, and ladder. Acoustic Doppler Velocimetry (ADV) and Optical Backscatter Sensor (OBS) measurements were taken at specific points around the cutter head. The variables of suction flow rate, cutter speed, and the thickness of cut were investigated to understand their specific effect on turbidity generation and turbulence production around the cutter head.

A near-field advection diffusion model was created to predict resuspension of sediment from a cutter suction dredge. The model incorporates the laboratory data to determine the velocity field as well as the turbulent diffusion. The model is validated with laboratory testing as well as field data.

Conclusions from this research demonstrate undercutting consistently produced larger point specific turbidity maximum than overcutting in the laboratory testing. An increase in suction flow rate was shown to increase production and decrease turbidity around the cutter head. In general, an increase in cutter speed led to an increase in turbidity. The thickness of cut produced less resuspension for a full cut versus a partial cut. Data for a “shallow cut” also produced less turbidity generation than partial cuts. The numerical model was compared to all laboratory testing cases as well as the Calumet Harbor and New Bedford cutter resuspension data and produced suitable MRA values for all tests. The numerical model produced higher point specific regions of turbidity for undercutting but produced larger mean values of turbidity for overcutting.

ACKNOWLEDGEMENTS

I would like to first thank my advisor, Dr. Robert Randall, for his advice, instruction, and patience throughout the time spent on this project. His ability to listen to my progress and provide guidance with my obstacles was invaluable in constructing this dissertation. I would also like to thank the other committee members, Dr. Billy Edge, Dr. Scott Socolofsky, and Dr. Achim Stoessel for their time and advice while completing this project.

Special thanks go to John Reed, the Haynes Coastal Laboratory Manager. His knowledge and advice on topics in the laboratory were invaluable. Many hours were spent in the laboratory on his part, helping to make sure that my project was working properly and safely. Thanks also go to the United States Army Corps of Engineers' Coastal Hydraulics Laboratory (CHL) Vicksburg, Mississippi who partially funded this research. Finally, I would like to thank my family for their support, love, and understanding.

TABLE OF CONTENTS

CHAPTER Page

LIST OF FIGURES

Page

Page

Page

LIST OF TABLES

NOMENCLATURE

θ_s	step angle [L]
L_{spuds}	spud distance [L]
L_a	step size [L]
x,y,z	spatial coordinates [L]
U,V,W	water velocities [LT^{-1}]
w_s	particle settling velocity [LT^{-1}]
D_x, D_y, D_z	diffusion coefficient in the x,y,z directions [L^2T^{-1}]
C	sediment concentration [ML^{-3}]
$\dot{m}_r$	source strength at the cutter [MT^{-1}]
$\hat{m}_r$	percent of material available for resuspension[-]
X	solids content by volume measured [-]
X_T	theoretical maximum of reduced solids [-]
t_c	thickness of dredge cut [L]
V_s	rate of swing [LT^{-1}]
D_d	diameter of discharge pipe [L]
V_d	flow velocity in discharge pipe [LT^{-1}]
TGU	turbidity generation unit [ML^{-3}]
$\forall_s$	volume of dredged material from one swing [L^3]
W_o	total quantity of dredging suspended solids generated [M]
f_{74}	fraction of particles < 74 μm [-]

f_0	fraction of particles smaller than particles with a critical resuspension initiatioin velocity equal to the water current [-]
γ	specific weight of dredge material [M/L^3]
C_{DT}	coefficient dependent on dredge type [-]
Q	flow rate [L^3T^{-1}]
π_n	linear regression parameters [-]
V_i	intake suction velocity [LT^{-1}]
V_t	cutter tip speed [LT^{-1}]
D_c	cutter diameter [L]
V_c	cutter blade tangential velocity [LT^{-1}]
ω	angular velocity [$radT^{-1}$]
R_c	cutter radius [L]
C_r	resuspended sediment above background concentration [ML^{-3}]
A, a, b, c, c'	regression coefficients [-]
ρ_w	density of water [ML^{-3}]
F, F_F, F_D	cut thickness parameters [-]
L_c	length of cutter [L]
d_{50}	mean sediment diameter [L]
D_f	thickness of a full cut [L]
$D_{\%}$	thickness of cut ratio [D]
$\dot{m}_s$	rate of sediment excavated by the cutter [MT^{-1}]

$\dot{m}_p$	rate of sediment entrained by the suction line [MT^{-1}]
C_S	in situ sediment concentration [ML^{-3}]
P	dredge production [L^3T^{-1}]
A_E	surface area of cutter exposed to washing [L^2]
A_T	total surface area of cutter [L^2]
h_r	sediment concentration initial condition height [L]
$\dot{m}_l$	rate of sediment that settles quickly [MT^{-1}]
D_i	suction inlet pipe diameter [L]
R_f	resuspension factor [-]
$\dot{V}_s$	volumetric in situ sediment removal [L^3T^{-1}]
P	production of the dredge [L^3T^{-1}]
Sg_s	specific gravity of the slurry [-]
V_D	slurry velocity in the discharge pipe [LT^{-1}]
A_A	advancing surface area of cutter blades [L^2]
A_{NA}	non-advancing surface area of the cutter blades [L^2]
x_p, y_p	spatial coordinate of cutter-mudline intersection [L]
z_p	vertical coordinate of cutter-mudline intersection [L]
θ	ladder angle [rad]
e_b	cutter length parameter [L]
D_f	depth of a fully submerged cutter [L]
A_B	back region surface area of cutter [L^2]

F_g	force due to gravity [MLT^{-2}]
ρ_s	density of sediment particle [ML^{-3}]
ρ_f	density of fluid [ML^{-3}]
$\forall_p$	sediment particle volume [L^3]
g	gravitational constant [LT^{-2}]
F_D	drag force of the particle [MLT^{-2}]
C_D	particle drag coefficient [-]
w_s	particle settling velocity [LT^{-1}]
A_p	sediment particle front area [L^2]
Re_p	particle Reynolds number [-]
d_p	particle diameter [L]
ν	kinematic viscosity of fluid [L^2T^{-1}]
μ_f	fluid dynamic viscosity [$ML^{-1}T^{-1}$]
W_*	dimensionless settling velocity [-]
D_*	dimensionless particle diameter [-]
R_1, R_2, R_3	Dietrich particle coefficients [-]
CSF	Corey Shape Factor [-]
a_p,b_p,c_p	particle length scale coefficients [-]
M	Powers value [-]
Sg_p	specific gravity of the particle [ML^{-3}]
w_s'	hindered settling velocity [LT^{-1}]
C_{sl}	slurry volumetric concentration [-]

n	Richardson-Zaki parameter [-]
N_c	rotational speed of the cutter [rpm]
F_c	cutting force [MLT^{-2}]
Γ_s	shaft torque [M^2LT^{-2}]
R	radial distance [L]
t_l	cut layer thickness [L]
p_b	pitch of the blades or teeth [rad]
κ	profile angle [degrees]
φ	angular position of the blade [rad]
p_c	cavitation pressure [$ML^{-1}T^{-2}$]
λ_c	hydrostatic pressure factor
ψ	optical backscatter output voltage [volts]
A_{obs}, B_{obs}	optical backscatter regression coefficients [-]
$\overline{u}_i$	mean value of velocity [LT^{-1}]
u_i'	fluctuating component of velocity [LT^{-1}]
$\tau_{reynolds\_ij}$	Reynold's stress tensor [$ML^{-1}T^{-2}$]
I	turbulence intensity [-]
$\vec{q}$	turbulent concentration flux [ML^{-1}]
c'	fluctuation from the mean concentration [ML^{-3}]
w_r	resultant uncertainty [-]
$\forall_C$	volume of material for each cut [L^3]
$\forall_r$	volume of material available for resuspension [L^3]

N_{DT}	number of blade swipes per time step [-]
BN	number of blades on the cutter [-]
dt	time step [T]
k_c , k_c'	size factors for the diameter and length of the cutter [-]
S_F	surface plane of sediment resuspension [L^2]
L_p	length of the cutter diameter perimeter exposed to washing [L].
tsr	cuttertip speed ratio[-]
$ptip$	prototype cutter tip speed [LT^{-1}]
$mtip$	model cutter tip speed [LT^{-1}]
Pe	Peclet number [-]
D_N	numerical diffusion [L^2T^{-1}]
$Cour_y$, $Cour_z$	Courant number in y and z direction [-]
λ_y , λ_z	diffusion number in y and z direction [-]
$\vec{V}$	velocity field [LT^{-1}]

CHAPTER I

INTRODUCTION

Cutter Suction Dredge

Cutter suction dredging operations are common practice for maintaining and deepening navigable waterways. Figure 1 provides a picture of a standard cutter suction dredge. The cutter suction dredge is a vessel with a cutter that excavates the sediment, a pumping system that creates suction to remove and transport the sediment, and a ladder to support both the cutter and suction line.

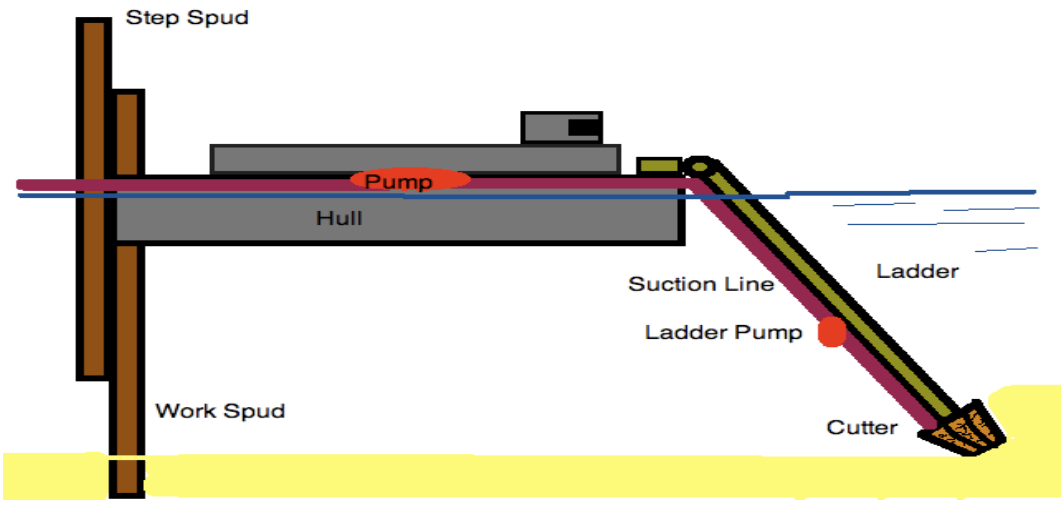

Figure 1. Picture of a Cutter Suction Dredge

This dissertation follows the *Journal of Waterway, Port, Coastal, and Ocean Engineering* format.

The cutter usually has five to eight blades that do the actual excavation of the sediment (Turner, 1996). The cutter can also have teeth or chisels mounted to the blades. Cutters are often defined as basket type cutters, or spider cutters and have serrated edge blades or flat blades depending on their geometry and structure. Cutter diameters range between 45.7 cm (18 in) to 335.3 cm (132 in) (Burger, 2003). A cross section of the cutter geometry is shown in Figure 2. The main function of the cutter is to excavate the material and create a mixture or "slurry" to be transported.

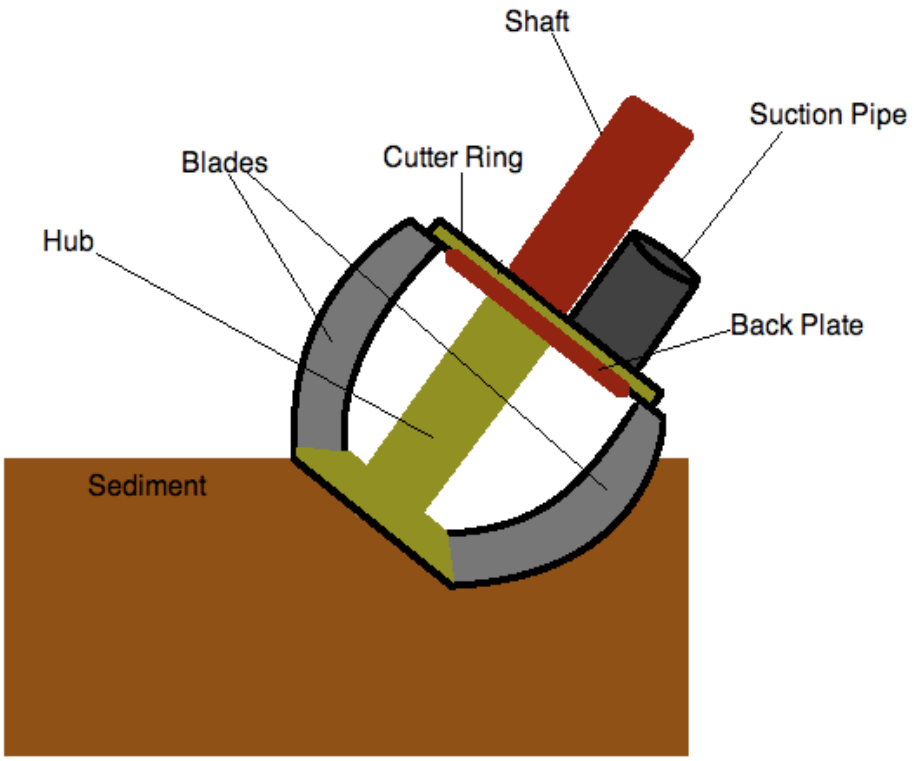

Figure 2. Side View of a Cutter

Material is cut by the cutter and is transported by a suction pipe. The suction pipe is mounted on the ladder and inserts through a back plate near the cutting blades. The back plate of the cutter can be either flat or conical. A centrifugal pump creates the suction in the suction line and pumps the slurry through the discharge pipeline that can typically range from a 15 cm (6 in) to a 112 cm (44 in) diameter pipeline (Huston and Huston, 1976). The classification of dredge size is usually defined by the diameter of the discharge pipeline. Typical solid content of the slurry in the pipeline ranges from 10 to 20 percent by volume.

The ladder of the cutter suction dredge provides a mounting location for the cutter and the cutter drive and distributes the necessary weight to make sure that the cutter is pushed into the sediment. The ladder is raised and lowered so that the cutting depth can be adjusted. The maximum working water depth for a cutter suction dredge without a ladder pump is approximately 30 m (90 ft) (Herbich, 2000). The angle of the ladder normally has a maximum cutting angle of 45 degrees from horizontal.

Operation of a Cutter Suction Dredge

The standard cutter suction dredge uses spuds and winches to advance forward and swing in either the starboard-port or port-starboard direction. When the dredge is stationed on one of the spud poles, winches on the dredge swing the dredge by pulling and slacking cables. Cables are fixed by side anchors set at fixed locations. When the dredge performs a starboard to port swing, the starboard winch slacks the starboard cable and the port winch haulls in the port cable. The angle that a cutter suction dredge swings is dependent upon the side anchor placement but usually reaches a maximum rotation at

30 degrees from the centerline on the starboard side and 30 degrees from the centerline on the port side (Turner, 1996).

Most of the production (actual entrainment of sediment in the pipeline) occurs when the dredge is on the work spud. The second spud is known as the “auxiliary” spud or “step” spud. In order for the dredge to advance into new material the dredge must alternate between the work spud and the step spud. This method is known as “stepping” or “setting” forward (Huston and Huston, 1976). Two different cutter suction dredge designs have been created for this procedure.

When both the work spud and the step spud are located on the stern of the vessel, a method known as “setting” is utilized (Turner, 1996). Referring to Figure 3 (left pane), the dredge has completed the previous swing and at point A reaches a suitable angle in the port direction to advance forward. At this point, the step spud is lowered and the work spud is raised. The dredge then swings back to starboard until the swing angle on the reverse side is large enough so that a significant advancement is made at point B. The work spud is then lowered and the step spud is raised so that the standard swing can be made. This swing moves from point B to point C, then swings in the port direction to point D. In order to make another step, the dredge then moves to point E where the step advancement can be made from point E to F, and the same pattern is followed (point F-G, point G-H).

Calculation of an estimate for the step angle θ_s [rad] can be predicted using the distance between the work and step spud L_{SPUDS} [L] and the desired forward advancing step size L_a [L](Turner, 1996)

$$\sin\theta_s = \frac{0.5L_a}{L_{SPUDS}} \tag{1}$$

The other design created to advance the dredge is known as the spud carriage. A diagram of this type of movement can also be seen in Figure 3 (right pane). In this case, the work spud is mounted on a moveable carriage known as the spud carriage. When the work spud is fixed to the bottom, the dredge advances forward or backward by adjusting the position of the spud carriage in relation to the dredge. The step spud is located on the stern of the vessel. When the dredge has advanced to the maximum of the relative displacement of the spud carriage to the dredge hull, the step spud is lowered and the work spud is raised. The work spud is then moved to the necessary starting position and lowered. Finally, the step spud is raised and the work can continue.

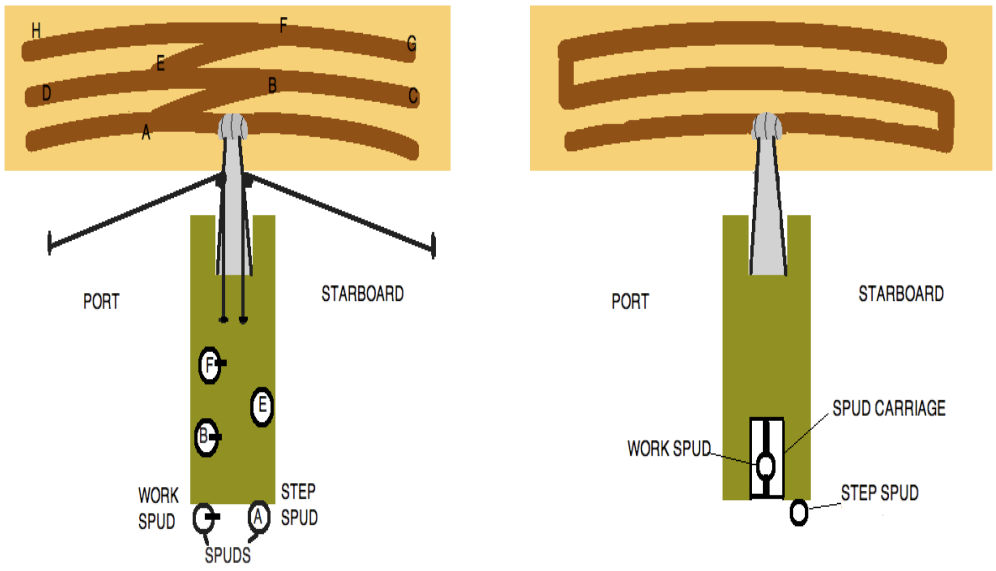

Figure 3. Cutter Pathway for Standard and Spud Carriage Cutter Suction Dredging

As the dredge is swinging from either port to starboard or starboard to port the cutter is always rotating in the same direction. Undercutting occurs when the tangential velocity of a blade at the top of a cutter is moving in the opposite direction of the ladder swing direction. Overcutting occurs when the tangential velocity of the top position for the blades of the rotating cutter is moving in the same direction as the ladder swing direction. A diagram of undercutting and overcutting can be seen in Figure 4.

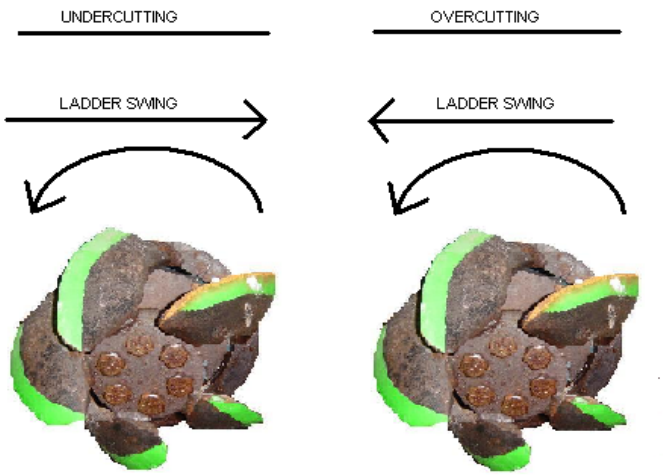

Figure 4. Two Cutter Heads Displaying Undercutting (left) and Overcutting (right)

Definition of Turbidity

The term “turbidity” has a plethora of definitions, however, the American Public Health Association (APHA, 2001) defines turbidity as “an expression of the optical property of a sample that causes light rays to be scattered and absorbed rather than transmitted in straight lines through a sample.” The description of turbidity analysis is also described by stating “attempts to correlate turbidity with the weight concentration of

suspended matter are impractical because the size, shape and refractive index of the particulate materials are important optically but bear little direct relationship to the concentration and specific gravity of suspended matter."

Turbidity is created from natural and human activities. Land erosion, mostly from agricultural practices, is the most abundant producer of turbidity in lakes, rivers, and estuaries. Turbidity is also caused from the agitation of bottom sediments caused from waves, currents, and winds as well as larger storm events such as hurricanes. Turbidity can also be caused from biological sources such as red tides and plankton blooms.

Dredging induced suspension of sediment has created aquatic environmental concerns that are important worldwide. The impacts of dredged material on the open ocean are discussed by Pequengat et al. (1978). The impacts are grouped into physical impacts, chemical impacts, and biological impacts. The increase in turbidity associated with cutter suction dredging operations is mainly categorized into the physical impacts. Cloudiness in the water column created from the turbidity often creates an unfavorable public response. As a result, monitoring dredging turbidity is important to the community at large.

The effects turbidity has on both aquatic plants and other organisms is difficult to ascertain because of the multiple variables that exist in the field and the diverse needs of different plant and animal species. These variables include the concentration of sediment, size and density distribution of the suspended material, the mineral composition of the material, and the organic material percentage. Nutrient exchange,

both uptake and release, is stated to increase from resuspension during dredging (Pequengat et al., 1978). Methods to remove turbidity from the water column predominately include settling and dispersion.

Turbidity Measurement Methods

Most currently used methods of turbidity measurement are either gravimetric or optical. However, it is difficult to relate the sediment concentrations and optical properties between different types of turbidity meters and units of measurement. Units used for turbidity measurement are also numerous. Gravimetric measurement techniques rely on collecting a sample and removing the sediment and then taking a "dry" measurement of the material from the sample. However, optical methods are more diverse and provide more variation in measurement techniques.

In the early 1900's the Jackson Turbidity Unit (JTU) was created. The unit was a relative measurement of the Jackson Candle Turbidity meter that consisted of a candle and glass tube. Samples were poured into the glass tube and the JTU was a notification of when the depth of the sample caused the candle light to diminish beyond visual standards. Around the same time period, the Secchi disc was also invented. The disc was designed to be white and to be lowered into the water column until it could no longer be visible to the human eye. In 1926 the Formazine Turbidity Unit (FTU) was developed as a relative measurement for using Formazine. The advantage of using Formazine was that a standard stock solution could be created and better measurement repeatability could be achieved. The Formazine standard solution has a JTU value of 4000 units.

In the 1970's, two types of turbidity sensors were created known as the transmissometer and the nephelometer. The transmissometer was designed to measure absolute transmission of a sample with an emphasis on the absorption of light caused by a sample. The transmissometer is known to be especially useful in calculating attenuation, however, it is criticized because it does not easily correlate with JTU or FTU measurement units.

The nephelometer and the Nephelometric Turbidity Unit (NTU) was accepted by APHA (2001) as the preferred turbidity measurement system. The NTU is a measure of the process of nephelometry where light is measured at a sensor 90 degrees to the incident beam rather than at a sensor 180 degrees to the incident beam as is prevalent in most other turbidimeter measurement systems. In this case, the amount of light scattered is the main focus of measurement. A transmissometer is also part of the device and measures the remaining light at 180 degrees. The nephelometer is very useful because the output signal is linear with increasing turbidity. Disadvantages of the system include its non-correlation with the JTU and the possibility of "stray light" entering the measurement testing environment and causing erroneous measurements.

Dredging Induced Turbidity Generation

The spillage from a cutter suction dredge is defined as the amount of material that is cut by the cutter but is not removed from the system by the suction line (Burger, 2003). This material can either settle to the bottom as a residual or become resuspended sediment (RSS) in the water column causing turbidity (Bridges et al., 2008). When the sediment is resuspended, a plume may form. The plume from the cutter suction dredge

normally stays near the bottom of the water profile but can travel in horizontal directions and affect the water quality in specific locations.

The generation of this spillage can be caused from the initial cutting and tangential velocity of the cutter blades as well as the mixture created from the cutter and the flow into the suction inlet (Burger, 2003). Both types of spillage can be affected by specific operating parameters of the cutter suction dredge including cutter rotational velocity, suction flow rate, thickness of cut, ladder angle, and ladder swing speed. By reducing the amount of spillage, the production of the dredge can be maximized and the turbidity generation can be minimized.

Several components of a cutter suction dredge have been known to cause the resuspension of sediment. Dredges with hulls whose drafts are close to the depth of cut can produce turbidity. The constant swinging of the vessel can create a turbulent environment and initiate resuspension. This is often the case when large dredges work in shallow regions. Dredge ladders can also create turbidity by dragging through sediment when the ladder is too long or when the angle of cut is too shallow.

Although the hull and ladder may produce some turbidity, the cutter has been defined as the most abundant turbidity generation mechanism on the dredge (Brahme, 1983). Therefore, cutter blades should be designed to guide material into the suction intake, thus increasing production and decreasing turbidity simultaneously. The number of blades is also stated to be important (Brahme, 1983). If there are not enough blades the amount of material cut with each blade may become too large and turbidity may be created. In certain situations, the cutter can actually be removed and the suction line can

be directly used to pick up material. This procedure can help reduce turbidity and has been used when conducting maintenance dredging.

Problem Definition and Dissertation Outline

The resuspension of sediment from cutter suction dredging can be caused from the initial cutting and tangential velocity of the cutter blades as well as the mixture created from the cutter and the flow into the suction inlet. This sediment resuspension can be affected by specific operating parameters of the cutter suction dredge including cutter rotational velocity, suction flow rate, thickness of cut, ladder angle, and ladder translational speed. By reducing the amount of resuspended sediment, the production of the dredge can be maximized and the turbidity generation can be minimized.

In order to predict the resuspended sediment created from a prototype cutter suction dredge, both physical and numerical model tests have been designed. Physical model tests use a dredge/tow carriage that has similar capabilities as a cutter suction dredge. The cutter speed, suction flow rate, and thickness of cut are investigated and turbidity and velocity data at specific points surrounding the cutter are examined in order to better understand the turbidity generation. The physical data is examined to understand turbulence characteristics of the cutter suction dredge as well as provide valuable input data for the numerical model.

The numerical model is an advection diffusion numerical computer model that predicts a source term based on the physics of the system and uses laboratory data to predict the flow field and turbulent diffusion around the cutter in the dredging environment. The operating parameters used to determine the turbidity generation from

the cutter include the cutter rotational velocity, the suction flow rate, the thickness of cut, the ladder angle, and the translational ladder speed. The source term model calculates the volume of sediment excavated and uses the forces created during dredging to predict the amount of resuspended material from each cut. This material is then entered as a flux into an advection diffusion model to examine the movement of sediment concentration surrounding the cutter. The variables are represented in the numerical model and validated through laboratory testing.

Objectives

The objectives of the dissertation research are:

1) Develop laboratory techniques for measuring near-field resuspended sediment concentrations and fluid velocity surrounding the cutter.
2) Analyze the measured resuspended sediment concentrations and velocities surrounding the cutter for the specific operating parameters of suction flow rate, cutter speed, and cut thickness.
3) Develop and verify a numerical model for predicting the near-field resuspended sediment concentrations surrounding the cutter.

Outline

The outline of the dissertation is to first state the previous literature and knowledge on the topic of resuspension from a cutter suction dredge. Chapter II includes information on previous numerical models developed for cutter suction sediment resuspension. Chapter III continues the literature review and discusses information on turbidity data collected from field tests.

The second section of this dissertation discusses the research completed for this study on the physical and computational testing of the turbidity generation of a cutter suction dredge. Chapter IV addresses the scaling laws involved with conducting turbidity experiments in the laboratory and the methods for relating the data to the prototype environment. Chapter V provides information on the physical testing methods used to investigate turbidity generation from a model cutter suction dredge. The laboratory facilities and the equipment utilized for the investigation are also discussed. Chapter VI provides the statistical description of the methods used to analyze the laboratory data and provides the actual results from the laboratory study.

The third part of this dissertation addresses the numerical model created for this study. Chapter VII addresses the description of the physics of the model as well as the key equations and general layout of the structure of the software. The model is compared to laboratory data as well as field data. Finally, in Chapter VIII, conclusions and recommendations for future research are addressed.

CHAPTER II

LITERATURE REVIEW

The numerical modeling of resuspended sediment from a cutter suction dredging operation can be subdivided into far-field modeling and near-field modeling. A diagram displaying the difference between the near-field and far-field is shown in Figure 5. Far-field models attempt to predict the sediment plume movement occurring beyond a few initial cutter diameters and often extend their domain to several hundred meters from the cutter. Near-field models predict the initial turbidity plume or "source term" of the cutter suction dredge and are used as initial conditions for far-field models.

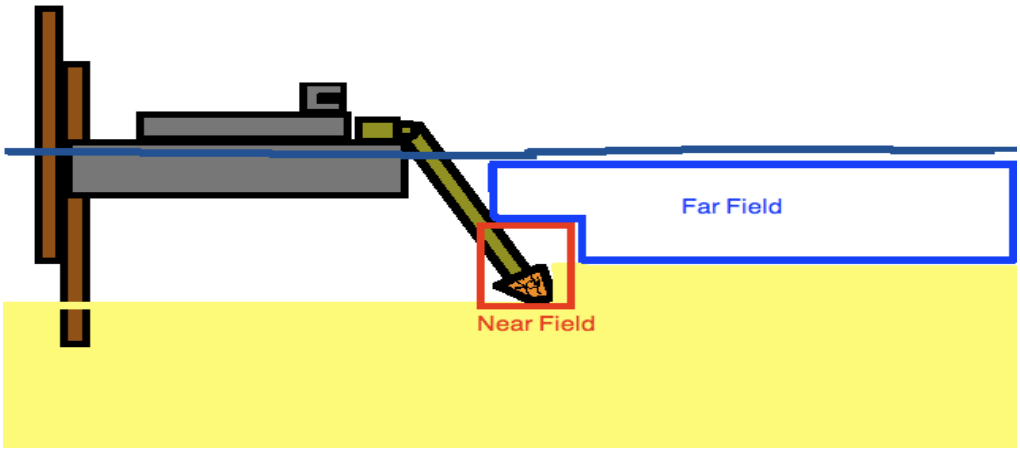

Figure 5. Near-Field and Far-Field Regions Surrounding the Cutter

Far-Field Modeling

Far-field numerical computer models are designed to predict the sediment plumes that are created from the resuspension of sediments during dredging operations. Although the far-field model is adequate at describing sediment concentrations away from the dredge, the far-field model requires a "source term" or near-field approximation of the amount of resuspended sediment to drive the far-field model.

Kuo et al. (1985) described the movement of a turbidity plume by modeling the plume as a series of repetitive thin disks that decrease in strength as they move away from the source. Over time the disk is assumed to spread out in the *x*, *y* and *z* directions, where *x* is in the flow direction [L], *y* is laterally across a dredge cut [L], and *z* is in the vertical direction [L]. In this case, a uniform flow field is assumed:

$$x = Ut \tag{2}$$

where U is the water velocity in the x direction [LT^{-1}] and t is time [T]. Also, if pure advection is assumed in the x direction then the concentration in the x direction is assumed as steady where:

$$\frac{\partial C}{\partial x} = 0 \tag{3}$$

and C is sediment concentration [ML^{-3}].

The movement of the sediment particles in the far-field are described by the equation:

$$\frac{dC}{dt} - w_s \frac{dC}{dz} = D_y \frac{d^2C}{dy^2} + D_z \frac{d^2C}{dz^2} \tag{4}$$

w_s is particle settling velocity [LT^{-1}], D_y is diffusion coefficient in the y direction [L^2T^{-1}], D_z is diffusion coefficient in the z direction [L^2T^{-1}].

The equation was solved by Kuo et al. (1985) by assuming a uniform flow field with constant U velocity in the x direction and a continuous source strength at the cutter head where x, y, and z are (0,0,0). The solution is stated as:

$$C(x,y,z) = \frac{\dot{m}_r}{\pi(D_y D_z)^{0.5}\frac{x}{U}} \exp\left[-\frac{y^2}{D_y\frac{x}{U}} - \frac{(z+w_s\frac{x}{U})^2}{D_z\frac{x}{U}}\right] \quad (5)$$

where U is water current velocity in the x direction [LT^{-1}] and $\dot{m}_r$ is source strength at the cutter [MT^{-1}]. The use of this equation has been incorporated into the DREDGE model developed by Hayes and Je (2000). An output display at the dredging depth z=0 from the DREDGE model for a typical cutter head dredge is shown in Figure 6.

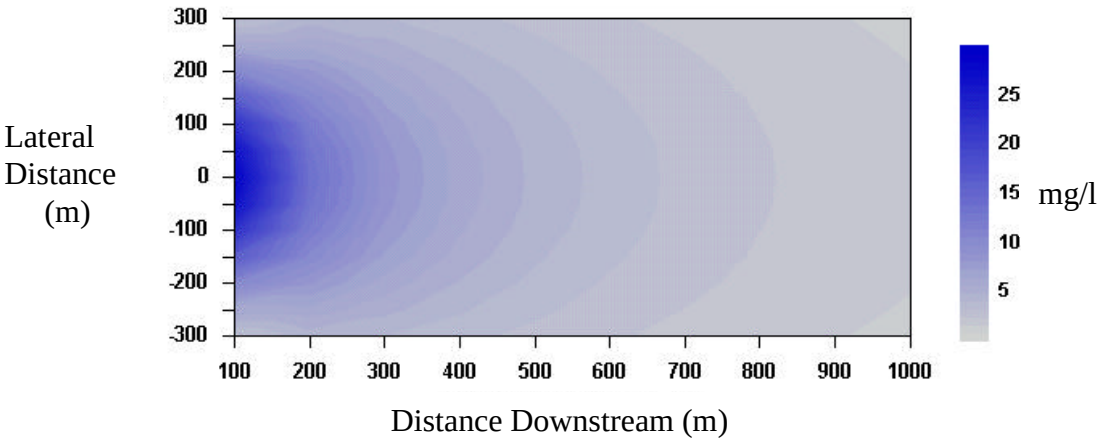

Figure 6. DREDGE Model Far-Field Output of Turbidity

Besides the model mentioned above, numerous sediment transport models exist (Chapra, 1997; Je, 1998) that also predict the transport of resuspended sediment in the far-field but all of these models require a source term $\dot{m}_r$ or near-field approximation. The next section describes the history of the development of a near-field model for a cutter suction dredge.

Near-Field Studies and Modeling

Yagi et al. (1975) described an investigation of turbidity in the near-field from a cutter suction dredge. Operating conditions that were significant for turbidity generation included shape and speed of the cutter, direction and rate of swing, discharge from the dredge pump, and the step distance. The study was conducted over two periods of testing. Work was conducted simultaneously with dredging work being conducted on Port Yokkaichi, Japan.

Seven test cases were examined with each test conducted twice. The two variables that were mainly investigated were the swing speed and the depth of cut. Cutter speed was held constant. No real trend was seen on swing rate for turbidity, and turbidity was noticed to be much less when swinging toward the left. Also, when the cutter was not rotated, turbidity was at a minimum. Maps of the distribution of turbidity were made for 20 m (65.6 ft), 60 m (196.8 ft), and 110 m (328 ft) around the cutter. Conclusions stated that the vertical distribution of turbidity around the cutter head followed an exponential decay as the location moved away from the cutter.

Yagi et al. (1975) utilized the data created from the field study to create a near-field approximation of cutter suction dredge turbidity generation. The method involved the calculation of the percent of material, $\hat{m}_r$, available for resuspension by comparing the theoretical maximum of dredged material in the dredge pipe versus the actual amount of dredged material in the dredge pipe. Yagi et al. (1975) used the report's field data to develop an empirical equation for the average mud content in the dredge pipe. Although the equations represents the effect of specific variables on resuspension, no applicable results were obtained. Also the equation is site specific and no correlation is stated for other types of cutter suction dredges. The equation for the percent of material available for resuspension $\hat{m}_r$ is:

$$\hat{m}_r = 1 - \frac{X}{X_T} \tag{6}$$

X is solids content by volume measured in discharge pipe by solids content meter [%] and X_T is theoretical maximum of reduced solids content in discharge pipe [%]

$$X_T = \frac{L_a t_c V_s}{\pi V_d D_d^{\,2}} \tag{7}$$

L_a advance distance per step [L], t_c is thickness of dredge cut [L], V_s is rate of swing [LT^{-1}], D_d is diameter of discharge pipe [L], V_d is flow velocity in discharge pipe [LT^{-1}].

Huston and Huston (1976) produced data from a field study for a cutter suction dredge with a suction pipe diameter of 68.6 cm (27 in) and discharge pipe diameter of 76.2 cm (30 in). The test had a 248.9 cm (98 in) diameter cutter with cutter speeds ranging from 0 to 35 rpm. The study was conducted in Corpus Christi, TX and

examined the effect of cutter speed and thickness of cut on sediment resuspension. The cutter was stated to be responsible for creating the largest percentage of dredge induced turbidity. Samples were taken at different depths with the final depth being just above the bottom of the cut. The findings showed an increase in turbidity only around the cutter with negligible effect in upper layers of the water column. Variability of turbidity around the cutter head was associated with the turbulence created in this region. However, turbidity was stated to increase with an increase in cutter rpm. It was stated that additional work should be done on relating the statistical relationship between cutter speed and turbidity generation.

Nakai (1978) proposed a TGU (Turbidity Generation Unit) method that predicted turbidity of a specific dredging operation based on the type of dredging operation as well as the sediment characteristics involved with the specific project. The TGU method covered different dredging operations including cutter head, trailing suction draghead, and clamshell and standard bucket dredging. Turbidity was highest for clays, followed by silts, and finally sands. Data was used from the Yagi et al. (1975) field study. A coefficient based on dredge type and the sediment environment was utilized to predict the quantity of resuspension created from a unit quantity of dredged material from the dredging operation. Although TGU values are presented for different dredging scenarios, data for determining the actual coefficient are not reported. TGU values are represented as:

$$TGU = \frac{f_{74}\ W_o}{f_o\ \forall_s} \tag{8}$$

TGU is Turbidity Generation Unit [ML^{-3}], $\forall_s$ is volume of dredged material from one swing [L^3], W_o is total quantity of suspended solids generated from dredging [M], f_{74} is fraction particles < 74 μm, f_0 is fraction of particles smaller than particles with a critical resuspension initiation velocity equal to the water current velocity. A conversion for equation 8 can be made to compensate for the dredging coefficients:

$$\frac{f_{74}}{f_o}\frac{W_o}{\forall_s} = \frac{f_{74}}{f_o} C_{DT}\,\gamma \tag{9}$$

where γ is specific weight of dredge material [ML^{-3}], C_{DT} is coefficient dependent on dredge type and soil conditions. The equation can be rewritten in terms of a near-field source strength:

$$W_O = TGU\left[\left(\frac{f_0}{f_{74}}\right)Q\right] \tag{10}$$

where Q is flow rate [L^3T^{-1}].

Hayes et al. (1984) presented information on a study of the turbidity created from a cutter suction dredge working in a river in Savannah, Georgia. The operating variables investigated were cutter speed, swing speed, and thickness of cut. Sampling tubes were located above the cutter head. Partial and full cuts were investigated with the highest suspended solids being reported for a full cut with a relatively high cutter speed. However, results were variable because of sampling tube location for full cuts versus partial cuts. The sampling tubes were located at a lower depth for full cuts and often experienced the effect of sediment collapsing. Other uncontrollable variables in the

study included variations in swing speed, cutter speed, and thickness of cut during the testing.

Hayes (1986) also reported on sediment resuspension from a cutter suction dredge in Calumet Harbor, IL. Water quality samples were taken within 3.05 m (10 ft) of the cutter and were used to compare a normal cutter suction dredging operation to a "matchbox" style (draghead) suction head. Velocity measurements of the current in the area as well as background water quality were investigated.

The dredge had a 30.5 cm (12 in) diameter discharge pipe and 35.6 cm diameter (14 in) suction pipe with a six blade serrated edge cutter. The cutter was 1.07 m (3.5 ft) in diameter and was 0.76 m (2.5 ft) long. Maximum speed of the cutter was 27 rpm. Constant swing speeds of 0.214 m/s (0.7 ft/s) and 0.34 m/s (1.1 ft/s) were investigated with 15, 20 and 27 rpm cutter speeds. Full cuts were used in the testing. Hoses were attached to a steel frame at six sampling locations near the cutter and water samples were drawn through the hoses using a centrifugal pump.

Samples were measured for suspended solids concentration and also analyzed for particle size distribution. Port to starboard swings had sampling point values that were relatively homogeneous while starboard to port swings produced a decreasing turbidity gradient as distance from the cutter increased.

Hayes (1986) used a least squares regression multiple variable analysis to create empirical models for both point and line source resuspension. The models were based on dimensionless parameters created from the key variables of suction velocity, cutter

speed, and ladder swing speed. Data did not allow for the thickness of the cut to become a variable in the equation.

A stepwise linear regression builds an equation one variable at a time by examining a group of variables and choosing the specific variable that explains the most variation at each step. One variable is selected and its coefficient is set. From here the remaining variation must be explained by the next highest variable.

The regression equation is stated to be only applicable to conditions that fall within the range of data from which the equation was derived. Input data to obtain values of the equation include the standard operating parameters as well as the direction of cut. Assumptions were made that stated the region of negligible turbidity was reached two cutter diameters above the post-dredging bottom.

Hayes (1986) assumed that since the source strength model was created for sediment resuspension directly at the cutter, the dynamics of the sediment including settling were assumed to be unnecessary. A sinusoidal mathematical equation was created to describe the movement of the cutter suction dredge. Using this equation in conjunction with the original resuspension equation, a point source model was derived. Line source models in both the downstream direction and in the lateral direction were also created using a similar method.

Hayes (1986) developed three dimensionless parameters for cutter resuspension using linear regression analysis:

$$\pi_1 = \frac{V_s}{V_i} \tag{11}$$

$$\pi_2 = \frac{V_t}{V_i} \tag{12}$$

$$\pi_3 = \frac{t_c + D_c}{2D_c} \tag{13}$$

where V_i is intake suction velocity [LT^{-1}], V_t is cutter tip speed [LT^{-1}], t_c is thickness of cut [L], D_c is cutter diameter [L] measured at the back ring of the cutter.

Hayes (1986) used a semi-ellipsoid flow approximation for the suction intake velocity. The cutter tip speed used in the dimensionless calculation was stated to be dependent upon whether the cutter is undercutting or overcutting. Here the cutter tip speed can be represented in terms of both types of cuts where:

Undercutting

$$V_t = V_c - V_s \tag{14}$$

Overcutting

$$V_t = V_c + V_s \tag{15}$$

and

$$V_c = \omega R_c \tag{16}$$

Here V_c is tangential velocity of the cutter blade [LT^{-1}], ω is angular velocity [T^{-1}], R_c is cutter radius [L]. The linear regression predicted resuspended sediment above background concentration C_r [ML^{-3}] with the equation:

$$C_r = A\pi_1^a \pi_2^b \pi_3^c \tag{17}$$

for a thickness of cut greater than the diameter of the cutter, and

$$C_r = A\pi_1^a \pi_2^b \pi_3^{c'} \tag{18}$$

for a thickness of cut less than the diameter of the cutter, where *A, a, b, c* are regression coefficients and c' is a regression coefficient based on the depth of cut.

During the study it was stated that most resuspension of sediment results from sediment that clings to the cutter blades during excavation and then sediment is washed off the blade. Hayes (1986) conducted the stepwise linear regression on Calumet Harbor field data and developed the relationship

$$C_r = \left(\frac{V_s}{V_i}\right)^{2.869} \left(\frac{V_t}{V_i}\right)^{1.027} \tag{19}$$

Andrassy and Herbich (1988) reviewed the effect of operational parameters used in dredging operations and their effect on resuspension of sediment for both laboratory and field data. Field data in the study included Calumet Harbor, James River, Savannah River, and Port Kanda, Japan. Laboratory data were included from Brahme (1983) and Hebrich and DeVries (1986). The investigation of cutter head diameter, cutter speed, suction speed, swing speed, thickness of cut, ladder angle, and sediment diameter showed no significant data trends.

Collins (1995) also used empirical methods to create source strength estimates for a cutter suction dredge. The models were derived using data from Savannah River, James River, and Calumet Harbor field studies (Chapter III). The empirical model was derived in the similar format as Hayes (1986) and also included parameters for partial and full cutting. Collins begins with the solution:

$$\frac{C_r}{\rho_w} = \left(\frac{V_s}{V_i}\right)^{2.848}\left(\frac{V_t}{V_i}\right)^{1.022} \tag{20}$$

Here ρ_w is the density of water [ML^{-3}]. These values are similar to Hayes (1986). However, Collins (1995) emphasizes the variation of the thickness of cut and the cutter length in the coefficient *a* (equation 16) and explores this variation with the factor F where:

$$F = F_F F_D \tag{21}$$

and

$$a = \log(F) = \log(F_F) + \log(F_D) \tag{22}$$

$$F_D = 1; \quad \textit{for full cut}$$

$$F_D > 1; \quad \textit{for nonfull cut}$$

The parameter F_D accounts for the type of cut and can be described as a function of cutter head penetration ratios for both partial cuts and full cuts. F_F is a function of the cutter length and the median sediment diameter and was calibrated with Calumet Harbor, Savannah River, and James River field data, yielding:

$$\left[\frac{\frac{L_c}{d_{50}}}{13.32}\right]^{7.04} = \log[2.05 + \log F_F] \tag{23}$$

$$F_D = 1.9039(D_{\%} - 1)^2 + 0.4116(D_{\%} - 1)^7 \tag{24}$$

$$D_{\%} = \frac{t_c}{D_f} \tag{25}$$

where L_c is cutter length [L], d_{50} is the mean sediment diameter [L], D_f is the thickness of a full cut [L] when the cutter is submerged in the sediment to a thickness of one cutter diameter. $D_{\%}$ is the ratio of the thickness of cut to a full cut.

Crockett (1993) created a near-field model for predicting resuspension from a cutter suction dredge. The model was based primarily on the geometric relationship of the area of the cutting blades that are available for being exposed to the mechanism of "washing", where sediment is removed from each cutter blade during its revolution in the water column. Crockett (1993) provides a derivation (Chapter IV) of this area for several types of cutting depths including full, partial, and very small thickness cuts.

The sediment resuspension equations utilized by Crockett (1993) were based on the assumption that material excavated by the cutter is either removed by entrainment of the suction line or transported by water current away from the cutter region in the form of a turbidity plume. These assumptions lead to a materials balance equation:

$$\dot{m}_s = \dot{m}_p + \dot{m}_r \tag{26}$$

where $\dot{m}_s$ is rate of sediment excavated by the cutter [MT^{-1}], $\dot{m}_p$ is rate of sediment entrained by the suction line [MT^{-1}], and $\dot{m}_r$ is source strength at the cutter [MT^{-1}].

In this case,

$$\dot{m}_s = C_s L_c t_c V_s \tag{27}$$

where C_s is in situ sediment concentration [ML^{-3}]. The mass rate of entrained sediment can be calculated from the production of the dredge:

$$\dot{m}_p = C_s P \tag{28}$$

where P is dredge production [L^3T^{-1}].

Although equations 26, 27, and 28 make it plausible to calculate $\dot{m}_r$ directly, several issues exist such as the quick re-settling of sediment particles (residuals) that make it difficult to entertain a direct mass balance. Hayes et al. (2000) makes note of this issue and provides an equation with added variables of concern for predicting the amount of sediment resuspension.

An empirical approximation was made for the source strength of resuspension for a cutter suction dredging operation. Crockett (1993) produced three linear regression equations for predicting the amount of resuspended sediment released during cutter suction dredging. The three equations are:

$$\dot{m}_r = 10^{46.03\left(\frac{A_E}{A_T}\right)}\left(\frac{\dot{m}_s^{1.43}}{\dot{m}_p^{0.43}}\right)\left(\frac{V_t}{V_i}\right)^{2.10} \tag{29}$$

$$\dot{m}_r = \dot{m}_s\left[10^{36.25\left(\frac{A_E}{A_T}\right)}\left(\frac{V_t}{V_i}\right)^{1.61}\right] \tag{30}$$

$$\dot{m}_r = 10^{50.70\left(\frac{A_E}{A_T}\right)}\left(\frac{\dot{m}_s^{2.85} V_t^{1.03}}{V_i^{2.82}}\right) \tag{31}$$

where A_E is surface area of cutter exposed to washing [L^2] and A_T is total surface area of cutter [L^2]. Crockett (1993) is able to also calculate the resuspended sediment concentration by converting the mass flow rate according to:

$$C_r = \frac{\dot{m}_r}{L_c h_r V_s} \tag{32}$$

where h_r is height above new cut elevation where the sediment concentration is equal to initial conditions [L]. Hayes (1986) determined from observations that h_r can be approximated as two cutter diameters and states that no study had been focused on the topic of experimentally calculating h_r.

Hayes et al. (2000) performed a stepwise linear regression model by utilizing field data from the Calumet Harbor, James River, Savannah River, and New Bedford field studies. Initial equations were used from Crockett (1993) and altered to create both a dimensional and non-dimensional equation for predicting the amount and percentage of resuspension released during a cutter suction dredging operation. The equations developed by Hayes et al. (2000) were based on the assumption that material excavated by the cutter is either removed by entrainment of the suction line, settled to the bottom, or transported by current away from the cutter region in the form of a turbidity plume. These assumptions lead to a materials balance equation:

$$\dot{m}_s = \dot{m}_p + \dot{m}_r + \dot{m}_l \tag{33}$$

where $\dot{m}_l$ is rate of sediment that settles quickly [MT^{-1}].

Field data from the four studies show that $\dot{m}_s$ is much greater than $\dot{m}_r$, and $\dot{m}_p$ is much greater than $\dot{m}_r$. However, Hayes et al.(2000) states that even a small amount of $\dot{m}_r$ can create a significant turbidity plume and that $\dot{m}_r$ is nearly impossible to measure

in the field. Therefore, Hayes et al. (2000) moves toward a linear regression approach based on the geometric surface area of the exposed cutter area.

Hayes et al. (2000) used a stepwise linear regression on 106 field observations based on the variables of $\dot{m}_r$ and log($\dot{m}_r$), $\dot{m}_s$, log($\dot{m}_s$), $\dot{m}_p$, log($\dot{m}_p$),V_s , log(V_s), V_T, log(V_T), V_i log(V_i), A_E/ A_C, and log(A_E/ A_C) to create the empirical *Dimensional Model* (DM)

$$\dot{m}_r = \left|V_s \pm \alpha \pi D_c\right|^{1.864} \left(\frac{4A_E}{\pi^2 L_c D_c} \right)^{14.143} \tag{34}$$

where α is the rotational speed of the cutter [radT^{-1}]. A *Non-Dimensional Model* (NDM) was also designed using dimensional analysis and the non-dimensional variable groups:

$$\pi_1 = \frac{\dot{m}_R}{\dot{m}_s} \tag{35}$$

$$\pi_2 = \frac{\dot{m}_s}{\dot{m}_p} \tag{36}$$

$$\pi_3 = \frac{V_s}{V_i} \frac{A_E}{A_C} \tag{37}$$

$$\pi_4 = \frac{A_E}{A_C} \tag{38}$$

$$\pi_5 = \frac{V_t}{V_i} \tag{39}$$

The linear regression from this analysis by Hayes et al. (2000) produced

$$\pi_1 = \pi_3^{1.804} \pi_5^{1.966} \tag{40}$$

Substituting in the necessary parameters, the *Non-dimensional Model* (NDM) is expressed as:

$$\dot{m}_r = \frac{C_s t_c D_c^{1.966} L_c^{2.966} V_s^{2.804} A_E^{1.804} \left| V_s \pm \alpha \pi D_c \right|^{1.966}}{Q^{3.770}} \tag{41}$$

Both the DM and the NDM resuspension values can be expressed as a percentage of the total sediment cut. This leads to a rearrangement of the DM and NDM equations into a fractional form calculated as:

$$\text{DM:} \qquad \hat{m}_r = \frac{\left| V_s \pm \alpha \pi D_c \right|^{1.864}}{C_s V_s t_c L_c^{15.143}} \left(\frac{A_E}{D_c} \right)^{14.143} \tag{42}$$

$$\text{NDM:} \ \hat{m}_r = \frac{\left(L_c D_c \right)^{1.966} \left| V_s \pm \alpha \pi D_c \right|^{1.966} \left(V_s A_E \right)^{1.804}}{Q^{3.770}} \tag{43}$$

A sensitivity analysis of both the DM and NDM showed that the DM was very sensitive to cutter speed and thickness of cut and not sensitive to pipe velocity while the NDM was very sensitive to pipe velocity. Both the DM and NDM were only slightly sensitive to swing speed. It was also noted that when predicting the average resuspended sediment rate the mean of both the port to starboard swing and the starboard to port swing should be calculated.

Wu and Hayes (2000) later utilized field data from the Lavaca Bay field study (Chapter III) to validate the models created from Hayes et al. (2000). The validation showed an overestimate with the NDM when predicting resuspended sediment. Hayes and Wu (2001) then proceeded to redefine the equations based on the updated field data.

Additional changes to the model include a newly defined step distance that was previously represented as the cutter length. With the new field data, a combination of 387 observations were utilized to create new DM and NDM equations using the stepwise linear regression expressed in terms of sediment loss percentage rate where:

$$DM: \qquad \hat{m}_r = \frac{(C_S t_c)^{0.676} V_s^{2.008}}{L_a^{13.899}} \left(\frac{A_E}{D_c}\right)^{14.575} \left(\frac{Q}{D_i^2}\right)^{0.805} \tag{44}$$

$$NDM: \hat{m}_r = \left(\frac{A_E}{L_a D_c}\right)^{13.503} \left(\frac{Q}{D_i^2 V_s}\right)^{0.388} \tag{45}$$

where D_i = suction inlet pipe diameter [L].

Hayes and Wu (2001) then used these approximations and field data to conduct a statistical analysis on resuspension from cutter suction dredges and validate that the information could be used as estimates of resuspension prior to dredging. The information was included in a simplified approach for predicting resuspension from different types of dredging operations. In this study, the amount of sediment resuspension from a cutter suction dredge is estimated using the equation:

$$\dot{m}_r = R_f f_{74} C_s \dot{V}_s \tag{46}$$

where R_f is resuspension factor i.e. percent loss of sediment and $\dot{V}_s$ is the volumetric in situ sediment removal [L^3T^{-1}]. The data showed the least sediment resuspension from a 45.72 cm (18 in) discharge diameter dredge followed by a 25.4 cm (10 in) discharge diameter dredge and a 30.48 cm (12 in) discharge diameter dredge respectively.

Burger (2003) investigated particle trajectories for rock cutting along a cutter suction blade with a computational fluid dynamics (CFD) program. The CFD simulated the particle trajectories with constant pump velocity and different cutter speeds. The model was verified analytically, however, the flow field around the cutter needed to be validated. Also, the model did not consider particle-particle interactions so the resulting plume from these particles paths was not modeled.

The models mentioned above have been useful in examining and predicting the quantity of sediment resuspension from a cutter suction dredging operation. However, to this date, a numerical model has not been created that is designed to investigate turbidity issues and predict the spatial distribution of resuspended sediment in the near-field domain of a cutter suction dredge. The models mentioned in this chapter are valuable for comparing the results of the numerical model designed for this dissertation and are of great importance for understanding the full range of prediction utilized to evaluate resuspended sediment quantities from a cutter suction dredging operation.

CHAPTER III

FIELD AND LABORATORY TESTING

Field Studies

Data collected during field studies are invaluable for understanding the complex systems involved with sediment plume modeling. Although sometimes expensive, these tests provide direct data to validate any model that is attempting to predict the mechanics of the problem. The following describes five field studies that provide necessary field data on cutter suction sediment resuspension. These studies include the Calumet Harbor, James River, Black River, New Bedford, and Lavaca Bay studies. Table 1 provides a summary of these studies and the dredging parameters involved with each study.

Table 1. Field Tests and Parameters

Field Test	Calumet	James River	Back River	Acushnet	Lavaca Bay
Dredge	Dubuque	Essex	Clinton	Ellicott 370	Tyro, Jr.
Discharge Diameter (m)	0.30	0.46	0.51	0.25	0.30
Cutter Diameter (m)	0.9	1.5	1.8	0.8	0.8
Cutter Speed (RPM)	15,20,27	20,28,32, 35,37,40	6.6,12,16	20	8.5,19
Cutter Tip Speed (m/s)	0.2-0.4	0.2-0.4	0.2-0.4	0.15	0.03-0.64
Production (m^3/hr)	33-56	504-2252	161-7379	28	28
Water Current (m/s)	0.0-0.07	0.1-0.8	0.03-0.8	0.0-0.07	0.0-0.07
Samples	12	15	28	51	10

The U.S. Army Corp of Engineers has conducted several studies on sediment resuspension from dredging operations. The research was conducted under the Improvement of Operation and Maintenance Techniques (IOMT) program and included studies of cutter suction dredging resuspension (Hayes et al., 1984; Montgomery and Raymond, 1984; Hayes, 1986).

Calumet Harbor

In this study the U.S. Army Engineering Research and Development Center combined their efforts with the Chicago District of the U.S. Army Corps of Engineers to compare the sediment resuspension of operating a matchbox suction dredge (dustpan type) versus operating a cutter suction dredge. The cutter suction dredge, DUBUQUE, used in the study had a 30.48 cm (12 in) inside discharge pipe diameter. The dredge had a cutter head diameter of 0.914 m (3 ft), with a cutter head length of 0.762 m (2.5 ft). The length of the ladder was 13.57 m (44.5 ft) and the thickness of cut was 0.914 m (3.0 ft). Swing speeds for the study were 0.21 and 0.335 m/s (0.7 and 1.1 ft/s) while cutter speed was varied between 15, 20, and 27 rpm.

Near-field water quality data were collected within 3.05 m (10 ft) of the point of dredging using six sampling stations surrounding the cutter head. The sampling locations were located on a designed steel frame structure that was mounted to the dredge ladder. Sampling tubes were positioned at each of the six sampling stations and water samples were taken every 30 minutes during six test periods each lasting 4 hours. Mean values of turbidity are displayed at the spatial sampling locations for both undercutting (Figure 7) and overcutting (Figure 8).

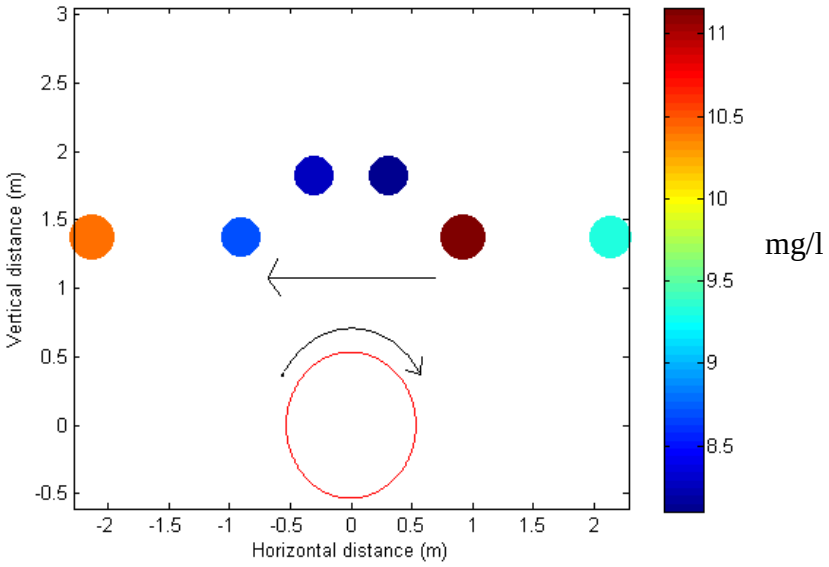

Figure 7. Calumet Harbor Turbidity Undercutting

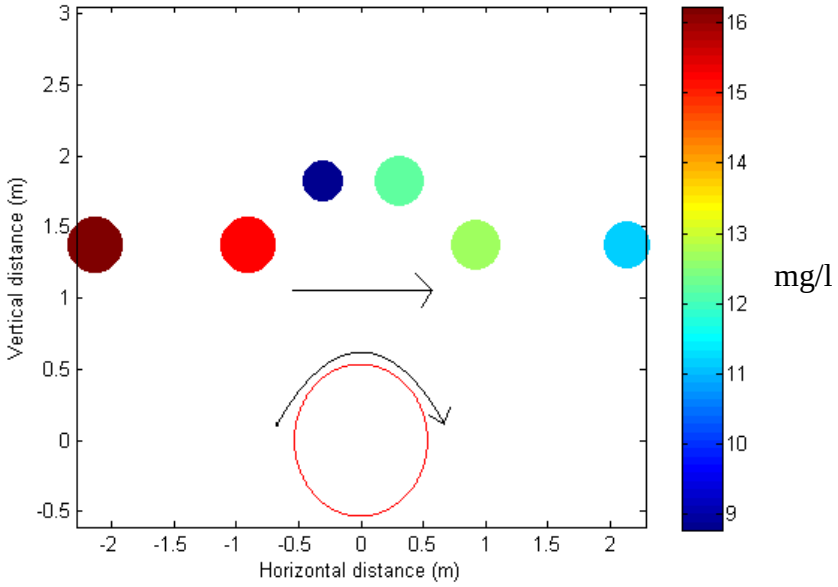

Figure 8. Calumet Harbor Turbidity Overcutting

The initial water quality standards and in situ sediment samples were taken prior to dredging. The in situ sediment consisted of a silty loam with 14.3% clay, 68.5% silt and 17.2 % sand. The analyzed sediment distribution showed that 82.8% of the material was able to pass through a #200 mesh sieve equating to a size of 72 μm. Moisture content was reported to be 71.1% while specific gravity was 2.71. Hayes (1986) reported an in situ sediment concentration of 926 g/l, however, because of the majority of the sediment has such a small grain size, the concentration later used in modeling was 767 g/l.

Conclusions from the study stated overcutting testing produced a higher resuspended sediment concentration than undercutting testing. Resuspension of sediment was stated to be primarily caused from the washing of the cutter blades.

James River

The Norfolk, Virginia District of the U.S. Army Corps of Engineers compared the effectiveness of a dustpan dredging operation versus a cutter suction dredging operation for removing contaminated sediment and minimizing sediment resuspension. The dredge used in the study was the ESSEX, a 45.72 cm (18 in) cutter suction dredge with a suction diameter of 53.34 cm (21 in). The cutter on the dredge was 1.52 m (5 ft) in diameter with a cutter length of 1.55 m (5.08 ft). The ladder on the ESSEX was 18.83 m (61.75 ft).

The in situ sediment properties were investigate and defined as a clay with silty characteristics with a moisture content of 44% and a specific gravity of 2.73, equating to an in situ sediment concentration of 554 g/l.

During testing the thickness of cut was 1.52 m (5 ft) which represents a fully submerged cutter. Although the only variable in the dredging operation was the cutter speed, the data collected from the study were not averaged over specific testing intervals and the swing speed of the ladder was often variable.

The time to swing from starboard to port was recorded as 5 min and the time to swing from port to starboard was recorded as 2.75 min (McLellan et al., 1989). The length of the dredge from the cutter to the spud location was 63.33 m (201.75 ft) while the dredge path width was recorded as 57.92 m (190 ft) (Raymond, 1984). Therefore the swing velocity can be averaged as 0.20 m/s (0.66 ft/s) from starboard to port and 0.36 m/s (1.2 ft/s) for port to starboard swings.

Crockett (1993) summarized and reported on the most pertinent data from the study that relates directly to the varied operating parameters. Collins (1995) published the data with assumptions on cutter speed and thickness of cut. Conclusions from the study stated a strong positive correlation of resuspended sediment with an increase in cutter speed and a negative correlation with an increase in suction flowrate.

Savannah River

The study was also conducted by the USACE Waterways Experiment Station and examined the parameters of cutter speed, swing speed, and thickness of cut on sediment resuspension. The study used the dredge CLINTON, a 50.8 cm (20 in) cutter suction dredge, and took place at the Back River of Savannah, Georgia. The dredge had a cutter head diameter of 1.83 m (6 ft), a cutter length of 1.52 m (5 ft), and a ladder length of 20.82 m (68.3 ft) (McLellan et al., 1989; Hayes et al., 1984).

The in situ sediment of the Back River was characterized as a silty clay with a moisture content of 44.3% (McLellan et al., 1989). The specific gravity and the *in situ* sediment concentration were estimated to be 2.7 and 1229 g/l respectively.

The method of sampling resuspended sediment was similar to both Calumet Harbor and James River studies and consisted of six sampling tubes mounted on steel tubing around the cutter head. Suspended solid background concentrations were recorded prior to dredging. Suction speed, cutter tip speed, swing speed, ladder angle, and production data were recorded as well as the suspended solid concentration data. Overcutting and undercutting data were both recorded. Data were reported for only two of the six tubes during full cutting situations because of sloughing that occurred during testing.

The thickness of cut was investigated for two testing situations. This first cut, consisted of a fully submerged cutter undercutting a bank of 6.09 m (20 ft). The second thickness of cut is recorded as approximately a 0.91 m (3 ft) cut. This material represents the second pass of the cutter over the material left behind from the first cut and is considered a partial cut in the study. Conclusions from the study stated an increase of resuspended sediment with an increase in cutter speed, a decrease in suction flowrate, and in increase in the thickness of cut.

Lavaca Bay

Lavaca Bay is part of the Texas Gulf Coast and is located between the cities of Galveston and Corpus Christi. The data from this study came from a Superfund report for pilot dredging studies to investigate the possibility of removing contaminated

sediment from the region. The data was collected in two phases with the field data used in this dissertation including the Phase II study conducted in shallow water. The depth of the water was approximately 0.30-0.91 m (1-3 ft) with a final dredging depth of 1.22 m (4 ft). The sediment consisted of silt and silty sand and ranged from 51.6% to 75.1% solids by weight.

The dredge was a 30.48 cm (12 in) cutter head dredge with a production range of 26.75-91.74 m^3/hr (35-120 yd^3/hr). Cutter speed was 8-9 rpm with a cutter diameter of 76.2 cm (30 in). The suction flow rate ranged from 0.16-0.27 m^3/s (5.5-9.5 ft^3/s). The concentration of solids in the discharge pipe ranged from 32-130 g/l. The swing speed of the dredge ranged from 0.27–0.37 m/s (0.9-1.2 ft/sec).

Resuspended sediment samples were collected 0.91–1.52 m (3-5 ft) from the cutter using a metal frame. Cutter speed, swing speed, overcutting and undercutting, cutting depth, cutting width, flow velocity, and solid concentration were recorded during testing. Conclusions of the study stated an increase in resuspended sediment with an increase in the summation of cutter speed and swing speed. Resuspended sediment also was concluded to be greater for overcutting.

New Bedford

A pilot study on hydraulic dredging was conducted in New Bedford Harbor, Massachusetts on the Acushnet River to investigate the effectiveness of hydraulic dredging on sediment removal for the area. The study included a standard cutter head dredge, a horizontal auger dredge, and a Matchbox dredge. In total 7,645 m^3 (10,000 yd^3) of material was removed from the site, 2,217 m^3 (2,900 yd^3) of which was

contaminated with polychlorinated biphenyls (PCBs). The USACE New England Division (USACE, 1990) managed the study and the Waterways Experiment Station offered assistance on the study as well. The in situ sediment concentration average was 1800 g/l and the sediment was classified as a sandy silt with a d_{50}=110 μm.

The cutter suction dredge used in the study was an Ellicott 370 Dragon Series with a 25.4 cm (10 in) discharge diameter. The discharge connected to a 20.32 cm (8 in) diameter pipeline. The cutter speed was run at 20 rpm and one test was run at 40 rpm. Swing speed was noted to be 0.15 m/s (0.5 ft/s) in both directions. The thickness of cut was 0.61 m (2 ft), with the width of each cut averaging 18.29 m (60 ft). The cutter diameter was noted to be 0.80 m (2.63 ft) and the cutter length was stated as 0.79 m (2.60 ft). The suction flow rate averaged at 7950 lpm (2100 gpm) while the solids concentration in the slurry averaged at 40 g/l. The estimated sediment release rate of the cutter suction dredge was noted as 12 g/s. It was also noted that prior sediment release estimates stated a sediment resuspension rate for a cutter suction dredge of 40 g/s.

During the study, production, total suspended solids of slurry, rate of advance, and swing direction were consistently recorded. The data recorded from the study were used to develop a sediment resuspension rate based on the depth of the water and the dredge swing speed. It was shown that an increase in cutter speed increased the resuspension rate significantly. It was also shown that the cutter head dredge had the lowest average resuspension rate when compared to the horizontal auger dredge and the matchbox dredge.

Six locations surrounding the cutter head were sampled to obtain TSS turbidity measurements. The location of the samples around the cutter as well as the mean values obtained for all measurements from the study can be seen in Figure 9 (undercutting) and Figure 10 (overcutting). Samples were taken every 15 minutes during the study.

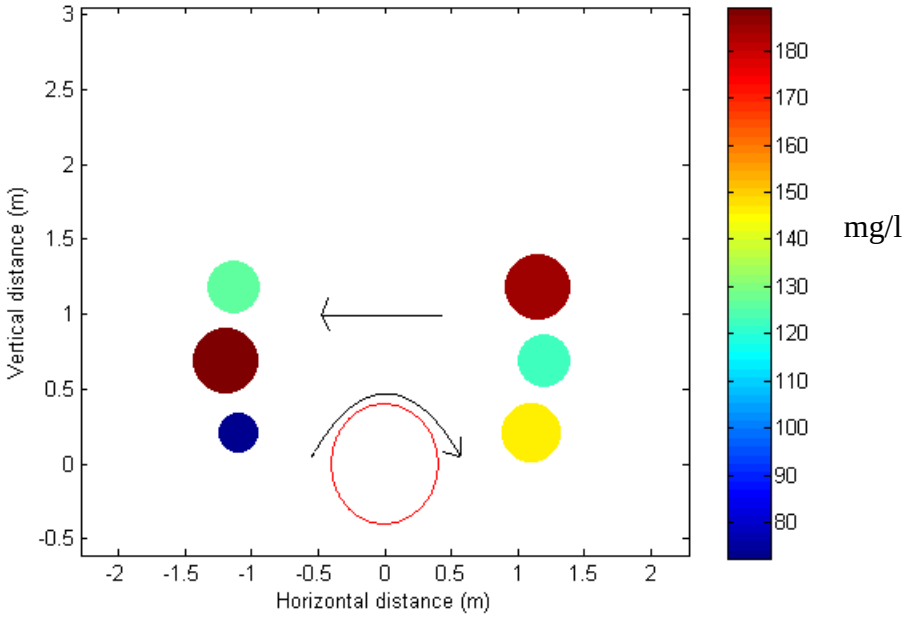

Figure 9. New Bedford Turbidity Undercutting

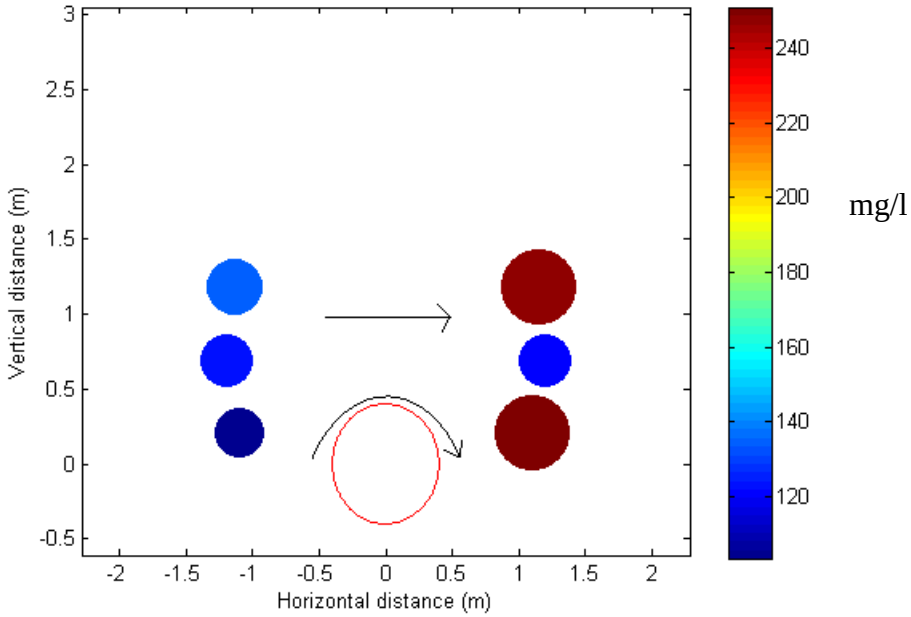

Figure 10. New Bedford Turbidity Overcutting

Laboratory Physical Model Studies

Physical model studies are conducted in a laboratory setting and provide a controlled environment to examine specific variables of interest when testing a complex problem. The physical model provides an economical method for testing dredging issues that might otherwise be impossible to investigate during field testing. The following is a description of previous laboratory testing that was conducted to understand the cutter suction dredging mechanics in hopes to maximize production and minimize the resuspension of sediment.

A cutter head flow visualization was conducted by Slotta (1968) to investigate the flow in and around the cutter head under different operating variables and their effect

on turbidity generation and dredging production. A 1:15 scale model with a back ring diameter of 16.5 cm (6.5 in) representing a 2.47 m (8.1 ft) diameter cutter head was tested in a Plexiglas tank. Hydrogen bubbles created by electrolysis provided visualization of the flow field. Dredge model similitude was investigated using the Buckingham Pi theory based on Reynolds, Froude, kinematic velocity, and cutter speed scaling with the conclusion that an accurate quantitative method for forecasting dredge model results was not yet available.

Joanknecht (1976) investigated cutter head performance for a 1.9 m (6.23 ft) diameter prototype cutter. Model scaling used were 1:3 and 1:4 scales, and the sand used had a median grain diameter of 200 μm. A Froude scaling relationship was applied based on the particle settling velocities and the median sediment diameter of the model and prototype bed sediment. Model to prototype relationships were also made for production rates and cutting forces.

Flow tests around the cutter as well as tests for cutting sand were conducted in the same tank (Mol, 1977a; Mol, 1977b; and Mol, 1977c). Cutting tests in sand used a sediment diameter of 120 μm with a cutter diameter of 0.6 m (1.96 ft). Tests were scaled using Froude scaling, and cuts were conducted using an inclined ladder angle of 30 degrees. Other important notes were that an outward flow tended to be created once the cutter reached a threshold speed. The flow field for the cutter head varied significantly between overcutting and undercutting dredging. Spillage from the cutter head was created once the cutter rotation reached a large enough quantity.

Miltenburg (1983) conducted sand cutting tests with cutter diameters between 0.32 m and 0.4 m (1.05 ft and 1.31 ft). Froude scaling laws were used and the flow and mixture forming processes inside the cutter were studied. Tests used a sediment diameter of 180 μm and the variable operating parameters included cutter speed, suction velocity, and swing speed. Conclusions from the study showed an increase in production with a decrease in cutter speed and increase in suction flowrate.

Brahme (1983) investigated the complex flow pattern around the cutter head. Work also focused on the amount of suspended sediment levels generated by the cutter head at different locations near the cutter head. The resuspended sediment levels were measured as a function of the dredge operating parameters. Operating parameters in the study included cutter rotation, suction, and swing of the cutter head. The three bed materials were fine sand, micro beads, and medium sand, having a median sediment diameter of 210 μm, 93 μm, and 390 μm, respectively.

Rotational speed of the cutter head varied from 75 rpm to 195 rpm. Swing velocity ranged from 1.22 to 9.1 cm/s (0.48 to 3.58 in/s). The two models size used were an 20.3 cm (8 in) cutter diameter and 5.1 cm (2 in) suction diameter and a 10.2 cm (4 in) cutter diameter with a 2.8 cm (1.1 in) suction diameter with a flow of 212 lpm (56 gpm) and 190 lpm (50 gpm) respectively.

Brahme (1983) collected samples in front of the cutter and reported turbidity values as high as 120 g/l. It was concluded that a significant decrease in turbidity occurred above the cutter when the distance above the cutter reached one suction pipe diameter. Turbidity in the horizontal direction became negligible when the distance

away from the cutter reached ten to fifteen suction pipe diameters. Resuspension on the back of the cutter was shown to be greater than in front of the cutter. The larger cutter produced a larger turbidity.

Herbich and Devries (1986) conducted a study to investigate the various operating parameters of the cutter head dredge on suspended sediment levels. A 1:8 scale model cutter head was used for a prototype dredge with a basket type cutter head. The diameter of the cutter was 82.9 cm (72 in) and the diameter of the suction pipe was 40.6 cm (16 in).

Operating parameters investigated included ladder angle, cutter rpm, and thickness of cut as related to the cutter diameter. Fine sands with a median grain diameter of both 100 μm and 200 μm were investigated. Five radial positions approximately 45.7 cm (18 in) vertically from the cutter head were fixed with syringes used for sampling resuspension. The study showed the turbidity is minimized when the thickness of cut is equal to the cutter diameter. A shallower cut is shown to increase turbidity while a cut that is larger than the cutter diameter may also increase turbidity because of sloughing. The study investigated cutting from 60 percent to 100 percent cutting thickness in relation to the cutter diameter. Cutter tip speeds were investigated and showed an increase in resuspension with increase in cutter tip speed. Increase in the ladder angle from 22 to 29 degrees in relation to the vertical created an increase in resuspension at the leading edge of the cutter but a decrease in resuspension in the trailing area of the cutting region. It was also shown that the amount of resuspension above the cutter head was very small.

Burger (2003) conducted laboratory tests to understand the path of single particles moving around and in the cutter head. Cutter head diameters of 0.3 m (.09 ft) to 0.4 m (0.12 ft) were investigated with a cutting angle of 45 degrees. The residence time (time of particle injection into the cutter head flow until it is entrained by the suction flow) was investigated with the variables of suction velocity, cutter speed, particle size and particle density. An increase in flow rate was shown to decrease particle residence time, however, no correlation for cutter speed was produced. Decreasing particle density tended to decrease the residence time, but the particle diameter effect was inconclusive. Burger found a cutter speed threshold ratio for particles being thrown out of the suction range and also discussed the importance of particle inertia. In this case, the threshold ratio is a relationship between the tangential cutting force and the drag force created from suction. It noted that particles were more easily thrown out of the suction range when swinging in the overcutting direction.

Randall et al. (1998) defined the standard necessities for conducting dredging research in a laboratory setting. Consequently, Glover (2002) and Glover and Randall (2004) reported on the preliminary design a dredge/tow carriage for the dredge/tow flume in the Haynes Coastal Engineering Laboratory. Randall et al. (2005) reported on the installation of the dredge carriage at the Haynes Coastal Engineering Laboratory and on the structural, mechanical, and electrical plans of the system. Henriksen et al. (2007) provided initial data and testing procedures used for conducting dredging research with a particular focus on resuspension studies for a cutter suction dredge. Henriksen and Randall (2008) reported mean values of resuspended sediment surrounding the cutter for

a model dredge carriage operating at different parameters of suction speed, cutter speed, and thickness of cut in relation to the cutter diameter. Henriksen (2009) conducted an intial investigation on the turbulence characteristics for a cutter suction dredge.

In summary, both the field models and the numerical models provide data that are invaluable for understanding dredging production and sediment resuspension from the cutter suction dredging operation. The laboratory techniques utilized are able to isolate the process to better understand the dynamics of the problem, while the field data is able to provide real working scenarios and demonstrate the variation and difficulty of testing and understanding the actual problem of interest.

CHAPTER IV

PROTOTYPE DREDGE TO MODEL DREDGE SCALING

This chapter reviews the important factors of sediment resuspension from a cutter suction dredging operation and discusses the importance of these variables for both prototype operations in the field and model testing in the laboratory. Previous methods for prototype to model conversions are discussed and the approach used by this investigator is stated.

Dredging Resuspension Parameters

The parameters involved with resuspended sediment transport from a cutter suction dredge are site specific and are dependent on the in situ sediment characteristics and the operating methods of the cutter suction dredge. In situ sediment characteristics include the grain size distribution and the solids concentration of the pre-dredged sediment (Collins, 1995). Dredging operating parameters include cutter rotation speed, suction intake speed, thickness of cut, swing speed, and ladder angle (Hayes, 1986). The design of the cutter is also very important. Cutter diameter and cutter length play an important role when comparing these dimensions in relation to the thickness of cut (Collins, 1995).

Cutter Speed

As the cutter is rotated, it guides sediment into the suction pipe. However, as cutter speed increases, the centrifugal force on sediment particles increase and particles have a greater tendency to be released outside the suction zone of influence (Huston and

Huston, 1976; Brahme, 1983; Herbich and Brahme, 1983; Burger, 2003). An increase in cutter speed can also increase the turbulence in the region. These two factors contribute to an increase in sediment resuspension as the cutter speed increases.

Suction Intake Speed

The suction pipe behind the cutter is designed to transport sediment that is released by the cutter to a specified discharge location. An increase of the suction (negative) pressure in the suction pipe increases the suction velocity field and removes sediment more quickly from the cutter region. Most researchers (Huston and Huston, 1976; Brahme, 1983; Herbich and Brahme, 1983; Collins, 1995; Burger, 2003) state that a stronger suction pressure will remove sediment more efficiently and decrease the amount of resuspended sediment.

Hayes (1986) proposed a semi-elliptical suction intake velocity field surrounding the cutter as:

$$V_i = \frac{Q}{\frac{\pi^2}{2} L_c R_c} \tag{47}$$

Where V_i is the suction intake velocity [LT^{-1}], Q is the flow rate [L^3T^{-1}], L_c is the cutter length, and R_c is the cutter radius [L]. This approximation is used to represent a suction pipe located at the center of the cutter and proposes that the suction intake is located in the center of the back ring of the cutter. However, the suction pipe entrance orientation is usually located below the center of the cutter. Also, some suction lines are also

positioned either to the left or right of the centerline of the cutter to help with dredging operations that mainly use one type of cutting (overcutting or undercutting).

Thickness of Cut

The amount of sediment released into the water column by each blade of the cutter is determined by the percentage of the cutter that is actually submerged into the in situ sediment. The percentage of cutter submersion is determined by the vertical displacement of the cutter relative to the top of the sediment (thickness of cut), the ladder angle, the cutter radius, and the cutter length. Collins (1995) hypothesized that these variables combine into a single factor known as the surface area exposed, "the fraction of cutter head surface not covered by sediment during the dredging operation." Although this hypothesis covers partial cutting, it does not reflect any sloughing or bulldozing effects of sediment resuspension that can increase as a cutter is buried further in the sediment past its diameter. In this case sloughing is the collapse or "avalanche" of sediment when a cutter is cutting a bank of sediment. Sloughing normally occurs in a region that is vertically above the cutter. Bulldozing mainly occurs from the pushing of sediment by the dredge ladder if the angle of the dredge ladder is too shallow. Therefore, it is suggested that a component of sediment resuspension may not only be attributed to the area of washing but also to variables such as sloughing and bulldozing.

Past researchers have looked at the thickness of cut (Nakai, 1978; Hayes, 1986; Herbich and DeVries, 1986; McLellan, et al. 1989). Nakai (1978) noticed an increase in resuspended sediment as the thickness of cut increased and attributed this due to sloughing. Both Hayes (1986) and Herbich and DeVries (1986) noticed a minimum of

sediment resuspension when the thickness of cut is equal to the cutter diameter and an increase in sediment resuspension as the thickness of cut increased above one cutter diameter. Hayes (1986) and McLellan, et al. (1989) also noted an increase in sediment resuspension as the thickness of cut decreased from a full cut of one cutter diameter to a partial cut less than one cutter diameter. Crockett (1993) hypothesized that this is due to "washing off" of the cutter blades when more of the blade surface area is exposed to the water.

Ladder Angle

Ladder angle is the angle that exists between the horizontal (water surface or sediment flat bad) and the centerline of the ladder. The angle that the ladder is set during dredging has been investigated to analyze its effect on sediment resuspension (Huston and Huston, 1976; Herbich and DeVries, 1986; Collins, 1995; Crockett, 1993; Hayes et al., 2000). The ladder angle has a strong effect on the orientation of the cutter in reference to the in situ sediment and determines the amount of material that the cutter excavates. This in turn has a strong effect on both the production rate and the turbidity generation. If the ladder angle is too small the ladder can also have an effect on turbidity production by bulldozing the sediment before the cutter can reach the sediment. If the sediment is bulldozed significantly, then a hill is formed and the sediment collapses and avalanches into the cutter.

Production

The dredge production rate is the amount of material removed from the dredging environment by the cutter suction dredge that actually is transported through the suction and discharge pipline. The in situ sediment concentration directly increases dredging production, while an increase in production inversely contributes to the amount of resuspended sediment. An increase in slurry flowrate also increases the production of the operation by entraining more sediment into the suction inlet. An estimate of production (Turner, 1996) for a cutter suction dredge can be expressed using the equation:

$$P = \frac{\pi D_D^{\,2}}{4} V_D Sg_s \tag{48}$$

where P is production of the dredge [L^3T^{-1}], Sg_S is specific gravity of the slurry [-], D_D is diameter of the discharge pipe [L], and V_D is slurry velocity in the discharge pipe [LT^{-1}].

Mol (1977b) investigated the $\omega R_C / V_i$ parameter on the trajectory of plastic particles (γ =1118 kg/m^3, d_{50}=200 μm) and stated that the parameter was important in determining the percentage of the production, defined as ratio of particles that were entrained into the suction inlet over the number of particles released into resuspension or settling. Particle velocity was studied and it was found that the suction velocity had a minimal effect on the particle movement. It was also shown that the production was greater for undercutting than for overcutting. Figure 11 displays the production percentage in relation to the investigated dredging parameter $\omega R_C / V_i$.

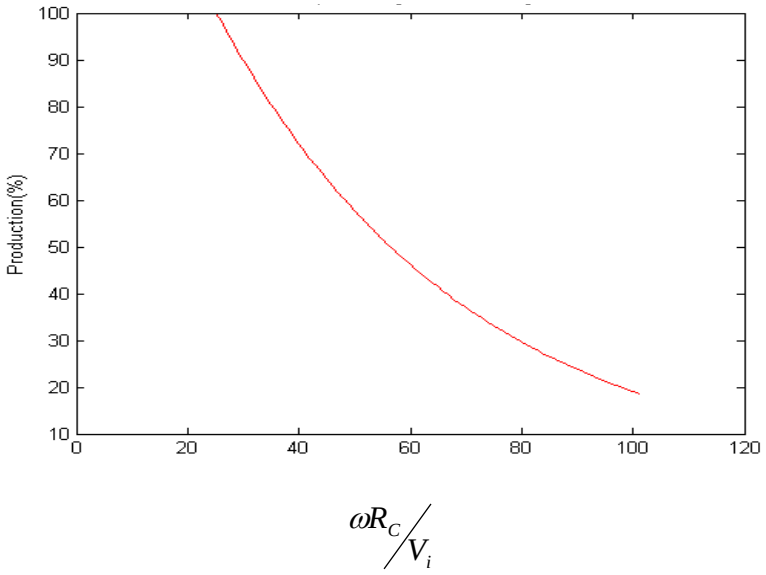

Figure 11. Production Percentage versus $\omega R_C / V_i$

Moret (1977) investigated particle trajectories for sand (d_{50}=500 μm) and fine gravel (d_{50}=1800 μm) and noted that smaller diameter particles stayed with the standard flow field of the cutter suction model dredge more than larger particles. It was shown that the drag force and gravitation force of larger particles was important for the particle trajectories altering from the standard flow pattern. The drag force and gravitational force was stated to sometimes balance each other for undercutting while the gravitational force in the overcutting dredging often lead to particles tangentially escaping the suction zone.

Mol (1977c) investigated production rates for both undercutting and overcutting dredging in sand (d_{50}=120 μm). Cutter speed, suction flow rate and swing speed were investigated to observe their effect on production rates. Production was measured as a ratio of the amount of sediment entrained by the suction line over the amount of material

cut from the sediment bank. The cutter speed and suction flow rate trends showed similar results to the production curve measured from the plastic bead study.

When looking at swing speed it was noted that production tended to increase when swing speed increased for undercutting testing while overcutting testing showed very little correlation between an increase in production and an increase in swing speed. The effect was attributed to a better mixing processes occurring for undercutting than for overcutting. It was noted that gravity may have a stronger effect for the overcutting tests and that this may be a reason for better production occurring for undercutting tests than overcutting tests.

Slotta et.al (1977) conducted an investigation on the geometric relationship of cutter height on production. The inner ring diameter of all the cutter heads was 0.38 m (1.25 ft). Tests were conducted with cemented gravel (d_{50}=25 mm) and on sand (d_{50}=200 μm). Cutter speed and swing speed were also variables investigated in the study. The ladder angle during the study was set at 45 degrees. An “almost linear” positive dependence occurred for swing speed with production. This was seen for both undercutting and overcutting tests. However, the efficiency (amount entrained in the suction pipeline versus amount cut) of the cutter suction dredge was not correlated with swing speed for overcutting, and tended to decrease with an increase in swing speed for undercutting. Geometrically, a shorter cutter head height led to better production and efficiency for undercutting but was not important for overcutting testing.

Miltenburg (1983) also investigated production and the geometric cutter head height while cutting sand. The cutter head diameters investigated with 0.32 m (1.05 ft)

and 0.4 m (1.31 ft). Froude scaling was used to relate the fluid velocities near the cutter head. Different types of cutter heads were examined with different back plate orientations and types of suction openings. When examining cutter speed and suction flow rate the production results were similar to previous results seen in Figure 11. Undercutting always produced a larger production rate than overcutting. Cutter swing speeds tested were 0.1-0.3 m/s (0.33-0.99 ft/s).

Cutter Washing Area

As stated previously, variables such as the thickness of cut, the ladder angle, the cutter radius, and the cutter length contribute to the amount of surface area exposed to a washing mechanism where the rotating cutter blades are exposed to water and the sediment can be resuspended. Both Hayes (1986) and Collins (1995) recognized that these variables contribute to a single factor known as the surface area exposed, "the fraction of cutter head surface not covered by sediment during the dredging operation."

Crockett (1993) explored this hypothesis by developing a geometric analysis of the cutter head that could be used to calculate the exposed washing area of a cutter blade and thus provide a parameter to investigate for exploring sediment resuspension factors. Crocket (1993) states that during the swing of the cutter head the trailing half section of the cutter head as well as the blade section that is above the sediment bank defines the total surface area exposed to washing as:

$$A_E = A_{NA} + A_A \tag{49}$$

where A_E is total washing surface area of the blades [L^2], A_A is advancing face surface area of blades in the sediment [L^2], and A_{NA} is non-advancing side surface area of the

cutter vulnerable to washing [L^2]. The advancing face surface area above the sediment profile A_A is dependent on the thickness of cut and the depth of cut and can be expressed in a system of equations:

$$A_A = \frac{1}{2}\left[x_p^2 + (z_p - 0.5D_c)^2\right]\tan\theta \tag{50}$$

$$x_p = -L_c\sqrt{1-\left(\frac{2z_p}{D_c}\right)^2} \tag{51}$$

$$z_p = \frac{D_c}{2}\left[q\left(\frac{t_c}{D_f}(q+1)-1\right) + \sqrt{\left[(1-q)^2\left(1-\left(\frac{t_c}{D_f}(q+1)-1\right)^2\right)\right]}\right] \tag{52}$$

where x_p is the x horizontal coordinate of the intersection of the mudline and the cutter [L], z_p is the z vertical coordinate of the intersection of the mudline and the cutter [L], and θ is the ladder angle [rad]. A layout of the spatial variables can be seen in Figure 12. Here, D_f is the depth of a full cut where the cutter is completely submerged in the sediment [L] and is calculated as:

$$D_f = \frac{D_c\cos\theta}{2}\left[1+q+\frac{2L_c\tan\theta}{D_c}\sqrt{1-q^2}\right] \tag{53}$$

where

$$q = \frac{1}{\sqrt{1+\left(\frac{2L_c}{D_c}\tan\theta\right)^2}} \tag{54}$$

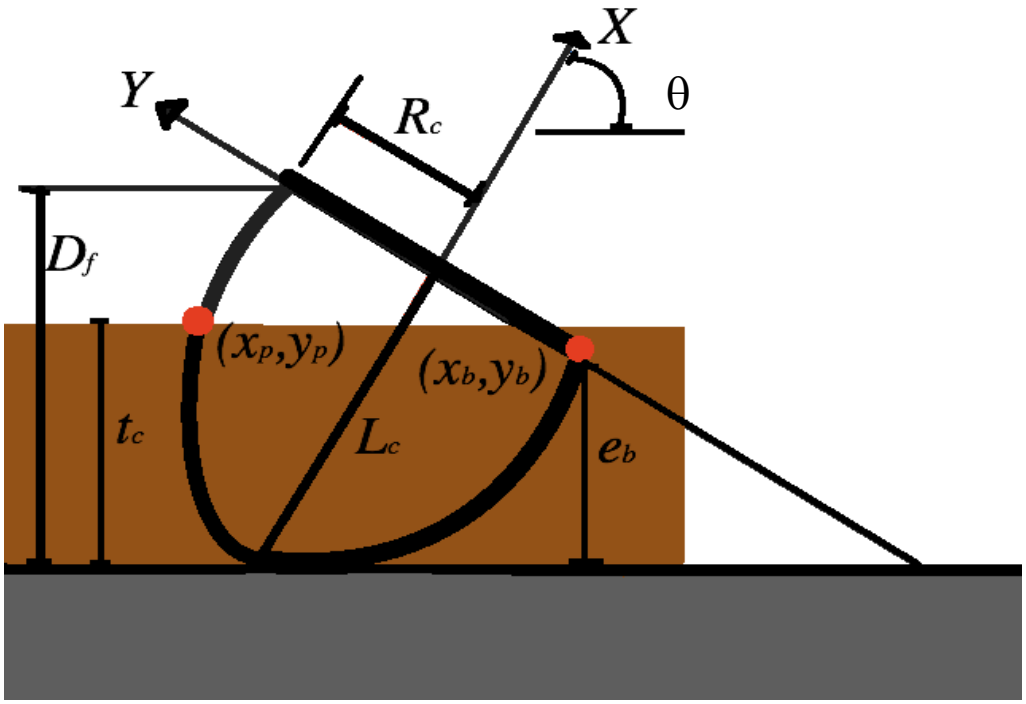

Figure 12. Orientation of Parameters for Calculating Cutter Area of Resuspension

When calculating the exposed section of the cutter behind the swinging direction, the surface area is approximated as half of the area of the total surface area of the cutter A_T [L^2]

$$A_C = 0.5\,A_T \tag{55}$$

and

$$A_T = \frac{\pi^2 L_c D_c}{4} \tag{56}$$

If the percentage of cut thickness to full cut depth, $D_{\%}$ *(*equation 25), is greater than or equal to 1 then none of the advancing surface area is exposed and the only exposed area is A_{NA}. However, if $D_{\%}$ is less than 1 then both A_A and A_{NA} contribute to the area of washing.

Collins (1995) determined the area A_A by subtracting the nonexposed area of washing by assuming an ellipsoid a_z submerged below the mudline for the nonexposed region. Following Collins (1995) equations:

$$A_A = 0.5\left(1 - a_z\right) \tag{57}$$

$$a_z = 1 - \left[1 - \left(\frac{2y_p}{D_C}\right)^2\right]^{0.5} \tag{58}$$

where y_p is the y horizontal coordinate of the intersection of the mudline and the cutter [L].

Conversely, Crockett (1993) takes a separate approach to calculating A_A and assumes an adequate advance for each cutter step so that the slope of the mudline is zero across the cutter. Also, the length parameter e_b [L] is utilized to determine a standard partial cut or a "shallow" cut where the complete length of the cutter blade is not submerged in the sediment bed when the blade is on the bottom of the cutter. Here:

$$e_b = \left| - R_c + R_c q + L_c \left(1 - q^2\right)^{0.5} \tan\delta \right| \cos\delta \tag{59}$$

if $t_c / e_b \geq 1$

$$A_A = 0.5\left[x_p^2 + \left(y_p - R_c\right)^2\right] \tan\delta \tag{60}$$

if $t_c / e_b \leq 1$

$$A_A = 0.5\left(\sqrt{x_p^2 + \left(y_p + R_c\right)^2}\right)\left(\sqrt{x_p^2 + \left(y_p - R_c\right)^2}\right)\sin\delta + 0.5\left(\sqrt{x_p^2 + \left(y_p + R_c\right)^2}\right)\frac{\sin\alpha\sin(\theta - \alpha)}{\sin\phi} \tag{61}$$

where

$$\delta = \sin^{-1}\left[\frac{2R_c}{\sqrt{x_p^2 + \left(y_p + R_c\right)^2}}\right] \tilde{=} \alpha \tag{62}$$

$$\phi = 180^\circ - \theta \tag{63}$$

Wu and Hayes (2000) recalculated the cutter area exposed to washing A_E to compensate for shorter step advances of the cutter where the step distance is less than the cutter length. A decrease in step distance creates an added surface area of washing, A_B [L^2] from the exposed back region of the cutter. Here:

$$A_E = A_{NA} + A_A + A_B \tag{64}$$

In situ Sediment

In situ sediment can be classified according to numerous variables some of which include grain size, grain shape, plasticity, and soil classification. All of these variables directly affect the settling time of the in situ sediment that is dredged. Numerous laboratory and field work has stated the importance of the settling rates of sediment particles when determining resuspended sediment concentration sources at the origin of dredging (Nakai, 1978; Brahme, 1983, Hayes, 1986, DiGiano, et al. 1993).

Nakai (1978) provided a model for dredging resuspension and isolated the estimation of resuspension to sediment particles smaller than 74 μm. This assumption

was based on the premise that larger particles tended to settle extremely quickly and thus did not contribute to the resuspension of the dredged material. Hayes (1986) also concluded 80% of the resuspended sediment collected during sampling of the Calumet Harbor study were smaller than 74 μm.

Particle Settling Velocity

The settling of sediment particles through the water column is an important physical property when examining the dynamics of the resuspension of sediment from a cutter suction dredge. After sediment is resuspended into the water column by the cutter, it begins to settle immediately because of the force of gravity.

Expressing the weight of the particle as:

$$F_g = \left(\rho_s - \rho_f\right) g \forall_p \tag{65}$$

where F_g is force due to gravity [MLT^{-2}], ρ_s is density of the particle [ML^{-3}], ρ_f is density of the surrounding fluid[ML^{-3}], $\forall_p$ is sediment particle volume [L^3], and g is gravitational constant [LT^{-2}]. As the particle falls through the water, the drag force is expressed as:

$$F_D = C_D \rho_f \frac{w_s^2}{2} A_p \tag{66}$$

where F_D is force due to the drag of the particle [MLT^{-2}] , C_D is particle drag coefficient [-], w_s is particle settling velocity [LT^{-1}], A_p is sediment particle front area [L^{-2}]. The dimensionless drag coefficient can be developed from the ratio of inertial and viscous forces expressed in the particle Reynolds number Re_p (dimensionless):

$$\mathrm{Re}_p = \frac{w_s d_p}{\nu} \tag{67}$$

Here d_p is particle diameter [L], ν is kinematic viscosity of fluid [L^2T^{-1}]. The drag coefficient is also dependent on the shape of the particle.

In order to find the terminal settling velocity for a sediment particle, a balance between the submerged weight of the particle and the drag force is recognized where:

$$\left(\rho_s - \rho_f\right) g \forall_p = C_D \rho_f \frac{w_s}{2} A_p \tag{68}$$

For particles Re_p <1 it is assumed that C_D =24/ Re_p. Thus, the drag force can be expressed as:

$$F_D = 3\pi\mu_f w_s d_p \tag{69}$$

where μ_f is the dynamic viscosity of the surrounding fluid [$ML^{-1}T^{-1}$]. From this, the Stokes (Dietrich, 1982) settling equation can be derived where:

$$w_s = \frac{\left(\rho_s - \rho_f\right) g d_p^2}{18\nu} \tag{70}$$

Although this equation has been extremely useful in the scientific community, its limitation is that it is confined functionally to small particles where the Re_p <1 and also assumes that the particles are perfectly spherical in nature.

In order to compensate for discrepancies between experimental data and theoretical principles, Dietrich (1982) conducted a review of previous particle settling descriptions and designed a set of equations to calculate the terminal settling velocity of

a natural particle. The method involved the use of a dimensionless settling velocity W_* and dimensionless particle diameter D_* where:

$$W_* = \frac{\rho_f w_s^3}{(\rho_p - \rho_f) g \nu} \tag{71}$$

$$D_* = \frac{(\rho_p - \rho_f) g d_p^3}{\rho \nu^2} \tag{72}$$

In the calculation of W_*, Dietrich (1982) used experimental data to incorporate size and density, shape of the particle, and roundness of the particle, expressing the dimensionless settling velocity as:

$$W_* = R_3 10^{R_1 + R_2} \tag{73}$$

where

Size and Density
$$R_1 = -3.76715 + 1.92944(\log D_*) - 0.09815(\log D_*)^2 - 0.00575(\log D_*)^3 + 0.00056(\log D_*)^4 \tag{74}$$

Shape
$$R_2 = \log\left(1 - \frac{1 - CSF}{0.85}\right) - (1 - CSF)^{2.3} \tanh(\log D_* - 4.6) + 0.3(0.5 - CSF)(1 - CSF)^{2.0}(\log D_* - 4.6) \tag{75}$$

Roundness
$$R_3 = \left[0.65 - \left(\frac{CSF}{2.83} \tanh(\log D_* - 4.6)\right)\right]^{(1+(3.5-M)/2.5)} \tag{76}$$

The Corey shape Factor *CSF* is (Corey, 1949):

$$CSF = \frac{c_p}{\sqrt{a_p b_p}} \tag{77}$$

where a_p is largest sediment particle length scale, b_p is middle length scale, and c_p is smallest length scale. A *CSF* of 1.0 represents a completely spherical particle. The value of M in the R_3 equation is derived from the Powers value (Powers, 1953). The Powers value is 6 for a perfectly round material and is 2-3 for particles that have a strong angularity.

Another component of concern when investigating the particle settling velocity include the effect of particle-particle interactions. Three ways that particle-particle interactions may change the settling rate of the particle include the possible increase in the viscosity of the mixture, particle-fluid-particle effects, as well as the hindering effect of collisions occurring during settling between particles.

Although the resuspension of sediment is not defined as a slurry in this dissertation, the distinction between the mixing zone and the resuspension zone represents an arbitrary boundary line between the region of slurry dynamics and resuspended sediment dynamics. Because these regions are adjacent and often intertwine in this problem, it is important to discuss the settling dynamics of the sediment particles in this region as well.

Wilson et al. (1996) provides an adequate review of slurry dynamics and suggests using Stoke's law for sediment particles smaller than 50 μm and using a Newtonian approximation for particles larger than 200 μm. In this case, the Newton equation is stated:

$$w_s = 1.73\left[gd_p(Sg_p - 1)\right]^{0.5} \tag{78}$$

where Sg_p is the specific gravity of the particle [ML^{-3}].

The Stoke's approach and the Newtonian approach provide estimates of settling velocity for a range of particles, but leave a gap in a critical range for slurry. Therefore, Wilson et al. (1996) provides a similar nondimensional approach as stated above, using nondimensionalized particle diameter and settling velocities. The text also provides a valid subroutine VTCALC in the appendix for calculating terminal velocity as well as the hindered settling velocity w_s' [LT^{-1}] where:

$$w_s' = w_s(1 - C_s)^n \tag{79}$$

and C_s is the slurry volumetric concentration (percent of slurry occupied by solids). The value of n is defined by Richardson-Zaki (1954) and is based on the Reynolds particle number. Typical values of n range between 2.4 and 4.6.

Model to Prototype Scaling Laws

Conducting testing for prototype conditions is often expensive and difficult. With prototype conditions the variables of interest can be difficult to isolate. Modeling prototype conditions in a laboratory provides a cost and time effective approach to obtaining much needed answers on specific variables of interest for a dredging operation. When testing in the laboratory, a model setup usually displays the physical process on a different geometric or time scale. Therefore, scaling laws are required to relate the physical process between prototype and model conditions.

When developing scaling laws it is important to determine the penalties. Here, specific physical process of interest may be scaled incorrectly and prototype to model comparisons will be difficult. However, model testing has proven to be an economical

and knowledgeable approach to learning about important questions in the scientific arena.

Dimensional Analysis is a method used to create scaling laws and minimize the number of variables needed when conducting an experiment (Munson et al., 2002). Setting up the variables that need to be explored can be important for creating scaling laws between model and prototype conditions and also minimizing the number of experiments needed to be completed.

When designing scaling laws, there are three main components that should be correlated between the prototype scale and the model scale. The three main components are the geometric, kinematic, and dynamic relationships between the model and the prototype (Munson et al., 2002). The geometric relationship exists between the length scales of the model and prototype while the kinematic relationship exists between both the length and time scale and reflect the similarity of velocity between the model and prototype conditions. The dynamic relationship consists of the length, time and force ratio's and is often the most difficult to achieve in the laboratory.

When scaling the model to prototype conditions it is helpful to combine the specific variables of interest into dimensionless groups. The Buckingham Pi theorem (Buckingham, 1914) is used to investigate the important variables in the problem and then determine the dimensionless groups for the best analysis. This is done by first defining the important variables of interest and their dimensions. A formula is then used to determine the number of pi terms with non-repeating variables. The system of interest can then be mathematically defined by a function composed of the nondimensional

groups. Common dimensionless groups often derived by Buckingham pi theory are reported in Table 2. The name and formula for each dimensionless group as well as a description of the force comparative ratio used in each group are displayed.

Table 2. Common Dimensionless Numbers used for Scaling (Munson et al., 2002)

Name	Grouping	Force Ratio
Reynolds #, Re	$\frac{\rho V \ell}{\mu}$	$\frac{inertia}{viscous}$
Froude #, Fr	$\frac{V}{\sqrt{g\ell}}$	$\frac{inertia}{gravitational}$
Euler #, Eu	$\frac{p}{\rho V^2}$	$\frac{pressure}{inertia}$
Cauchy #, Ca	$\frac{\rho V^2}{E_v}$	$\frac{inertia}{compressibility}$
Strouhal #, St	$\frac{\omega \ell}{V}$	$\frac{local\ inertia}{convective\ inertia}$
Weber #, We	$\frac{\rho V^2 \ell}{\sigma}$	$\frac{inertia}{surface\ tension}$
Mach #, Ma	$\frac{V}{c}$	$\frac{inertia}{compressibility}$

When scaling a model cutter suction dredge to a prototype dredge there are several variables that must be scaled. These variables include:

- cutter head diameter
- cutter rotational speed
- ladder swing speed
- suction velocity
- sediment diameter and density

When modeling these variables it is difficult to achieve similarity in all aspects between model and prototype conditions. Typical geometric scaling of the cutter head region, including the cutter, back ring, and suction mouth usually are on the scale of (1:6) and can go as low as a (1:10) model to prototype scaling. Testing in prototype conditions can be very difficult because of fluctuations in environmental variables such as wind, water currents, water waves, sediment size, and sediment bottom profile. Conducting visual flow studies of a cutter suction dredge in a prototype environment is also extremely difficult because of water visibility issues.

Researchers (Slotta, 1968; Joanknecht, 1976; Burger, 2003; Glover, 2002; Miedema, 1987) agree that when modeling hydraulic dredging it is not possible to match all of these criteria using the same set of scaling laws. However, if the limits of the model scaling laws are provided, then it is assumed that the model is acceptable for the understanding of physical processes that the investigator is interested in exploring.

Slotta (1968) used hydrogen bubbles to visualize the flow field around the cutter head. These tests focused on the improved dredging techniques with the use of a back

plate and used both Reynolds numbers and Froude numbers when utilizing the Buckingham's Pi Theorem. In this case a normalized velocity ratio between the cutter speed and the suction velocity was defined as the most important parameter in the study.

Joanknecht (1976) also created scaling laws for comparing the actual cutting of the cutter head and the movement of sand with a d_{50} =200 μm into the suction pipe. Froude scaling was used where the ratio was created between the terminal velocity of the particles and the suction velocity.

Research conducted at Delft hydraulics (Mol, 1977c; Moret, 1977) on sand particles also examined the effect of dredging performance and set up model testing based on Froude scaling. The ladder angle for these tests was set at 30 degrees. An important correlation noted during the testing was seen between the axial and centrifugal forces created by the action of the cutter head rotation alone (without the suction line effect). In this case it was found that the axial component is strongest at the front of the cutter, causing fluid or slurry to be entrained into the suction region. However, near the back of the cutter and near the cutter plate the centrifugal force created by the cutter causes sediment to be sent out of the suction region and consequently lifted as resuspended sediment.

In these studies a specific ratio between the cutter speed and the suction flow rate was shown to have a threshold value where the trajectory of particles caused by the centrifugal force or the cutter rotation would exceed the axial flow forces of the cutter and the suction line and consequently lead to the resuspension of sediment. In these tests a cutter diameter of 0.6 m was used with a threshold value of:

$$\frac{\omega R_C}{V_i} = 0.42 \tag{80}$$

occurring for both undercutting and overcutting testing. This threshold value increased to values between 0.5 (undercutting) and 0.6 (overcutting) when the cutter was allowed to rotate freely in the water column and not completely submerged in a sediment bank.

(Moret, 1977) also noted that the flow field for undercutting was significantly different than for overcutting. It was stated that varying the operating parameters of cutter speed and suction flow rate did not dramatically change the characteristics of the flow field.

When examining the effect of swing speed, Mol (1977a) stated that the flow field created with the addition of the swinging ladder could be created theoretically by a superposition of the stationary flow and the swing speed translational flow field.

Previous scale laws for modeling cutter head dredging have been conducted by several researchers. Joanknecht (1976) assumes Froude scaling as the dominant method because of the assumption that the gravitational force is the main force acting on the resuspended sediment during dredging. Joanknecht (1976) also directly states that the scaling for the fall velocity of the sediment particle and the suction speed should be the same for prototype and model scaling.

Burger (2003) used the dimensionless Navier-Stokes equations and the dimensionless equations of particle motion to create scaling laws for testing the trajectory of a single particle in the flow field of the cutter head. In this case, Burger states that the Reynold's number is large enough to neglect the viscous forces. In this case, scaling of the laboratory experiments can be scaled according to the Euler number.

It is also noted that the time scale can be based on the entrainment time for a particle when the suction force is dominant or can be the cutter speed when the centrifugal force of the cutter is dominant.

Burger (2003) used the dimensionless equation of motion to analyze a single particle and considered drag, lift, added mass, gravity, buoyancy, and pressure when explaining the forces on a single particle. Using this equation requires that the Strouhal and Froude scaling be the same for prototype and model conditions. It is noted that the cutter tip speed and the suction speed must also be scaled according to Froude scaling. Burger (2003) scaled the particles reaction to movements from the flow field with a ratio of the terminal velocity of the particle and the gravity constant and used Strouhal scaling to address this topic.

Scaling Equations

Slotta (1968,1974) conducted a flow visualization study around the cutter head. The main focus of the study was to see how flow changed with different operating parameters and how the flow field led to turbidity generation and consequently resuspended sediment. The tests used a 1:15 geometric scaling and used hydrogen bubble release in a Plexiglas tank. Four main scaling equations were created to compare model to prototype conditions.

$$\left[\frac{V_i D_c}{\nu}\right]_m = \left[\frac{V_i D_c}{\nu}\right]_p \tag{81}$$

$$\left[\frac{V_i^2}{gD_c}\right]_m = \left[\frac{V_i^2}{gD_c}\right]_p \tag{82}$$

$$\left[\frac{\omega D_c}{V_i}\right]_m = \left[\frac{\omega D_c}{V_i}\right]_p \tag{83}$$

$$\left[\frac{\omega Q^{0.5}}{H_i^{0.75}}\right]_m = \left[\frac{\omega Q^{0.5}}{H_i^{0.75}}\right]_p \tag{84}$$

where:

$$H_i = \frac{V_i^2}{2g} \tag{85}$$

These set of equations were developed using Buckingham Pi theory (Buckingham, 1914). Equation (81) and equation (82) are scaled to the Reynold's and Froude number, respectively, while equation (83) and equation (84) review the kinematics of the system relating to the velocities of the cutter speed and the sediment pick up function. It was noted that equation (80) and equation (81) were not well correlated with the data collected from the experiment but equation (83) and equation (84) did match up well with the parameters used during model dredging. It is important to note that neither, production, swing speed, or cutting forces were measured during testing. The testing did not incorporate ladder swing and the production meter was not set up for testing.

Joanknecht (1976) used Froude scaling to investigate cutter head dynamics for 1:3 and 1:4 scales with a d_{50} =200μm. The Froude scaling was applied to the sediment diameter of model and prototype sediment where:

$$\left[\frac{w_s}{\sqrt{gd_{50}}}\right]_m = \left[\frac{w_s}{\sqrt{gd_{50}}}\right]_p \tag{86}$$

The model testing satisfied the condition by using the same sediment as the prototype environment. Froude scaling was also used for the cutter rotation and the swing speed where:

$$\left[\frac{V_s}{\sqrt{gD_c}}\right]_m = \left[\frac{V_s}{\sqrt{gD_c}}\right]_p \tag{87}$$

$$\left[N_c\sqrt{\frac{D_c}{g}}\right]_m = \left[N_c\sqrt{\frac{D_c}{g}}\right]_p \tag{88}$$

Here N_c is the rotational speed of the cutter [RPM]. Fluid and sediment particle modeling was scaled according to the particle settling velocity and the suction inlet velocity where:

$$\left[\frac{w_s}{V_i}\right]_m = \left[\frac{w_s}{V_i}\right]_p \tag{89}$$

Based on the Froude scaling relationships other scaling ratios were created for flow rate, cutting force, and cutting power.

$$\left[\frac{Q}{D_c^{2.5}}\right]_m = \left[\frac{Q}{D_c^{2.5}}\right]_p \tag{90}$$

$$\left[\frac{F_c}{D_c^3}\right]_m = \left[\frac{F_c}{D_c^3}\right]_p \tag{91}$$

$$\left[\frac{\Gamma_s}{D_c^4}\right]_m = \left[\frac{\Gamma_s}{D_c^4}\right]_p \tag{92}$$

where F_c is the cutting force [MLT^{-2}] and Γ_s is the shaft torque [M^2LT^{-2}].

Brahme and Herbich (1986) studied the flow field around the suction inlet to examine the sediment pickup behavior of the system. The scaling of the tests included a dimensionless parameter describing the velocity field where:

$$\frac{Q}{R^2 V} = \text{Velocity Field (Dimensionless)} \tag{93}$$

Using this formula, the magnitude of the velocity field at a point can be determined if the flow rate and radial distance R [L] from the suction intake is known and the flow is assumed constant. It was also noted that the velocity field was strongly dependent on the flow rate.

In regards to sediment pick up behavior, the scaling of the velocity component created by the suction is only important where the magnitude of the velocity component is on the same order of magnitude as the particle settling velocity. Glover and Randall (2004) state that because the scaling of the velocity field is strictly dependent on suction flow rate, the sediment pickup behavior can be scaled with the Brahme and Herbich (1986) approach according to the equation:

$$\left[\frac{Q}{D_c^2 w_s}\right]_m = \left[\frac{Q}{D_c^2 w_s}\right]_p \tag{94}$$

This equation allows for easy geometric scaling of different prototype cutterheads even when only one model cutter head is investigated and takes into account both the velocity of the fluid and the particle settling velocity for numerous types of dredging conditions. Therefore, equation 92 is chosen as a scaling law for the modeling of this work.

Cavitation occurs when the pressure of the fluid in the system is lowered to a magnitude below the vapor pressure. In this case, bubbles often form and collapse, causing damage to the cutter blade. These bubbles affect the flow field and consequently the sediment settling characteristics. Miedema (1987) investigated the scaling laws occurring between model and prototype and stated that if both model and prototype exemplify a cavitating cutting system then it is essential that the blade angle at the start of each cut should be the same angle. Miedema (1987) also predicts the thickness of each cut for a single blade of the cutter with:

$$t_l = \frac{60\,V_s}{N_c p_b}\cos(\varphi)\cos(\kappa) \tag{95}$$

where t_l is cut layer thickness [L], p_b is pitch of the blades or teeth [rad], κ is profile angle [rad] , φ is angular position of the blade [rad]. A schematic of the profile of the equation can be seen in Figure 13.

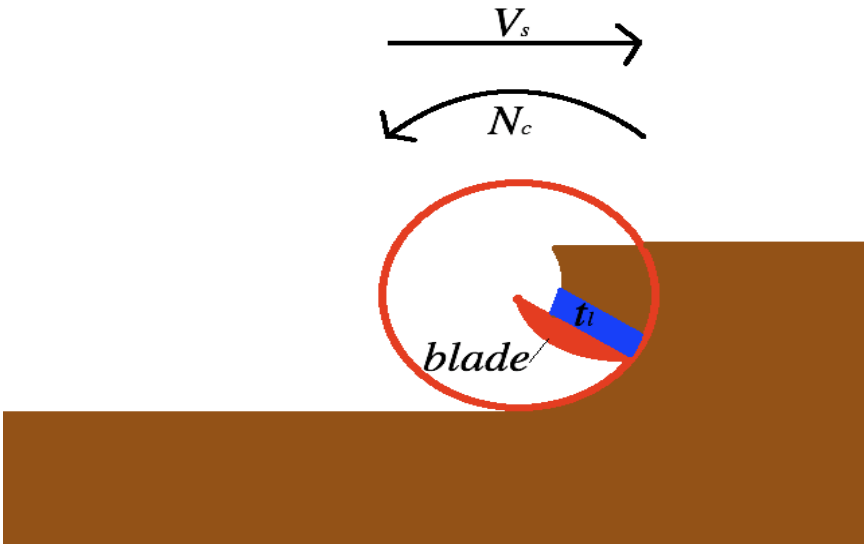

Figure 13. Cut Layer Thickness in Relation to Cutter Head Geometry and Kinematics. (Revised from Miedema, 1987)

In order for the model to prototype scaling to be correct, the thickness of cut must be geometrically identical in its ratio to the cutter geometry. This correct scaling is ascertained by scaling the cutter tip speed to the swing speed according to the equation:

$$\left[\frac{N_c D_c}{V_s}\right]_m = \left[\frac{N_c D_c}{V_s}\right]_p \tag{96}$$

Scaling the effect of cavitation properly can be especially important when testing the cutting forces during dredging. If the pore pressure reaches a low enough value for cavitation, the cutting force involved with the excavation of sediment solely relies on digging depth and discounts the cutting speed. In order for cavitation to occur, Miedema

(1995) provides a predictive equation for cavitation based on digging depth, blade angle, cutter head rpm, layer thickness, and sediment characteristics.

$$\left(\frac{d_1}{c_1}\right)\left(\frac{k_m}{e}\right)\frac{z_d + 33}{V_c t_l} < 1 \tag{97}$$

Cutting forces are represented here as d_1 / c_1 and based on the blade angle. The sediment properties are expressed in terms of k_m / e. It is important to note the effect of blade angle on cavitation, where an increase in the blade angle will cause a larger cavitation effect.

Miedema (1987) designed a scaling factor for cavitation between model and prototype conditions by first calculating the prototype cavitation pressures $[p_c]_p$ [$ML^{-1}T^{-2}$] model cavitation pressures $[p_c]_m$ [$ML^{-1}T^{-2}$] and then providing a ratio of the two creating the "hydrostatic pressure factor". This equation assumes that the soil mechanics for both prototype and model sediment are identical.

$$[p_c]_p = [\rho_f g(z_d + 33)]_p \tag{98}$$

$$[p_c]_m = [\rho_f g(z_d + 33)]_m \tag{99}$$

$$\lambda_c = \frac{z_p + 33}{z_m + 33} \tag{100}$$

Where λ_c is the hydrostatic pressure factor, g is the gravitational acceleration [LT^{-2}], and z is the digging depth [L].

In order to maintain this scaling, the pore pressure ratio must be equal to the hydrostatic pressure factor. Since the pore pressure is dependent on cutter rpm and layer thickness, Miedema(1987) provides other scaling laws including:

$$(N_c)_m = (N_c)_p \frac{1}{\lambda_c}\left[\frac{(D_c)_p}{(D_c)_m}\right]^2 \tag{101}$$

Miedema(1987) also develops a scaling law for the swing speed of the cutter by setting the angular position of the blade for cavitation equal for both model and prototype. Once this rationalization is established, the scaling law for model to prototype swing speed is developed.

$$(V_s)_m = (V_s)_p \left[\frac{(D_c)_p}{(D_c)_m}\right]\frac{1}{\lambda_c} \tag{102}$$

Glover and Randall (2004) subdivided the previous scaling laws into three categories including sediment pick-up scaling, Reynolds and Froude scaling, and cutter cavitation scaling. Previous cutter suction model testing (Slotta, 1968; Joanknecht, 1976; Brahme and Herbich, 1986; Burger, 1997, 2003; Glover and Randall, 2004) have focused on the sediment pick-up approach for model to prototype scaling. The scale laws based on the cavitation process require an extremely fast cutter head speed that is unfeasible for most model testing. However, when cutter speed reaches a maximum threshold, the flow field may neglect the effect of the suction velocity because it is overpowered by the tangential velocities created by the cutter rotation. When examining the kinematic scaling laws between a model and a prototype, the model for a hydraulic

dredge would need digging depths or pressures that are not feasible in a testing environment. Therefore, for the purpose of this work the sediment entrainment behavior will provide the basis for model to prototype scaling.

When approaching the model to prototype testing using sediment entrainment it is important to understand the effect of the suction inlet. The flow rate through the suction line creates a radial velocity field into the suction mouth. This flow field draws sediment into the suction line, however, before any entrainment of particles occurs, the cutter must first excavate the sediment. Glover and Randall (2004) state that the volume of material excavated by the model cutter is a geometric ratio based on the geometric, kinematic, and dynamic scaling involved. Therefore, the amount of sediment entrained by the suction line should also pick up the amount of sediment defined by the geometric ratio of excavated sediment.

Glover and Randall (2004) also provide an example of the radial velocity field created by a vertical suction line and compare two suction inlets with a geometric scale of 1:2. In this case the larger suction line has a flow rate twice as large as the smaller suction line. In order for the two suction zones to obtain geometric similarity, the zone of entrainment for the pipe with the larger diameter must have a radius that is twice as large as the smaller suction line. This zone of entrainment increases in size if the particle settling time becomes less or if the flow rate increases.

When scaling the cutter speed, previous methods (Slotta, 1968; Burger, 1997, 2003) used the suction inlet velocity as the other variable in the scaling ratio. Glover and Randall (2004) used the assumption of flow rate dependence rather than suction

velocity dependence and used the dimensionless velocity field (Brahme and Herbich, 1986) to derive an equation for the scaling of cutter speed, N_c, to particle settling velocity, w_s, where:

$$\left[\frac{N_c D_c}{w_s}\right]_m = \left[\frac{N_c D_c}{w_s}\right]_p \tag{103}$$

Swing speed scaling for model to prototype comparisons was also derived from previous scaling laws using the concept of the swinging motion contributing a velocity field component. Using the concept of kinematic similarity, the swing speed, V_s, can be substituted into equation 103.

$$\left[\frac{V_s}{w_s}\right]_m = \left[\frac{V_s}{w_s}\right]_p \tag{104}$$

Other scaling issues of interest include sediment parameters involved with the in situ sediment prior to dredging such as the density of the material. Different sediment densities exhibit different settling times even when their diameters are similar. Other sediment parameters that are difficult to scale include the compactness of sediment as well as cohesiveness of sediment. Due to similar sediment being used in both model and prototype modeling, equal suction velocity was also used

$$\left[\frac{w_s}{V_i}\right]_m = \left[\frac{w_s}{V_i}\right]_p \tag{105}$$

For the purpose of this dissertation it was determined that sediment pick-up is the predominant scaling issue for the study. Therefore, the settling velocity of the sediment was chosen as the primary scaling variable. Other equations exist for model to prototype

comparison; however, not all components can be satisfied. Based on the premise of scaling the sediment settling properties, equation (94), equation (103), and equation (104) were used to create the model to prototype comparisons.

Table 3 displays a comparison between the model dredge carriage and a typical 30.48 cm (12 in) dredge (prototype 1) and a 60.96 cm (24 in) dredge (prototype 2) based on the scaling laws chosen for this study. This table demonstrates that the prototype flow rate that should be used for this comparison is adequate for the 30.5 cm (12 in) dredge but is probably slightly low when compared to standard 61 cm (24 in) dredging operations. Cutter speed for the 30.5 cm (12 in) prototype dredge is within operating range but is slightly low for the 61 cm (24 in) dredge. Also, the prototype swing speed used for this comparison is much less than would be seen in the field.

The sediment that was used for this dissertation was sediment that was available to the researcher during the testing period. In the future, the sediment used for examining resuspension should have a smaller sediment size to better represent dredging model requirements. This would solve any issues for suction flow rate, cutter rpm, and ladder swing speed.

Table 3. Model and Prototype Operating Parameters for a Cutter Suction Dredge (Henriksen et al., 2008)

Parameter	**Model**	**Prototype 1**	**Prototype 2**
Scale	1:1	3:1	6:1
Cutter Diameter	34.3 cm (13.5 in)	102.9 cm (40.5 in)	205.8 cm (81 in)
Depth of Cut	20.3 cm (8 in)	60.9 cm (24 in)	121.8 cm (48 in)
Sediment d_{50}	0.26 mm	0.26 mm	0.26 mm
Settling Velocity	30.9 mm/s	30.9 mm/s	30.9 mm/s
Suction Diameter	10.2 cm (4 in)	30.5 cm (12 in)	61 cm (24 in)
Suction Flow Rate	1135.5 LPM (300 GPM)	10,220 LPM (2,700 GPM)	40,882 LPM (10,800 GPM)
Cutter speed	86 RPM	29 RPM	14 RPM
Max Swing Speed	1.73 cm/s (0.68 in/s)	1.73 cm/s (0.68 in/s)	1.73 cm/s (0.68 in/s)

When determining the variables of interest and the scaling of these variables in a physical model test, there are usually several approaches depending on the main variables of interest. Unfortunately it is normally extremely difficult to scale and physically model a testing situation in a laboratory setting and still retain all variables encompassed in the field. For the purpose of this dissertation, the sediment fall velocity was used as the main scaling variable. Using this method removes such variables as the cutting depths and pore pressures. However, the interest of this dissertation is resuspenion of sediment and therefore must focus primarily on the sediment dynamics of sediment resuspended in the water column.

CHAPTER V

PHYSICAL MODEL CUTTER SUCTION DREDGE TESTING

Haynes Coastal Engineering Laboratory

In September 2003, the Barrett G. Hindes Foundation provided funds that were used to contract Oilfield Electric Marine, a subsidiary of Rowan Companies, and Digital Automation and Control Systems Inc. to construct a dredge/tow carriage for the dredge/tow flume in the Haynes Coastal Engineering Laboratory. The goal of building the dredge/tow carriage was to create an environment to investigate multiple types of dredging schemes as well as provide towing functionality for other ocean engineering testing.

Dredge/Tow Flume

The dredge/tow flume provides an exceptional environment to test different types of dredging situations including cutter heads, suction heads, drag heads, and hopper placement. The dredge/tow flume is 45.6 m (149.5 ft) long, 3.66 m (12 ft) wide, with a maximum water depth of 3.05 m (10 ft). The flume also contains a 7.56 m (24.8 ft) long by 1.52 m (5.0 ft) deep sediment pit that is ideal for dredge testing. There are windows located in the region of the sediment pit. The windows are particularly useful in flow visualization studies around the cutter head. Four axial flow pumps provide the capability of pumping 2,233 l/s (35,000 gpm) of water through the flume. These pumps can simulate a current for modeling sediment resuspension in the near-field and far-field. A schematic of the dredge/tow flume is shown in Figure 14 that shows the diffuser for

current generation, location of the sediment pit, and the weirs for controlling water depth.

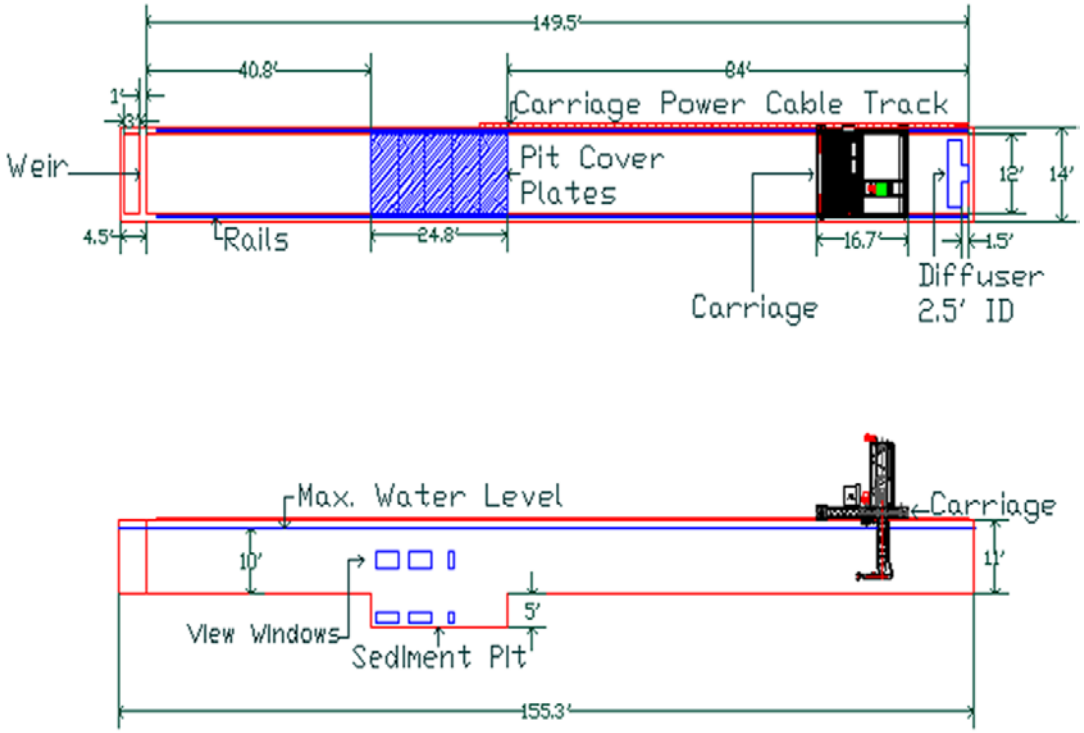

Figure 14. Plan and Side Views of Dredge/Tow Flume (dim in ft, divide by 3.28 for m).

Dredge/Tow Carriage

The dredge/tow carriage was conceptually designed by Glover and Randall (2004), installed in the Spring of 2004, and became operational in 2005 (Randall et al., 2005). The model dredge consists of a carriage, ladder, and cradle. The cradle moves the ladder side-to-side in the flume to simulate the swinging of a cutter head dredge. The model dredge carriage has both an upper vertical ladder as well as an articulating ladder

at the bottom of the vertical ladder. This allows both vertical movement as well as an adjustable angle between 0 and 50 degrees with the horizontal. A Dredging Supply Company cutter is attached to the end of the articulating ladder and the suction inlet is located immediately behind the cutter. The dredge carriage has a GIW Industries centrifugal dredge pump with a 10 cm (4.0 in) suction inlet diameter and a 7.6 cm (3.0 in) discharge outlet. Figure 15 provides drawings for the dredge/tow carriage system while Table 4 displays the operational capabilities of the system. Figure 16 illustrates the model dredge sitting on the rails of the dredge/tow flume.

Table 4. Working Parameters of the Dredge/Tow Carriage

Category	**Characteristic**
Maximum Carriage Speed	2 m/s (6.6 ft/s)
Distance to reach constant speed	3.1 m (10 ft)
Total Dredge/Tow Carriage Weight	4545 kg (10,000 lb)
Cradle Weight	1364 kg (3,000 lb)
Ladder Weight	909 kg (2,000 lb)
Carriage Power	Two 3.8 kW (5 hp) motors
Cutter Power	7.5 kW (10 hp)
Pump Power	14.9 kW (20 hp)
Side to Side Cradle Motor Power	1.1 kW (1.5 hp)
Vertical Ladder Motor Power	1.1 kW (1.5 hp)
Articulating Ladder Position Motor Power	0.5 kW (0.8 hp)
Dredge Pump Flow Rate	Maximum 1893 lpm (500 gpm)
Dredge Pump Size	10.4 cm (4 in), suction; 7.62 cm (3 in), discharge
Swing Travel	1.6 m (5.3 ft) on either side of flume centerline
Ladder Angle	0 to 50 degrees from horizontal

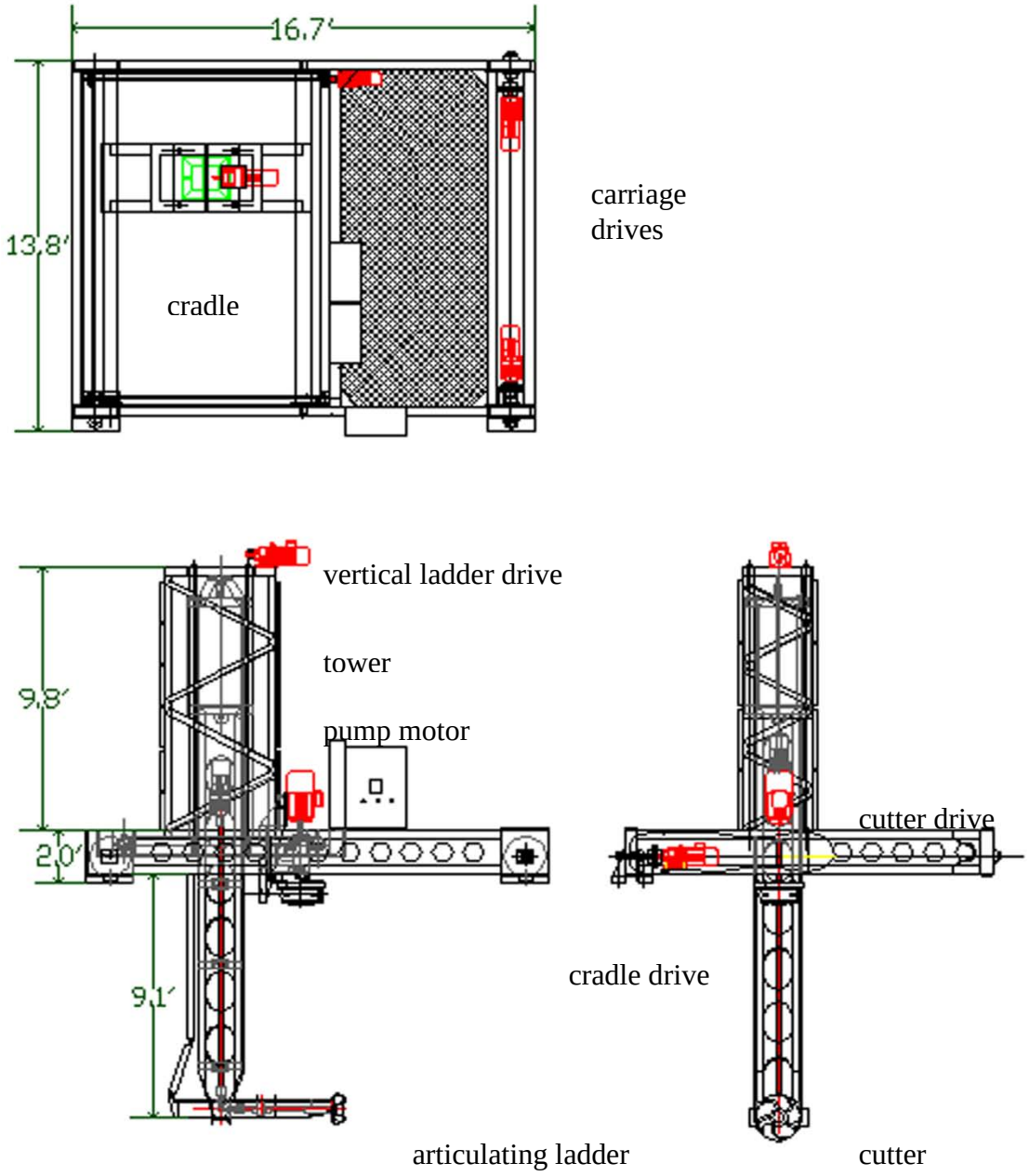

Figure 15. Dredge/Tow Carriage Assembly Drawing (dims in ft, divide by 3.28 for m)

Figure 16. Dredge/Tow Carriage Sitting atop the Dredge/Tow Flume and Sediment Pit

Dredge Cutter Specifications

The cutter attached to the dredge/tow carriage is a flat blade cutter with five outer blades. The outer ring is 26.7 cm (10.5 in) in diameter with blade tips extending to a diameter of 34.3 cm (13.5 in). The orientation of the cutter on the dredge carriage represents the same dynamics that exist on a standard cutter suction dredge. In this setup both undercutting and overcutting can be tested. A picture of the cutter on the dredge/tow carriage is shown in Figure 17.

Figure 17. Picture of the Flat Blade Cutter

Following initial installation and testing of the dredge/tow carriage in 2005, additional modifications were made to complete the model dredge carriage. These modifications include:

- Installation of a magnetic flow meter and nuclear density gauge
- Purchase and installation of a Tri Flow slurry sand separation system for the separation of sediment with water
- Completion of the data acquisition system for recording and transferring all data entries and controlling the automation of the dredge carriage

- Purchase of Acoustic Doppler Velocimetry and Optical Backscatter instruments for sediment resuspension measurements
- A hopper barge for storing dredged sediments

The completion of these additions to the dredge/tow carriage allows for dredging laboratory research to be conducted thoroughly and quickly, and is especially helpful when conducting resuspension studies.

Dredge Carriage Instrumentation

Magnetic Flow Meter

Figure 18 shows the setup of the flow meter on the dredge/tow Carriage. The flow meter is a Krohne IFC 090 K magnetic flow meter that has a 4-20 mA output signal. The output data from the flow meter is sent to the data acquisition system so that the flow of slurry or water can be monitored. The flow meter is mounted inline in a vertical section of the 7.6 cm (3 in) discharge line. Calibration of the flow meter was completed with a zero calibration in still water and then checking the calibration by filling a graduated 946.35 l (250 gallon) container and recording the time to completion of fill.

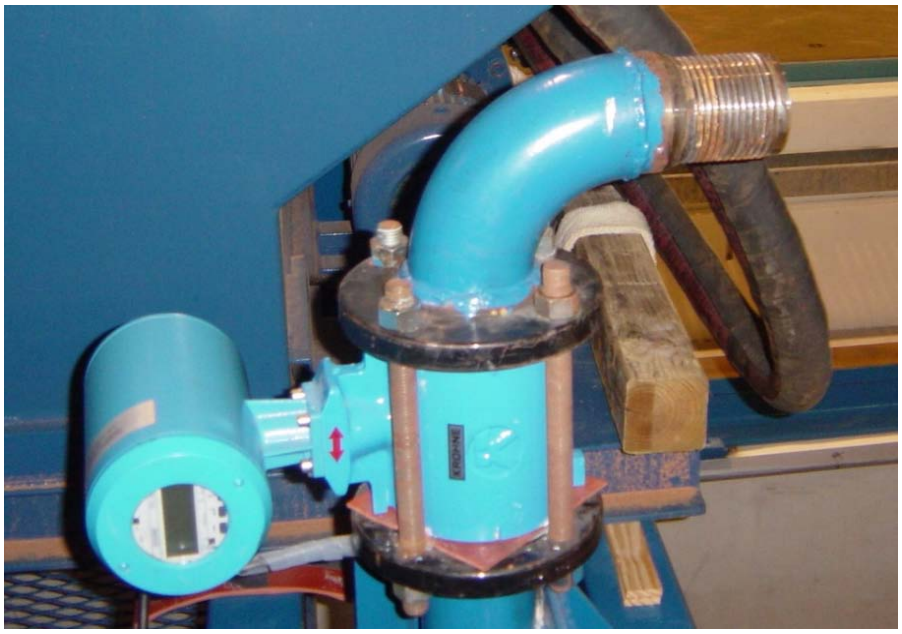

Figure 18. Magnetic Flow Meter Installation on the Dredge/Tow Carriage

Nuclear Density Gauge

The nuclear density gauge (Figure 19) installed on the Dredge/Tow Carriage is an Ohmart Vega DSG radiation based density measurement system. The system contains a gamma-based density gauge with a sealed Cesium 137 source in a source holder with a scintillation detector. The density gauge is clamped on the 7.6 cm (3 in) vertical discharge pipe just below the flow meter and the output is a 4 to 20 mA signal. Calibration of the density gauge was completed by taking data samples using a sand filled tube of known density and also when only water was in the system. The sand filled tube was inserted into the discharge pipe and the instrument reading was adjusted to the in situ specific gravity (2.00) of the saturated sand in the pipe.

Figure 19. Ohmart Vega DSG Nuclear Density Gauge

Pressure Sensors

Omega pressure sensors were installed at both the suction line and discharge line of the dredge/tow carriage pump system. Both sensors are installed within one meter of the pump suction entrance (suction sensor) and discharge exit (discharge sensor). The sensors were calibrated by placing a handheld digital manometer in line with each sensor. A picture of the pressure sensor and the data recorded during calibration can be seen in Figure 20.

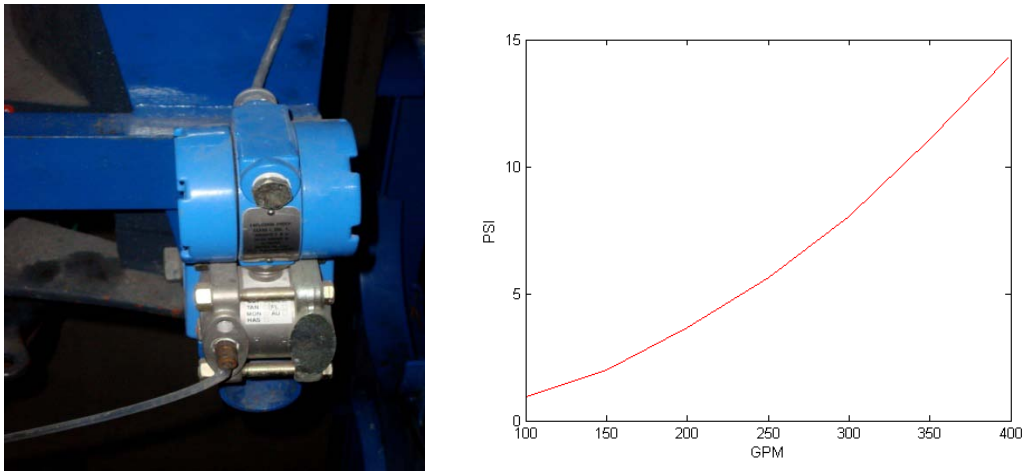

Figure 20. Pressure Sensor and Calibration Curve

Data Acquisition System

Randall et al. (2005) describes the data acquisition system for the dredge/tow carriage. However, modifications and additions to the system have made the operation of the dredge carriage more functional and easy to use. The data acquisition system is run through a graphical user interface on a standard PC and is able to access a manual operating station as well as all of the necessary drives needed to operate the dredge/tow carriage. Figure 21 shows the manual operating station adjacent to the dredge automation personal computer. The PC is also able to record data from the installed gauges and simultaneously execute programmable dredging simulations. The graphical user interface (GUI) used to control the data acquisition system is shown in Figure 22.

Figure 21. Manual Control System (left) Next to PC Automation System (right)

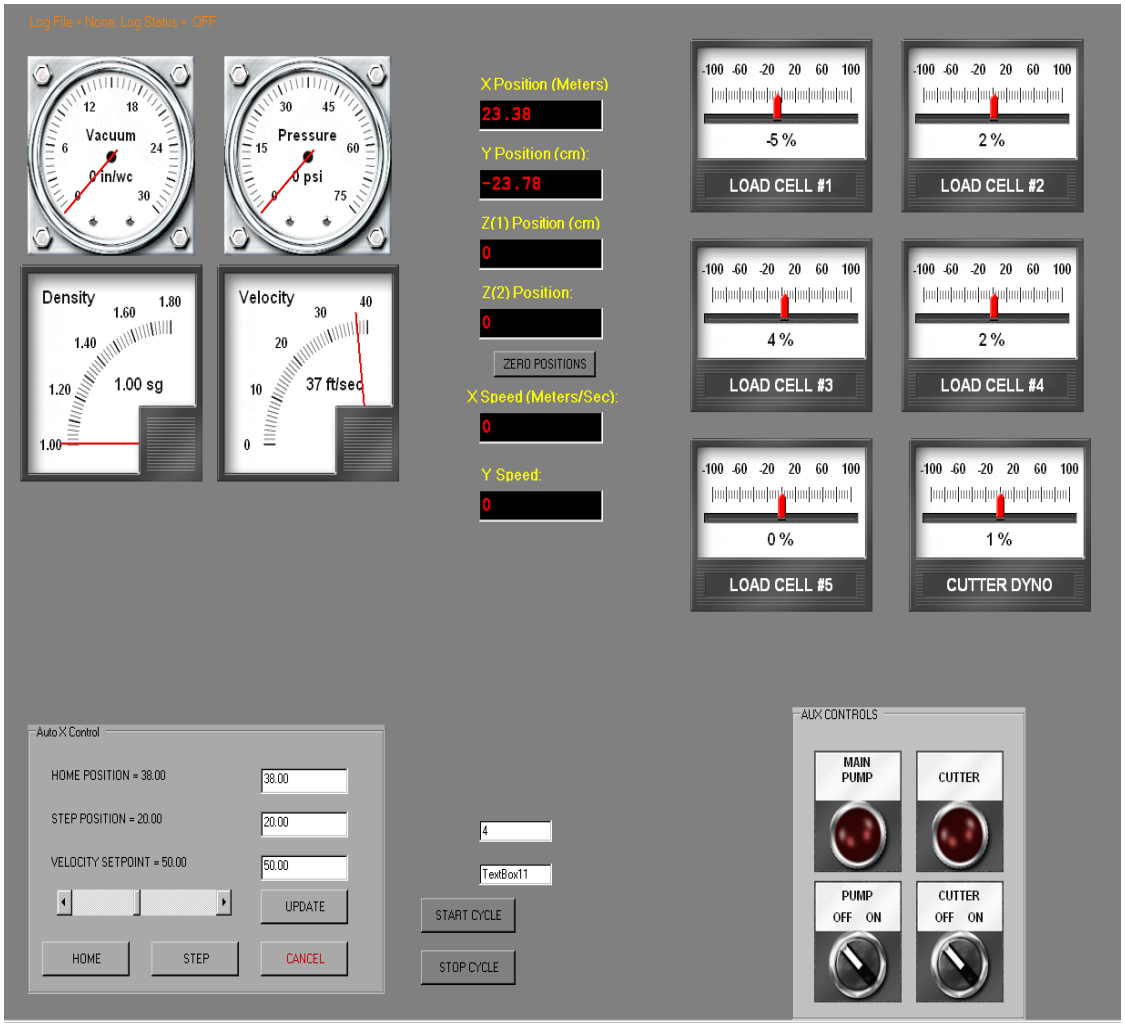

Figure 22. Graphical User Interface (GUI) for Controlling the Dredge/Tow Carriage

The graphical user interface is able to maneuver the dredge/tow carriage with the push of a button and is especially useful for initiating pre-defined dredging cycles. This allows complete repetition of testing situations. The graphical user interface also displays real time data to the user so that the dredging operation can be instantly monitored.

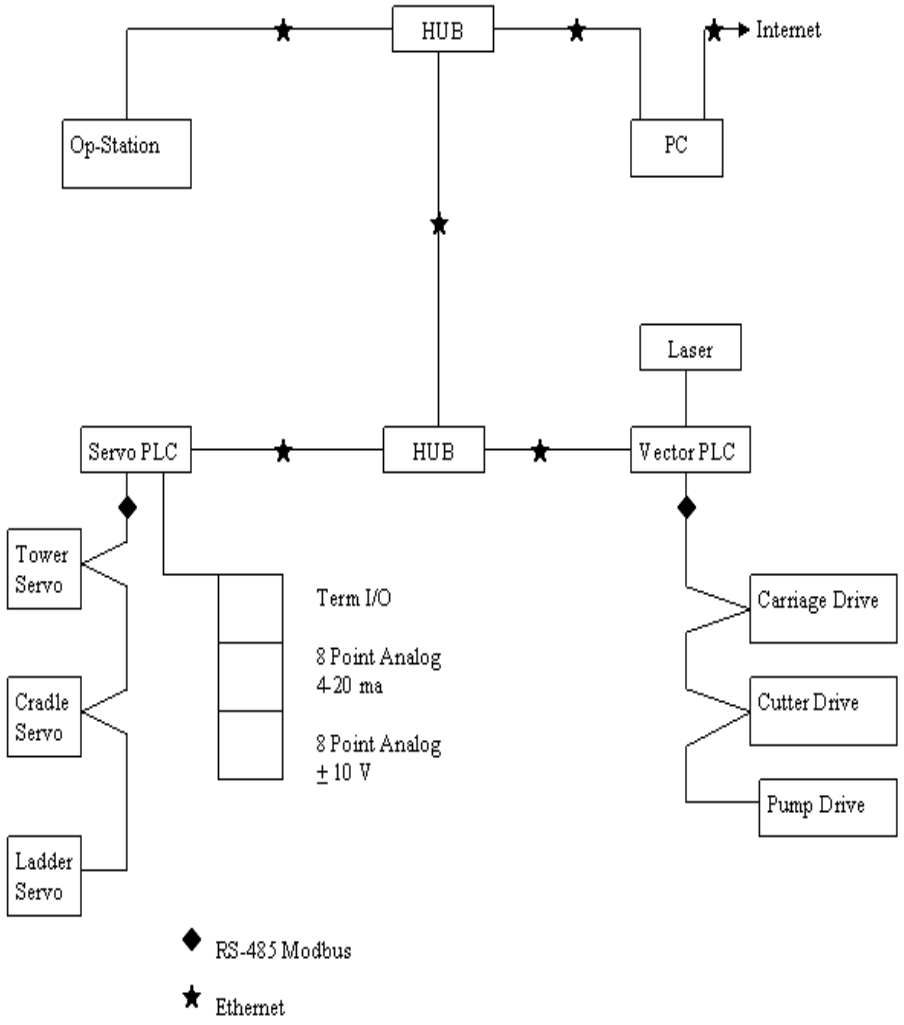

Figure 23. Schematic of the Dredge/Tow Carriage Data Acquisition System

Figure 23 displays the schematic of the data acquisition system and the individual components associated with the operation of the dredge carriage. The graphical user interface (GUI) is located in the personal computer (PC). However, it is important to note that the control of the carriage can be manually controlled from the operator station location. In manual or GUI controlled modes, network hubs relay and

obtain information to/from the servo and vector programmable logic computers (PLC). The Servo PLC's control and obtain data for the tower, cradle, and ladder movements. The Vector PLC controls and obtains data for the movement of the carriage, cutter and pump movements. Data for the horizontal position of the carriage along the tank is obtained through the Vector PLC via a laser shown in Figure 24.

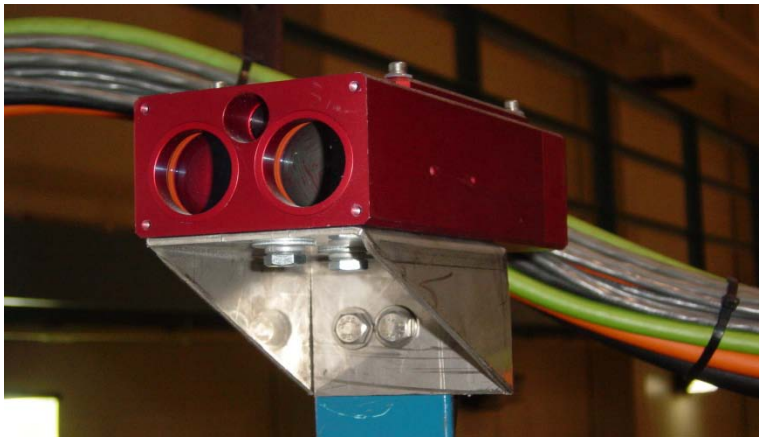

Figure 24. Horizontal Position Laser Mounted on the Dredge/Tow Carriage

Confined Placement Area

A confined placement area (CPA) was constructed out of cement blocks in the dredge/tow tank as shown in Figure 25. The CPA is a temporary structure that can easily be removed from the dredge/tow tank. The CPA allowed for a suitable location to transport the removed dredge material so that turbidity measured during testing is caused by the direct action of the cutter suction entry location and not from the discharge of any sediment. A picture of the CPA filled after dredging can is shown in Figure 26.

Figure 25. Confined Placement Area Pre-Dredging

Figure 26. Confined Placement Area Post-Dredging

After this study, a hopper barge (Fig 27) was also installed for further studies on cutter suction production. The hopper barge is 6.1 m long by 3.4 m wide by 1.5 m deep (20 ft long by 11 ft wide and 5 ft deep) and the hopper internal dimensions are 4.9 m long by 2.1 m wide by 1.5 m deep (16 ft long by 7 ft wide by 4 ft deep). The hopper is constructed with 3/32 steel plate and the total internal volume is 14.1 m^3 (18.5 yd^3). For a slurry velocity of 3 m/s (9.8 ft/s), the estimated pumping time until full is 57 min for overflow and 17 min for no overflow. The hopper barge floats on the water in the tank and is attached to the carriage. The hopper is positioned over the sediment pit in the dredge/tow tank and the bottom door is opened to return the sediment to the pit. Draft measurements are used to determine the weight of slurry in the hopper.

Figure 27. Dredging Hopper for Containment of Dredge Material

Acoustic Doppler Velocimetry Sensors

Acoustic Doppler Velocimetry (ADV) Sensors are used in measuring water velocities at specific points. The sensors send an acoustic signal to a parcel of water and measure the Doppler shift of the signal to calculate the velocity of the water parcel. Both Sontek and Nortek sensors were used in this study. All sensors used in this study were three dimensional sensors that can measure the velocity components of *u*, *v*, and *w*. The Sontek sensors were programmed with Sontek software to take velocity measurement samples at 8Hz and the Nortek sensors were programmed with Nortek Vectrino software to take velocity measurements at 48Hz. Figure 28 shows pictures of the Nortek and Sontek ADV.

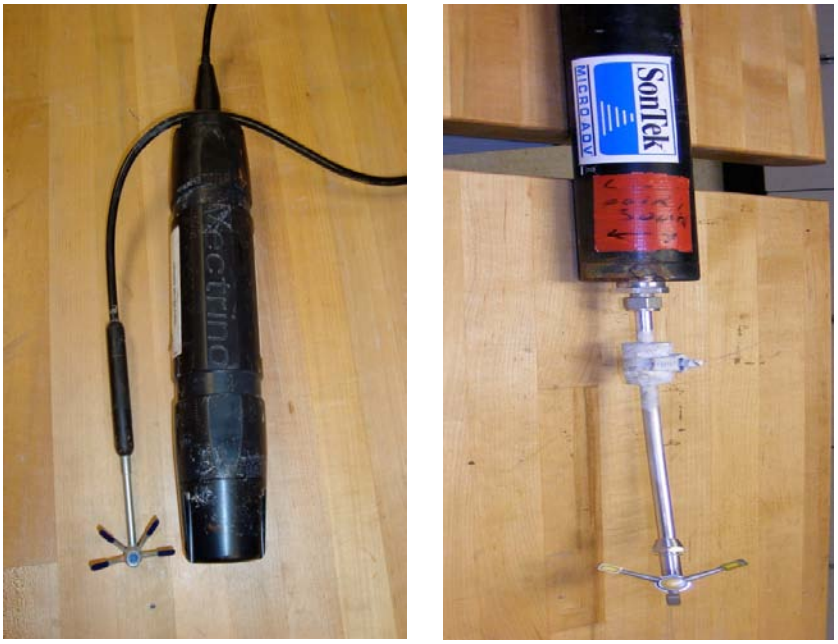

Figure 28. Nortek (left) and Sontek (right) ADV Sensors

Optical Backscatter Sensors

Optical backscatter sensors (OBS) are used extensively to increase sampling densities of resuspended sediment (RSS) for in situ measurements. The sensors function by emitting infrared light and measuring the transmission (Downing, 2005). The infrared radiation is quickly attenuated by water, therefore the infrared beam does not travel large distances. This allows the OBS sensor to measure very exact point locations in the range of 2.5 cm (1 in) to 20.3 cm (8 in) relative to the receiver head.

The OBS sensors have a nearly linear response to particles in turbid water (Downing, 2005). The OBS sensors that are used to record turbidity measurements in the dredge/tow tank are the OBS3+ sensors. These sensors contain a high intensity infrared emitting diode (IRED), four photodiode detectors, and have a turbidity range of 0-4,000 nephelometric turbidity units (NTU's). The IRED provides a beam with a half power point location at 50 degrees in the axial plane and 30 degrees in the radial plane. The best sampling point exists 5 cm away from the sensor. Figure 29 shows a picture of the sensor and demonstrates the linear characteristics of the sensor to the sediment used in the tow tank.

Saturation of the OBS sensor can occur when values reach significantly high concentration levels. For mud, saturation may start at concentrations of 20 g/l while values of saturation for sand occur at 50 g/l. Most aquatic applications utilize the linear section of the OBS sensor so that a single equation can be used:

$$C_r = A_{obs} \psi + B_{obs} \tag{106}$$

where ψ is optical backscatter output [volts], and A_{obs} and B_{obs} are regression coefficients.

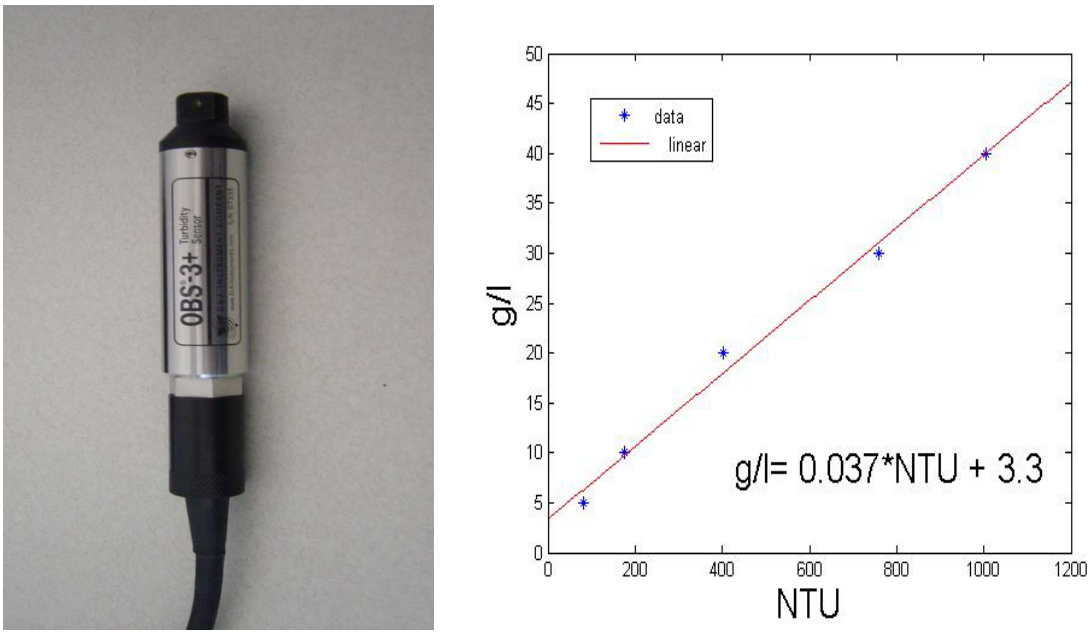

Figure 29. OBS3+ Sensor (left) and Calibration Curve for NTU to grams/liter (right)

The calibration curve constructed for the OBS3+ sensor was constructed with the sediment pit sand by placing the OBS3+ sensor in a container with a known concentration of the sediment and measuring the concentration while the sediment was kept in suspension with a mechanical stirring apparatus.

When calibrating the OBS sensor to the sediment concentrations, there are several issues that exist including sediment diameter, shape and color (Downing, 2005). Connor and De Visser (1992) reported on the sediment diameter effect on OBS output

voltage. Glass beads were used so that the shape and color of the particles did not contribute to the study. An inverse power law regression was used to fit the data and it was stated that further research was needed to understand the OBS output with sediment properties. It was also noted that obtaining an accurate calibration with sediment particles larger than 150 μm was difficult because of the inability of a larger sediment diameter to remain in suspension. Figure 30 displays OBS voltage output for a range of sediment diameters.

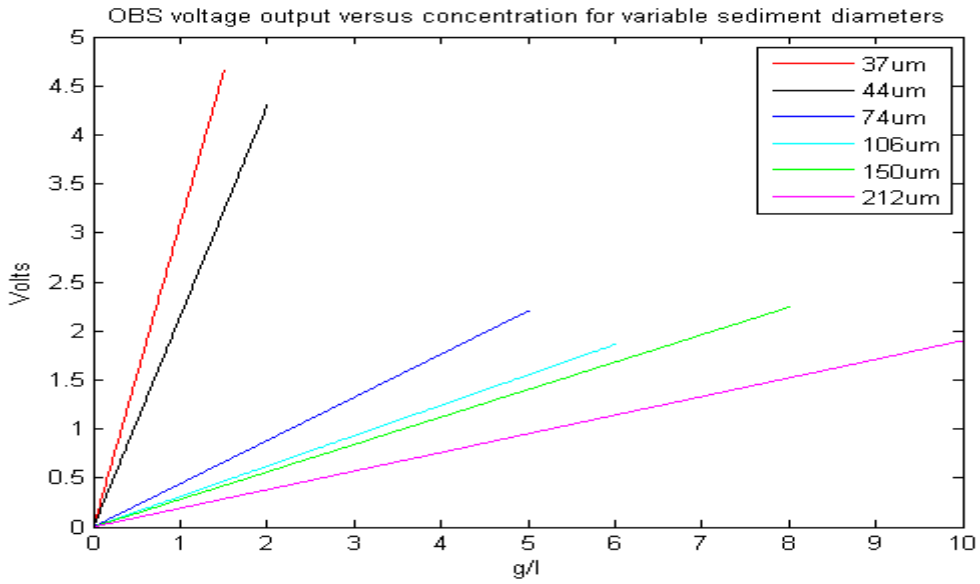

Figure 30. OBS Voltage Output for Sediment Concentrations with Different Sediment Diameters (Downing, 2005)

The operation of the OBS3+ sensors is controlled using a Campbell Scientific CR10X data logger. A trigger was built to initialize simultaneous data recording between the OBS sensors and the ADV sensors. A picture of the CR10X data logger and

trigger setup is illustrated in Figure 31. Figure 32 shows the computers and equipment utilized for collecting data from the four ADV and four OBS sensors.

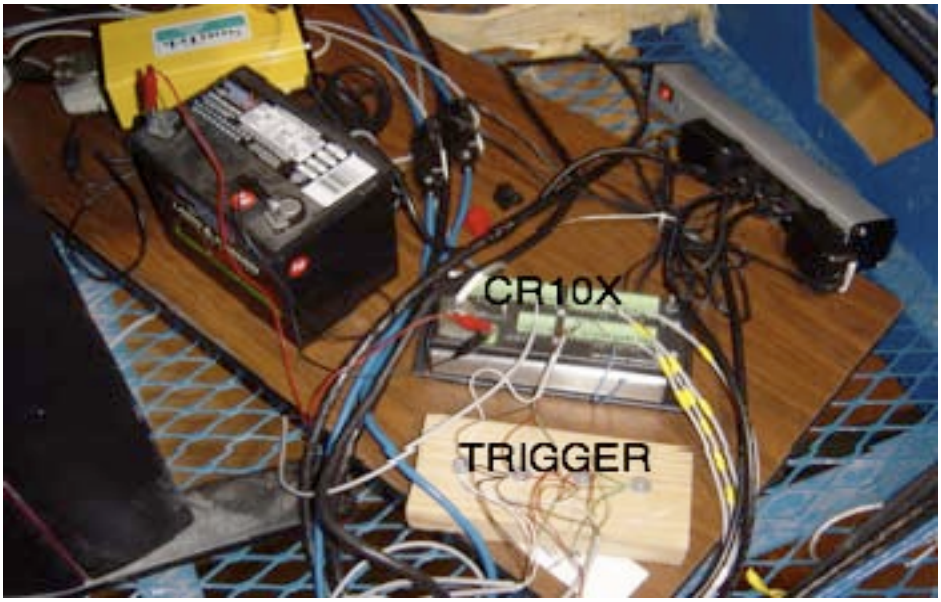

Figure 31. Picture of the CR10X Data Logger with Trigger Setup

Figure 32. Picture of the Data Acquisition Arrangement of the ADV and OBS Sensors

Data Collection Mounting System

A mounting system was designed and installed around the cutter so that four ADV sensors and four OBS instruments were positioned for sampling. An underwater camera was also attached to the mounting system as shown in Figure 33. The ADV and OBS sensors were mounted so that wake effects are minimized. The sensors were set in a spatial cross section representing the spatial turbidity at the back line of the cutter. This cross section was chosen because visually it produced the highest turbidity region when viewing the dredging operation. A total of 20 points were measured around the cutter. Table 5 and Figure 34 display the spatial coordinates of each sampling point in relation to the center of the cutter and the displayed reference of orientation.

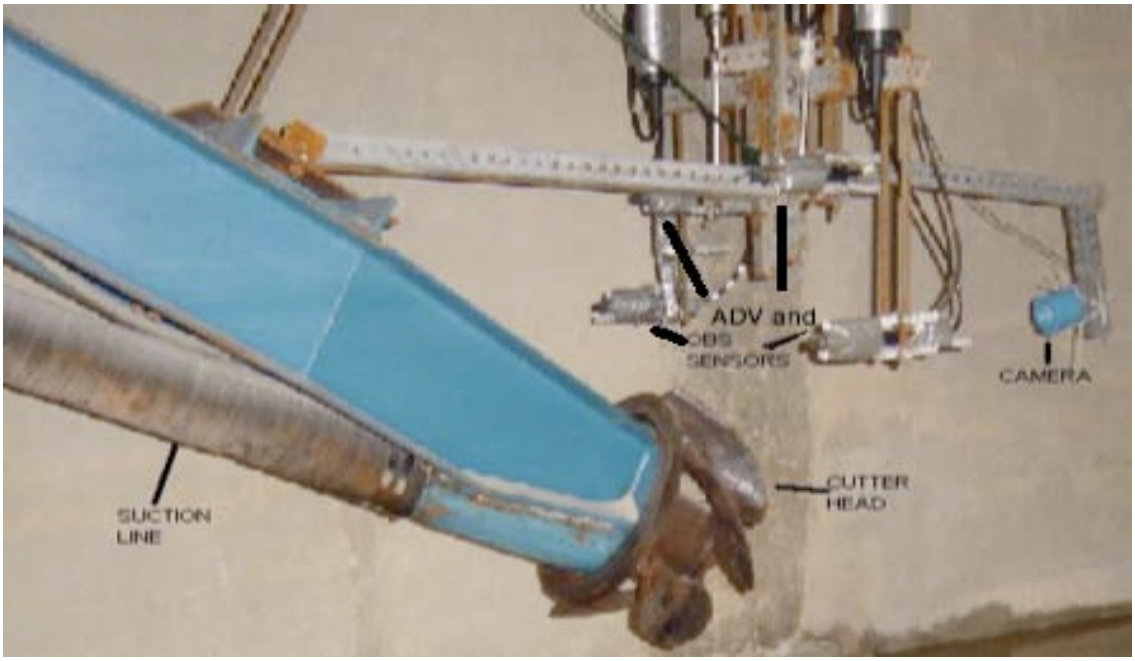

Figure 33. Side View of the Data Collection Mounting System

Table 5. Spatial Location of Sampling Points Surrounding the Cutter

Point	Y	Z	Point	Y	Z
P1	**12.7 cm**	**35.5 cm**	**P11**	**-12.7 cm**	**35.5 cm**
P2	**12.7 cm**	**45.7 cm**	**P12**	**-12.7 cm**	**45.7 cm**
P3	**20.3 cm**	**30.4 cm**	**P13**	**-20.3 cm**	**30.4 cm**
P4	**20.3 cm**	**40.6 cm**	**P14**	**-20.3 cm**	**40.6 cm**
P5	**20.3 cm**	**50.8 cm**	**P15**	**-20.3 cm**	**50.8 cm**
P6	**33.0 cm**	**15.2 cm**	**P16**	**-33.0 cm**	**15.2 cm**
P7	**33.0 cm**	**25.4 cm**	**P17**	**-33.0 cm**	**25.4 cm**
P8	**40.6 cm**	**10.1 cm**	**P18**	**-40.6 cm**	**10.1 cm**
P9	**40.6 cm**	**20.3 cm**	**P19**	**-40.6 cm**	**20.3 cm**
P10	**40.6 cm**	**30.4 cm**	**P20**	**-40.6 cm**	**30.4 cm**

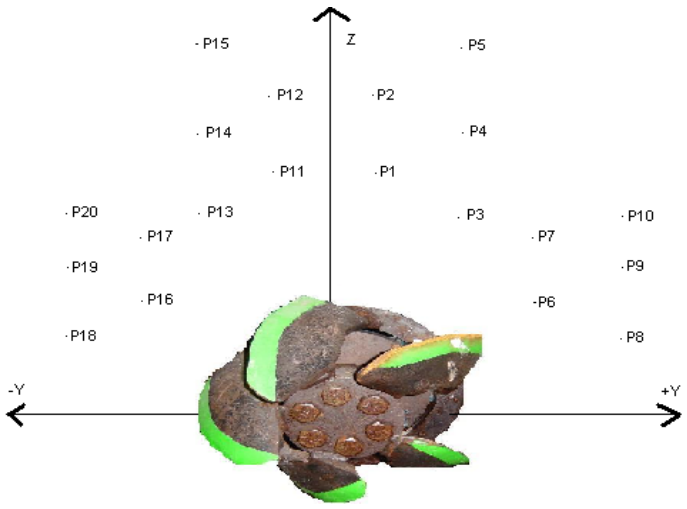

Figure 34. Spatial Map of Sampling Points Surrounding the Cutter

Sediment Characteristics

Beach sand with a d_{50} of 260 μm was available in the sediment pit and used for this study. Figure 35 shows the logarithmic profile of the standard sieve analysis for the sediment. Table 6 displays the standard geological parameters for the sediment.

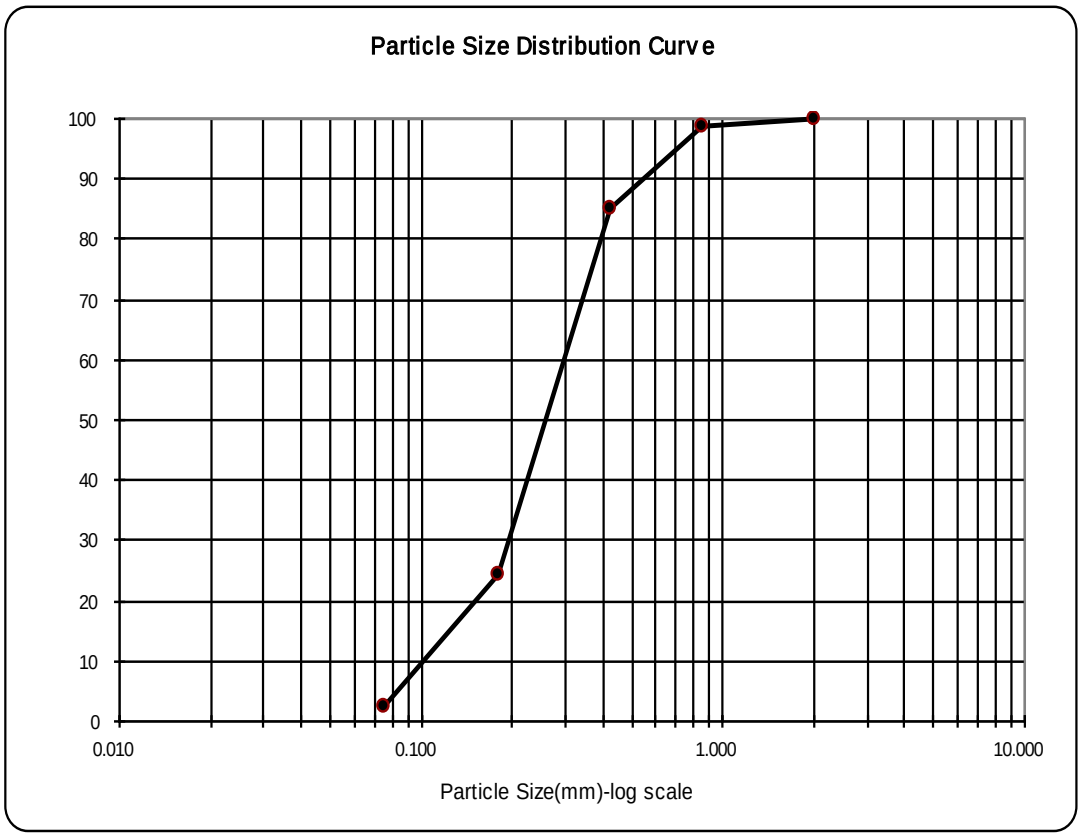

Figure 35. Logarithmic Profile of Particle Size of Sediment Pit Sand

Table 6. Sieve Analysis and Characteristics of Sediment Pit Sand

D10 (μm)	**110**
D30 (μm)	**250**
D50 (μm)	**260**
D60 (μm)	**300**
Cohesive Soil Fraction	**3%**
Repose Angle (deg)	**30**
Critical Shields parameter	**0.046**
Soil density	**2650 kg/m^3**

Laboratory Measurement of Sediment Resuspension

Ninety cuts were made during the testing. The tests included initial preliminary testing for slower cutter speed tests to simulate prototype conditions as well as the tests conducted for the main study. A cut was made in the overcutting direction followed by a cut in the undercutting direction. After six cuts were made, the tank was drained and the water was pumped out of the sediment pit with a submersible sump pump. The sediment was then manually transported from the confined placement area back to the sediment

pit and smoothed. Water was slowly pumped back into the dredge/tow tank in preparation for the next testing cycle.

The data acquisition system allowed for repeatable cutting conditions in the sediment pit. At the beginning of each cut, the cutter and pump were turned on and the ladder was lowered to the desired cutting depth. Once the desired cutting depth was reached, the cutter was momentarily stopped so that the ADV sensors, OBS sensors, and the dredging data collection system could be triggered. After triggering, the cutter was returned and the ladder swing was made. A constant swing speed of 1.73 cm/s (0.68 in/s) was utilized and the articulating ladder angle was also held constant at 24 degrees from horizontal.

Testing Matrix

The parameters investigated in this study were the suction velocity, cutter rotation speed, and the thickness of cut in the sediment. Seven test cases were examined. These seven tests are outlined in Table 7. Tests with the letter A are undercutting while tests with the letter B are overcutting. Test case one was repeated three times for each sampling position so that repeatability could be achieved. The other test cases were conducted so that the necessary operating parameter comparisons could be made.

Table 7. Testing Matrix for Cutter Suction Testing Parameters

Test Case	Cutter Speed (RPM)	Suction (GPM)	Thickness of Cut (in)	Type of Cut
Case1A	86	150	8	Undercutting
Case1B	86	150	8	Overcutting
Case2A	86	200	8	Undercutting
Case2B	86	200	8	Overcutting
Case3A	86	300	8	Undercutting
Case3B	86	300	8	Overcutting
Case4A	58	150	8	Undercutting
Case4B	58	150	8	Overcutting
Case5A	116	150	8	Undercutting
Case5B	116	150	8	Overcutting
Case6A	86	150	4	Undercutting
Case6B	86	150	4	Overcutting
Case7A	86	150	12	Undercutting
Case7B	86	150	12	Overcutting

CHAPTER VI

DISCUSSION OF LABORATORY RESULTS

The data collected during the laboratory study were recorded from the dredge/tow carriage instrumentation by the data acquisition system and from the OBS and ADV sensors. The data from the dredge/tow carriage instrumentation were used to record the dredging operation parameters and calculate the production of the cutter suction system. The turbidity characteristics of each set of dredging tests were investigated by analyzing the OBS and ADV data.

Dredge/Tow Carriage Data

The dredge/tow carriage instrumentation provided data on the flow rate, the slurry specific gravity, and the suction and discharge pressures during each dredging test. These data were used to conduct a statistical analysis on the results for each test and also calculate the production based on Equation 48. Figure 36 demonstrates a typical data set from the data acquisition system for a dredging test. It is important to notice that the beginning of the test shows where the dredge pump must be turned off momentarily to start the cutter. This procedure has since been altered so that the pump does not need to be turned off before the cutter begins. The data analysis used to construct Table 8 utilized only a sample of the data set that was most representative of a steady state test and minimized any boundary effects.

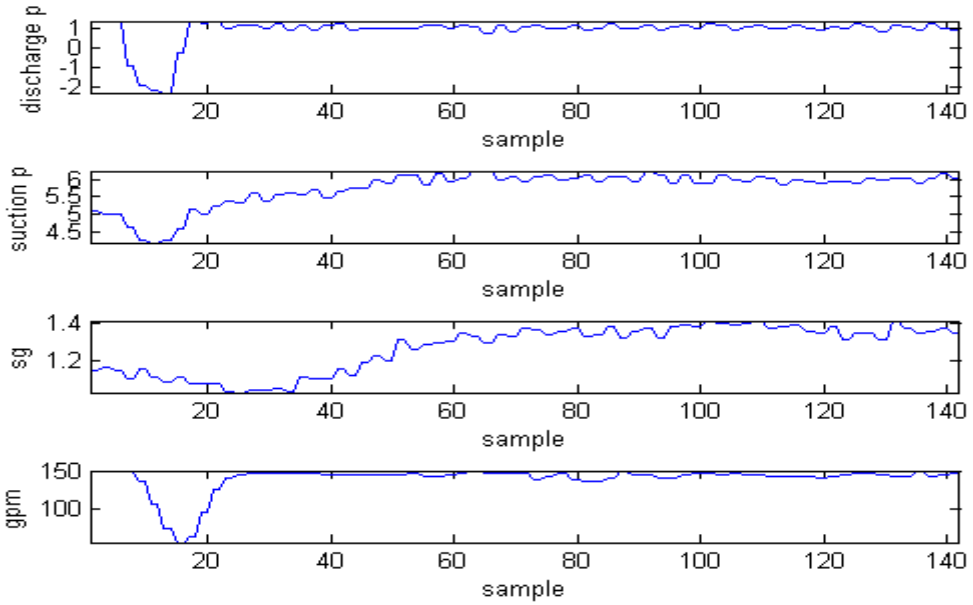

Figure 36. Raw Dredge Carriage Data

Table 8. Production Table for Each Laboratory Test Case [m^3/hr]

TEST	MEAN	STD
Case1A	6.12	2.01
Case1B	5.46	2.17
Case2A	9.66	3.47
Case2B	8.89	2.63
Case3A	12.53	4.12
Case3B	11.72	2.49
Case4A	8.97	3.08
Case4B	3.14	1.36
Case5A	8.88	1.82
Case5B	8.46	4.68
Case6A	1.97	1.58
Case6B	1.88	1.80
Case7A	9.32	4.87
Case7B	13.07	4.21

Reviewing Table 8, the production was consistently greater for undercutting for all test Cases 1-6. However, when the thickness of cut was equal to one cutter diameter, the testing produced a larger production rate for overcutting (Case 7). The flow rate also demonstrated a strong linear effect on the production for both undercutting and overcutting (Cases 1-3). Cutter speed did not show a strong correlation with predicting production for undercutting but did have a direct correlation showing an increase in production with an increase in cutter speed for overcutting. These results agree with prior testing and demonstrate that the mechanics of dredging production can vary significantly and are strongly dependent on the suction speed and the thickness of cut as well as the cut type (undercutting and overcutting).

A review of Table 9 demonstrates that the slurry specific gravity was consistently greater for undercutting than overcutting for all partial cut testing. The full cut (thickness of cut equal to one cutter diameter) testing (Case 7 and Case7B) agreed with production data and was greater for overcutting. The flow rate data was consistent in the range of interest of the 150 gpm and 300 gpm testing, however, some variation existed in the 200 gpm testing. The discharge pressures reflected this occurrence at 200 gpm, however, the suction pressure did not show this variation during the 200 gpm testing.

Table 9. Dredge Carriage Parameters for Each Test Case

TEST	N	GPMM	GPMSD	SGM	SGSD	DPM	DPSD	SPM	SPSD
Case1A	14	148.70	2.26	1.19	0.06	1.19	0.21	5.42	0.48
Case1B	14	149.38	2.97	1.17	0.07	1.26	0.23	5.21	0.53
Case2A	6	218.07	27.85	1.20	0.06	4.55	1.57	5.79	0.76
Case2B	6	238.37	40.48	1.17	0.03	5.57	2.63	5.71	0.39
Case3A	5	299.58	7.38	1.19	0.06	10.17	0.26	6.70	0.96
Case3B	5	304.64	3.70	1.18	0.03	10.01	0.24	6.44	0.94
Case4A	4	146.77	1.93	1.28	0.04	1.74	0.70	4.45	1.51
Case4B	5	152.47	0.74	1.08	0.04	1.75	0.61	3.93	1.33
Case5A	6	147.99	2.54	1.28	0.05	1.55	0.69	4.91	1.42
Case5B	6	150.16	5.59	1.27	0.16	1.71	0.65	4.43	1.45
Case6A	6	152.50	0.52	1.06	0.04	1.43	0.34	4.52	0.34
Case6B	6	153.47	0.92	1.05	0.05	1.44	0.37	4.42	0.74
Case7A	4	140.43	4.39	1.31	0.17	1.18	0.44	5.84	0.77
Case7B	3	136.45	9.54	1.46	0.17	1.43	0.48	5.82	0.48

N=Number of Tests
GPMM=Flow rate mean (gpm)
GPMSD=Flow rate standard deviation
SGM=Specific gravity mean (dimensionless)
SGSD=Specific gravity standard deviation
DPM=Discharge pressure mean (psi)
DPSD=Discharge pressure standard deviation
SPM=Suction pressure mean (inHg)
SPSD= Suction pressure standard deviation

Turbidity Data Analysis

General Observations

The resuspension of sediment caused from undercutting was three to six times greater than resuspension created from overcutting. In general, resuspension generation was highest relatively close to the initial sediment release point of the cutter. Here, sediment is initially "washed" off the cutter blade. As the blade rotates there is less material to be removed from the blade surface. This produces a decreasing gradient of turbidity as sediment is released from the cutter blade. The gradient of decreasing turbidity is also strong in the vertical direction. This strong diffusion gradient is attributed to the large amount of turbulence and strong dissipation created from the cutter head.

Repeatability of Experiment

The repeatability of the experiment was fairly consistent. Although the test is governed by a large amount of turbulence, general trends and mean values were shown to be repeatable. A display of the raw data directly from the four OBS sensors can be seen in Figure 37. Data are truncated for data analysis but show the spikes caused by the boundary conditions at the beginning and end of testing.

The raw data from cut 122 OBS-3+ provide a particularly good example of the boundary condition that occurs during the test run. Repeatability was more consistent when overcutting than when undercutting and also was more consistent as the thickness of cut decreased. The 30.2 cm (12in) cut was more difficult for repeatability and for

data analysis because the data tended to show random turbidity spikes instead of a continuous source of resuspension.

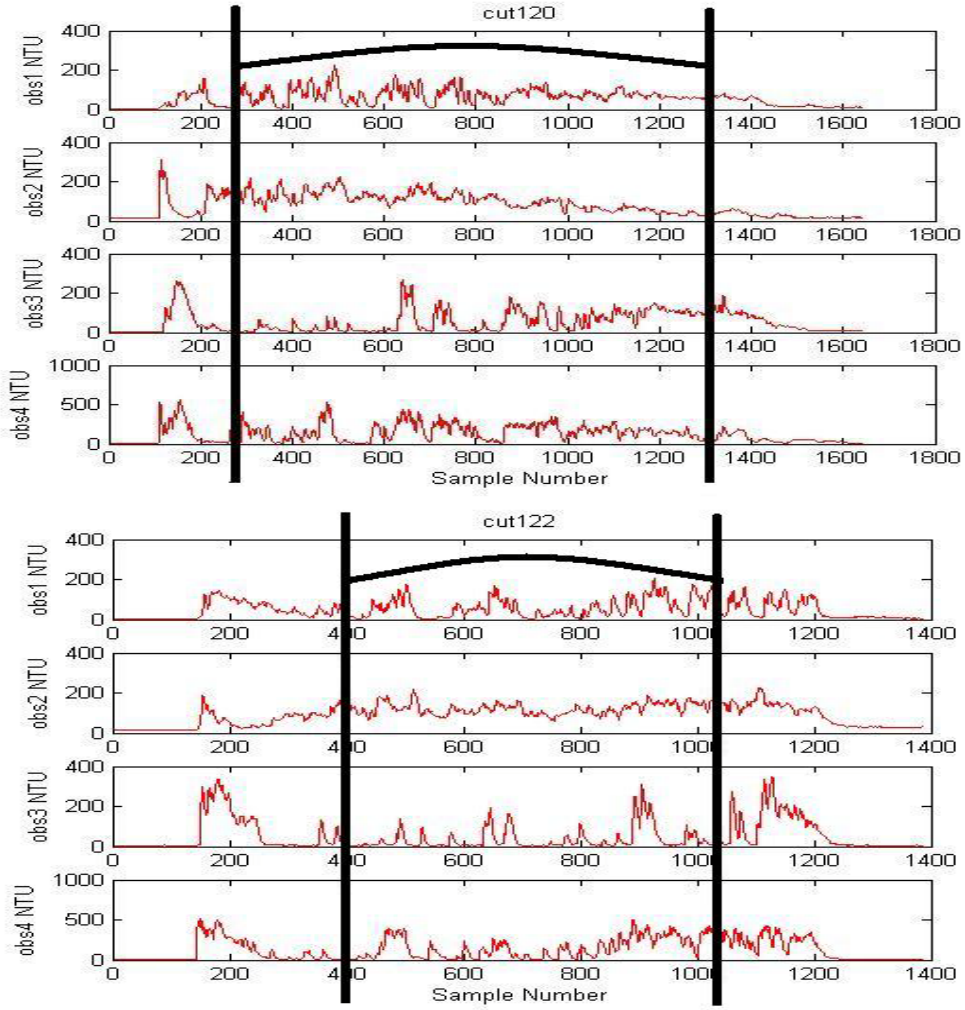

Figure37. Repeatable Experimental Data Showing Data Truncation

In order for the statistical parameters of the turbidity generation to be determined correctly, the recorded data had to be truncated to account for boundary effects. The

data truncation was necessary because of boundary effects caused by the walls of the sediment pit. When the cutter was either started next to the wall or finishing a cut and approaching the wall, a large increase in turbidity was observed that differed from the mean value created during most of the cutting process. A picture of the boundary effect caused from the sediment pit wall is illustrated in Figure 38.

Figure 38. Boundary Effect Seen During Dredging

Analysis of the data showed that the raw OBS and ADV data tended to demonstrate two phases during each test. The typical trend of the data was to begin with a strong amount of turbidity generation at the beginning boundary condition (BC). This was followed by a Phase 1 (P1) condition where the turbidity generation was minimal,

followed by a Phase II (P2) condition where a stronger turbidity generation occurred. The pattern of this data is seen simultaneously in the OBS and ADV data and represents the general pattern seen in all testing in the laboratory. An example of the shift in turbulence and turbidity generation can be seen in Figure 39. Tables from this analysis of Phase I and Phase II as well as the initial data analysis are located in Appendix C.

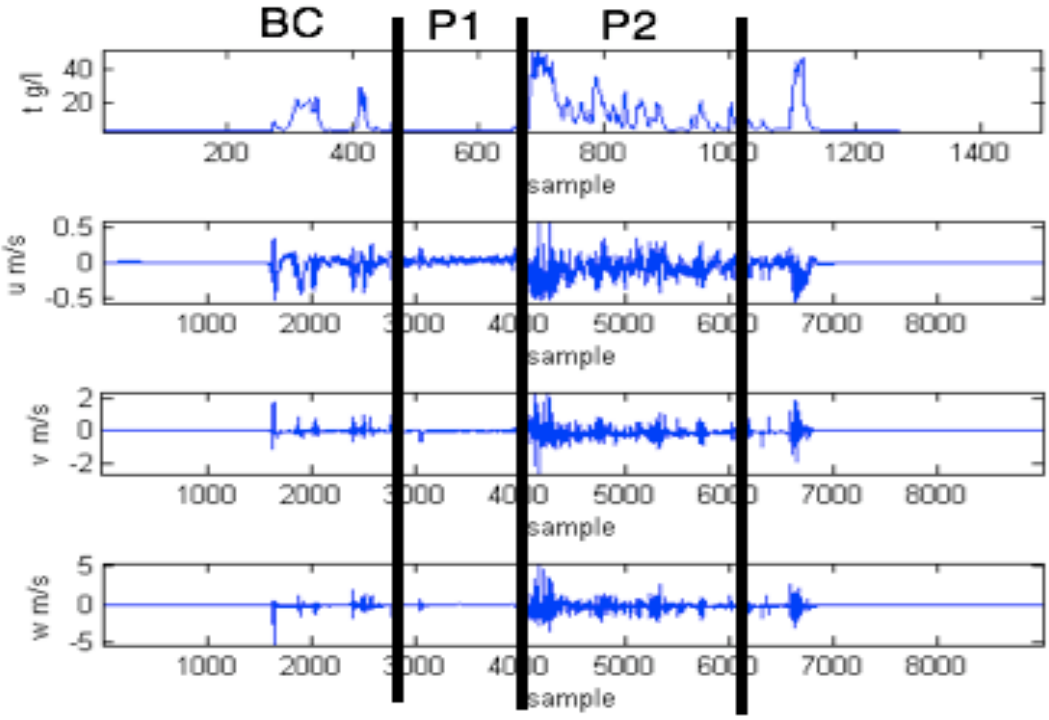

Figure 39. Raw Data from the OBS and ADV Data

Spatial maps of the mean turbidity were made for each test case. These maps represent the mean turbidity created during the testing period and are created for both undercutting and overcutting. It is important to note that all spatial maps generated for

this dissertation are designed to show the strength of the variable using both the color and the size of the circle. Graphs were also created for each point surrounding the cutter. Point comparisons were created to examine the effect of the flow rate, the cutter speed, and the thickness of cut variation described in the testing matrix (Table 7). Figure 40 and Figure 41 display the spatial maps of turbidity for Case 1A and Case 1B tests. The turbidity spatial maps for all tests are displayed in Appendix D. It is important to note that not all points were obtained for the twelve inch cut (Case 7A and Case 7B). This is due to the possibility of damage to the OBS and ADV sensors when placing them close to the sediment bed.

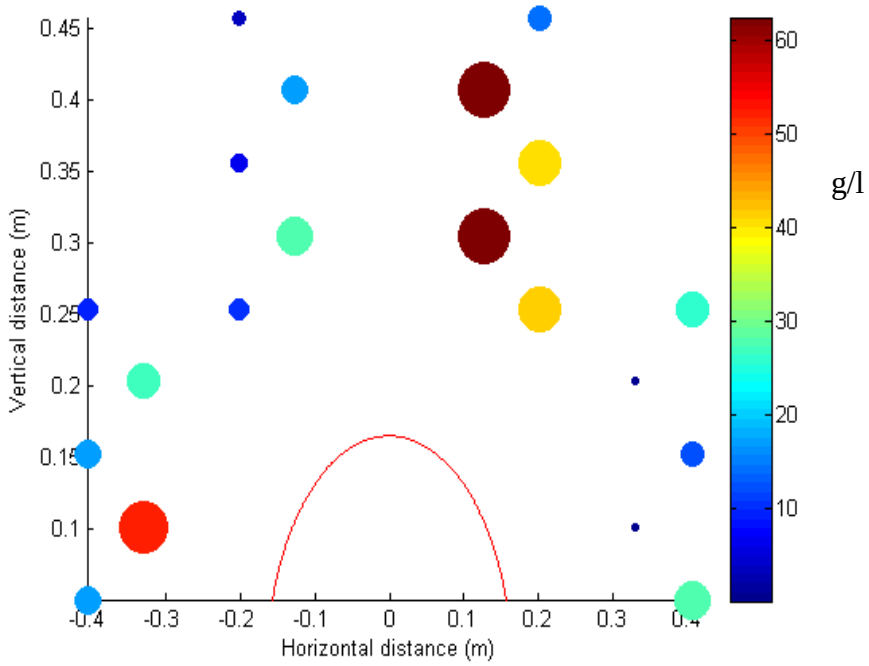

Figure 40. Case 1A (567.75 LPM=150GPM) Spatial Map of Mean Turbidity for Undercutting.

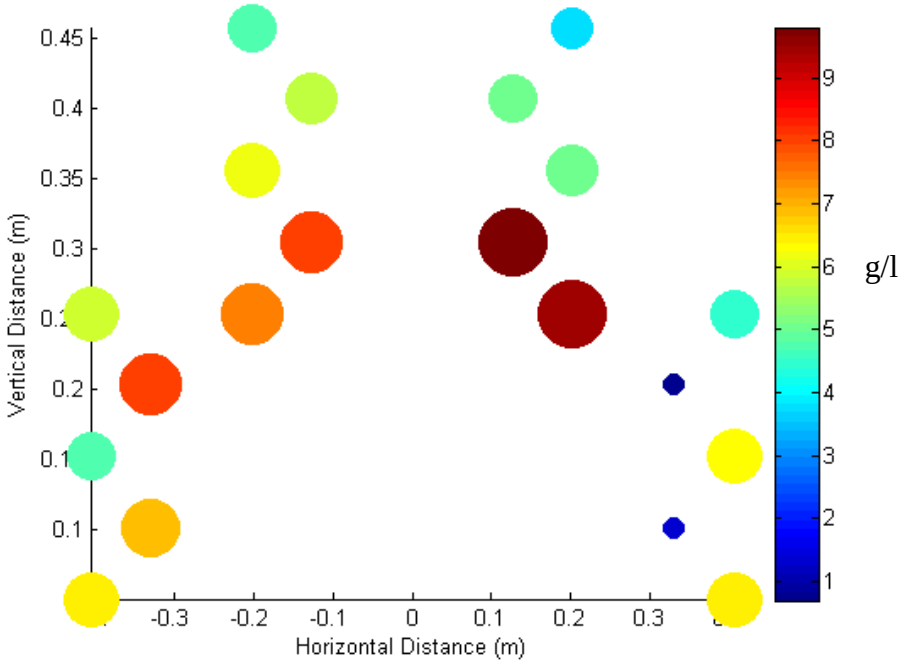

Figure 41. Case 1B (567.75 LPM=150GPM) Spatial Map of Mean Turbidity for Overcutting.

Flow Rate Comparison

Figure 42 provides point comparisons at each sampling point surrounding the cutter head. The flow rate comparison showed that in the overcutting scenario the majority of points showed minimum resuspension at 200 gpm. It is interesting to note that most points showed an increase in turbidity at 300 gpm. This is counterintuitive to the standard idea of an increase in flow rate causing a decrease in turbidity. This effect was thought to be due to an increase in turbulence caused by the higher flow rate and is investigated in the turbulence analysis section of this dissertation.

The spatial orientation of the turbidity surrounding the cutter for all three flow rates show a general pattern where the highest concentrations occur at point 1, 2, and 3

for undercutting and point 6 for overcutting. As the cutter rotates, more washing occurs and locations such as point 11, 12, 13, and 14 show much less turbidity. In general, all three cases follow the general pattern of the highest turbidity concentrations existing within one cutter diameter from the edges of the cutter. Point 2 in the undercutting testing is an exception to this, with relatively high resuspension values constantly occurring in this region.

The strongest spatial turbidity gradient surrounding the cutter is seen in overcutting testing, with the trend moving toward negligible turbidity 2-2.5 cutter diameters from the cutter. Overcutting testing also shows a strong spatial concentration gradient, however, point 1, 2, and 3 do not have high turbidity values when compared to other points. It is interesting to note that a significant decrease in turbidity is seen for undercutting at point 8 and point 9 as suction increases. These points are the initial excavating point for material where the suction effect is strong.

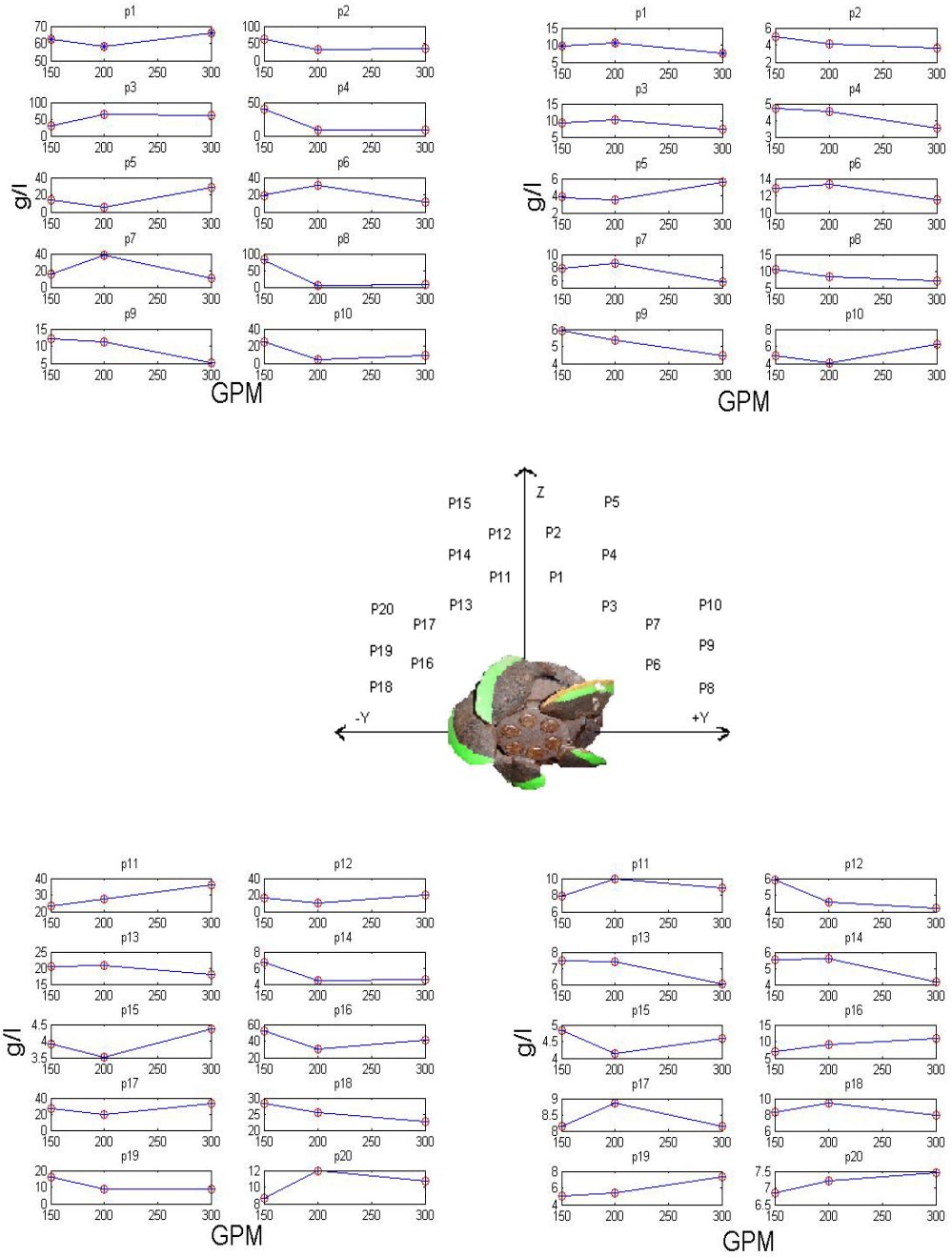

Figure 42. Point Comparison of Flow Rate for Undercutting (left) and Overcutting (right). Multiply GPM by 3.785 to obtain LPM

Cutter Speed Comparison

Although lower cutter speeds may have certain points that provide larger values of resuspension, the turbidity of points within one cutter diameter around the cutter increases as cutter speed increases. This effect is most prevalent in points close to the initial excavation release location (point 1, 3, 6, and 8). The effect is more pronounced in the overcutting testing and is especially observed at point 6 and point 8. It is also interesting to note the strong spatial gradient existing in the vertical direction. This gradient is strongest in the undercutting testing at the highest RPM but is also seen in the other cases. Although the middle cutter speed (Case 1A) shows some differences, the results generally follow assumptions (Hayes, 1986) that state negligible turbidity values existing two cutter diameters away from the tip blades in the vertical direction.

The maximum value seen from all dredging operations was seen in Case 5A (116 rpm). These points of high turbidity existed at extremely low vertical locations horizontally far from the cutter. Most points in the overcutting tests showed the generalized trend of increasing turbidity with increasing rpm. However, some locations in the undercutting tests surrounding the cutter actually showed a maximum turbidity generation at 86 rpm (Case 1A) with a decrease in turbidity at the highest cutter speed of 116 rpm. These points represent the highest points of turbidity generation in Case 1A and are the locations where sediment is initially released due to washing.

Observing the spatial maps, it is observed that at the lowest cutter speed testing (Case 4A) most of the sediment resuspension is concentrated at point 1, with little

resuspension occurring at other usually high turbidity points (point 2, point 6, and point 8). In this case, sediment stays on the cutter blade until it reaches the release point, but because the cutter speed is less, the sediment is not thrown as high up in the water column. However, in Case 5A the increase in cutter speed causes washing to occur earlier and an initial increase in resuspension at the initial excavation points (point 6 and point 8) with relatively less resuspension occurring elsewhere.

Thickness of Cut Comparison

Figure 44 shows that the thickness of cut mostly presented a maximum resuspension of sediment for the 20.2 cm (8 in) cut. The 30.2 cm (12 in) cut represents more of a "full cut" and agrees with previous reports by producing the lowest turbidity levels. The 10.1 cm (4 in) cut produced less turbidity than the 20.2 cm (8 in) cut but still more than the 30.2 cm (12 in) cut. This 10.1 cm (4 in) cut represents a "shallow cut" whose dynamics are discussed by Crocket (1993). In this case, the amount of material picked up by the blade is still available to "washing" but the amount of material is simply less.

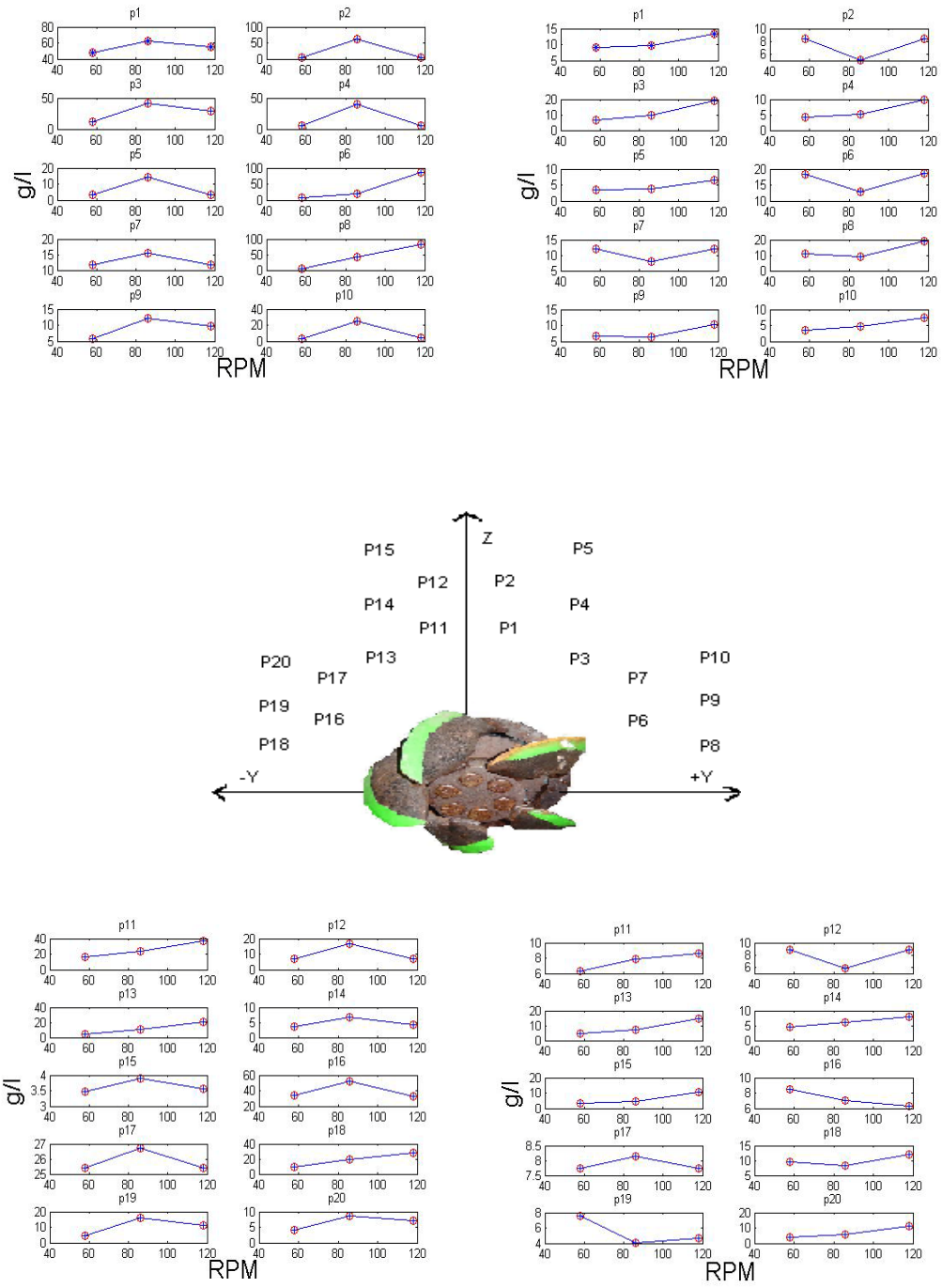

Figure 43. Point Comparison Mean of Cutter Speed (RPM) for Undercutting (left) and Overcutting (right)

It is interesting to note that the spatial gradient in the vertical direction is not as strong in the shallow cut. Instead, the spatial turbidity is segregated with the entire excavating release side of the cutter being more turbid than the other side. This effect is strongest with the overcutting testing in Case 6A. Instead of turbidity being focused in points 1, 2, 6, and 8, higher turbidity values exist on the entire right side (points 1-10) relative to points on the left (points 11-20).

Case 7A showed the highest values at point 6 and point 16. However, these data were only obtained for the undercutting test. Because point 6 and point 16 are so close to the sediment bed, the effect of sloughing may be substantial in this region. If point 6 and point 16 are removed from the analysis, it is interesting to note the similarity between the undercutting test and overcutting test for Case 7A. The general pattern of the overcutting and undercutting spatial maps show strong similarity. Although point 1 and point 11 could not be recorded for the overcutting test, point 10 represents a higher resuspension level and displayed similar values for both tests.

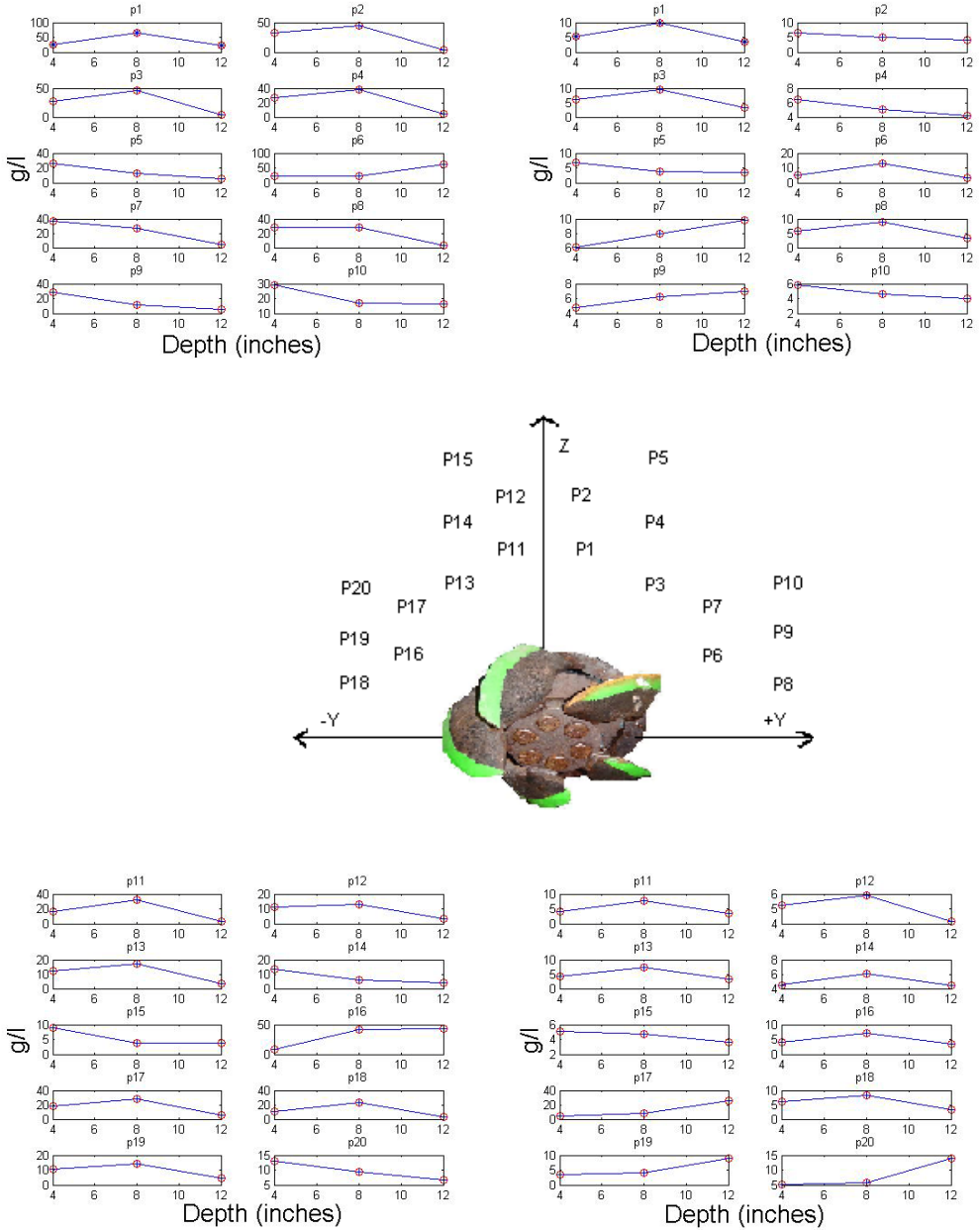

Figure 44. Point Comparison of Thickness of Cut for Undercutting (left) and Overcutting (right) Multiply by 2.52 to obtain Depth in cm.

Turbulence Analysis

Specific turbulence parameters also were investigated for this data analysis. The statistical derivation of turbulence can be found in many texts including Newman (1977) and Pope (2000) and relies on separating each velocity vector from the ADV data into a mean and fluctuating part :

$$u_i = \overline{u}_i + u_i' \tag{107}$$

where the bar notes the mean value and u' is the fluctuating component [LT^{-1}].

Substituting into the Navier Stoke's equation, the cross-correlation terms remain with the mean statistics. The cross-correllation terms are called the Reynold's stress tensor [$ML^{-1}T^{-2}$] :

$$\tau_{reynolds\_ij} = \overline{-\rho_f u_i' u_j'} \tag{108}$$

It is also possible to calculate turbulence intensity and concentration flux for each velocity component. The turbulence intensity (dimensionless) for each velocity component is

$$I = \frac{\sqrt{\overline{u_i'^2}}}{\overline{u_i}} \tag{109}$$

and the turbulent concentration flux [$ML^{-2}T^{-1}$] is

$$\vec{q} = u_i' c' \tag{110}$$

where c' is the fluctuation from the mean concentration [ML^{-3}] .

The specific variables of turbidity, turbulence intensity for the *V* and *W* velocity components, and concentration flux for the *V* and *W* velocity components were analyzed.

Tables C1-C15 display mean, standard deviation, and maximum values of these variables for all test cases (Appendix C). The specific variables analyzed included turbulence intensity for the *V* and *W* velocity components and concentration flux for the *V* and *W* velocity components. The mean velocity field for each test case was created and can be found in Appendix D. Examples of the mean velocity field can be seen for Case 1A (Figure 45) and Case 1B (Figure 46).

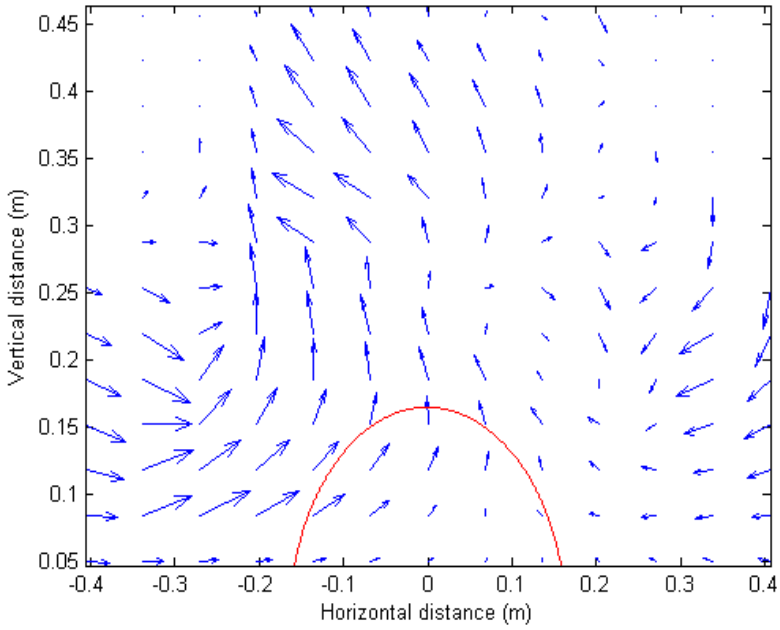

Figure 45. Spatial Map of Velocity Field (m/s) for Case1A

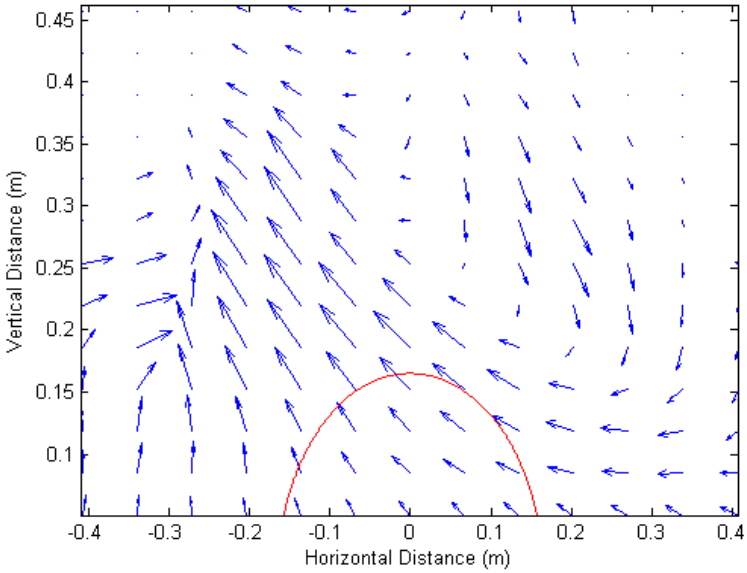

Figure 46. Spatial Map of Velocity Field (m/s) for Case 1B

When examining these velocity fields spatial maps were also created of the velocity field in relation to the cutter tip speed ratio. The purpose of this investigation was to understand if the velocity field could be directly scaled to the cutter tip speed when predicting flow fields for different cutter speeds. For instance, if the cutter speed was increased by a certain percentage, would the flow velocities at specific points also increase by that percentage? In this case, the cutter tip speed ratio is defined as:

(111)

Review of the cutter tip speed ratio spatial maps (Appendix D) shows similar ratios of velocities for *V* and *W* in the flow field when the cutter tip speed is adjusted. Because cutter tip speed ratio values were similar for different cutter speeds, it is

assumed that the scaling of the flow field for the numerical model discussed in Chapter VII can be directly proportional to the cutter tip speed ratio.

Spatial maps of turbulence intensity for Case 1A (Figure 47) and Case 1B (Figure 48) were created as well as the concentration flux for Case 1A (Figure 49) and Case 1B (Figure 50). These maps represent the turbidity generation mechanisms created during the testing period. It is important to note that not all data point collection could be obtained for the twelve inch cut. This is due to the possibility of damage to the ADV and OBS sensors when placing them so close to the sediment bed.

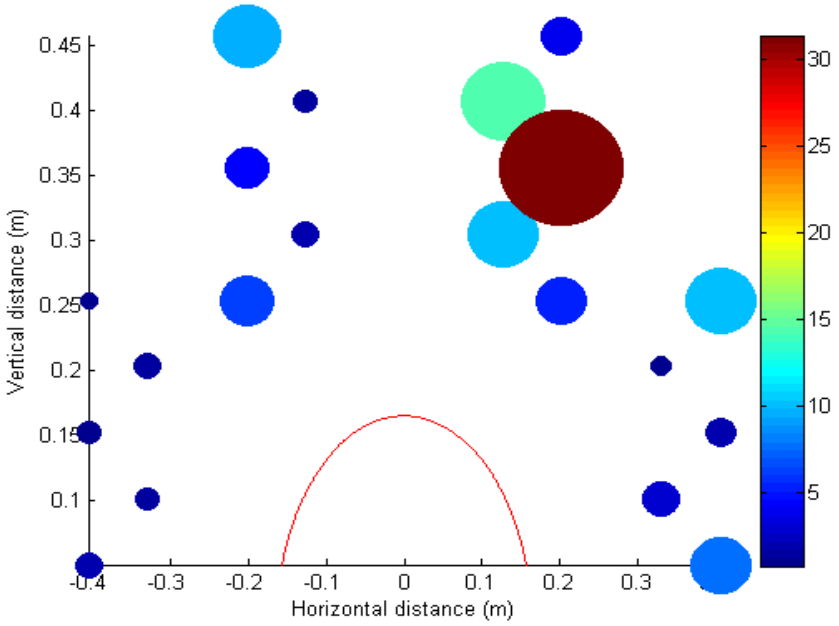

Figure 47. Spatial Map of Turbulence Intensity of Velocity *V* for Case1A

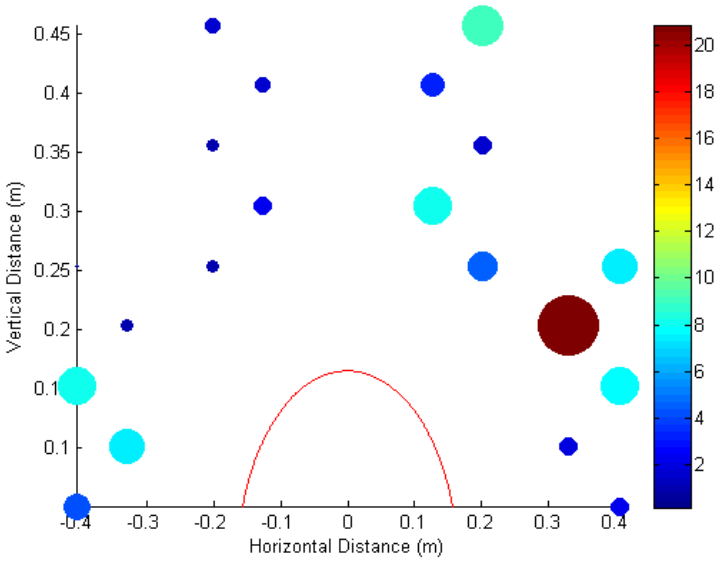

Figure 48. Spatial Map of Turbulence Intensity of Velocity *V* for Case1B

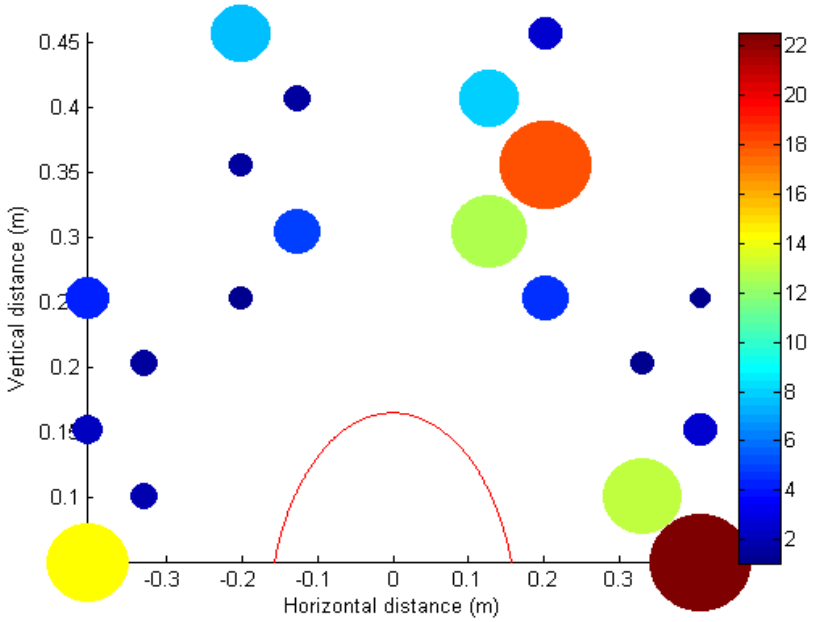

Figure 49. Spatial Map of Turbulence Intensity of velocity *W* for Case1A

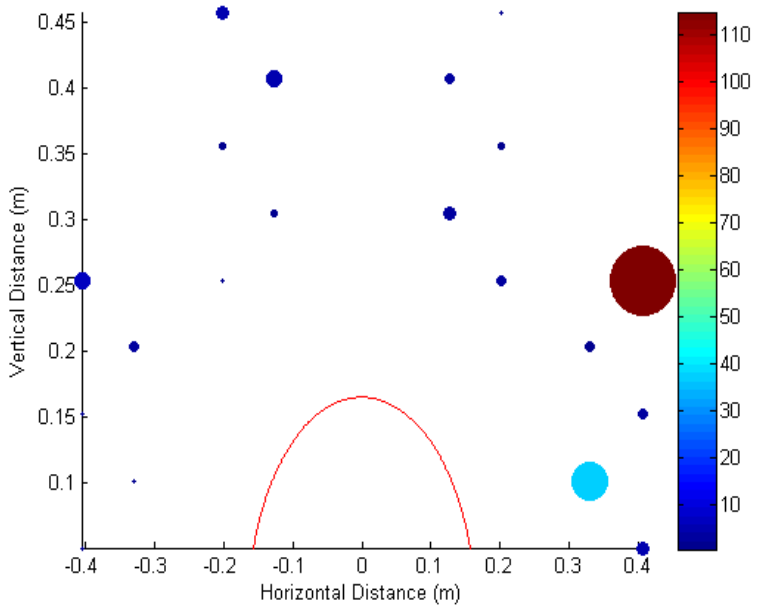

Figure 50. Spatial Map of Turbulence Intensity of Velocity *W* for Case1B

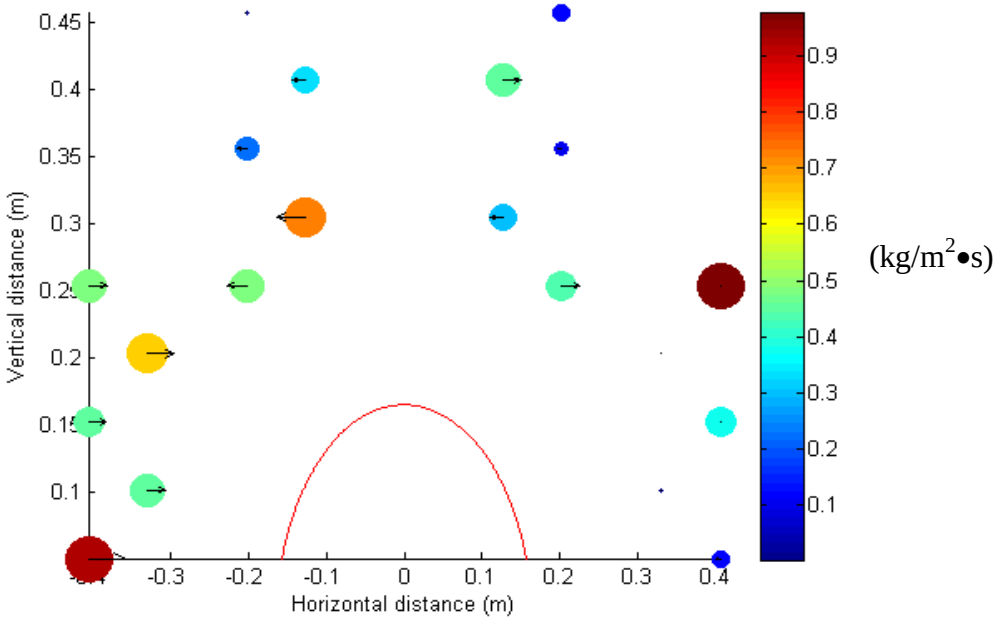

Figure 51. Spatial Map of Concentration Flux of Velocity *V* for Case1A

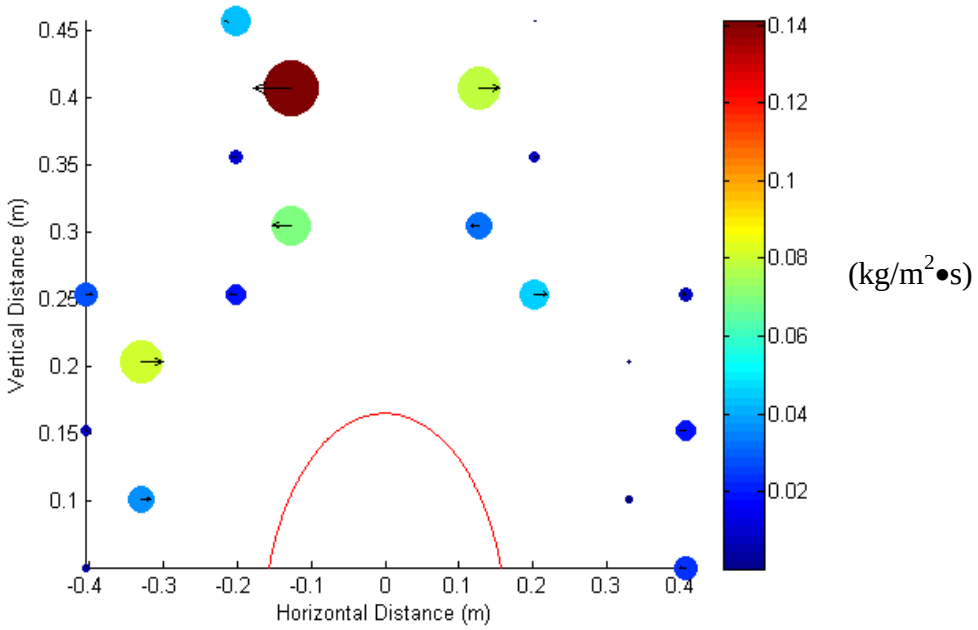

Figure 52. Spatial Map of Concentration Flux of Velocity *V* for Case1B

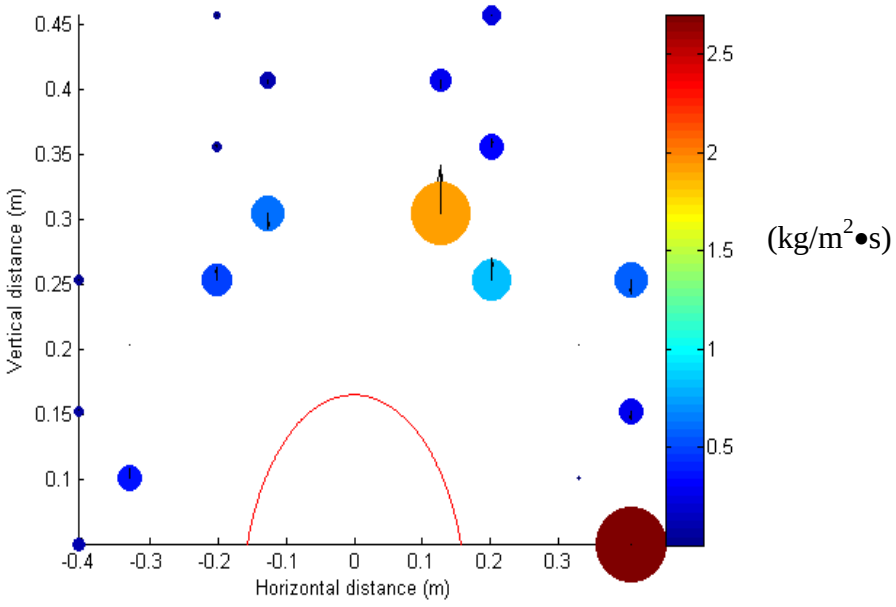

Figure 53. Spatial Map of Concentration Flux of Velocity *W* for Case1A

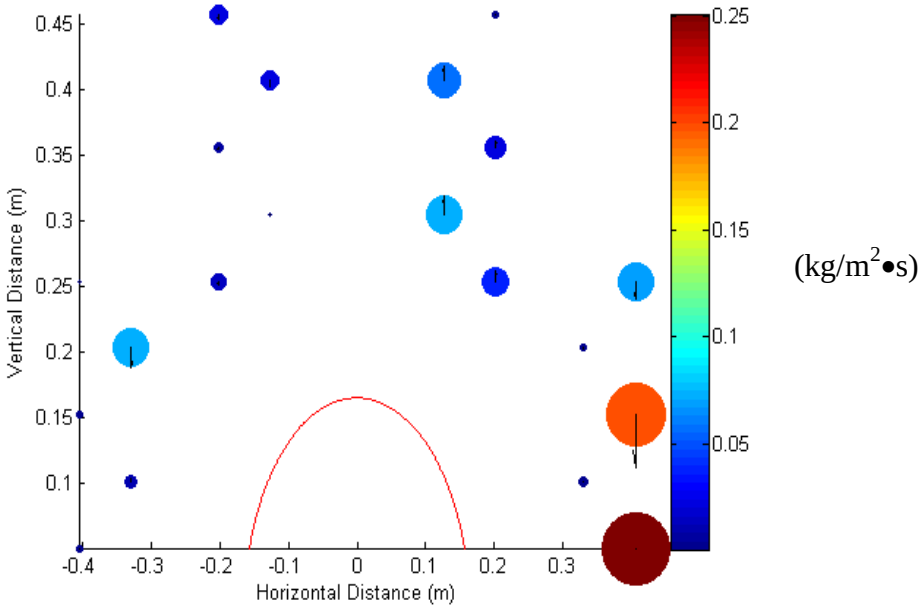

Figure 54. Spatial Map of Concentration Flux of Velocity *W* for Case 1B

Undercutting and Overcutting

In most cases, larger mean and maximum turbidity values were seen for undercutting testing. No major differences were seen for turbulence intensity for the *V* component of velocity between undercutting and overcutting. It was found that turbulence intensity for the *W* component of velocity was generally stronger for overcutting. However, turbulence intensity for the *W* component was stronger for undercutting when comparing Case 4A to Case 4B (slow rpm) and Case 7A to Case 7B (full cut).

When examining the effect of cut type on the concentration flux, the data consistently shows a stronger concentration flux in the *V* velocity component for undercutting. This mainly occurs at points 11-15 and is in the region that sees a greater

amount of washing during undercutting testing. Undercutting also produced the largest amount of concentration flux for the *W* velocity component for all tests.

Flow Rate Comparison

In general, all three cases follow the general pattern of the highest turbidity values existing within one cutter diameter from the edges of the cutter. The spatial orientation of the turbidity generation surrounding the cutter for all three flow rates show a general pattern where the highest turbidity and turbulence intensity usually occur at points 1-4 for undercutting and points 1-4 and point 11 for overcutting.

The flow rate comparison showed that in the undercutting scenario the majority of points showed minimum turbidity at 200 gpm. This is counterintuitive to the idea that an increase in suction flow rate is expected to cause a decrease in turbidity. However, the maximum value of turbidity for Case 1, Case 2, and Case 3 did tend to decrease slightly as the flow rate increased for undercutting. The turbulence intensity for the *V* velocity component decreased as flow rate increased while the turbulence intensity for the *W* velocity component had the lowest mean value but the highest single value at point 2 for the 200 gpm case of undercutting. No major difference was seen for turbidity and turbulence between the overcutting cases of Case 1B, Case 2B, and Case 3B.

Data values for the concentration flux in the *v* direction for Case 1A, Case 2A, and Case 3A tended to show a decrease in concentration flux as flow rate increased. It is also found that Case 1A displays a much larger value of concentration flux in the *V* direction than Case 2A and Case 3A. This may be due to the increase in suction reaching a threshold and preventing the sediment from traveling away from the cutter for

undercutting. The maximum concentration flux for the *W* component of velocity was seen in Case 2. Overcutting showed a slight decrease in the *V* concentration flux as flow rate increased and negligible effect on *w* concentration flux as flow rate increased.

Cutter Speed Comparison

Although the middle cutter speed (Case 1) shows some discrepancies, the results generally follow results from Hayes (1986) that state negligible turbidity generation is found two cutter diameters away from the tip blades in the vertical direction. The largest turbidity values are seen in Case 1A for undercutting and Case 5B for overcutting. It is interesting that the highest values for the undercutting tests were observed for the middle cutter speed. The overcutting data agrees with the general principle that turbidity generation increases when a threshold is reached for an increase in cutter speed.

Turbulence intensity for the *V* velocity component of undercutting displayed the largest values at the highest cutter speed followed by Case 4A and Case 1A. Overcutting testing showed the strongest V turbulence intensity at the slowest cutter speed Case 4B followed by Case 5B and Case 1B. Turbulence intensity for the *W* velocity component was maximum for the fastest cutter speed (Case 5) but showed higher values for Case 4A (slowest speed) than Case 1A. However, turbulence intensity for the *W* component of velocity was directly proportional to cutter speed for the overcutting testing.

Concentration flux for the *V* component of velocity was directly related to cutter speed for undercutting but did not display a specific correlation for overcutting. No significant difference was seen for concentration flux in the *W* direction on the basis of cutter speed for both undercutting and overcutting testing.

Thickness of Cut Comparison

The thickness of cut results showed a maximum resuspension of sediment for the 20.2 cm (8 in) cut. The 30.2 cm (12 in) cut represents more of a "full cut" and agrees with previous reports by producing the lowest turbidity levels. However, the single point 11 showed an unusually high turbidity value that skews the mean value of turbidity around the cutter. During the testing this point of interest is extremely close to the ground during the full cut and probably displays more of the mixing dynamics discussed by Burger (2003) rather than the turbulent diffusion dynamics that this dissertation is interested in examining. This skewed point was only produced during undercutting testing and did not occur during overcutting. The 10.1 cm (4 in) cut also produced less turbidity than the 20.2 cm (8 in) cut and in general still more than the 30.2 cm (12 in) cut. This 10.1 cm (4 in) cut represents a "shallow cut" whose dynamics are discussed by Crocket (1993). In this case, the amount of material picked up by the blade is still available to "washing" but the amount of material is simply less.

Turbulence intensity for the *V* component of velocity was highest for the shallow cut Case 6A for undercutting tests with little difference for Case 1A and Case 7A. Conversely, Case 6B produced the lowest values of *V* turbulence intensity for overcutting. The turbulence intensity for the *W* component of velocity increased directly as the thickness of cut increased for undercutting. The 20.2 cm (8in) cut showed the highest values of *W* turbulence intensity followed by the 30.2 cm (12in) cut and the 10.1 cm (4in) cut respectively.

The effect of cut thickness on the concentration flux in the *V* velocity direction increases as cut thickness increases for both overcutting and undercutting. Concentration flux in the *W* velocity direction also displayed a strong correlation with cutting depth. In this case, as the depth of cut increased the concentration flux also increased in the downward (negative) direction. This correlation is especially strong in the undercutting testing.

Uncertainty Analysis

The reported dredging variables of dredging production, resuspended sediment, turbulence intensity, and concentration flux stated in this chapter represent the characteristics of the testing environment. The variables are calculated through data analysis and analytical principles. To be confident in these calculations, it is important to understand the uncertainties that exist with the measurement instrumentation and how these uncertainties translate into the variables calculated for this dissertation.

When a result, F, is a function of a number of independently measured variables $x_1, x_2, x_3, \ldots, x_n$ the expression is stated:

(112)

If w_r represents the resultant uncertainty and $w_1, w_2, w_3, \ldots, w_n$ represent the uncertainty for all measured independent variables, then the uncertainty of the resultant is expressed (Holman, 1989):

(113)

This method was used to understand the uncertainties associated with the calculation of dredging production, turbulence intensity, and concentration flux. Table 10 shows the accuracy of the measurement equipment and Table 11 shows the uncertainties of the calculated variables of interest.

Table 10. Accuracy of Laboratory Equipment

Measurement Device	**Accuracy**
Flowmeter	$\pm$ 0.3 % measured velocity
Nuclear Density Guage	$\pm$ 1% of measured reading
Optical Backscatter Sensor	$\pm$ 2% of measured reading
Acoustic Doppler Velocimetry	$\pm$ 1% of measured velocity (Sontek) $\pm$ 0.5% of measured velocity (Nortek)

Table 11. Uncertainty of Calculated Variables

Variable	**Uncertainty**
Production	$\pm$ .052 m^3/hr
Turbulent Intensity	$\pm$ 1% of calculated intensity
Concentration Flux	.016 kg/m^2*s

The results above are calculated using nominal values 1.2 for slurry specific gravity, and 30 cm/s for ADV velocity. The optical backscatter sensor utilized a nominal value of 45 g/l. The results of this uncertainty analyses demonstrate that the variables calculated in this dissertation display a range of uncertainty that is within the limits of acecceptable values for this dissertation.

CHAPTER VII

CUTTER SUCTION RESUSPENSION NUMERICAL MODEL

The near-field sediment resuspension numerical model generated for a cutter suction dredge is a combination of a source term model and a two dimensional advection diffusion model. The mechanics and hydraulic environment of a cutter suction dredge creates a source of sediment resuspension. This source of sediment is then transported away from the source region by advection and turbulent diffusion in the near-field region.

Source Strength Model

The source strength for a cutter suction dredge is predicted through mathematical algorithms and is difficult to measure with conventional testing methods. Since the source strength model cannot be directly derived from field and laboratory measurements, the model requires assumptions based on the physics of the environment. These assumptions can be analyzed with laboratory and field data, but are difficult to define as absolute because of the complexities of the problem.

The source strength estimate for this source model utilizes the physics of sediment resuspension in the immediate geometry of the cutter head. The variables included in this region include the sediment characteristics, cutter head geometry, and dredge operation parameters of cutter speed, suction speed, and thickness of cut. The laboratory and field studies described in the previous chapters provide the basis for the proper numerical validation of the source model described in this chapter.

The source strength of resuspended sediment from the cutter suction dredging operation can be defined as the mass of sediment released temporally into the near-field water domain directly surrounding the cutter head. This amount of sediment released per second is defined as $\dot{m}_r$ [MT^{-1}] and does not include any sediment that existed as background resuspended sediment prior to dredging.

In order to calculate the term $\dot{m}_r$, it is necessary to estimate this parameter from the physics involved in and around the cutter head. Calculating $\dot{m}_r$ involves parameters including the depth of cut, the cutter speed, the cutter diameter, and the suction flow rate. These inputs allow the approximation of the sediment volume from each cut of the cutter blade. A representation of this volume can be seen in Figure 55 for an undercutting scenario.

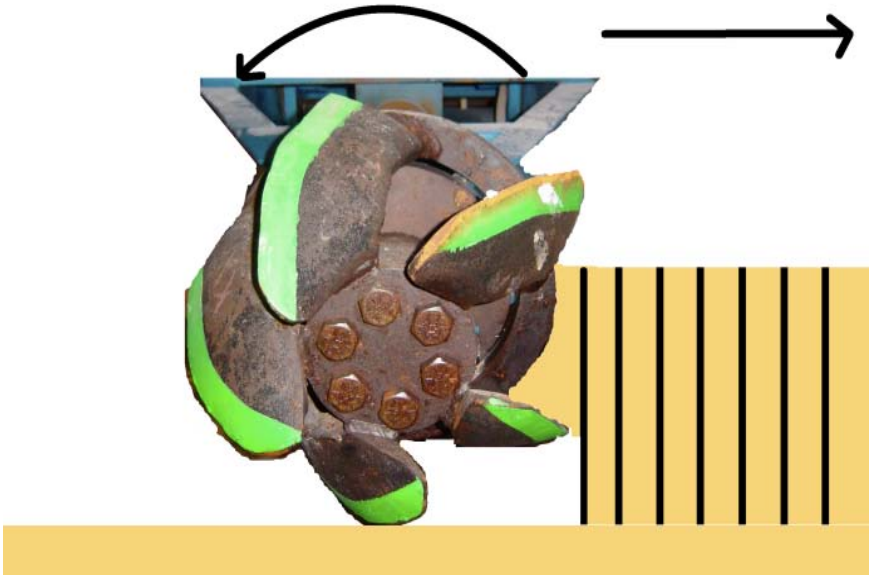

Figure 55. Sediment Volume per Cut.

For this numerical model a derivation of Miedema (1995) was used where:

$$\forall_C = R_C t_l L_C \cos(\theta) \tag{114}$$

$$t_l = \frac{V_s}{N_c} \tag{115}$$

Once this volume is known the cutter speed allows a calculation of the centrifugal force along the cutter blade. The other force on the volume of sediment is caused by the drag of the suction from the suction inlet of the dredge. The model for calculating the $\dot{m}_r$ term is able to discretize the volume of sediment along the cutter blade and calculate how much sediment is resuspended away from the suction zone of the cutter suction dredge.

Determining the equilibrium between the shearing force caused by the suction and the tangential force along the blade radius is calculated using a force balance equation; however, the complex interactions involved in this region better suit a predicted value using experimental data. For this model, experimental data from Mol (1977b) was used to predict the specific point along the cutter blade radius, R_{C_i}, where the sediment was defined as sediment contributing to the resuspension. In this case, the blade radius was discretized and the critical radius length was determined using:

Undercutting & Overcutting $$R_{C\_i} = \frac{0.48 V_i}{\omega} \tag{116}$$

A spatial layout of the amount of material released for resuspension can be seen in Figure 56. In this case the dredging setup is shown as well as the amount of material (green) released along the radius of the cutter.

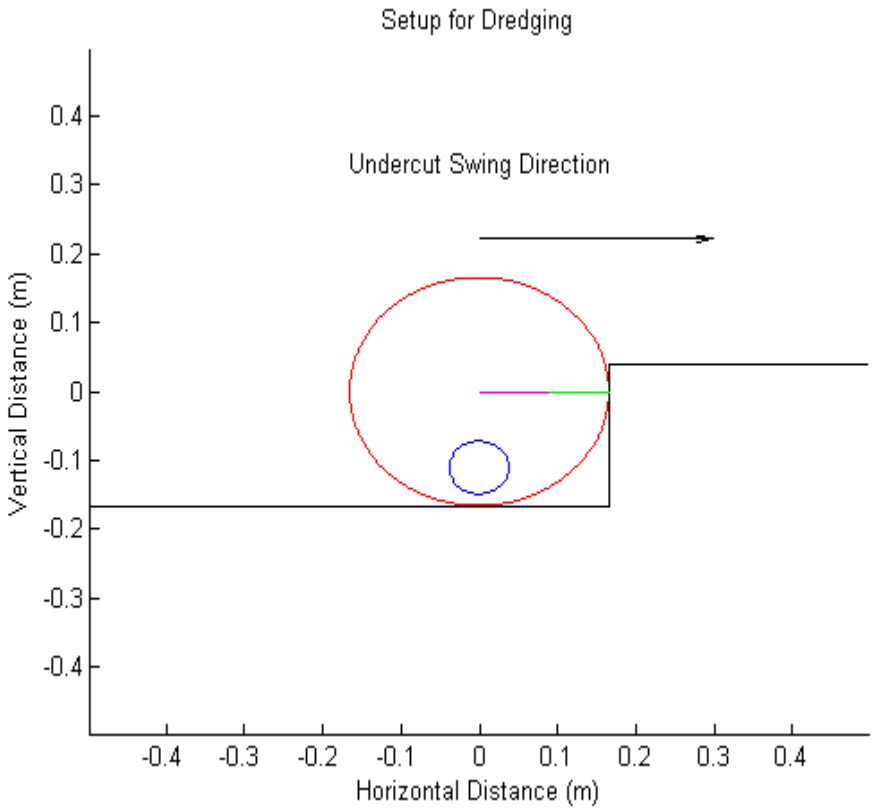

Figure 56. Dredging Setup Spatial Layout

Calculating the volume of material available for resuspension was completed with the equation:

$$\forall_r = \left(R_C - R_{C\_i}\right) t_l L_C \cos(\theta) \tag{117}$$

In order to quantify the source term per time step for the near-field model the approach taken in this work is to calculate the material available for resuspension along each cutter blade and determine the number of blade cuts (expressed as a ratio) per time step. This number of blade cuts is defined as:

$$N_{DT} = \frac{RPM * BN * dt}{60} \tag{118}$$

where *BN* is the number of blades on the cutter and *dt* is the time step [T]. The amount of sediment resuspended from one cutter blade is then multiplied by N_{DT} and then distributed over the region of concentration flux (region of washing). If *dt* is equal to 1 then:

$$\dot{m}_r = \forall_c C_s N_c \tag{119}$$

The amount of sediment that is released is quantified as the source term model and is entered into an advection diffusion model as a flux of sediment being released.

Concentration Flux

The flux of resuspended sediment is defined as the product of a concentration of resuspended sediment moving over a source surface or boundary with a specific velocity distribution. In order to determine the concentration flux, definitions are needed for the geometry of the boundary, the fluid movement at the defined boundary, and the concentration of resuspended sediment at the defined boundary. Therefore the following equation must be satisfied where:

$$\dot{m}_r = \int_{SA} \vec{q} \bullet \partial(SA) = \int_{SA} C\vec{V} \bullet \partial(SA) \tag{120}$$

Here *SA* is the surface area of the defined boundary [L^2].

Source Geometry

When modeling a source term, the source geometry is either defined as a point, line, or surface. The choice of geometry for the source term is dependent on the physics of the system, the laboratory and field data available as well as the computational time involved in solving the problem. It is difficult to place turbidity and velocity sensors extremely close to the cutter head to obtain true source data. Therefore, it is necessary to define the source geometry as an estimate of the exposed surface area of the cutter vulnerable to sediment release.

During the washing of the cutter blades, a concentration of resuspended sediment exists at the cutter blade region. This region of washing creates a resuspended source geometry with the surface geometry area S_F [L^2]. Collins (1995) states that the surface over which this source geometry exists is larger than the predefined S_F where the surface is expressed as:

$$S_F = (1 + k_c) D_C \left(1 + k_c'\right) L_C \tag{121}$$

where k_c and k_c' are size factors for the diameter and length of the cutter. Also, when the depth of the water becomes critical, the depth of water replaces $(1 + k_c) D_C$ for the source geometry calculation.

Crockett (1993) utilizes a source geometry based on a surface region defined over the length of the cutter as well as the height above the cutter where the sediment concentration is assumed to be negligible. The surface geometry for Crockett (1993) is defined as a plane perpendicular to the swing direction where:

$$S_F = L_c h_r \tag{122}$$

Crockett (1993) assumed a surface plane perpendicular to the swing direction and calculated the flux concentration based on the assumption:

$$\dot{m}_r = C_r L_c h_r V_s \tag{123}$$

The source strength model for this dissertation demonstrates the physics of washing by defining the surface region of release according to the perimeter of the blade that is actually exposed to washing and resuspends the sediment with any upward vertical motion. Therefore, the physics are similar to Collins (1995) in that an area of washing is determined for sediment release, but the area of washing neglects any component of the washing area which poses a negative vertical velocity component, believing that this washing would directly contact the sediment bed and would not contribute significantly to the upward vertical resuspension of sediment. The area of the surface region of release is therefore constrained to the upper half of the cutter and decreases as the thickness of cut increases.

It is important to remember that the surface region overlaps the perimeter of the top half of the cutter diameter and always travels the cutter length in the *x* direction. Therefore, the surface region of this numerical model is defined as:

$$S_F = L_c L_p \tag{124}$$

where L_p is length of the cutter diameter perimeter exposed to washing [L].

In order to convert the turbidity concentration into the standard [ML^{-3}] results, the flux must be modified in the model according to the equation:

$$C_R = \frac{\dot{m}_r}{L_c L_p V_t} \tag{125}$$

This calculation allows for the concentration to be discretized per unit length. The discretization of this concentration flux is discussed in the numerical domain section of this chapter.

Velocity Structure

Previous studies have used the velocity at the top of the cutter (Hayes, 1986; Crockett, 1993; Collins, 1995; Hayes et al., 2000) as a representation of the velocity structure at all points on the source geometry. In order to obtain a more accurate velocity structure, the velocity for this numerical model is discretized along the geometry and calculates the net velocity at each point along the washing region. An example of the velocity field is demonstrated for the source region for both a partial cut for overcutting (Figure 57) and a full cut for undercutting (Figure 58). Although the water velocity structure is also affected by eddies created by the ladder swing as well as the suction speed these influences are neglected at the cutter source geometry.

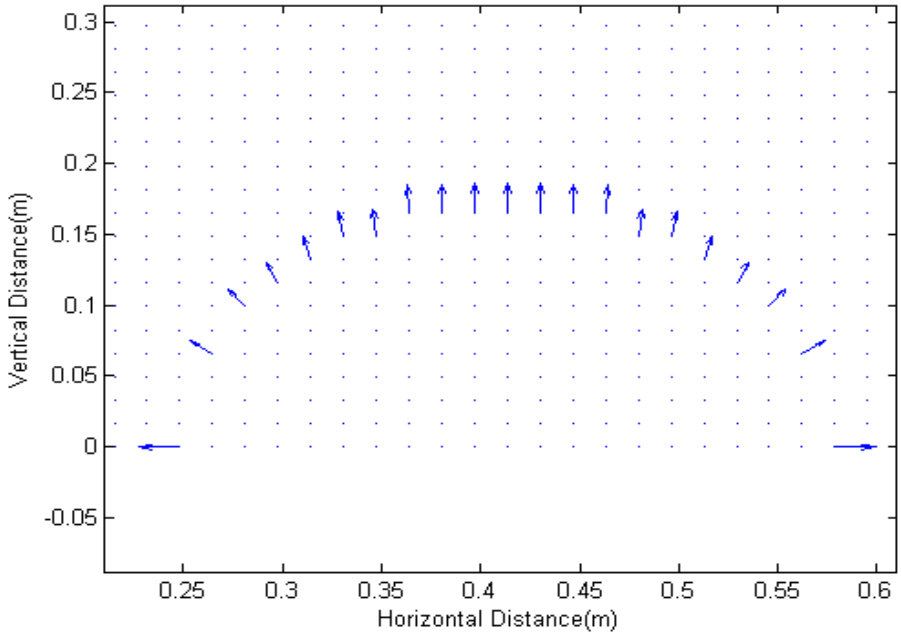

Figure 57. Velocity Field at Cutter for a Partial Cut (Overcutting).

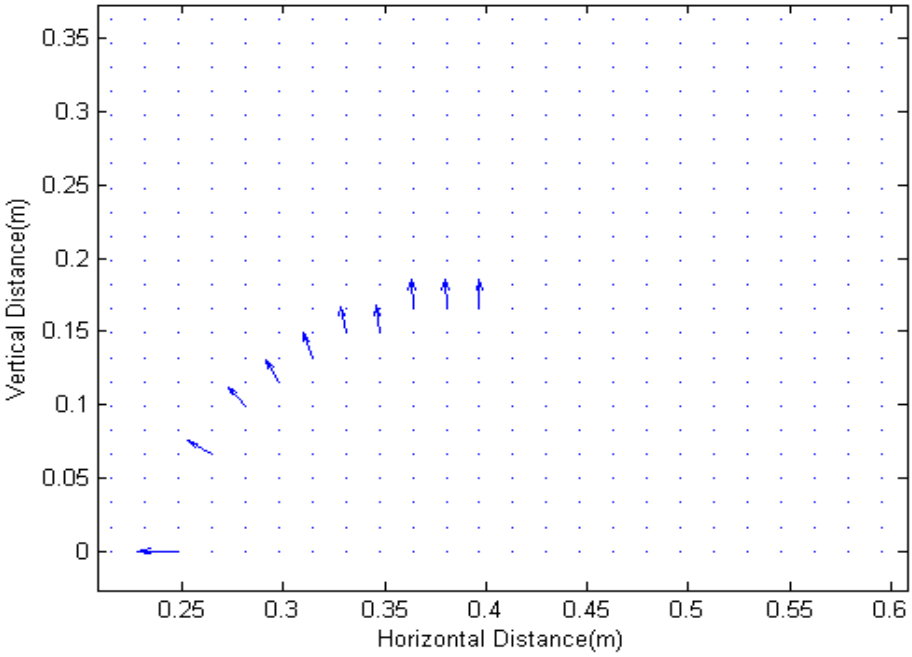

Figure 58. Velocity Field at Cutter for a Full Cut (Undercutting)

Source Concentration

In order to convert the mass source terms to a source concentration, the mass source strength must be divided by the source geometry and the velocity structure of that boundary. The concentrations predicted from these calculations are designed to represent the resuspended sediment concentrations that exist on the surface of the source geometry boundary.

Crockett (1993) assumed a surface plane perpendicular to the swing direction and calculated the flux concentration based on the assumption:

$$C_r = \frac{\dot{m}_r}{L_c h_r V_s} \tag{126}$$

For the numerical model presented in this dissertation the flux must be converted to the turbidity concentration according to the equation:

$$C_r = \frac{\dot{m}_r}{L_c L_p V_t} \tag{127}$$

This model represents the release of sediment due to the tangential speed of the cutter instead of the translational swing speed of the cutter used by Crockett (1993). Distribution of the concentration around the washing area of the cutter is designed to reflect a weighted release of sediment in the washing region. To accomplish this design, the mass of resuspended sediment is distributed linearly across the washing region where:

$$\dot{m}_r = \sum_i^N \dot{m}_{r\_i} \tag{128}$$

$$\dot{m}_{r\_i} = 0.5(i-1)^2(i-2)^2 \tag{129}$$

A spatial representation of this discretization can be seen in Figure 59.

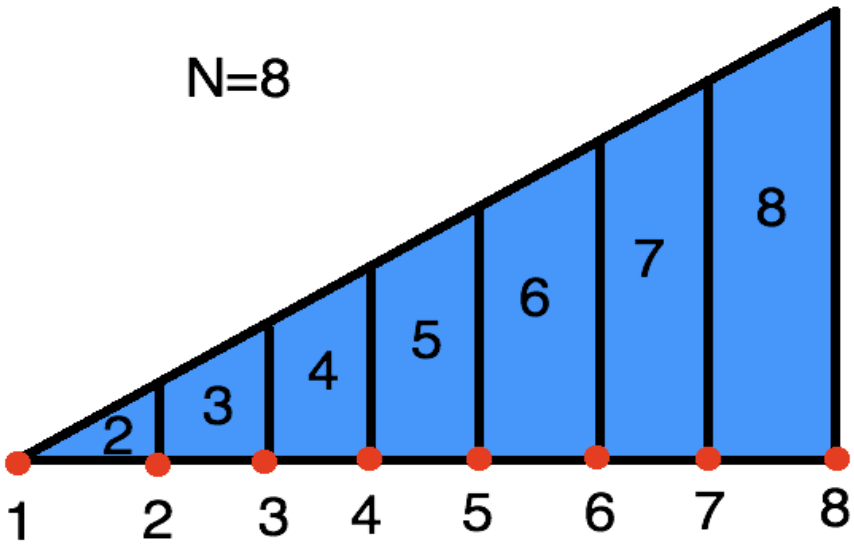

Figure 59. Method of Mass Distribution for Concentration Flux.

Advection Diffusion Model

The numerical solution reported is designed to predict the near-field spatial source approximation for sediment resuspension for a cutter suction dredge. The specific approach for this dissertation is to use a two dimensional finite difference method to show the evolution in time of sediment resuspension from the dredging operation. The resulting model provides a vertical profile of resuspension along the most turbid line in the swinging path of the cutter (above the back ring of the cutter).

The numerical finite difference model requires input parameters such as constant flux of sediment into the model, input velocity and diffusion, as well as the mean sediment diameter. These variables control the movement of the concentration of sediment.

The governing equations that describe the transport of resuspended sediment surrounding the cutter head are meant to reflect an extremely turbulent environment where the components of advection, turbulent diffusion, and the settling velocity of the sediment particles control the dynamics of the environment. Therefore, a transport equation in the vertical plane will be used. A full derivation of the transport equation can be found in Appendix B. The transport equation in three dimensions is:

$$\frac{\partial C}{\partial t} + U\frac{\partial C}{\partial x} + V\frac{\partial C}{\partial y} + W\frac{\partial C}{\partial z} = D_x\frac{\partial^2 C}{\partial x^2} + D_y\frac{\partial^2 C}{\partial y^2} + D_z\frac{\partial^2 C}{\partial z^2} \tag{130}$$

For this study, concern only deals with the most turbid line of the cutter head. This implies a steady condition in the *x* direction where:

$$\frac{\partial C}{\partial x} = 0 \tag{131}$$

It is thus possible to neglect the *x* direction and its components. Consequently, the transport equation in three dimensions reduces to a two dimensional equation in the *y-z* plane.

$$\frac{\partial C}{\partial t} + V\frac{\partial C}{\partial y} + W\frac{\partial C}{\partial z} = D_y\frac{\partial^2 C}{\partial y^2} + D_z\frac{\partial^2 C}{\partial z^2} \tag{132}$$

Furthermore, in order to compensate for the settling velocities of the resuspended sediment. Equation 132 must be further modified in the *z* direction where:

$$\frac{\partial C}{\partial t} + V\frac{\partial C}{\partial y} + W\frac{\partial C}{\partial z} - w_s\frac{\partial C}{\partial z} = D_y\frac{\partial^2 C}{\partial y^2} + D_z\frac{\partial^2 C}{\partial z^2} \tag{133}$$

Here w_s is the particle settling velocity [LT^{-1}] and is derived using equations from Dietrich (1982). It is important to note that this slip velocity prediction may have some discrepiencies in representing the true nature of the problem. This is due to the particle interactions that occur in the turbulent region of this problem.

Model Boundary Conditions

In order to solve the governing equation in the *y*-*z* plane, specific initial conditions and boundary conditions are needed. These include an initial condition with an initial zero concentration in the domain of the model as well as boundary conditions of the velocity and diffusion fields. The velocity field and diffusion field are defined prior to the time-stepping of the advection diffusion model, remain constant, and drive the model throughout the computation. Other boundary conditions include the constant flux input along the specific flux region in the bottom of the discretized domain as well as reflective boundary conditions along the surrounding borders.

Advection and Diffusion Calculations

In order to determine the advective and diffusive fields for the numerical model, laboratory data was implemented and then interpolated over the domain. Advective and diffusive matrices were completed by interpolating advective and diffusive fields for

laboratory tests based on cut type (undercutting and overcutting) and on the thickness of cut (Case 1A, Case 1B, Case 6A, Case 6B, Case 7A, Case 7B). After the specific advective and diffusive fields are interpolated for each test case, a second interpolation is used to create the advective and diffusive fields based on the thickness of cut ratio entered by the user. Since the Reynolds number for the cutter rotation is significantly large (100,000), scaling for the advective field neglects any viscous effects and is scaled directly to the cutter tip speed ratio. This ratio is defined as:

$$tsr = \frac{ptip}{mtip} \tag{134}$$

where *tsr* is tip speed ratio, *ptip* is prototype cutter tip speed [LT^{-1}], *mtip* is model cutter tip speed [LT^{-1}]. Scaling the diffusion field is completed with a separate approach and uses the dimensionless Peclet number:

$$Pe = \left(\frac{LV}{D_y}\right)_M = \left(\frac{LV}{D_y}\right)_P \quad , \quad Pe = \left(\frac{LW}{D_z}\right)_M = \left(\frac{LW}{D_z}\right)_P \tag{135}$$

In this case the length scale is the cutter diameter and the velocity is the cutter tip speed so that equation 135 becomes:

$$Pe = \left(\frac{D_c tipspeed}{D_y}\right)_M = \left(\frac{D_c tipspeed}{D_y}\right)_P \quad , \quad Pe = \left(\frac{D_c tipspeed}{D_z}\right)_M = \left(\frac{D_c tipspeed}{D_z}\right)_P \tag{136}$$

Finite Difference Method

Once the boundary and initial conditions have been set and the advective and diffusive fields have been interpolated equation 133 can be solved using a suitable finite

difference method. The approach used in this research utilizes a Modified Euler Method time-stepping approach (Burden and Faires, 2001):

$$C(y,z,t_{i+1}) = C(y,z,t_i) + \frac{dt}{2}\left[f(t_i, C(y,z,t_i)) + f((t_{i+1}, C(y,z,t_{i+1})) + dt^* f(t_i, C(y,z,t_i))\right] \quad (137)$$

Here the function f is the discretized solution to the transport equation:

$$f = -V(y,z)\frac{dC}{dy} - W(y,z)\frac{dC}{dz} - w_s(y,z)\frac{dC}{dz} + D_y\frac{d^2C}{dy} + D_z\frac{d^2C}{dz} \quad (138)$$

with the following discretization applied:

$$\frac{dC}{dy} = \frac{C_{j+1,k} - C_{j-1,k}}{2\Delta y} \quad (139)$$

$$\frac{dC}{dz} = \frac{C_{j,k+1} - C_{j,k-1}}{2\Delta z} \quad (140)$$

$$\frac{d^2C}{dy^2} = \frac{C_{j+1,k} - 2C_{j,k} + C_{j-1,k}}{\Delta y^2} \quad (141)$$

$$\frac{d^2C}{dz^2} = \frac{C_{j,k+1} - 2C_{j,k} + C_{j,k-1}}{\Delta z^2} \quad (142)$$

Numerical Diffusion and Model Stability

Numerical diffusion occurs from computational error created from the discretization in time and space. These errors occur in finite-difference schemes and lead to solution error where the correct solution is either over predicted or under predicted. Therefore, a correct finite-difference solution is obtained when the numerical diffusion is subtracted from the physical diffusion.

The discretization method used in the spatial domain for the finite-difference transport equation is the centered difference method in space. This method has been

shown to not produce numerical diffusion (Chapra, 1997). Conversely, the temporal discretization involved with the finite-difference scheme does produce numerical diffusion D_N [L^2T^{-1}] and can be calculated for example in the *y* direction as (Chapra, 1997).

$$D_N = \frac{V^2 \Delta t}{2} \tag{143}$$

Therefore, for the model produced, the maximum numerical diffusion was calculated using the cutter tip speed and was subtracted from the entire diffusive field for both D_y and D_z.

The stability of finite-difference solutions can also be affected by the advective component of the model. Positivity occurs when the advective movement is significantly greater than the diffusion involved in the same domain (Chapra, 1997). Positivity can be avoided if the Peclet number is less than 2.0. Mathematically, in the *y* and *z* directions:

$$P_E = \frac{V \Delta y}{D_y} < 2.0, \qquad P_E = \frac{W \Delta z}{D_z} < 2.0 \tag{144}$$

In order to satisfy this constraint, the maximum velocity is the cutter tip speed and the minimum diffusion from the D_y or D_z field is utilized in the calculation.

The Courant number is also often used to obtain stability when dealing with the advective component of the finite-difference scheme (Chapra, 1997). Here the Courant number is defined in both the y and z directions as:

$$Cour_y = \frac{V \Delta t}{\Delta y} \quad , \qquad Cour_z = \frac{W \Delta t}{\Delta z} \tag{145}$$

Values for the Courant number normally range between 0.5 to 1.0.

Stability can also be obtained from constraints imposed by diffusion. For instance, the diffusion number λ provides stability:

$$\lambda_y = \frac{D_y \Delta t}{\Delta y^2} \quad , \quad \lambda_z = \frac{D_y \Delta t}{\Delta z^2} \tag{146}$$

It is noted (Chapra, 1997) that a lambda value of 0.5 produces oscillating solution errors while a lambda value of 0.25 is effective in preventing solution error.

In order to obtain numerical stability for the finite-difference model created for this dissertation, a dual constraint was used by employing both the Courant number and the diffusion number. Model calculations used a Courant number of 0.5 and a diffusion number of 0.25. Test runs for this model are run with a mean diffusion for D_y and D_z that is calculated from the entire diffusive field. This allows a faster run time but at a cost to a more exact solution of the representation of the problem.

Numerical Model Refinement

Conservation of Mass

In order for the total mass input into the system to remain constant the flow field must follow the law of mass conservation. This law requires that the flow field be nondivergent and can be stated mathematically (Munson et al., 2002):

$$\nabla \bullet \vec{V} = 0 \tag{147}$$

where ∇ is the gradient operator and $\vec{V}$ is the velocity field. This equation assumes that the fluid is incompressible. The numerical model is a two dimensional model. Therefore, equation 147 can be simplified to obtain the expression:

$$\frac{\partial V}{\partial y} + \frac{\partial W}{\partial z} = 0 \tag{148}$$

The flow fields used to derive the model were all divergent and can be seen in Appendix E. Since all flow fields were divergent, mass was lost from the domain during every simulation. In order to compensate for the mass loss and adhere to the law of mass conservation, the total mass input into the system was monitored at each time step. This amount of mass was compared to the amount of mass considered in resuspension (in the domain of the model) at the current time step. Mass lost due to the divergent flow field was then returned to the numerical simulation domain. In this case, the amount of mass returned over the domain at each node depended on the current resuspended mass that existed at each node. This weighted distribution used to compensate for the mass loss was shown to equal the total mass lost at each time step when summed over the domain.

Model Validation

Validation of the numerical model to the laboratory and field data was conducted on all laboratory tests as well as the Calumet Harbor and New Bedford field data. In order to evaluate the effectiveness of the numerical model, a mean absolute error (MAE value) was evaluated. The MAE value can be defined as:

$$MAE = \frac{1}{N}\sum_{1}^{N}\frac{\left|x_i - f_i\right|}{\bar{x}} \tag{149}$$

Here x_i represents data set values, f_i represents model values at the same data point, and N is the number of samples. Table 12 displays the MAE values for all laboratory tests as well as the Calumet Harbor and New Bedford tests for undercutting and overcutting. The simulation time for each test is also reported Table 12. An MAE value of 0.0 represents a perfect fit of the numerical model data to the experimental data.

Table 12. MAE Values for All Simulations

Test	Simulation Time	MAE
Case 1A	20s	27.26
Case 1B	20s	11.29
Case 2A	20s	30.05
Case 2B	20s	21.44
Case 3A	20s	19.10
Case 3B	20s	5.20
Case 4A	20s	8.29
Case 4B	20s	4.80
Case 5A	20s	28.97
Case 5B	20s	21.49
Case 6A	20s	18.65
Case 6B	20s	4.16
Case 7A	20s	19.35
Case 7B	20s	8.73
Calumet Harbor (undercut)	30s	33.78
Calumet Harbor (overcut)	30s	27.29
New Bedford (overcut)	30s	45.66
New Bedford (overcut)	30s	48.97

In order to evaluate this model for $\dot{m}_r$ both laboratory tests and field tests were investigated. Since previous models estimate $\dot{m}_r$ across a vertical plane perpendicular to the swing direction, a mean was taken of concentration from the output of the model across a line one diameter above the cutter and one diameter across the cutter. This mean was then used to derive $\dot{m}_r$ according to Equation 125.

Table 13 displays the predicted values for Crockett (1993), Hayes et al. (2000) as well as the current numerical model of investigation for all of the laboratory tests for this dissertation as well as field tests for the Calumet Harbor and New Bedford sites. Examining the laboratory testing, the numerical model consistently produced lower values of $\dot{m}_r$ than values predicted from Crockett (1993). Comparing the results of the numerical model from this dissertation to Hayes et al. (2000) showed that the numerical model was particularly sensitive to suction intake V_i. Both Crockett (1993) and Hayes et al. (2000) demonstrate a stronger sensitivity to thickness of cut t_c than the numerical advection diffusion model. In this case, the coefficient involved with the influence of the exposed washing area for both Crockett (1993) and Hayes et al. (2000) are not designed to predict laboratory results and vary significantly to results from the advection-diffusion model tested in this dissertation.

Field data predictions for all three models showed stronger similarity than laboratory comparisons. This is due to the premise that both Crockett (1993) and Hayes et al. (2000) are primarily designed for field data. Although the mean source strength for overcutting was greater than undercutting in all numerical models, maximum values of turbidity at point locations agree with laboratory results and were greater for undercutting tests run by the numerical model (Appendix E). In this case the location and geometry of exactly how a mean source strength is determined is very important in the resultant source strength predicted by the numerical model.

Table 13. Sediment Resuspension $\dot{m}_r$ Values for All Simulations

TEST	CROCKETT	HAYES et al	HENRIKSEN
Case 1A	247.9	42.3	65.4
Case 1B	252.9	43.1	77.3
Case 2A	156.1	42.3	123.4
Case 2B	158.6	43.1	145.9
Case 3A	81.2	42.3	14.9
Case 3B	82.5	43.2	17.6
Case 4A	123.7	18.9	12.3
Case 4B	126.9	19.4	15.9
Case 5A	413.6	76.5	138.0
Case 5B	418.4	77.5	148.7
Case 6A	522.9	320.3	56.3
Case 6B	531.4	326.3	60.3
Case 7A	5.7	1.03	53.7
Case 7B	5.8	1.05	69.7
Calumet U	40.7	77.7	120.81
Calumet O	80.2	251.1	147.05
NewBedford U	40.5	284.7	305.92
New Bedford O	72.5	359.1	431.68

Although the model adequately predicts sediment resuspension from a cutter suction dredge, comparing the movement of the sediment plume in the model to the sediment plume recorded during laboratory testing reveals that the diffusive field for the numerical model is an underestimate of diffusion to laboratory predictions. In this respect the plume created numerically is mostly controlled by the advective environment. This is probably due to the averaging of the diffusive field. In this case, the averaging of the diffusive field smoothes the diffusive domain and may weaken the turbulent diffusion representation in critical regions of the model.

The diffusive field of this model is averaged so that the model can be run efficiently for the user community. Although simulations were created for a heterogeneous diffusive field and run successfully, the runtime for these simulations was extraneous. Therefore, it was decided that the model would be best suited to predict resuspended sediment with a homogenous diffusive field.

Model Structure and User Environment

The structure of the model development can be seen in the flowchart in Figure 60. The output of the model provides the spatial concentrations of resuspended sediment surrounding the cutter. Besides providing the development of the near-field spatial concentrations of resuspension surrounding the cutter, the model is also able to generate a point source located one diameter above the top center of the cutter.

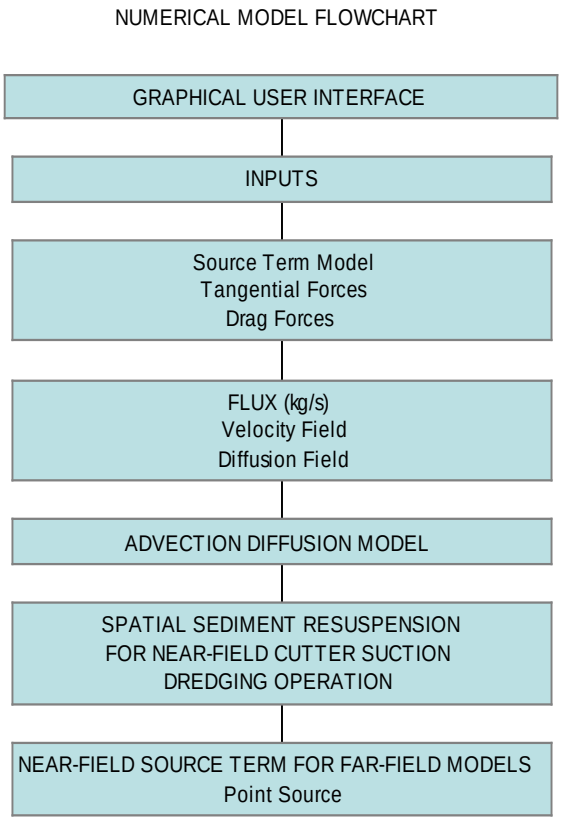

Figure 60. Numerical Model Structure

Graphical User Interface

The graphical user interface provides a location for the model user to enter the necessary variables of model input and distributes a direct visual output that is easy for the user to obtain. Components of the graphical user interface (GUI) can be seen in Figure 61 and include the dredging setup, the spatial near-field sediment resuspension concentration surrounding the cutter, and a far-field display. The far-field output uses the $\dot{m}_r$ mean point source approximation and the far-field equations from Kuo et al. (1985). A closer view of the far-field output can be seen in Figure 62. The GUI can be

easily opened by simply running the Matlab program NFCRM (Near-Field Cutter Resuspension Model.

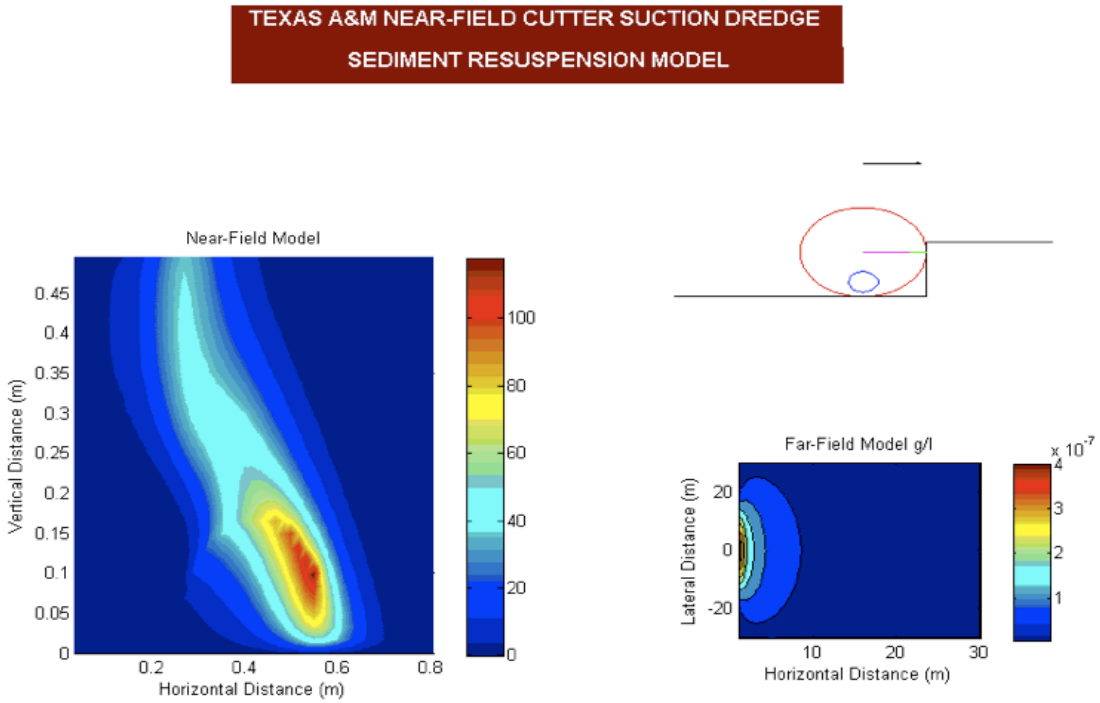

Figure 61. GUI Output for NFDRM Model

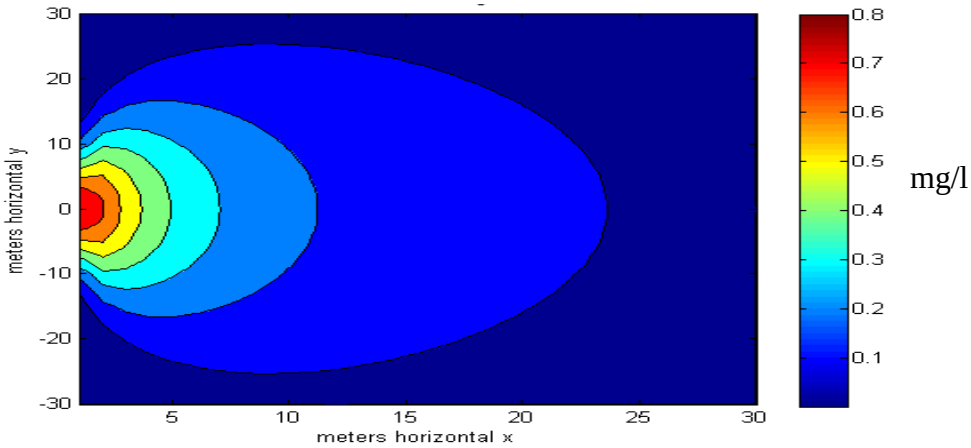

Figure 62. Far-Field Resuspension Output

CHAPTER VIII

CONCLUSIONS

The data collected from the dredge/tow carriage at the Haynes Coastal Engineering Laboratory are beneficial for understanding the resuspension of sediment created during cutter head dredging operations and are used in conjunction with cutter suction dredging field data to validate a near-field cutter head sediment resuspension numerical model. The ability to control the dredge/tow carriage from a PC allows for repeatable experiments in a laboratory setting and provides a more accurate method to identify the source term for a cutter suction dredging operation.

Undercutting consistently produced great spatial turbidity values than overcutting in the laboratory testing. An increase in suction flow rate was shown to increase production and decrease turbidity around the cutter head, but at the highest flow rate turbidity was shown to actually increase at specific spatial locations around the cutter. In general an increase in cutter speed led to an increase in turbidity, however, the increase in turbulence with cutter speed may also lead to a faster turbulent diffusion rate for some areas surrounding the cutter. The thickness of cut followed previous trends and produced less resuspension for a full cut versus a partial cut. Data for a “shallow cut” also was produced and showed less turbidity generation than partial cuts. This is probably due to less material being picked up by the cutter and being washed into the area surrounding the cutter. Cross correlation of both velocity and turbidity measurements were utilized to investigate the turbulence characteristics of surrounding the cutter head during dredging.

These results were used to determine the diffusion field for each specific laboratory test case.

A near-field numerical model was designed to predict the resuspension of sediment around the cutter head. The numerical model is composed of a source term model as well as an advection-diffusion model to predict the evolution in time of the resuspension of sediment during cutter suction dredging. Both the advective field and the diffusion field for the numerical model are derived from interpolation of laboratory data and the thickness of cut. Scaling of the velocity field is directly proportional to cutter tip speed while the scaling of the diffusion field is based on the Peclet number. The source term model is able to determine the amount of sediment suspended from the cutter blade based on a balance between the suction force and the tangential force from cutter rotation. The surface region for the flux of sediment is dependent on undercutting and overcutting and utilizes a weighted distribution over the washing region. The numerical model was compared to all laboratory testing cases as well as the Calumet Harbor and New Bedford cutter resuspension data and produced a suitable range of MRA values. Results agreed with previous numerical models by predicting a greater mean source term for overcutting but also agreed with laboratory testing by predicting greater point turbidity values at specific locations for undercutting.

It is noted that the numerical diffusive field used to predict the laboratory test cases is less than expected, especially for partial cuts. This is due to the use of a mean value used for each diffusion coefficient and is necessary for the numerical model to run in a reasonable amount of time.

Future Research

The possibilities for future studies using the dredge/tow carriage are widespread and also include cutter head swing speed variation, ladder angle for cutting, mud or clay cutting, water current effect on turbidity, bank height effects on sediment flow to the cutter head, and production versus spillage testing. Future testing should also focus on different cutter head types as well as different adaptors to the cutter head to prevent resuspension.

Although the mixture forming process has been initially reviewed by several authors (Slotta, 1968; Mol, 1977a; Burger, 2003), future studies should also attempt to model the particle-particle dynamics in this highly complex environment. Future understanding of the mixture forming process would greatly increase the exactness of the source term and allow for a better understanding of the flux into the resuspension domain.

Because the resuspension of sediment does not only occur in two dimensions it would also be very beneficial to sample in three dimensions and develop a three dimensional numerical transport model. This would be especially useful in examining dredging in water currents. All of these research topics would help further the understanding of dredging and help the economy as well as the environment.

REFERENCES

American Public Health Association (APHA). (2001). *Standard Methods for the Examination of Water and Wastewater*, 20th ed., Washington , DC.

Andrassy, C. and Herbich, J., (1988). "Generation of Resuspended Sediment at the Cutterhead," *The Dock and Harbour Authority*, 68, (797), 207-216.

Brahme, S. B. (1983). "Environmental Aspects of Suction Cutterheads." Dissertation, Ocean Engineering Program, Civil Engineering Department, Texas A&M University, College Station, TX.

Brahme, S.B., and Herbich, J.B. (1986). "Hydraulic Model Studies for Suction Cutterheads." *Journal of Waterway, Port, Coastal and Ocean Engineering*, ASCE, 112, (5), 590-607.

Bridges, T.S., Ells, S., Hayes, D., Mount, D.,Nadeau, S.C., Palermo, M.R., Patmont, C., and Schroeder, P. (2008). "The Four R's of Environmental Dredging: Resuspension, Release, Residual, and Risk." *Technical Rep. No. ERDC /EL TR-08-4* Dredging Operations and Environmental Research Program, Vicksburg, MS.

Buckingham, E. (1914). "On Physically Similar Systems: Illustrations of the Use of Dimensional Equations." *Phys. Rev.* 4, (4), 345-376.

Burden, R., and Faires, J., (2001) *Numerical Analysis.* Wadsworth Group., Pacific Grove, CA.

Burger, M. (2003). "Mixture Forming Processes in Dredge Cutterheads." Ph.D. Dissertation, Delft University of Technology, The Netherlands.

Burger, M.D. (1997). "Mixture Forming in a Cutterhead." *Proc. of the Central Dredging Congress Dredging Days,* CEDA, Amsterdam, The Netherlands.

Chapra, S.C., (1997). *Surface Water Quality Modeling.* McGraw-Hill, New York, NY.

Collins, M.A. (1995). "Dredging-Induced Near-Field Resuspended Sediment Concentrations and Source Strengths," *Miscellaneous Paper D-95-2,* US Army Engineer Waterways Experiment Station, Vicksburg, MS.

Conner, C.S. and De Visser A.M., (1992). "A Laboratory Investigation of Particle Size Effects on an Optical Backscatter Sensor." *Marine Geology* 108, 151-159.

Corey, A.T.,(1949) “Influence of Shape on the Fall Velocity of Sand grains.” MS thesis, Colo. A&M College, Fort Collins.

Crockett, T.R. (1993). “Modeling Near-Field Sediment Resuspension in Cutter Head Suction Dredging Operations.” M.S. thesis, University of Nebraska-Lincoln.

Dietrich, W. E. (1982). “Settling Velocity of Natural Particles.” *Water Resources Research*. 18, (6), 1615-1626.

Downing, J. (2005). *User Manual for the OBS-3 Sensor.* D&A Instruments, Logan, UT.

DiGiano F., Miller, C., and Yoon, J., (1993). “Predicting Release of PCBs at Point of Dredging,” *Journal of Environmental Engineering*, 119. (1),72-89, January.

Glover, G. J. and Randall, R. E. (2004). “Scaling of Model Hydraulic Dredges with Application to Design of a Dredge Modeling Facility,” *Journal of Dredging Engineering*, Western Dredging Association (WEDA), 6, (2), September.

Glover, G.J. (2002). “Laboratory Modeling of Hydraulic Dredges and Design of Dredge Carriage for Laboratory Facility.” M.S. thesis, Texas A&M University, College Station, TX.

Hayes, D. (1986). “Development of a Near Field Source Strength Model to Predict Sediment Resuspension from Cutter Suction Dredges,” *M.S. thesis*, Mississippi State University, Starkville, MS.

Hayes, D.F. and Je, C.H. (2000). *DREDGE Module User’s Guide.* Department of Civil and Environmental Engineering, Univeristy of Utah, Salt Lake City, UT

Hayes, D.F.and Wu, P. (2001). “Simple Approach to TSS Source Strength Estimates,” *Proc. of the WEDA XXI and TAMU 33 Annual Conference*, Houston, TX, June 25-27, 2001.

Hayes, D.F., Crockett, T.R., Ward, T.J., and Averett, D. (2000). “Sediment Resuspension during Cutter head Dredging Operations.” *Journal of Waterway, Port, Coastal, and Ocean Engineering*, 126(3), May/June 2000, ASCE.

Hayes, D., Raymond, G., and McLellan, T. (1984). “Sediment Resuspension from Dredging Activities,” *Proc. of the ASCE Specialty Conference, Dredging 84’*. American Society of Civil Engineers, Clearwater Beach, FL.

Henriksen, J. (2009). "Investigation of Turbulence Characteristics for Model Cutter Suction Dredging Operation," *PIANC De Paepe Williams Award,* Pittsburg, Pennsylvania, July 2009.

Henriksen, J. and Randall, R. (2008). "Laboratory Near-Field Turbidity Data for a Cutter Suction Dredging Operation," *Proceedings of the Western Dredging Association Twenty-eighth Technical Conference and Thirty-ninth Annual Texas A&M Dredging Seminar,* St. Louis, MI.

Henriksen, J., Randall, R., DeJong, P., and Sonye, S. (2007). "Initial Experiments and Data Acquisition for the Model Dredge Carriage," *Proc. of 18th World Dredging Congress,* Lake Buena Vista, FL.

Herbich, J. (2000). *Handbook of Dredging Engineering*. McGraw-Hill, New York, NY.

Herbich, J. and DeVries, J. (1986). "An Evaluation of the Effects of Operational Parameters on Sediment Resuspension During Cutter head Dredging Using a Laboratory Model Dredge System," *Report No. CDS 286,* Center for Dredging Studies, Texas A&M University, College Station, TX.

Herbich, J.B., and Brahme, S.B., (1983). "Literature Review and Technical Evaluation of Sediment Resuspension During Dredging," *Report No. COE-266* Ocean and Hydraulic Engineering Group, Texas A&M University, College Station, TX.

Holman, J. (1989). *Experimental Methods for Engineers*. 5th edition. McGraw-Hill, New York, NY.

Huston, J.W., and Huston, W.C. (1976). "Techniques for Reducing Turbidity with Present Dredging Procedures and Operation." *Technical Report D-76-4*, U.S Army Engineer Waterways Experiment Station, Vicksburg, MS.

Je, C.H. (1998). Modeling the Transport of Flocculating Suspended Sediments Resulting from Dredging Operations. Ph.D. Dissertation, University of Utah, Salt Lake City, UT.

Joanknecht, L.W.F. (1976). "A Review of Dredge Cutter Head Modeling and Performance." *Proc. of the Seventh World Dredging Congress, WODCON VII*, San Francisco, CA, pp. 995-1016.

Kuo, A. Welch, C., Lukens, R. (1985). "Dredge Induced Turbidity Plume Model," *ASCE Journal of Waterway, Port, Coastal, and Ocean Engineering*, 111, (3), May.

McLellan, T.N., Havis, R.N., Hayes, D.F., Raymond, G.L., (1989). "Field studies of sediment resuspension characteristics of selected dredges." *Technical Report HL-89-9*, US Army Engineer Waterways Experimental Station, Vicksburg, Miss.

Miedema, S.A. (1995). "Production Estimation Based on Cutting Theories for Cutting Water Saturated Sand." *Proc. of the 14th World Dredging Congress*, WODCON XIV, Amsterdam, the Netherlands, pp. 255-275.

Miedema, S.A. (1987). "Calculation of the Cutting Forces When Cutting Water Saturated Sand." Ph.D. Dissertation at Delft University of Technology, Delft, The Netherlands.

Miltenburg, C.J.M. (1983). "Flow and Mixture Forming in Large Cutterheads." Laboratory of Soil Transportation, Delft University of Technology, Delft, The Netherlands.

Mol, A. (1977a). "Flow In and Around a Cutter Head: Part II, Rotating Freely in Water: Injections with Dye." Delft Hydraulics Laboratory, Delft, The Netherlands.

Mol, A. (1977b). "Flow In and Around a Cutter head: Part III, Flow in a Cutter head With an Artificial Breach, Injections with Pieces of Plastic." Delft Hydraulics Laboratory, Delft, The Netherlands.

Mol, A. (1977c)."Cutting Tests in Sand." Delft Hydraulics Laboratory, Delft, The Netherlands.

Montgomety, R. and Raymond, G. (1984) "Overview of Corps Research Program on Dredging Contaminated Sediments," *Proc. of the 8th U.S./ Japan Experts Meeting*, Tokyo, Japan, U.S. Army Engineer Water Resources Support Center, Ft. Belvoir, VA.

Moret, G.E. (1977). "Flow Around and In a cutter head Part IV. Flow Around a Cutter Head Placed in an Artificial Bank; Injections of Coarse Sand, Fine Gravel and Artificial Pieces of Clay." Delft Hydraulics, Delft, The Netherlands.

Munson, B.R., Young, D.F., Okiisi, T.H., (2002). *Fundamentals of Fluid Mechanics*. Wiley & Sons, Inc. Fourth Edition, New York, NY.

Nakai, O. (1978). "Turbidity Generated by Dredging Projects," *Proc. of the 3rd U.S. / Japan Experts Meeting*, US Army Engineer Resources Support Center, Ft. Belvoir, VA.

Newman, J.N. (1977). *Marine Hydrodynamics*. MIT Press, Cambridge, MA.

Pequengat, W.E., Smith, D.D., Darnell, R.M., Presley, B.J., and Reid, R.O. (1978). "An Assessment of the Potential Impact of Dredged Material Disposal in the Open Ocean," *Technical Report D-78-2*. U.S. Army Engineer Waterways Experiment Station, Vicksburg, MS.

Pope, S. (2000). *Turbulent Flows*. Cambridge University Press, New York, NY.

Powers, M.C. (1953). "A New Roundness Scale for Sedimentary Particles," J. *Sediment. Petrol.* 23,117-119.

Randall, R., DeJong, P., Sonye, S., Krippner, N., and Henriksen, J. (2005). "Laboratory Dredge Carriage for Modeling Dredge Operations," *Proc. of the Western Dredging Association Twenty-fifth Technical Conference and Thirty-seventh Annual Texas A&M Dredging Seminar*, Editor, New Orleans, LA.

Randall, R. E., Edge, B. L. and Cox, D. T. (1998). "Laboratory Needs for Dredging and Dredged Material Disposal," *Proc. of 15th World Dredging Congress*, 17-31, Las Vegas, NV.

Raymond, G. (1984). "Techniques to Reduce the Sediment Resuspension Caused by Dredging," Miscillaneous Paper HL-84-3, US Army Engineer Waterways Experiment Station, Vicksburg, MS.

Richardson, J.F. and Zaki, W.M. (1954). "Sedimentation and Fluidization: Part I." *Trans. Inst. Chem Engrs.*, 32, 35-53.

Slotta, L.S. (1968). "Flow Visualization Techniques Used in Dredge Cutter Head Evaluation." *Proceedings of WODCON II*, Rotterdam, The Netherlands, 56-77.

Slotta, L.S., (1974) "Cutterhead Research and Standardization," *Proc. of the Fifth World Dredging Conference*, WODCON V, Hamburg,Germany, 437-474.

Slotta, L.S., Joanknecht, L.W.F., Emrich, R.K., (1977). "Influence of Cutterhead Height of Dredge Production." *Second International Symposium on Dredging Technology*, Texas A&M University, College Station, TX.

Turner, T. (1996). *Fundamentals of Hydraulic Dredging.* American Society of Civil Engineers, Reston, VA.

USACE (1990). "New Bedford Harbor Superfund Pilot Study." *Evaluation of Dredging and Dredge Material Disposal*. United States Army Corps of Engineers, New England Division.

Wilson, K. C., Addie, G.R., Sellgren, A., and Clift, R., (1996). *Slurry Transport Using Centrifugal Pumps.* Champman and Hall Publishing. Second Edition.

Wu, P.Y. and Hayes, D.F., (2000). "Verification and Enhancement of TSS Source Strength Models for Cutter Dredges." *World Dredging, Mining, and Construction*, 36, (6), August.

Wu. P.Y. (2001). "Verification and Modification of TSS Source Strength Models for Hydraulic Cutter Dredging Operations." *Proc. of the WEDA XXI and TAMU 33 Annual Conference*, Houston, TX.

Yagi, T., Miyazaki, S., Yashikumi, O., Koreishi, A., Sato. Y., Saito, M., Nakazono, Y., Masuda, K., Koro, S., Shibuya, Y., Kikuchi, K., and Kikuya, T. (1975). "Effect of Operating Conditions of Hydraulic Dredges on Dredging Capacity and Turbidity," *Technical Note 228*, Port and Harbour Research Institute, Ministry of Transport, Yokosuka, Japan.

APPENDIX A

MANUAL FOR CONDUCTING DREDGING USING THE FACILITIES AT THE HAYNES COASTAL ENGINEERING LABORATORY

The purpose of this manual is to describe methods used to conduct dredging research using the cutter suction dredge/tow carriage at Texas A&M University. The manual is designed to cover both the hardware and software issues for dredging research as well as the laboratory strategies utilized for dredging in this laboratory to date. Although this manual provides a general layout of the methods used in the laboratory, it is important to realize that it should be read and used in a flexible manner for each specific laboratory investigation and that the material herein does not obligate the writer or administration for any liabilities that may exist when following this manual to conduct specific investigations. It is important to remember that although the manual provides a general layout for conducting dredging research, each laboratory investigation is different in its own right and specific alterations may have to be made from this general strategy described.

As to date, the equipment used for dredging research includes the dredge/tow carriage, the dredging hopper, and the sediment-slurry separator. The dredge/tow carriage has measuring sensors including a flow meter, a nuclear density gauge, a horizontal location laser, pressure sensors to measure pump pressure and force sensors to measure cutting forces. Other instruments used in the laboratory include the laser depth

measuring system, the OBS (optical backscatter sensors), the ADV (Acoustic Doppler Velocimetry) sensors, and pressure sensors. Camera equipment used in the dredging research included an underwater camera as well as a dvd recorder placed in the sediment pit recording windows and hand held cameras. A layout of the dredging hardware and a layout of the sensors and cameras can are seen in Figure A1 and Figure A2 respectively. The following paragraphs describe the operation and layout of all of this equipment so that future engineers can easily conduct research in the laboratory.

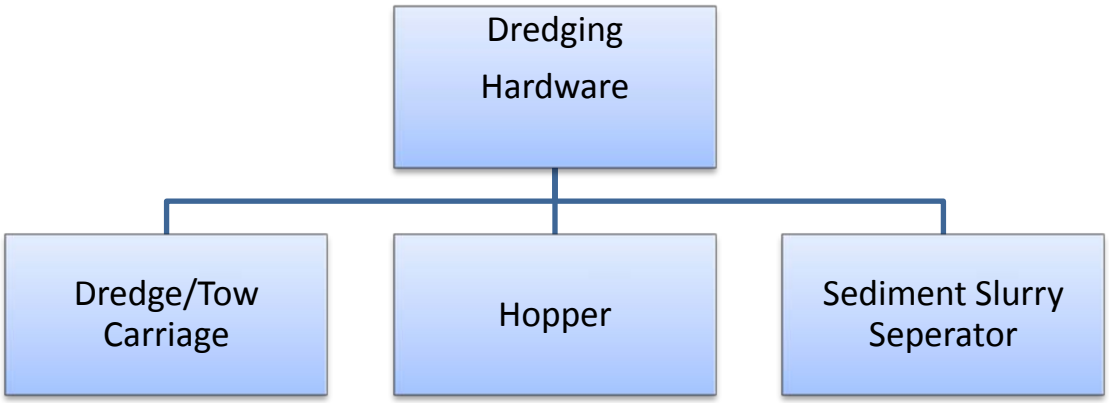

Figure A1. Dredging Hardware in the Laboratory

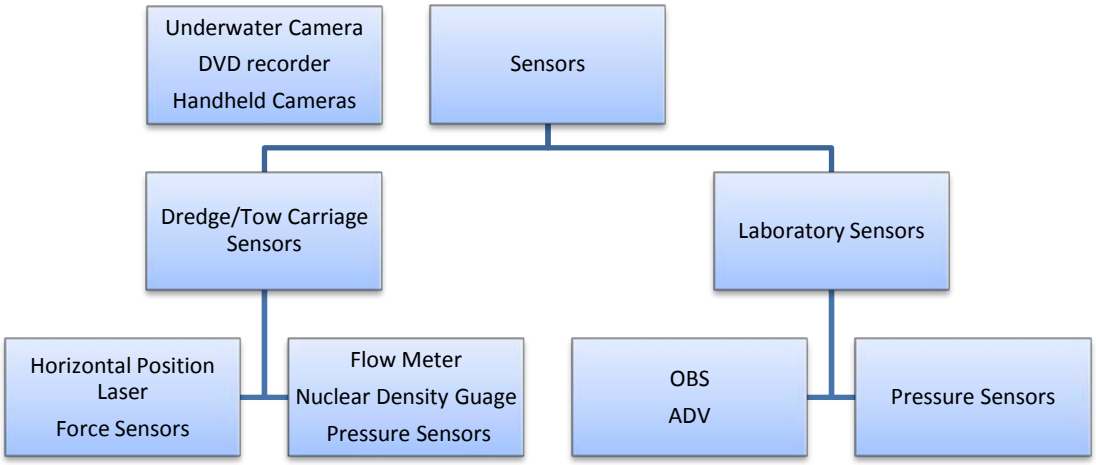

Figure A2. Cameras and Sensors in the Laboratory

Operation of the dredge/tow carriage

The dredge carriage was installed in 2004 and is the primary device for conducting dredging research. It is installed on the rails and the ladder of the dredge carriage can be separated from the cradle if necessary. When removing the entire ladder (including the articulating ladder and cutter) it is suggested that a new piece be constructed that will help in setting the ladder down and lifting it up with the crane. This device has not yet been created but should be built so that the ladder removal and installation procedure could be made easier.

The dredge carriage is designed to move the cutter in the x (East-West), y(South-North), and z(up-down) directions. The carriage can be controlled either by hand or by the computer. The first thing that must be done is for the emergency stop to be pulled

out and then the fuse at the extreme southeast tank wall must be turned to clockwise and then counter clockwise. When the fuse is set, a small light will turn on at the south electric box on the dredge carriage showing that the 480 volts is being delivered.

To move the carriage in the x direction, the operator simply turns the manual operating hardware to the hand position (normally it is in the off position) and the operator can then make the carriage move in the x direction.

Moving the ladder in the y and z directions is slightly more demanding. In this case, the operator must log into the computer and begin the dredging software. The software is nice because it provides a visual display of the spatial location of the dredge carriage and allows for the dredge carriage to be automated.

If an operator wants to move the ladder in the y or z location they must open the software and then go to the top of the page where it says enable. When enable is clicked a bar will come up that allows the operator to enable both the y and z movement. Once this is enabled the operator can then switch the manual operating software to hand and move the ladder in all three directions. The software also provides a pathway to turn on the pump and the cutter.

Changing the operating parameters of the Dredge Carriage

The variables that can be changed for the dredge carriage operation are:

1. The x translation speed
2. The y translation speed (ladder swing speed)
3. The z translation speed (ladder rising and lowering speed)
4. The cutter rotation speed

5. The pump speed.

All the components described above are changed by entering the separate drives of the dredge carriage. Handhelds for three of the drives are located on the carriage.

1. The x translation speed is controlled with the main drive of the carriage. In order to access this drive simply pick up the hand held and enter the percent of the maximum rpm that is desired. It is important to note that the maximum rpm can also be changed to increase the velocity of the carriage. In order to change any parameter on the handheld the operator must travel to the specific parameter using the arrow keys and then press the enter arrow, the value input, and the enter arrow again. If a mistake is made while entering the value, simply press the escape key. There are also other parameters that can be adjusted on this handheld to adjust how the dredge carriage moves. These include the jog speed (how fast it gets to its speed) and other parameters. It is also important to note that setting the maximum rpm for the carriage must be done twice, once for the direction north and once for the direction south.

The electrical system provided is designed predominantly around four major design criteria:

1. Control and data acquisition (accuracy and reliability)
2. Mobility of mechanical system (motion in x, y and z planes)
3. Flexibility
4. Safety for personnel and equipment

The electrical system uses the latest state-of-the-art technology available on the market in order to fulfill the design criteria for the dredge/tow carriage. It is also designed to meet the need for accurate control and reliable data acquisition. Every motor on the system is controlled either by digital variable frequency drives (VFDs) operated in vector control or by servo drives. The VFDs and servo drives provide accurate rates of acceleration, constant velocities and speeds (RPM), exact linear movements, and the necessary torque to the motors as needed to maintain the desired operating set points. In conjunction with these control capabilities they also broadcast, via RS485 communication interface, all of this data to the supervisory control and data acquisition (SCADA) system. These data will then be manipulated by the SCADA personal computer (PC) for logging and/or display purposes. In-line dynamometers, tension/load cells, laser range meters, flow, pressure, and vacuum transmitters, and density meters are also employed as part of the data acquisition system.

In order for the electrical system to meet the mobility requirements of the dredge/tow carriage the system is broken down into four major components: The carriage, the cradle, the tower and the ladder as shown in the previous drawings. The carriage is designed to remain permanently attached to the track and moves east and west along the X-axis. The cradle can be removed, as per the design requirement, and supports the tower which moves north and south along on the Y-axis on guide rails mounted inside the cradle. The tower supports and carries the ladder which moves up and down along the Z-axis on guide rails inside the tower assembly. As the dredge/tow carriage moves in the X, Y and Z axis, the electrical system accommodates for this range of motion not

only efficiently but in a manner that would limit the total stress on the power, control, and sensor cables. The electrical design for the carriage motion utilizes a power track system which is a totally enclosed cable carrier that operates in a similar manner to the treads on a military tank. The power track provides the capability to cable the primary 480 VAC, 3-phase power and 120 VAC, 1-phase control power from the local, fixed-mounted disconnect breaker box to the mobile dredge/tow carriage system's carriage VFD cubicle in a safe and efficient manner. The power track system also allows operations of up to 34.5 m (113 ft) of travel, at speeds of over 122 m/min (400 ft/min) and acceleration rates above 0.31 m/s^2 (1 ft/sec^2). To meet the design requirement of a removable cradle all of the components and wiring related to that system are designed in a manner that allows it to be isolated from the permanently mounted carriage. Plugs and receptacles mounted on the side of the carriage VFD cubicle are used to cable the 480 and 120 VAC power to the removable cradle. The cradle PLC and VFD cubicles along with cradle related motors, sensor devices, and wiring are attached to and completely supported by the cradle assembly. By designing the system in this manner the cradle can be removed with a minimum amount of effort. This design also allows the carriage system to remain safe by eliminating exposure to deadly voltage sources through use of receptacle covers as well as functional by means of a local mounted carriage VFD HMI (human-machine interface). For cradle motion, the electrical design utilizes a free floating cable harness that attaches to the carriage and tower using highly flexible cable. The flexible cable harness carries the power, control, and sensor feedback signals to and from the cradle VFD and PLC cubicles and the ladder mounted components. For ladder

motion, all the sensor signals are terminated inside a single interface junction box mounted on top of the ladder. This allows the use of more robust multiconductor cables, capable of handling the extensive, repetitive operation, to carry the feedback signals to the cradle PLC cubicle. This design will reduce the stress on the smaller, more delicate sensor wires which remain stationary on the ladder. Finally, the SCADA system (described later in this paper) utilizes two Ethernet radio systems. The radio telemetry setup eliminates all hardwired communication and sensor feedback cables from the carriage mounted PLC to the SCADA PC based remote operating system.

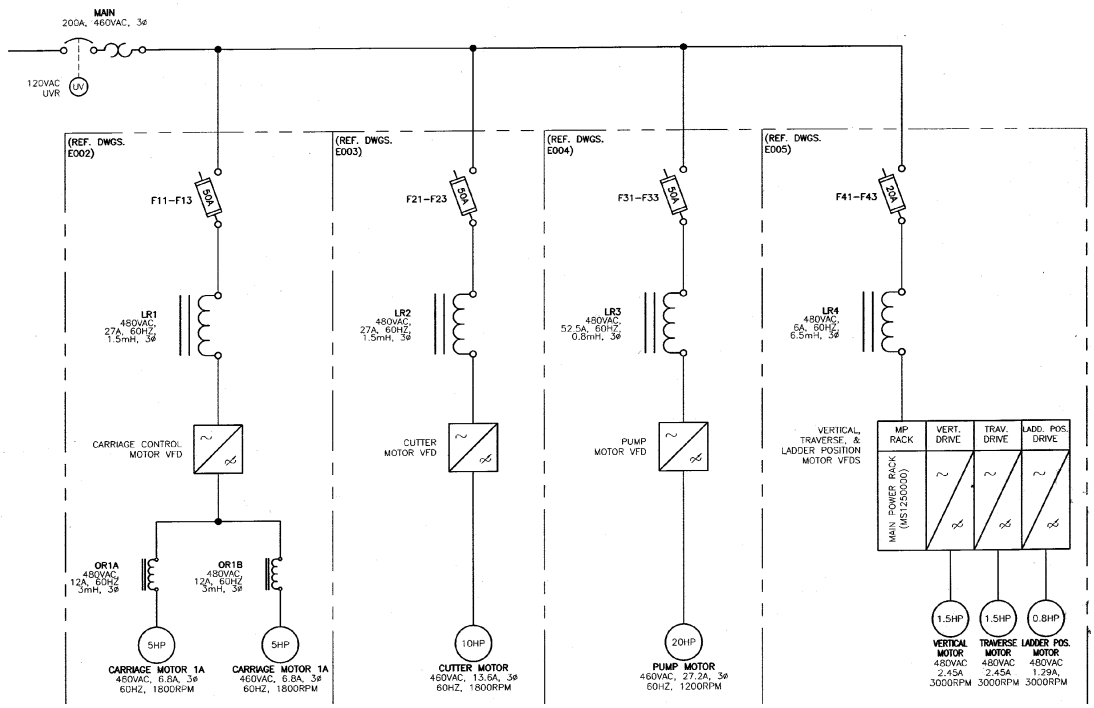

Figure A3. Electrical supply for dredge/tow carriage drive motors

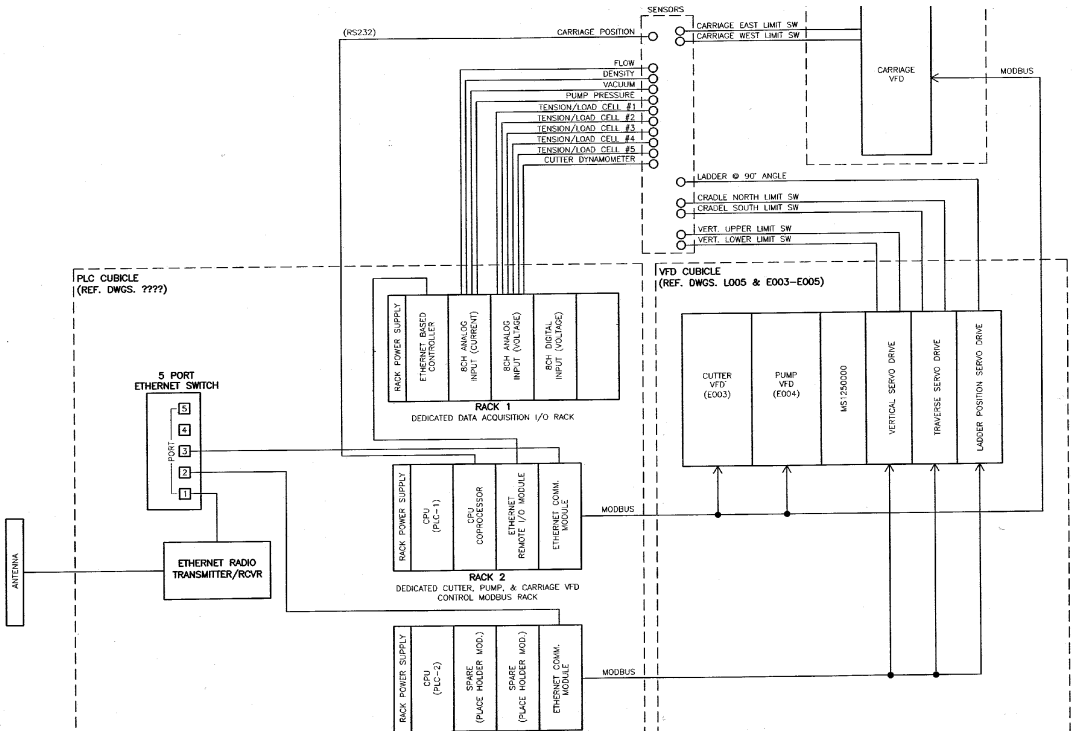

Figure A4. Electrical control and data channels for the dredge/tow carriage

The flexibility of the electrical system was also taken into account while in the designing stages of the project. All of the VFDs and PLCs provided are digitally operated and controlled, microprocessor based systems. The VFDs supplied to control the carriage, ladder pump, and cutter motors were intentionally oversized so that if future demands should require higher torque and horsepower requirements only the motors will need to be changed. The VFDs supplied for the carriage, ladder pump, and cutter motors are also identical in size as are the Servo Drives supplied for the vertical position, traverse control, and ladder angle motor systems. This allows all of the systems to be interchangeable. This will also reduce the amount of spare parts required as well as aid in trouble shooting. The VFDs supplied for the carriage, ladder pump, and cutter motors

can also be operated in over five (5) different modes of control: V/Hz constant and variable torque, sensorless vector (also known as vector control frequency feedback), vector control with speed feedback, or torque (master-slave) control. The remote console is designed to be powered by any standard 120 VAC receptacle which allows it to be setup and operated from almost anywhere within the laboratory facility. The 480 VAC, 3-phase power and the 120 VAC, 1-phase control power are isolated from one another so that the control system can be powered, if desired, by a separate, clean, uninterrupted power source. This assists in preventing dirty power from interrupting or contaminating the data acquired by the data acquisition system. By doing this it also allows the SCADA system and sensor elements to remain energized even if the main 480 VAC power to the building is lost, thereby, preventing loss of communication between the carriage mounted PLC and remote mounted PC. If power is accidentally or unintentionally deenergized to the system a laser range meter is used to recover the position of the carriage once power is reapplied. This eliminates the need to "home" or "re-zero" the carriage as would have to be done if the position of the carriage were calculated by counting pulses from an encoder. This will also allow the system to resume operation with a minimal amount of delay. Even the cabling pulled for the 480 VAC and 120 VAC is over sized by over 200% so that the systems on the dredge/tow carriage can be increased in size, if desired, without having to replace the original cable installed.

Personnel safety, equipment safety, and protection also played a vital role in the design of the electrical system. The main 480 VAC, 3-phase power for the dredge/tow

carriage system can be deenergized and locked-out by means of a 480 VAC, 200A panel mounted circuit breaker located on the southwest corner of the dredge/tow flume.. The emergency stop feature for the dredge/tow carriage utilizes a failsafe UVR (Under Voltage Release) on the 200A feeder breaker which will trip the breaker in the event of power loss to the UVR.

The power required to energize the UVR is provided by the remote console. If the remote console is removed from the facility the main 480 VAC feeding the dredge/tow carriage system cannot be energized. This should prevent any unauthorized operation of the equipment. The emergency stop can also be activated by either using the hardwired E-stop mounted on the front of the remote console, or will automatically be activated in the event of loss of radio communication between the remote mounted SCADA PC and carriage mounted PLC. The brake systems on the carriage, ladder angle, traverse, and vertical position motors require power to release the brake. In the event of power loss on the 480 VAC system all of the brakes will automatically apply.

Each VFD is equipped with its own isolation, fused disconnect switch and, as mentioned in the first paragraph of this section, the 480 VAC and 120 VAC power feeding the cradle electrical system is protected by individual circuit breakers per power source. All of the cabling installed on the dredge/tow carriage that carries 480VAC or 120VAC power is run using offshore rated armored and sheathed cable certified for use in Class 1 Division 1 hazardous regions. Also every cubicle located on the dredge/tow carriage (carriage VFD, cradle VFD, and cradle PLC cubicle) is equipped with a door

mounted “480 VAC POWER AVAILABLE” and/or “120 VAC POWER AVAILABLE” LED push-to-test pilot light(s), where applicable.

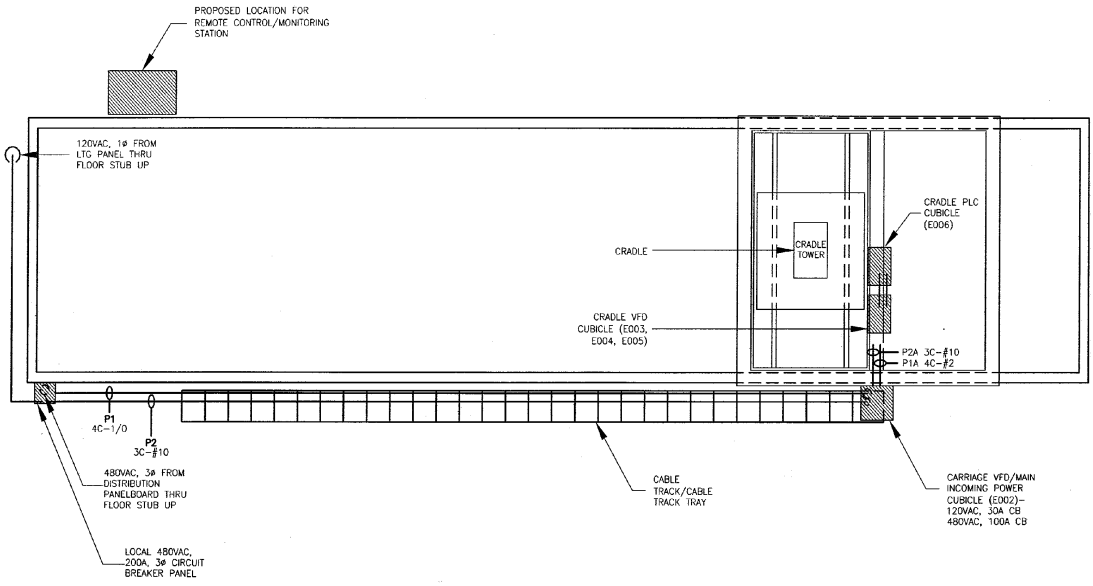

Figure A5. Electrical power cable track for dredge/tow carriage

In conjunction with the personnel safety features mentioned the dredge/tow carriage is also designed with components that will aid in protection of the system’s equipment. Physical end-stop barriers are mounted on the carriage rails to keep the carriage from running off the flume. Proximity switches are installed to prevent over-travel on the carriage, cradle, ladder, and ladder cutter angle systems. If any of these limits are reached the system is programmed to halt all motion in those directions. Each VFD and Servo Drive is also equipped with their own built-in safety features such as over-speed, over-current, over-voltage, speed/position deviation limits exceeded, and 480 VAC supply power loss faults. These built-in features will prevent erroneous

operations of the motors that could result in bodily harm or damage to the mechanical systems.

Data Acquisition System

The Supervisory Control and Data Acquisition (SCADA) system consists of a PC/joystick console located at the user/operator desk and a PLC system located on the dredge/tow carriage. Communication between the dredge/tow PLC and the user/operator station is completed by an advanced industrial wireless Ethernet link that is immune to interference from normal “Wi Fi” systems. Hardwire emergency stops are in place to override PLC control.

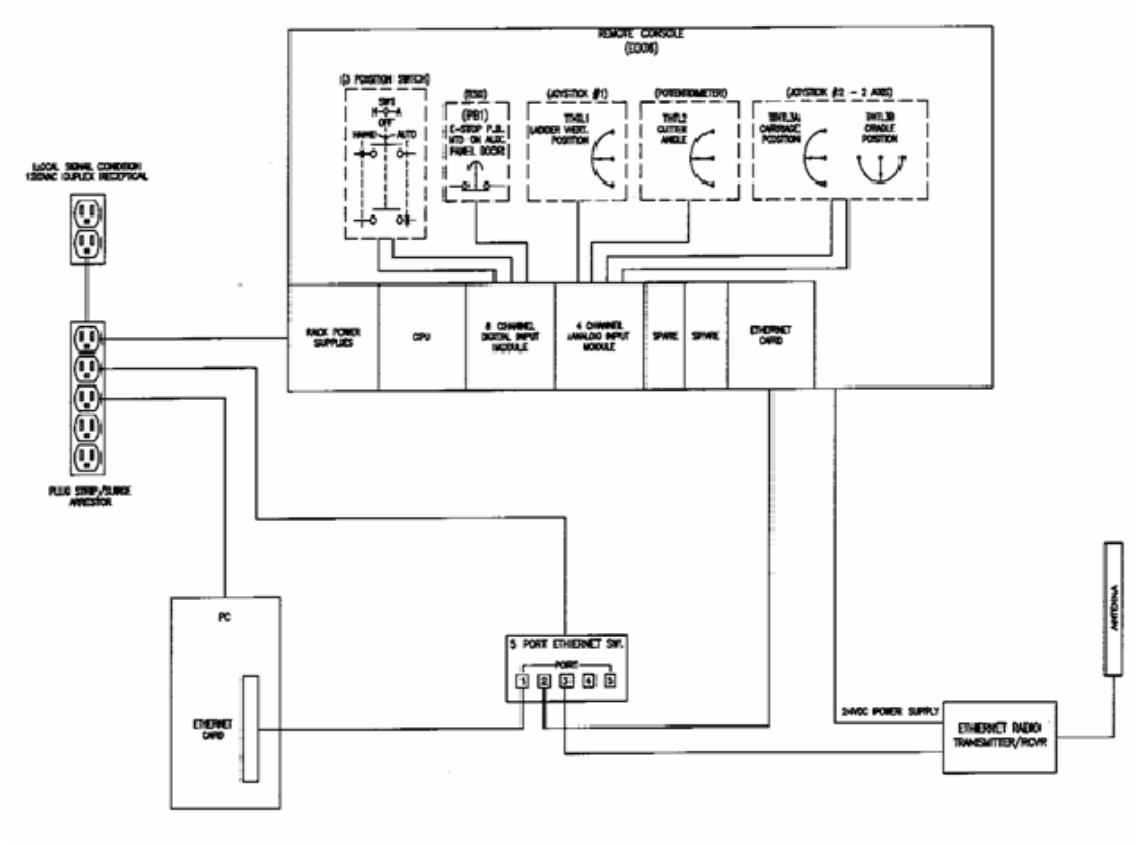

Figure A6. Schematic of SCADA and remote control console

The SCADA PC serves two basic functions. First is the collection and recording of data gathered by the dredge/tow carriage PLC. The data are stored in files that are available for analysis. Real time data are displayed on the PC monitor and are available for use by the operator. Also, the SCADA PC can perform real time calculations on the incoming data. The second function of the SCADA PC is to provide a method of developing 'recipes' of instructions for the dredge/tow carriage. These 'recipes' of instructions are developed using a Microsoft ® Viso flowchart format. A library of 'recipes' can be stored on the SCADA PC.

The SCADA joystick console provides a means to manually control the dredge/tow carriage system. Data from instrumentation can be recorded in either 'Auto Mode' (controlled by the SCADA PC) or 'Manual Mode' (controlled by the SCADA joystick console.) The SCADA joystick console is also used for maintenance functions that require the movement of the dredge/tow carriage.

The SCADA PLC system is located on the dredge/tow carriage and is responsible for controlling the motor/servo drives and collecting the instrumentation data for transmission to SCADA PC. The SCADA PLC system contains its own program to insure the motor drives are still in control in the event of a radio link loss.

The SCADA communication link is provided by two Ethernet radio modems each located at the dredge/tow carriage and the user/operator station. This link uses spread spectrum technology to prevent interference or intervention from typical

commercial “Wi Fi” systems. In the event of radio or other failure, a hardwired emergency stop is provided to disconnect power from the dredge/tow carriage.

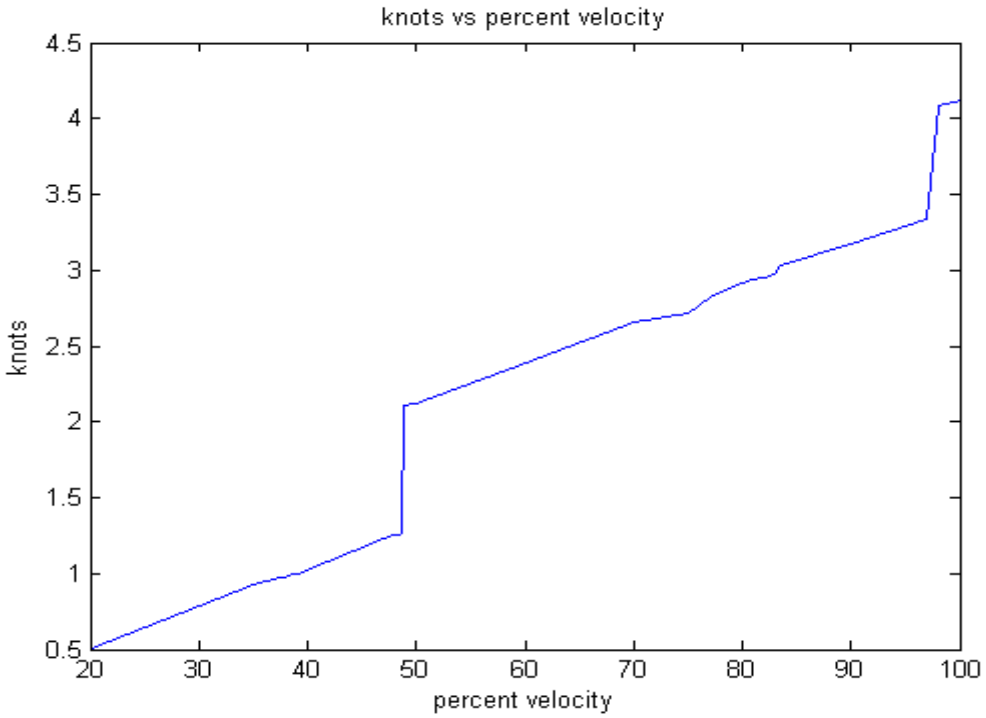

Figure A7. Tow Carriage Velocity from Variable Speed Drive Input.

The carriage speed in knots versus the input percent velocity that a carriage operator inputs into the computer is shown in Figure A7. This output is for a forward maximum horsepower of 3300hp. It is important to notice the jumps that occur in specific regions. The reason for these jumps it undetermined.

Guidelines for Running the Dredge Carriage

1. Make sure that the hand control is set to the off position and the emergency stop is pulled out. Go turn on the breaker switch. You will know that the dredge carriage is on when the small white light on the south side box of the dredge carriage turns on.

2. Unlock the dredge carriage computer box where the mouse and keyboard are located. Access the dredge carriage automation system through the executable.
3. Click the hand control box to automation if movement of the dredge carriage is to be done through the computer. **Warning: If the carriage was previously stopped before with the emergency stop, clicking over to the auto control will cause the carriage to finish the sequence formerly commanded by the operator.** In order to prevent this make sure that cancel has been pressed on the computer screen before switching over to auto control.
4. Working in the auto mode: Enter the home position, step position and percent velocity that the dredge carriage should travel. Press "update" to enter these values into the left hand side of the display. When the user wishes to step to a desired position the user should press the "step" button. When the user wishes to for the dredge carriage to travel to the home position the user should press the "home" button.
5. When the user is finished with the automation program. Turn the hand control to the "off" position. Close down the automation computer system. If the dredge carriage will not be used for some time, hit the emergency stop as well.
6. Working in the hand mode: **Be advised that the dredge carriage is programmed to travel at 100% of its velocity when working in the hand mode.** Note that the automation computer does not have to be turned on to work in this mode.

7. When done working in the hand mode: Move the hand control to the "off" position. If the dredge carriage will not be used for some time, hit the emergency stop as well.

Control for the Carriage Drive using the OEM handheld device located on the carriage.

The following is a list of the locations a dredge carriage operator must travel to in the OEM handheld menu in order to make changes on dredge carriage parameters including velocity, acceleration, and deceleration.

Menu 4

P.4.12-This location is the motor regeneration kilowatt limit. As the carriage decelerates, energy is actually generated by the dredge carriage. This energy travels back to the power source. In order for this energy not to overload the power source, a trip mechanism is used when the power created by the deceleration of the dredge carriage is too large. When the trip mechanism is triggered the emergency break is released. **It is important to note that the deceleration limit is actually controlled by this parameter.** This parameter makes it easier to break but also makes the tripping mechanism easier to set off. It is currently set at 1.3 kilowatts. In order for this parameter to increase it is suggested that resistors be purchased. These resistors could dissipate the energy created during the deceleration phase.

Note: If the trip mechanism occurs, the OEM handheld will prompt the carriage operator to reset the values by a "reset?". Here the operator should press "3" to reset the carriage. If the operator is not prompted with the "reset ?" command they should press the "?" button to initiate the reset sequence.

Menu 5

P.5.16-This location provides the maximum rpm that the carriage can go up to. It is currently set at 3000 rpm. This allows the carriage to travel at 2m/s in the East direction.

When we use the automation system we tell it a percent velocity to travel. The percentage is a percentage of the given rmp in the P5.16 menu.

P.5.15-This location provides the maximum rpm that the carriage can go up to when moving in the west direction. It is currently set at 300rpm. This provides protection when traveling back to the carriage's home location if the home location is at the east end of the tank.

Menu 6

P6.00-P6.03 provide the parameters for a four quadrant acceleration system including

P6.00-Acceleration Forward

P6.01-Decelartion Forward

P6.02-Acceleration Reverse

P6.03-Deceleration Reverse

Here the Forward direction would be in the West moving direction and the Reverse direction would be in the East moving direction.

The acceleration or deceleration is based on a percentage of the top speed. For example if the top speed were 2m/s and the Acceleration Forward was 10% while the

Deceleration Forward was 20% the carriage would accelerate at .2m/s^2 until it reached 2m/s and the Decelerate at .4m/s^2.

Troubleshooting

When the cradle or ladder is run to its limit in either position or power, the system automatically shuts off and should be reset. This can be accomplished by resetting the breakers to the servo drives and PLC's. A picture of the breakers and servodrive for the ladder are shown in Figure A12. It is also necessary to switch these breakers to the inactive position when hooking up directly to any PLC using the FMtools software. Using FMtools, directly connects the user to the cradle or ladder PLC without running through the data acquisition system. From here, the user can reset the limiting breaks and control the servodrives.

When setting up FMtools, the breaker should be set inactive. The proper cable and computer should be attached to the PLC and then the breaker can be returned to the active position. After the necessary programming of the PLC is completed, the breaker should once again be set inactive, the cable removed, the primary setup reestablished, and the breaker reset to active.

Figure A8. Breakers and Ser Dvorive for Ladder and Cradle Control

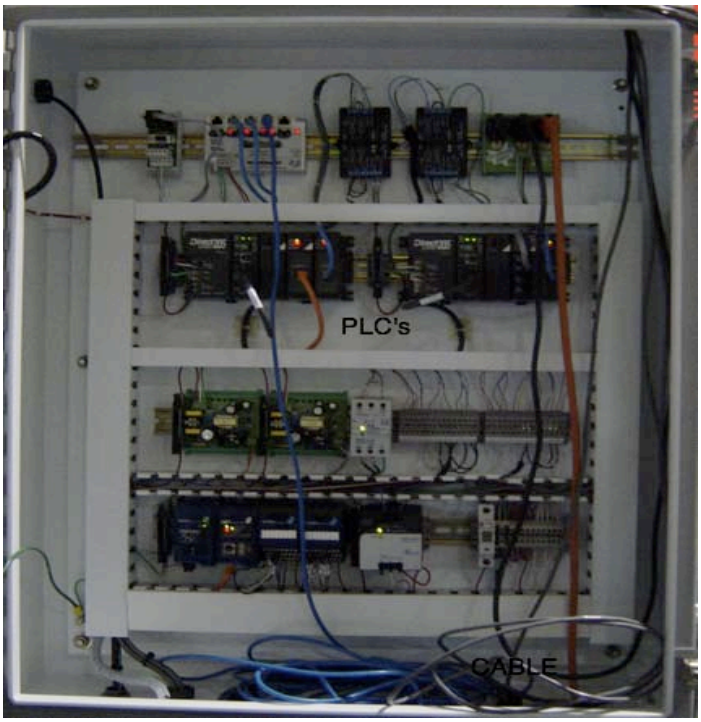

Figure A9. Picture of PLC location on Dredge/Tow Carriage

APPENDIX B

DERIVATION OF THE ADVECTION DIFFUSION TRANSPORT EQUATION

The derivation of the sediment transport equation involves both advective and diffusive terms (Nicholson, 1979) and can be derived by considering a specific volume with the dimensions dx,dy,and dz. The influent flux of solute into the volume in the x direction can be stated as

$$FLUX_I = \rho CUdydz \tag{B1}$$

where U is the turbulent velocity in the x direction

The effluent flux can be stated as:

$$FLUX_E = \left(\rho CU + \frac{\partial}{\partial x}(\rho CU)x \right) dydz \tag{B2}$$

The net flux is therefore:

$$FLUX_N = -\frac{\partial}{\partial x}(\rho CU)dxdydz \tag{B3}$$

Expanding this to three dimensions the rate of change of solute in the volume is:

$$-\frac{\partial}{\partial x}(\rho CU)dxdydz - \frac{\partial}{\partial x}(\rho CV)dxdydz - \frac{\partial}{\partial x}(\rho CW)dxdydz \tag{B4}$$

The time rate of change of the solute mass in the volume can also be states as:

$$\frac{\partial}{\partial t}(\rho C)dxdydz \tag{B5}$$

These two expressions can be equated where:

$$\frac{\partial}{\partial t}(\rho C) = -\frac{\partial}{\partial x}(\rho CU) - \frac{\partial}{\partial y}(\rho CV) - \frac{\partial}{\partial z}(\rho CW) \tag{B6}$$

The assumption is then made that the solute concentration is small enough to not affect the density of the solution. In this case the conservation of solute mass can then be written as:

$$\frac{\partial}{\partial t}(C) = -\frac{\partial}{\partial x}(CU) - \frac{\partial}{\partial y}(CV) - \frac{\partial}{\partial z}(CW) \tag{B7}$$

Since the flow is considered turbulent equation A7 can be expanded to:

$$\frac{\partial}{\partial t}(\overline{C} + C') = -\frac{\partial}{\partial x}\left((\overline{C} + C')(\overline{U} + U')\right) - \frac{\partial}{\partial y}\left((\overline{C} + C')(\overline{V} + V')\right) - \frac{\partial}{\partial z}\left((\overline{C} + C')(\overline{W} + W')\right) \tag{B8}$$

Because the temporal mean of the fluctuation is zero and the product of a steady quantity and fluctuation is zero the fluctuating components of the equation can be removed. Therefore,

$$\frac{\partial}{\partial t}(\overline{C}) = -\frac{\partial}{\partial x}(\overline{CU}) - \frac{\partial}{\partial x}(\overline{CU'}) - \frac{\partial}{\partial y}(\overline{CV}) - \frac{\partial}{\partial y}(\overline{CV'}) - \frac{\partial}{\partial z}(\overline{CW}) - \frac{\partial}{\partial z}(\overline{CW'}) \tag{B9}$$

Conservation of mass states:

$$\frac{\partial \overline{U}}{\partial x} + \frac{\partial \overline{V}}{\partial y} + \frac{\partial \overline{W}}{\partial z} = 0 \tag{B10}$$

Therefore the conservation of solute mass reduces to

$$\frac{\partial}{\partial t}(\overline{C}) = -\frac{\partial}{\partial x}(\overline{CU'}) - \frac{\partial}{\partial y}(\overline{CV'}) - \frac{\partial}{\partial z}(\overline{CW'}) - \overline{U}\frac{\partial \overline{C}}{\partial x} - \overline{V}\frac{\partial \overline{C}}{\partial y} - \overline{W}\frac{\partial \overline{C}}{\partial z} \tag{B11}$$

Fick's law of molecular diffusion is then used to express the fluctuating components on the right hand side of equation A11 where:

$$\overline{CU'} = -D_x\frac{\partial \overline{C}}{\partial x} \tag{B12}$$

$$\overline{CV'} = -D_y\frac{\partial \overline{C}}{\partial y} \tag{B13}$$

$$\overline{C'W'} = -D_w \frac{\partial \bar{C}}{\partial z} \tag{B14}$$

Substituting these terms into equation A11 and then dropping the bars results in:

$$\frac{\partial}{\partial t}(C) = \frac{\partial}{\partial x}\left(D_x \frac{\partial C}{\partial x}\right) + \frac{\partial}{\partial y}\left(D_y \frac{\partial C}{\partial y}\right) + \frac{\partial}{\partial z}\left(D_z \frac{\partial C}{\partial z}\right) - U\frac{\partial C}{\partial x} - V\frac{\partial C}{\partial y} - W\frac{\partial C}{\partial z} \tag{B15}$$

This equation is the three-dimensional advection diffusion equation for suspended sediment transport. The first three times represent the diffusion while the second three terms represent the advection. This equation can model the transport of resuspended sediments by applying a particle settling term.

APPENDIX C

TABLES DEVELOPED FROM TURBIDITY AND TURBULENCE ANALYSIS

The following tables display the data analysis conducted during this research on the specific variables on turbidity, turbulence intensity, and concentration flux. The data analysis was conducted for the data in its entirety as well as for the separate phases (Phase 1and Phase 2) recognized in the research. It is important to note that negative concentration flux values seen for concentration flux in the y or z direction (V or W velocities) is representative of the direction of the flux with the positive y direction being left to right when facing the front of the cutter and positive z direction being down to up.

Table C1. Turbidity for lab testing (g/l)

Test	Mean	Std	Max
C1	23.9	19.0	62.4
C1B	5.8	2.3	9.8
C2	17.6	18.0	65.0
C2B	6.0	3.2	10.5
C3	20.6	19.8	66.1
C3B	5.51	3.23	10.8
C4	8.49	11.95	47.36
C4B	5.10	3.11	10.99
C5	17.2	17.4	55.24
C5B	9.18	4.93	19.1
C6	16.45	10.17	33.26
C6B	4.15	2.34	6.8
C7	273.6	924.4	3703.3
C7B	6.93	6.88	25.65

Table C2. V velocity turbulence intensity for Lab Testing

Test	Mean	Std	Max
C1	5.9	7.15	31.38
C1B	4.7	4.8	20.8
C2	3.75	3.05	12.82
C2B	3.7	2.9	9.7
C3	3.16	3.4	10.4
C3B	5.66	7.5	30.35
C4	5.20	8.89	38.19
C4B	51.7	207.8	934.4
C5	9.69	18.74	71.5
C5B	8.03	20.5	93.6
C6	13.0	27.16	121.77
C6B	3.20	2.71	10.7
C7	5.88	8.20	32.63
C7B	5.16	5.77	18.11

Table C3. W velocity turbulence intensity for lab testing

Test	Mean	Std	Max
C1	6.35	6.4	22.6
C1B	10.1	25.9	114.9
C2	4.18	5.76	27.1
C2B	8.5	21.8	99.0
C3	8.5	14.3	53.6
C3B	9.58	21.15	90.95
C4	7.97	13.35	60.6
C4B	6.1	11.06	50.8
C5	8.75	26.3	120.1
C5B	20.04	79.64	358.3
C6	1.50	1.44	6.43
C6B	0.765	0.80	3.13
C7	12.3	29.04	119.3
C7B	2.64	3.81	14.3

Table C4. V concentration flux (kg/m*s) for lab testing

Test	Mean	Std	Max
C1	0.15	0.46	0.97
C1B	-.004	.05	.08
C2	-0.02	0.415	0.74
C2B	-.006	0.07	0.133
C3	-0.01	0.35	0.59
C3B	-0.003	0.08	0.18
C4	0.0581	0.214	0.718
C4B	0.02	0.05	0.123
C5	0.21	0.57	1.36
C5B	-0.03	0.143	0.197
C6	-0.02	0.144	0.236
C6B	-0.0012	0.01	0.02
C7	-3.78	16.0	2.04
C7B	0.026	0.09	0.21

Table C5. W concentration flux (kg/m*s) for lab testing

Test	Mean	Std	Max	Min
C1	-0.02	0.46	1.91	-2.7
C1B	-.02	0.07	0.07	-0.25
C2	0.22	0.63	2.3	-0.33
C2B	-0.03	0.07	0.12	-0.22
C3	0.07	0.57	1.75	-0.87
C3B	-0.03	0.09	0.07	-0.32
C4	0.022	0.09	0.34	-0.12
C4B	-0.02	0.07	0.05	-0.224
C5	0.05	0.33	1.36	-0.33
C5B	-0.05	0.13	0.06	-0.46
C6	-0.006	0.18	0.30	-0.59
C6B	-0.005	0.01	0.004	-0.03
C7	-1.67	6.7114	1.10	-26.7
C7B	-0.03	0.07	0.02	-0.18

Phase 1

Table C6. Turbidity for lab testing (g/l) Phase 1

Test	Mean	Std	Max
C1	14.24	14.65	54.5
C1B	5.26	2.31	9.48
C2	9.55	12.65	57.31
C2B	5.24	2.95	10.15
C3	9.31	9.72	42.44
C3B	5.11	3.41	11.68
C4	7.02	10.10	38.52
C4B	4.47	2.65	9.42
C5	16.75	17.36	63.72
C5B	8.62	6.29	21.16
C6	7.44	5.26	17.44
C6B	4.36	2.43	7.8
C7	373.12	1040.4	3703.3
C7B	5.27	3.90	14.27

Table C7. V velocity turbulence intensity for Lab Testing Phase 1

Test	Mean	Std	Max
C1	4.78	4.64	18.86
C1B	4.60	5.00	16.95
C2	3.97	3.96	14.93
C2B	6.29	13.42	60.99
C3	5.82	6.35	21.85
C3B	17.11	47.96	208.27
C4	5.91	10.27	44.9
C4B	5.68	5.59	20.46
C5	9.07	14.93	65.26
C5B	7.73	12.64	47.83
C6	14.81	51.39	239.92
C6B	3.08	4.15	16.83
C7	16.49	45.48	185.13
C7B	3.15	3.97	12.74

Table C8. W velocity turbulence intensity for Lab Testing Phase 1

Test	Mean	Std	Max
C1	3.17	3.06	12.84
C1B	2.37	1.92	6.65
C2	13.2	42.46	191.44
C2B	1.97	1.66	6.49
C3	6.21	11.86	54.14
C3B	3.02	2.62	7.97
C4	8.98	17.67	61.26
C4B	9.35	24.14	109.82
C5	7.34	12.43	48.26
C5B	6.45	14.68	66.29
C6	0.69	0.41	1.74
C6B	1.87	5.13	23.38
C7	3.39	4.26	13.6
C7B	4.29	7.37	22.3

Table C9. V concentration flux (kg/m*s) for lab testing Phase 1

Test	Mean	Std	Max	Min
C1	0.109	0.542	1.682	-1.359
C1B	0.0009	0.0366	0.107	-0.0713
C2	0.069	0.318	0.882	-0.620
C2B	-0.004	0.0929	0.196	-0.232
C3	-0.0631	0.598	1.110	-1.851
C3B	-0.007	0.071	0.213	-0.148
C4	0.043	0.297	1.19	-0.529
C4B	0.023	0.0518	0.205	-0.044
C5	-0.0127	0.498	1.210	-0.981
C5B	0.019	0.194	0.576	-0.307
C6	-0.002	0.060	0.133	-0.103
C6B	0.0003	0.017	0.042	-0.054
C7	-14.8	59.85	1.400	-239.27
C7B	0.017	0.045	0.136	-0.036

Table C10. W concentration flux (kg/m*s) for lab testing Phase 1

Test	Mean	Std	Max	Min
C1	-0.035	0.259	0.426	-0.554
C1B	-0.008	0.0351	0.053	-0.093
C2	0.053	0.165	0.603	-0.181
C2B	-0.007	0.036	0.024	-0.141
C3	0.169	0.538	1.915	-0.916
C3B	-0.006	0.041	0.052	-0.113
C4	-0.059	0.261	0.041	-1.152
C4B	-0.023	0.079	0.099	-0.268
C5	-0.034	0.419	1.372	-0.892
C5B	-0.067	0.086	0.056	-0.289
C6	-0.006	0.052	0.099	-0.125
C6B	-0.006	0.024	0.006	-0.105
C7	-7.58	29.91	0.019	-119.74
C7B	-0.003	0.018	0.025	-0.052

Phase 2

Table C11. Turbidity for lab testing (g/l) Phase 2

Test	Mean	Std	Max
C1	27.2	23.9	77.1
C1B	6.33	2.60	11.18
C2	21.3	22.16	74.36
C2B	6.29	3.45	11.89
C3	23.58	23.64	75.82
C3B	6.27	3.60	11.97
C4	9.53	14.36	59.08
C4B	5.77	3.48	12.89
C5	17.86	17.71	59.33
C5B	9.66	5.47	21.42
C6	16.85	11.05	34.62
C6B	4.33	2.47	7.84
C7	239.3	923.8	3703.3
C7B	8.21	9.22	33.91

Table C12. V velocity turbulence intensity for Lab Testing Phase 2

Test	Mean	Std	Max
C1	8.84	21.13	95.82
C1B	10.94	24.3	108.8
C2	7.59	17.59	80.01
C2B	4.01	6.85	31.49
C3	2.66	3.32	13.12
C3B	7.01	11.63	39.64
C4	2.76	2.51	10.48
C4B	11.3	22.3	92.45
C5	5.48	7.21	30.55
C5B	3.36	3.21	14.63
C6	16.31	41.65	182.17
C6B	3.69	7.23	33.1
C7	7.95	17.49	72.08
C7B	3.93	4.35	14.68

Table C13. W velocity turbulence intensity for Lab Testing Phase 2

Test	Mean	Std	Max
C1	5.60	6.85	26.0
C1B	3.46	3.9	15.27
C2	3.30	3.62	14.68
C2B	4.76	11.47	52.85
C3	3.75	5.18	21.44
C3B	9.59	24.02	108.39
C4	33.63	115.67	521.67
C4B	4.06	4.29	17.01
C5	4.48	8.69	40.12
C5B	28.89	116.65	524.17
C6	1.28	0.79	2.72
C6B	0.77	0.83	3.608
C7	5.43	7.87	27.0
C7B	4.14	6.98	24.43

Table C14. V concentration flux (kg/m*s) for lab testing Phase 2

Test	Mean	Std	Max	Min
C1	0.12	0.256	0.614	-0.312
C1B	0.013	0.03	0.072	-0.041
C2	0.016	0.3258	0.615	-0.575
C2B	0.009	0.062	0.174	-0.100
C3	-0.005	0.280	0.396	-0.809
C3B	-0.002	0.088	0.193	-0.224
C4	0.046	0.191	0.59	-0.289
C4B	0.029	0.07	0.201	-0.064
C5	0.288	0.59	1.85	-0.87
C5B	0.012	0.088	0.1574	-0.227
C6	-0.021	0.085	0.177	-0.201
C6B	-0.003	0.008	0.012	-0.026
C7	-0.044	0.298	0.263	-1.115
C7B	0.043	0.099	0.239	-0.085

Table C15. W concentration flux (kg/m*s) for lab testing Phase 2

Test	Mean	Std	Max	Min
C1	-0.012	0.358	0.49	-1.217
C1B	-0.017	0.08	0.134	-0.317
C2	0.025	0.199	0.693	-0.417
C2B	-0.016	0.076	0.150	-0.242
C3	-0.0178	0.1426	0.260	-0.434
C3B	-0.008	0.112	0.247	-0.322
C4	0.019	0.099	0.296	-0.252
C4B	-0.037	0.103	0.054	-0.394
C5	0.11	0.363	1.10	-0.382
C5B	-0.027	0.1316	0.1614	-0.402
C6	0.022	0.099	0.264	-0.1612
C6B	-0.004	0.014	0.016	-0.049
C7	0.064	0.304	1.19	-0.155
C7B	-0.009	0.100	0.209	-0.224

APPENDIX D

ORIGINAL FIGURES OF DREDGING PARAMETERS

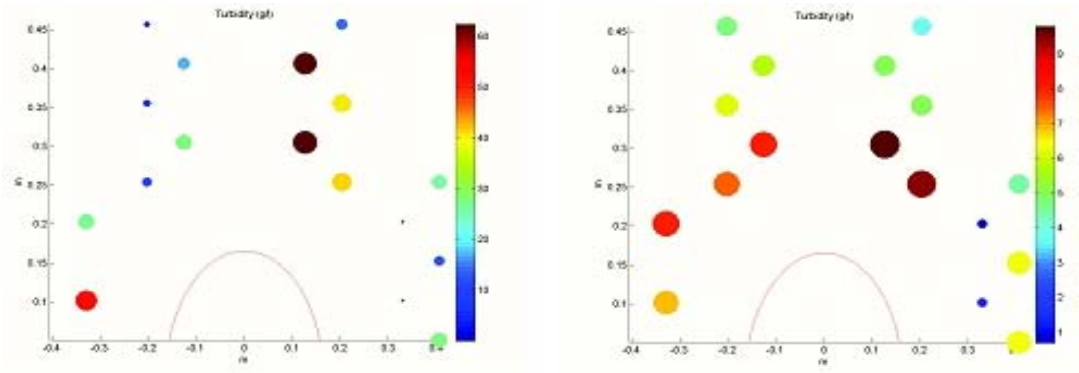

Figure D1. Turbidity (g/l) for case 1a (left) and case 1b (right)

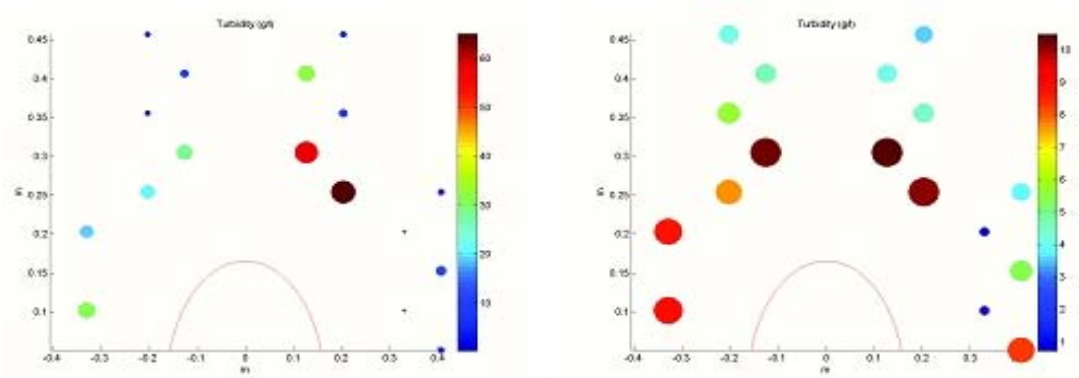

Figure D2. Turbidity (g/l) for case 2a (left) and case 2b (right)

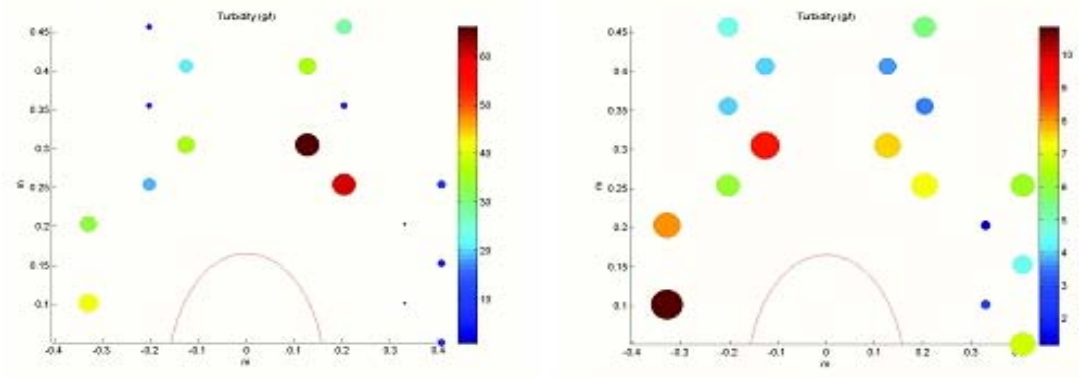

Figure D3. Turbidity (g/l) for case 3a (left) and case 3b (right)

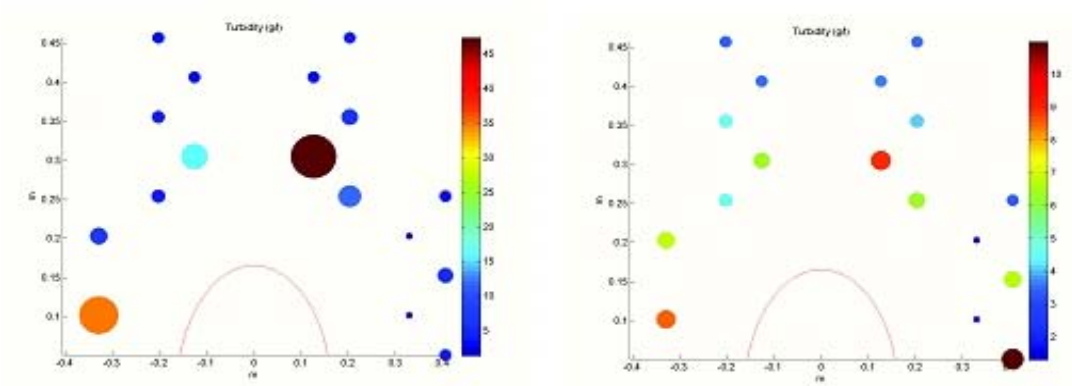

Figure D4. Turbidity (g/l) for case 4a (left) and case 4b (right)

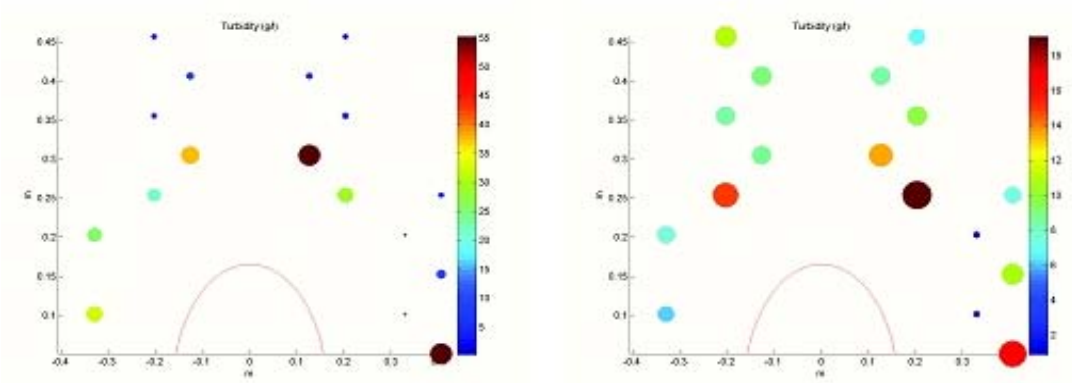

Figure D5. Turbidity (g/l) for case 5a (left) and case 5b (right)

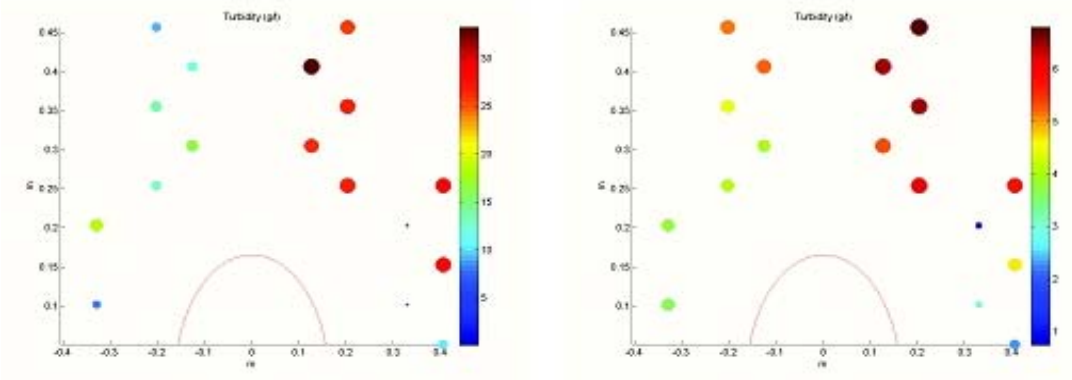

Figure D6. Turbidity (g/l) for case 6a (left) and case 6b (right)

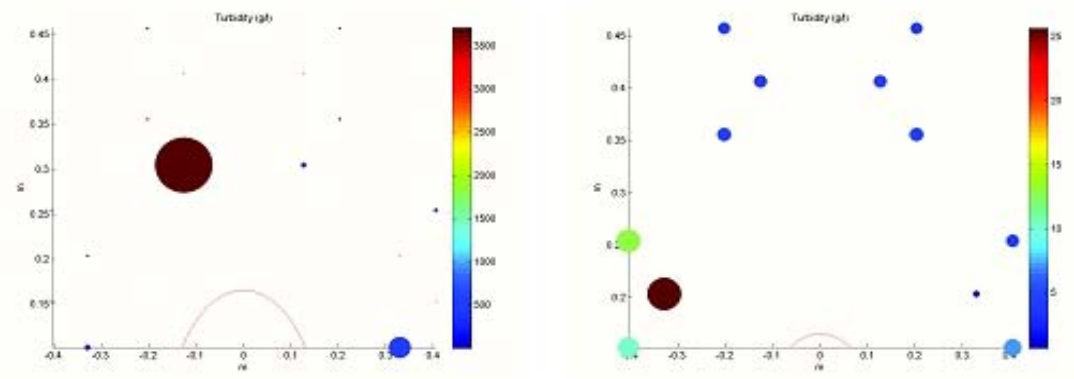

Figure D7. Turbidity (g/l) for case 7a (left) and case 7b (right)

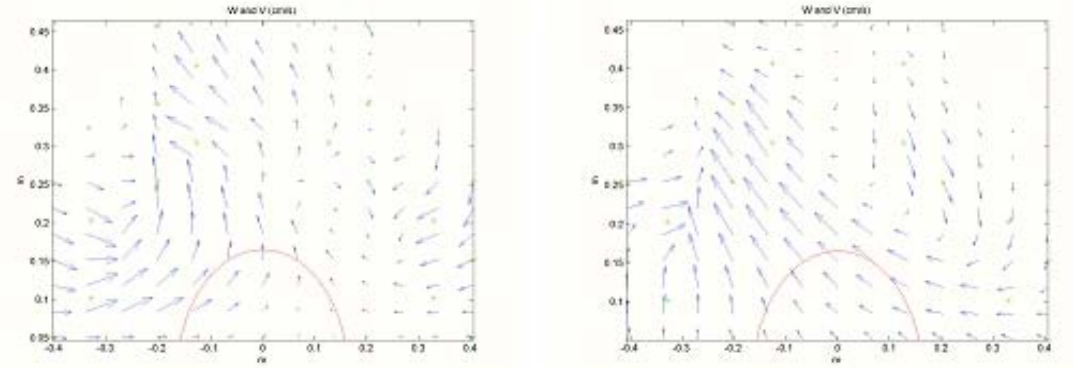

Figure D8. V and W Velocity Field (m/s) for case 1a (left) and case 1b (right)

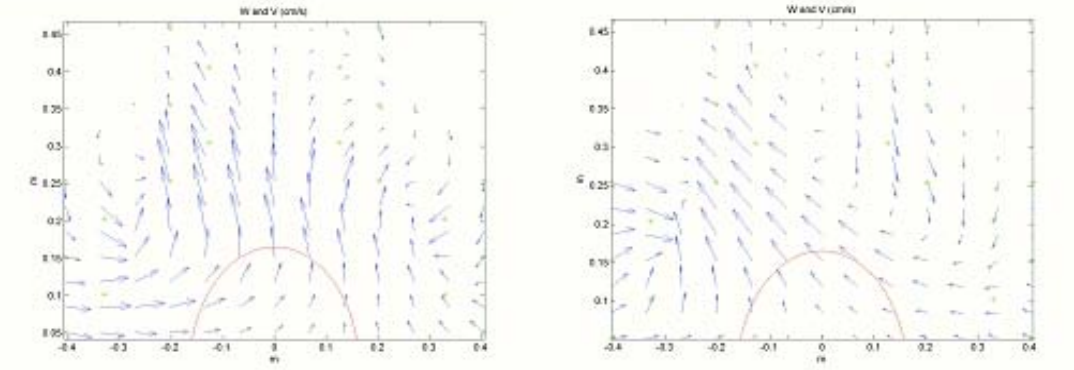

Figure D9. V and W Velocity Field (m/s) for case 2a (left) and case 2b (right)

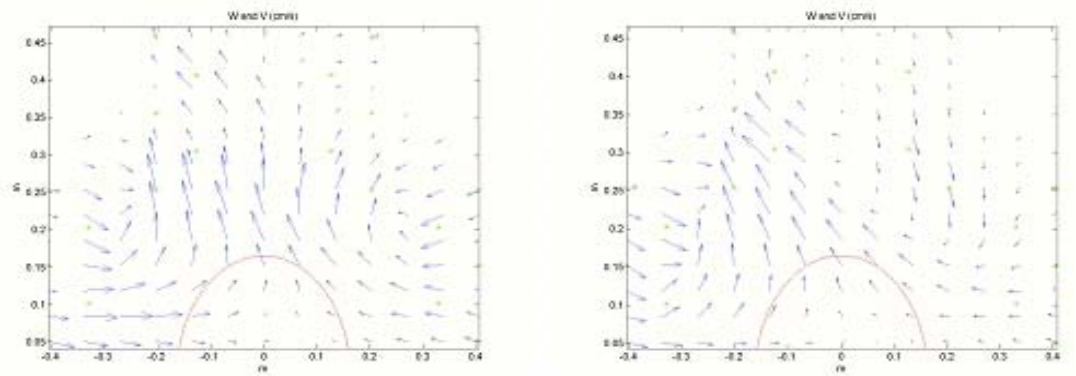

Figure D10. Velocity Field (m/s) for case 3a (left) and case 3b (right)

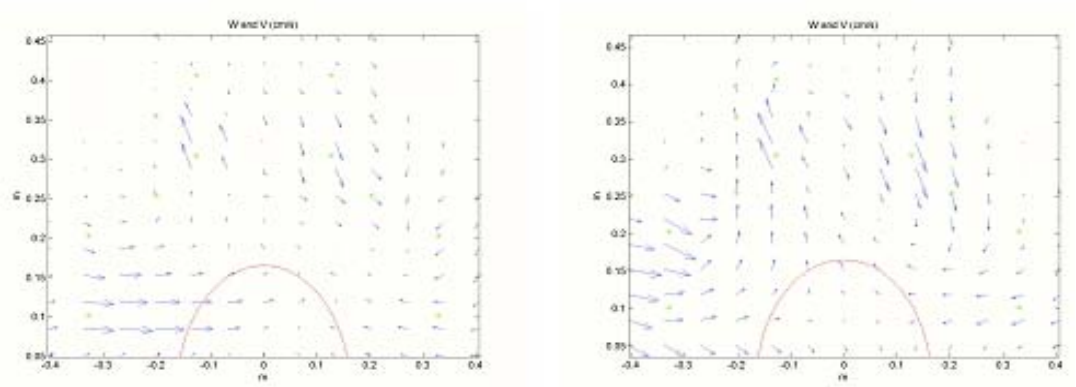

Figure D11. Velocity Field (m/s) for case 4a (left) and case 4b (right)

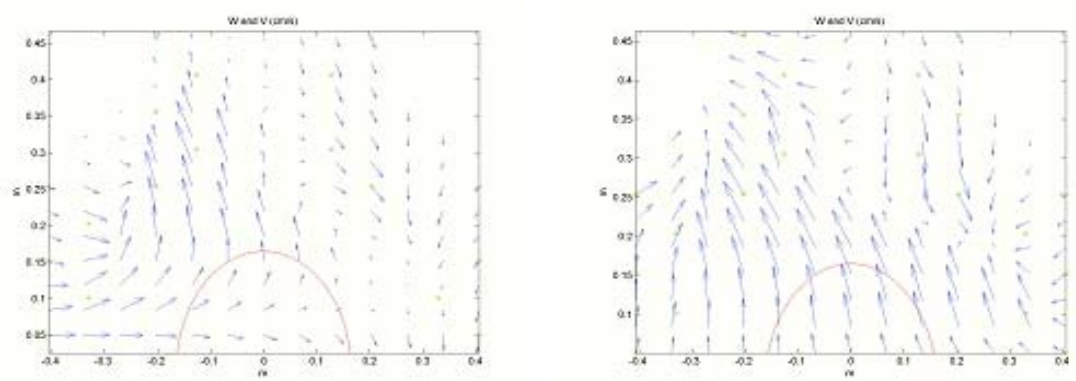

Figure D12. Velocity Field (m/s) for case 5a (left) and case 5b (right)

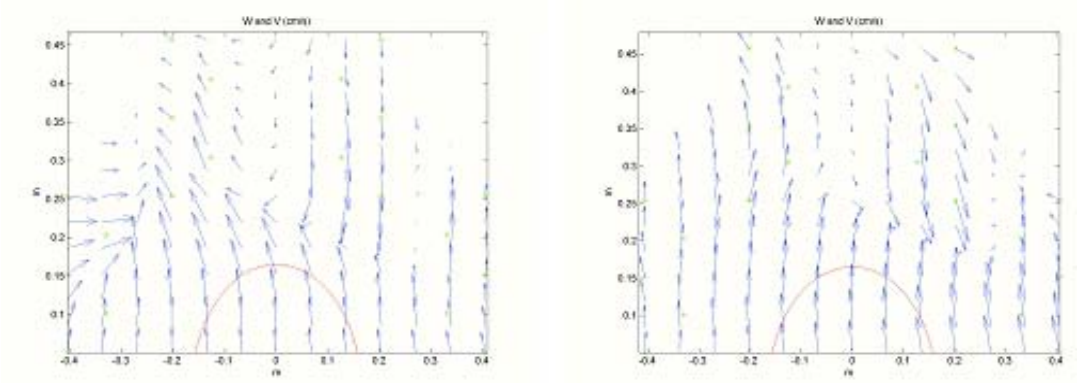

Figure D13. V and W Velocity Field (m/s) for case 6a (left) and case 6b (right)

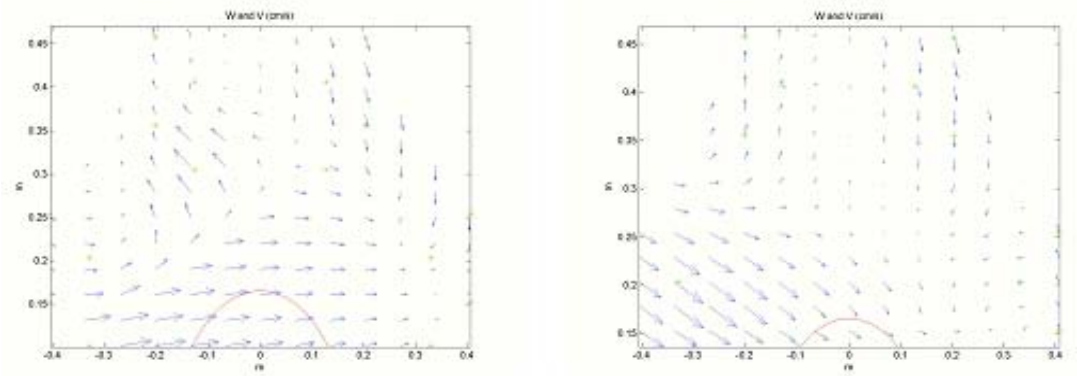

Figure D14. V and W Velocity Field (m/s) for case 7a (left) and case 7b (right)

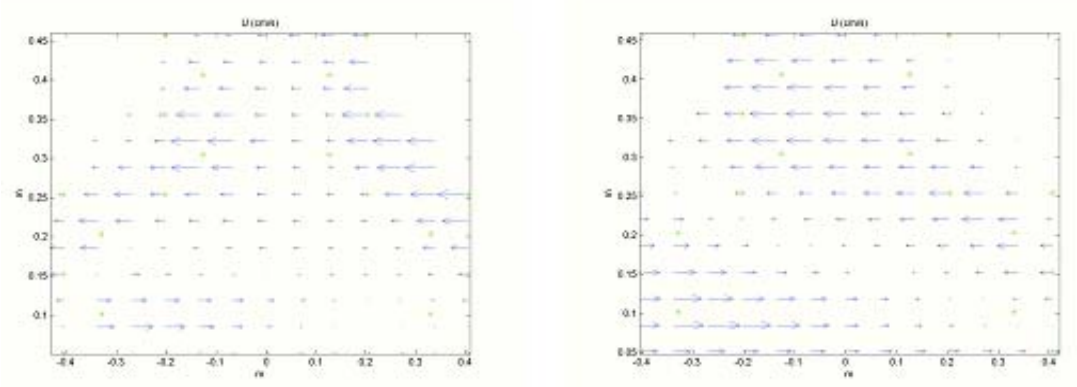

Figure D15. U Velocity Field (m/s) for case 1a (left) and case 1b (right)

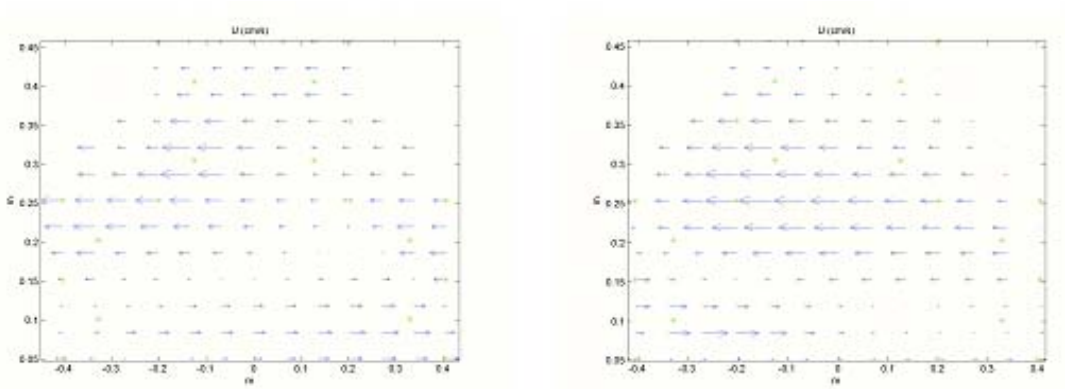

Figure D16. U Velocity Field (m/s) for case 2a (left) and case 2b (right)

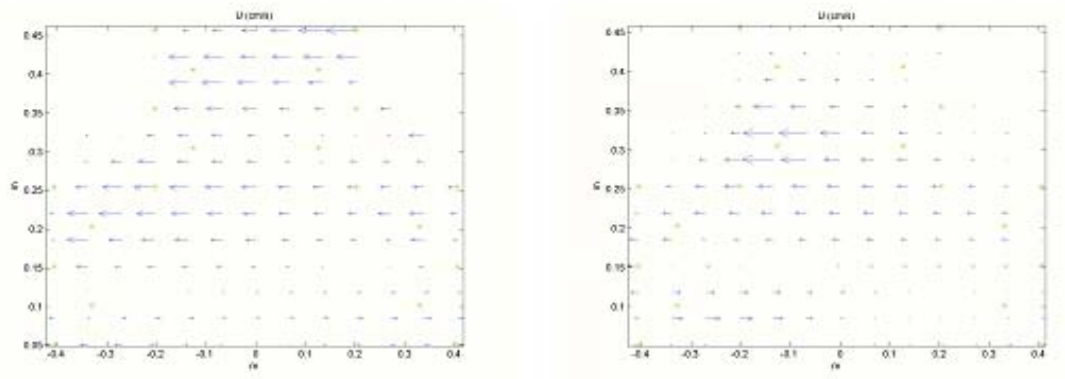

Figure D17. U Velocity Field (m/s) for case 3a (left) and case 3b (right)

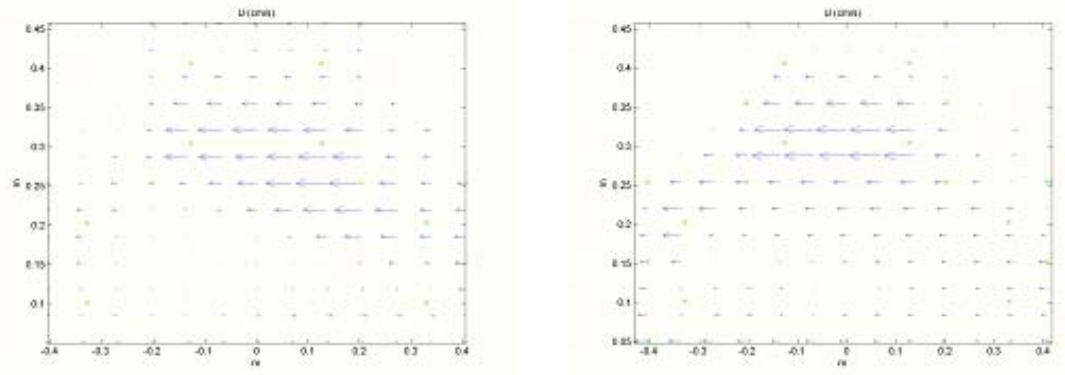

Figure D18. U Velocity Field (m/s) for case 4a (left) and case 4b (right)

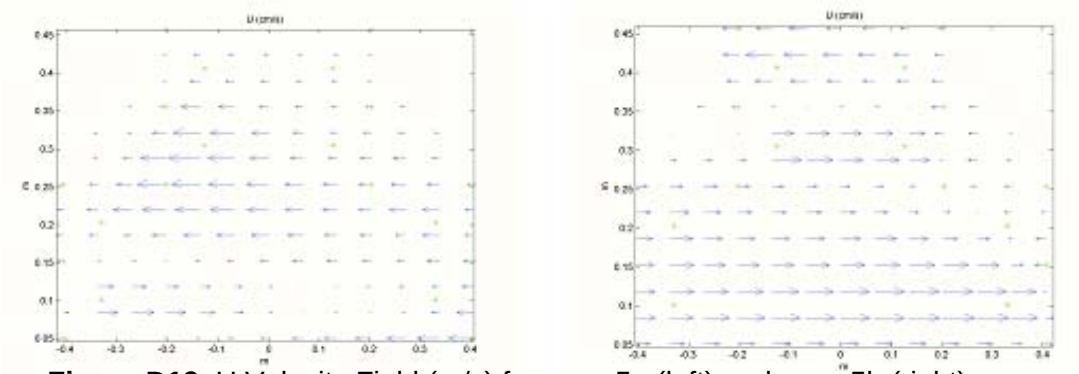

Figure D19. U Velocity Field (m/s) for case 5a (left) and case 5b (right)

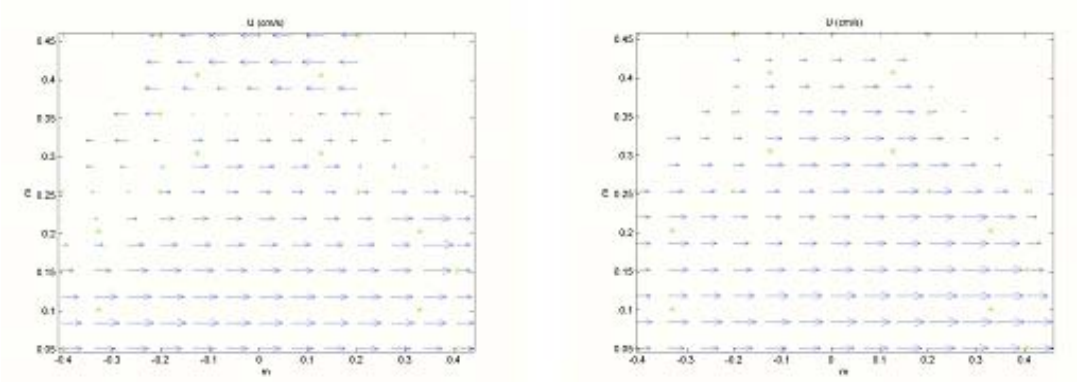

Figure D20. U Velocity Field (m/s) for case 6a (left) and case 6b (right)

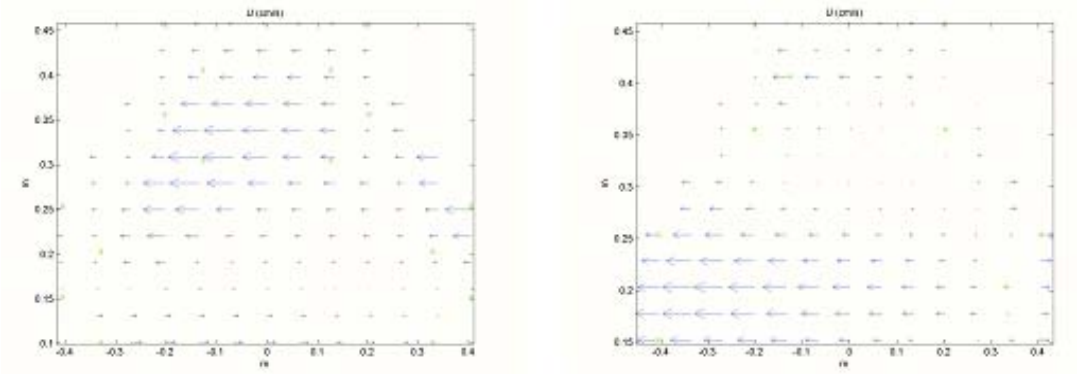

Figure D21. U Velocity Field (m/s) for case 7a (left) and case 7b (right)

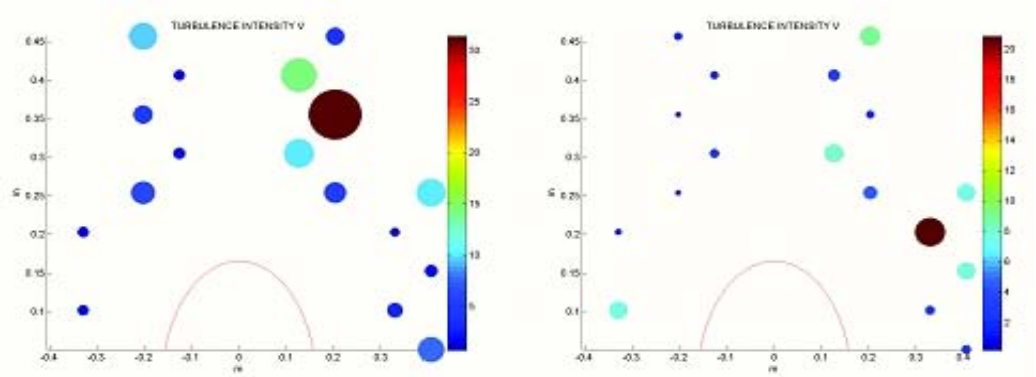

Figure D22. Turbulence Intensity for case 1a (left) and case 1b (right)

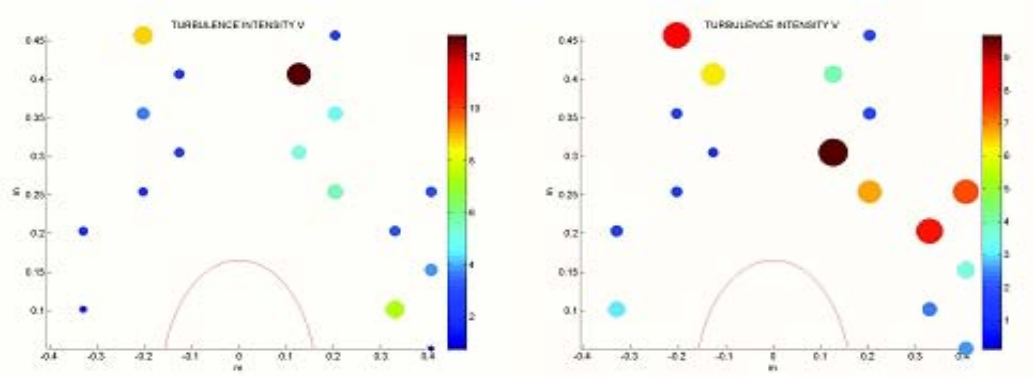

Figure D23. V Turbulence Intensity for case 2a (left) and case 2b (right)

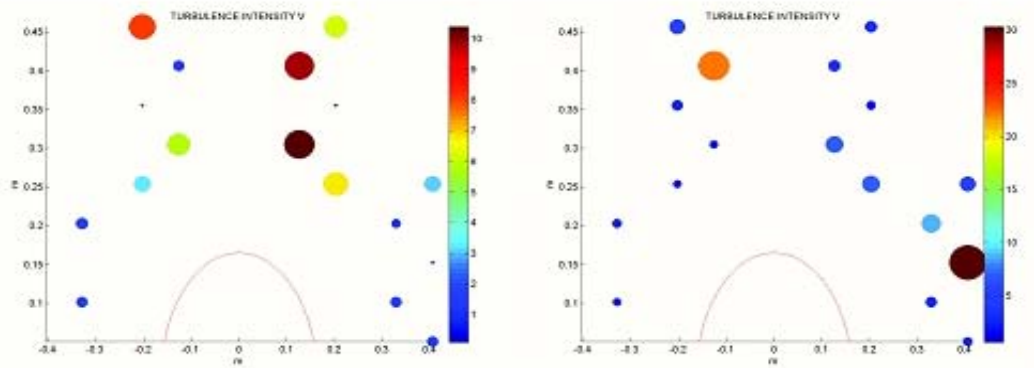

Figure D24. V Turbulence Intensity for case 3a (left) and case 3b (right)

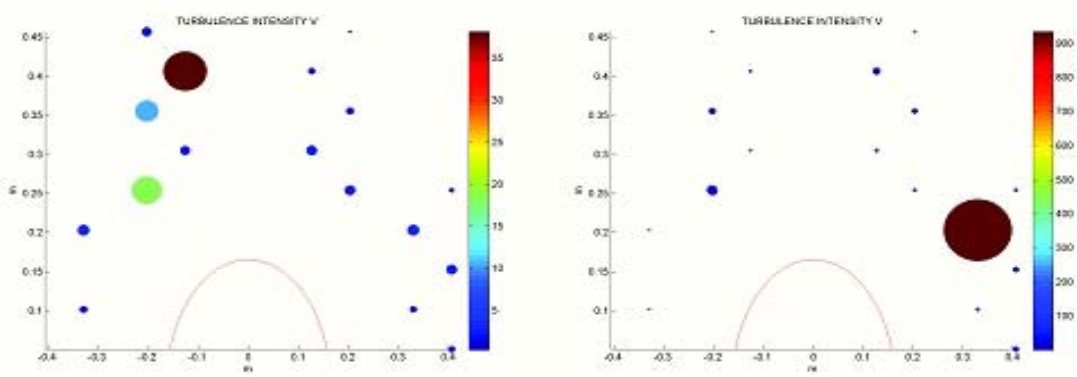

Figure D25. V Turbulence Intensity for case 4a (left) and case 4b (right)

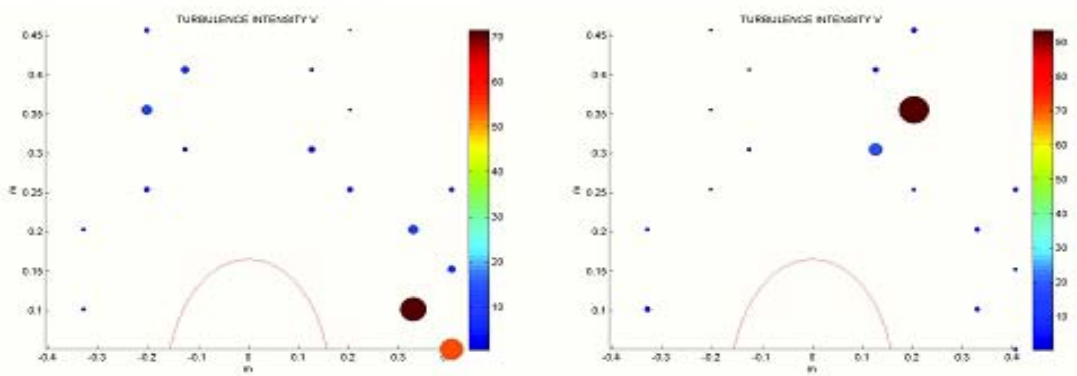

Figure D26. V Turbulence Intensity for case 5a (left) and case 5b (right)

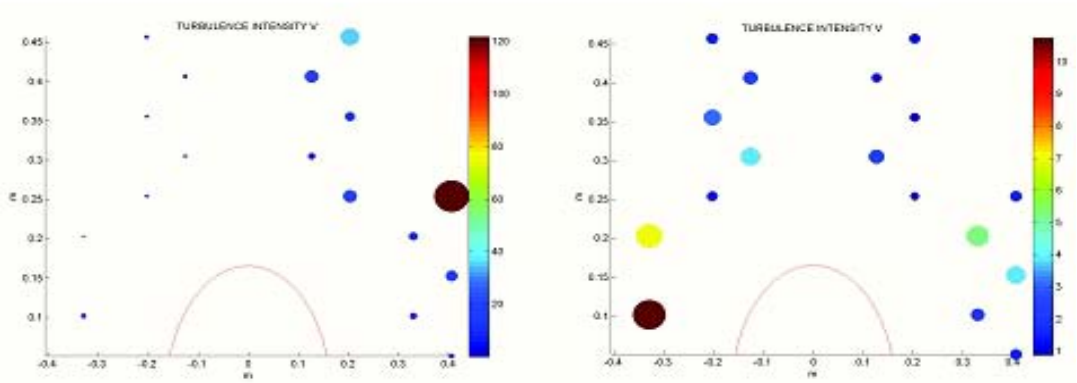

Figure D27. V Turbulence Intensity for case 6 (left) and case 6b (right)

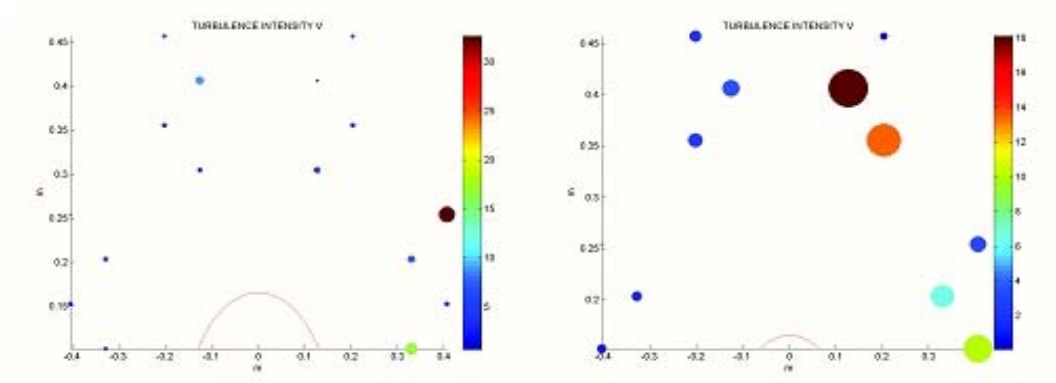

Figure D28. Turbulence Intensity for case 7 (left) and case 7b (right)

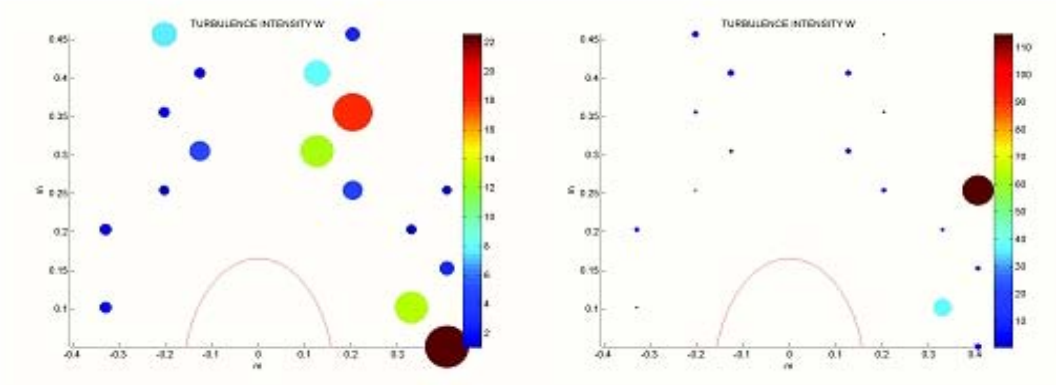

Figure D29. W Turbulence Intensity for case 1 (left) and case 1b (right)

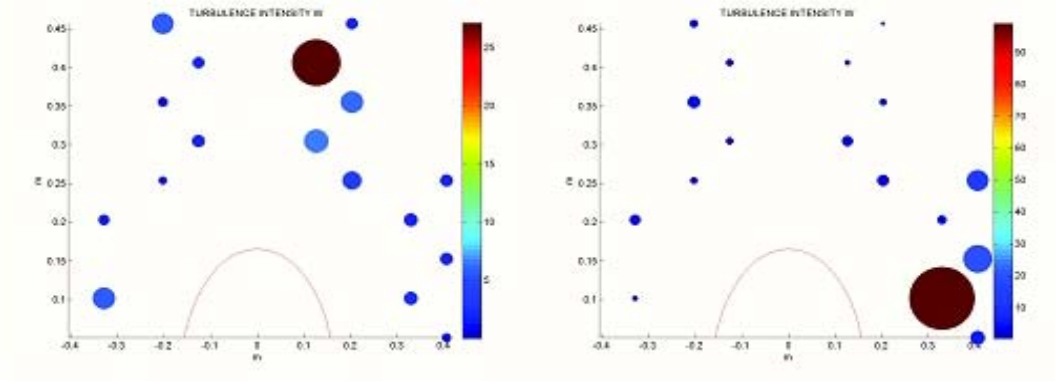

Figure D30. W Turbulence Intensity for case 2 (left) and case 2b (right)

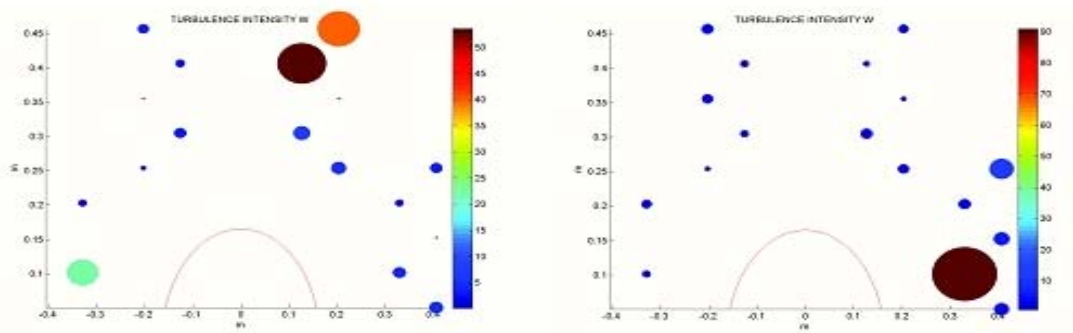

Figure D31. W Turbulence Intensity for case 3 (left) and case 3b (right)

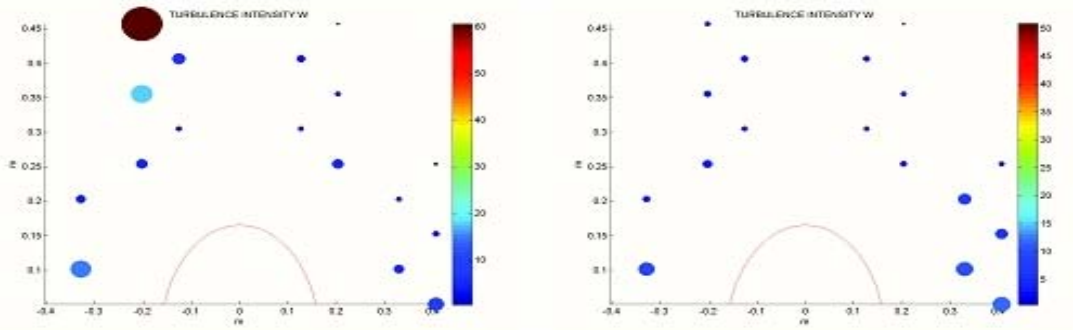

Figure D32. W Turbulence Intensity for case 4 (left) and case 4b (right)

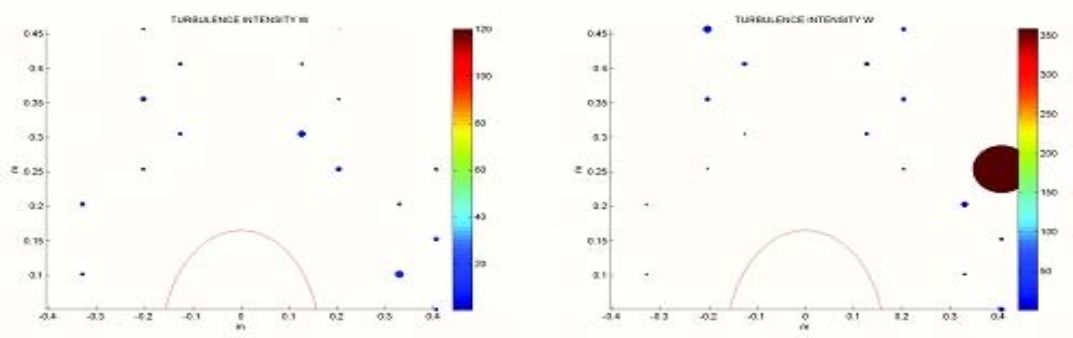

Figure D33. W Turbulence Intensity for case 5 (left) and case 5b (right)

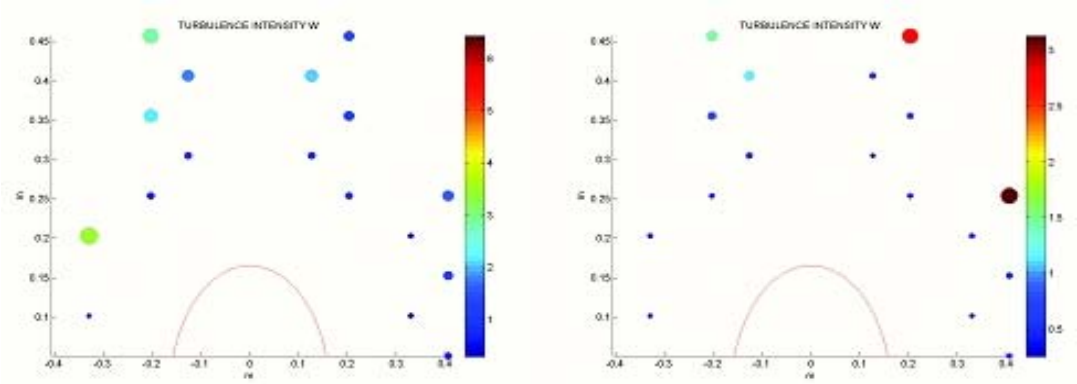

Figure D34. W Turbulence Intensity for case 6 (left) and case 6b (right)

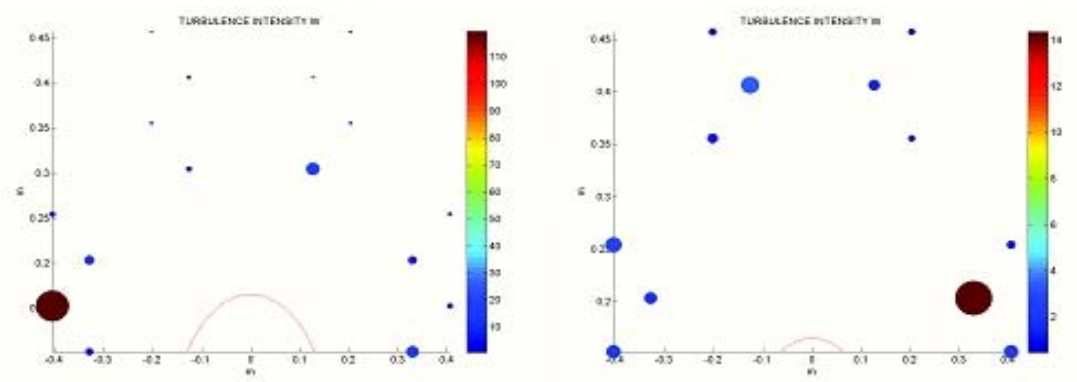

Figure D35. W Turbulence Intensity for case 7 (left) and case 7b (right)

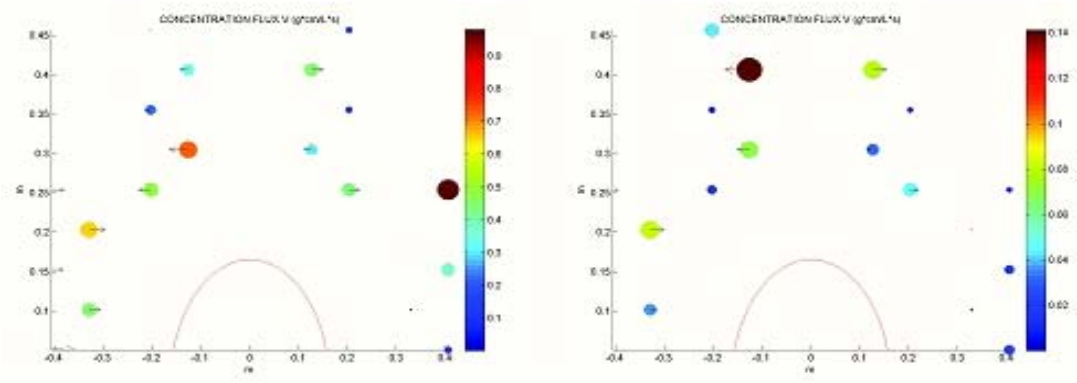

Figure D36. V Concentration Flux (g/m3) for case 1 (left) and case 1b (right)

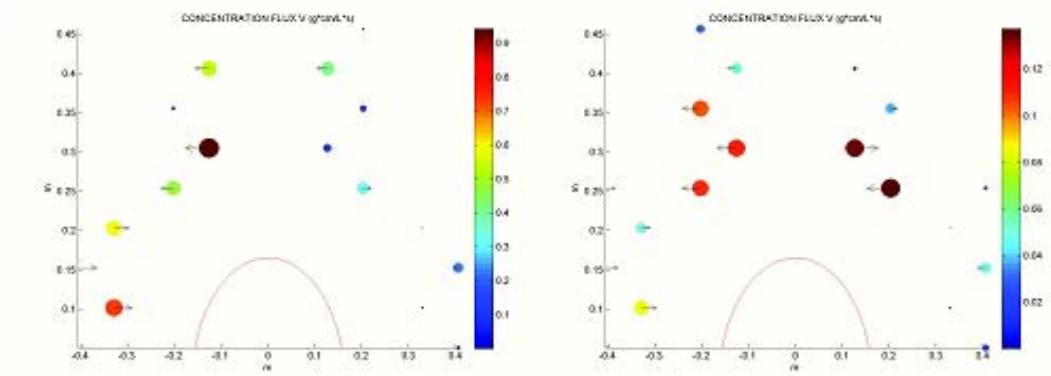

Figure D37. V Concentration Flux (g/m3) for case 2a (left) and case 2b (right)

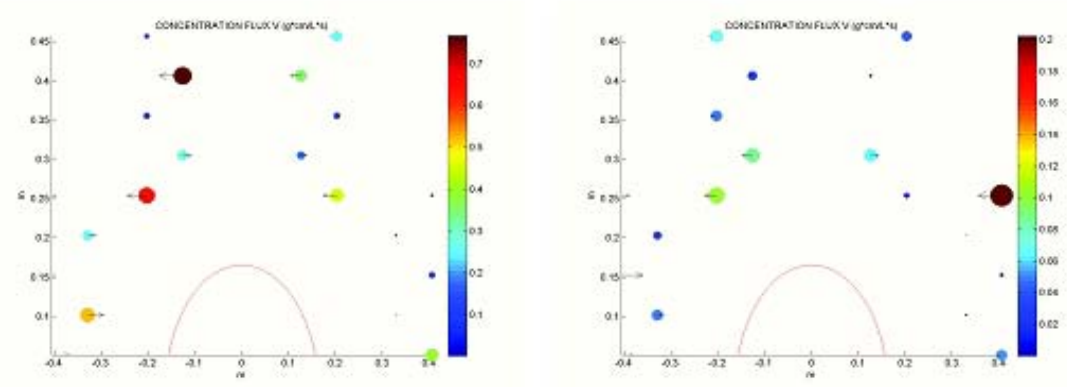

Figure D38. V Concentration Flux (g/m3) for case 3a (left) and case 3b (right)

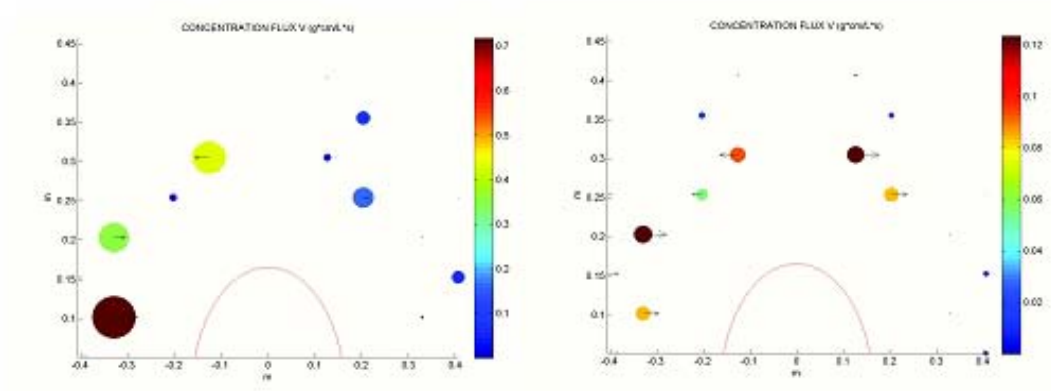

Figure D39. V Concentration Flux (g/m3) for case 4a (left) and case 4b (right)

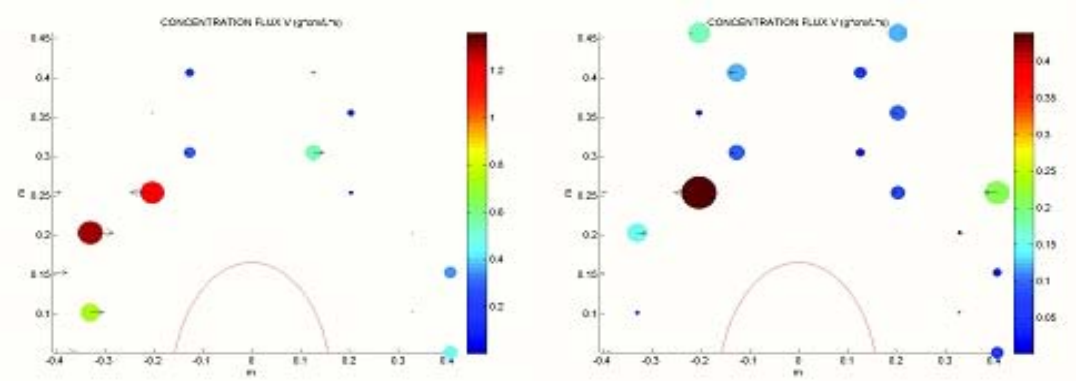

Figure D40. V Concentration Flux (g/m3) for case 5 (left) and case 5b (right)

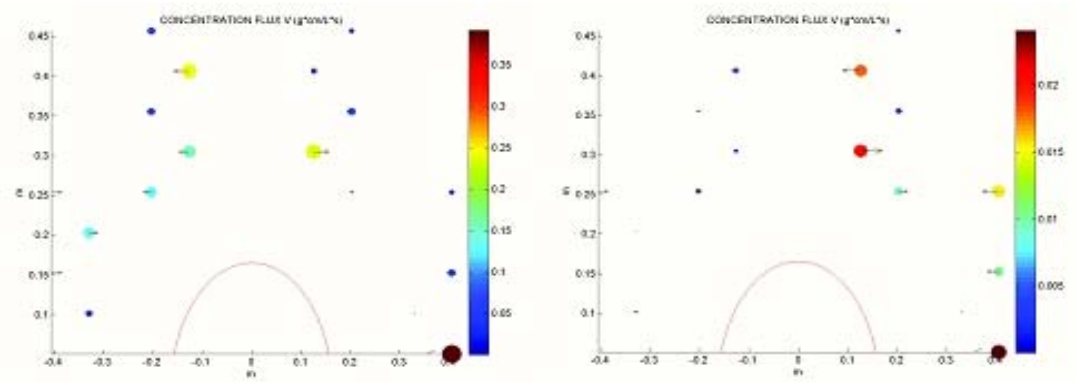

Figure D41. V Concentration Flux (g/m3) for case 6 (left) and case 6b (right)

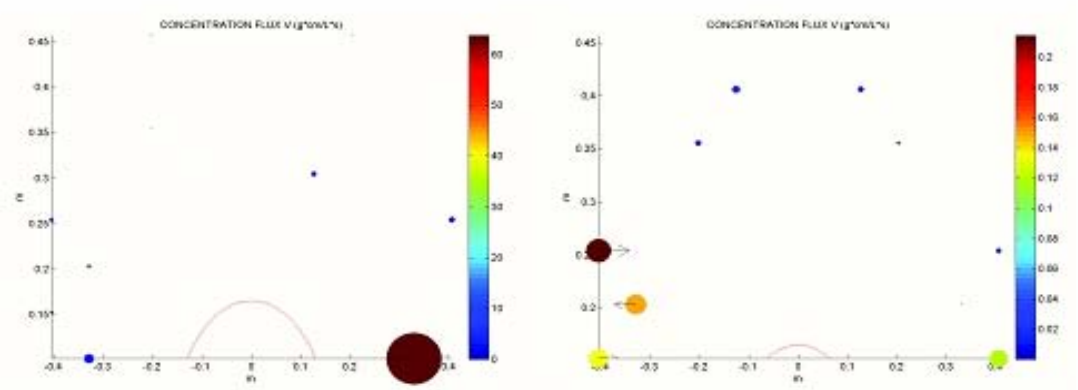

Figure D42. V Concentration Flux (g/m3) for case 7 (left) and case 7b (right)

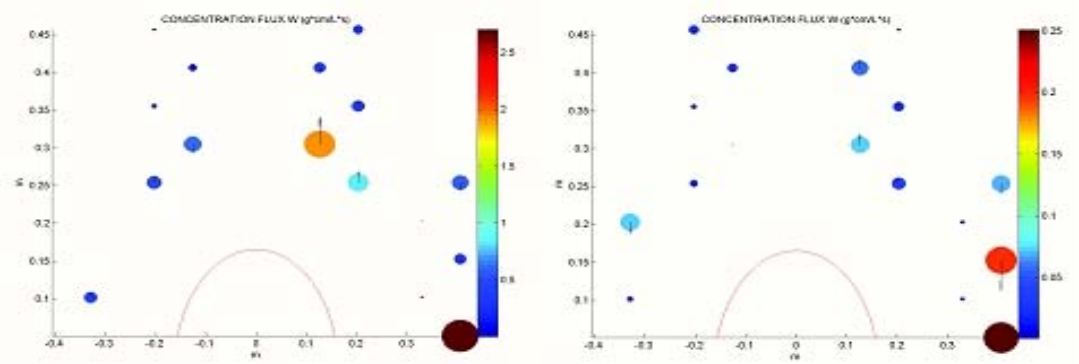

Figure D43. W Concentration Flux (g/m3) for case 1 (left) and case 1b (right)

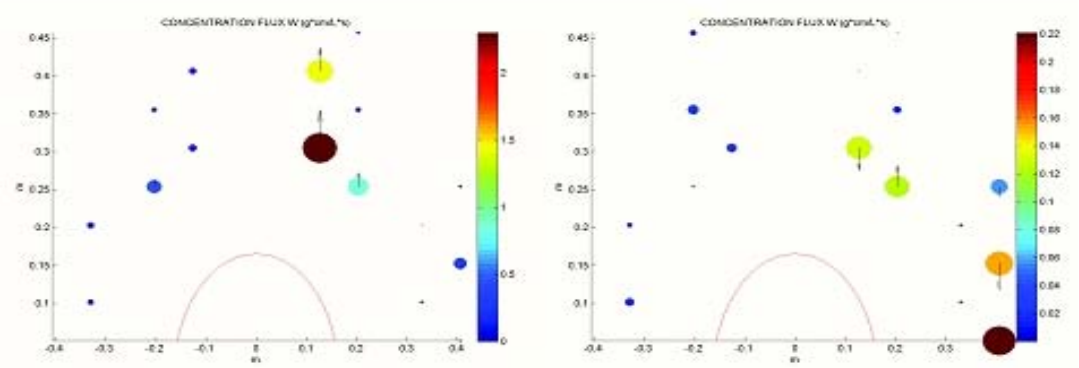

Figure D44. W Concentration Flux (g/m3) for case 2 (left) and case 2b (right)

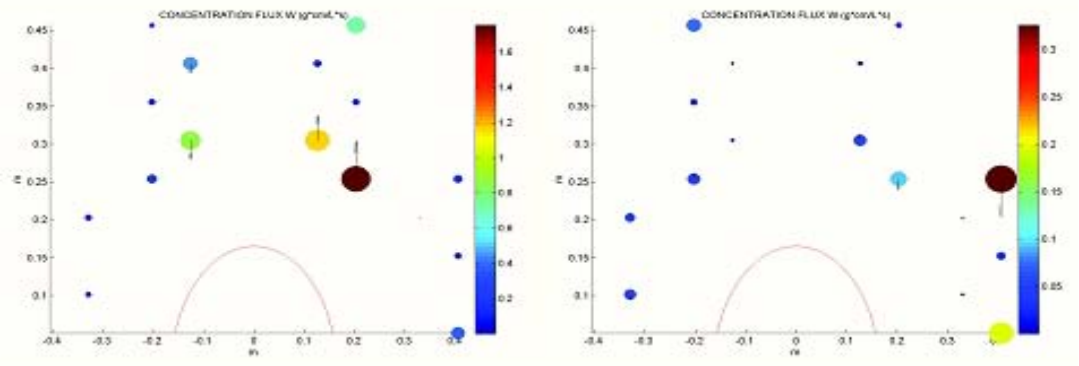

Figure D45. W Concentration Flux (g/m3) for case 3 (left) and case 3b (right)

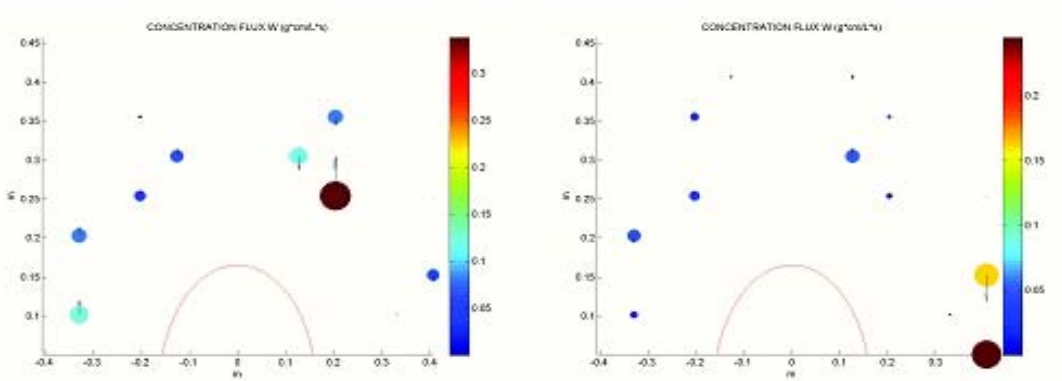

Figure 46. W Concentration Flux (g/m3) for case 4 (left) and case 4b (right)

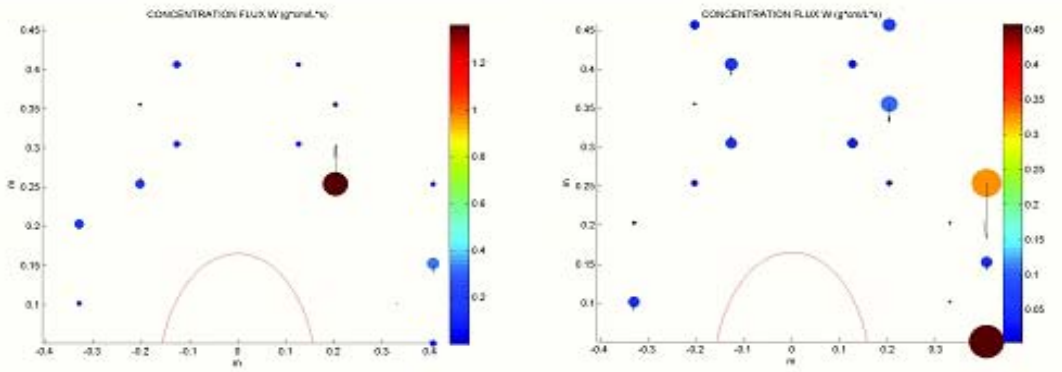

Figure D47. W Concentration Flux (g/m3) for case 5 (left) and case 5b (right)

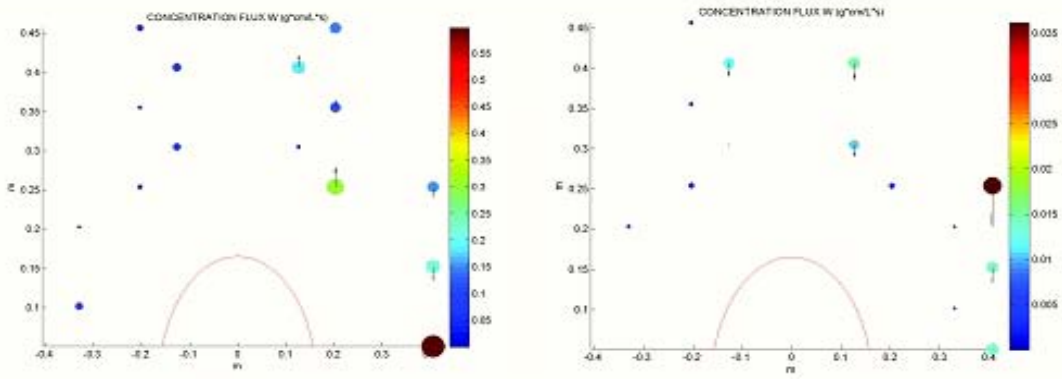

Figure D48. W Concentration Flux (g/m3) for case 6 (left) and case 6b (right)

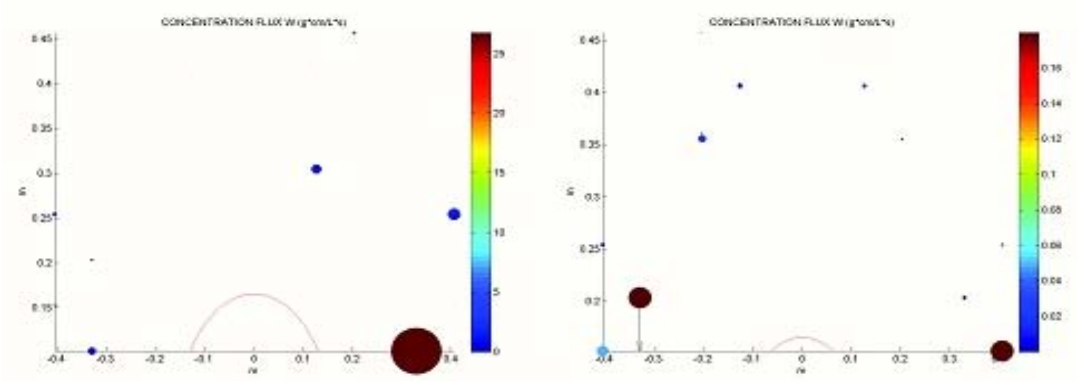

Figure D49. W Concentration Flux (g/m3) for case 7 (left) and case 7b (right)

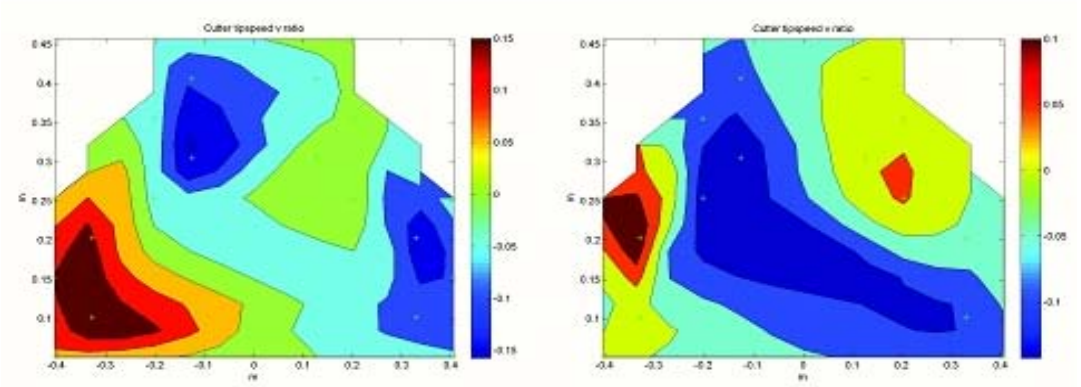

Figure D50. V Cutter Tip Speed Ratio for case 1 (left) and case 1b (right)

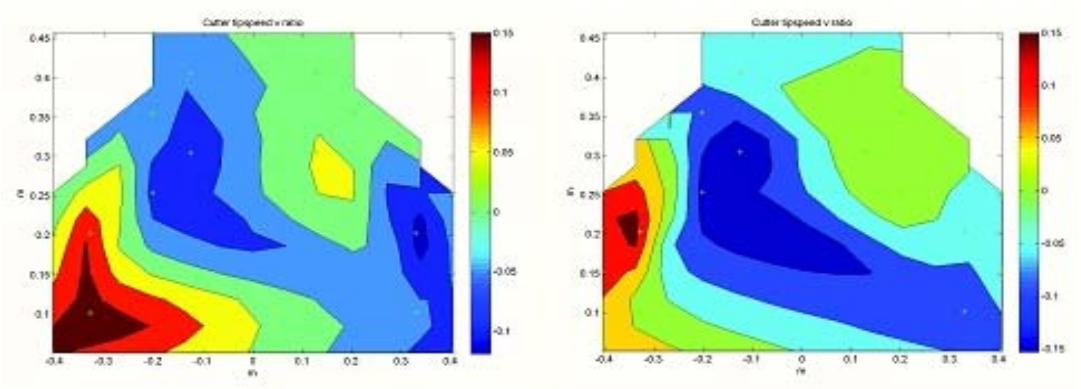

Figure D51. V Cutter Tip Speed Ratio for case 2 (left) and case 2b (right)

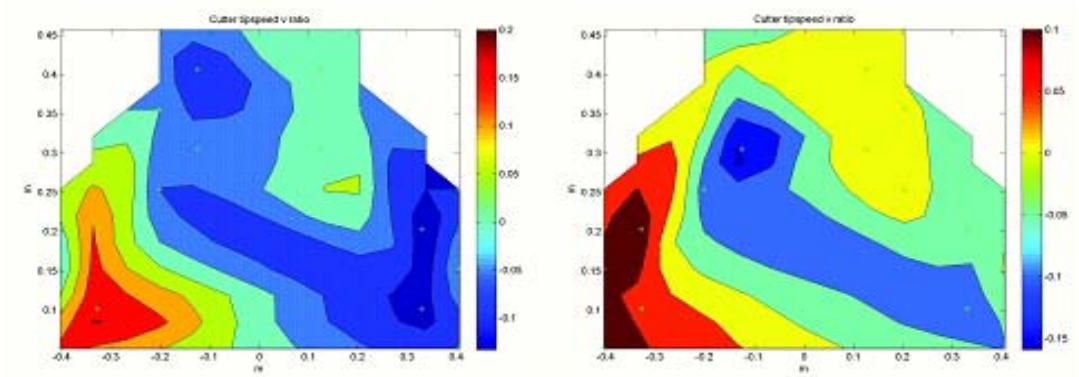

Figure D52. V Cutter Tip Speed Ratio for case 3 (left) and case 3b (right)

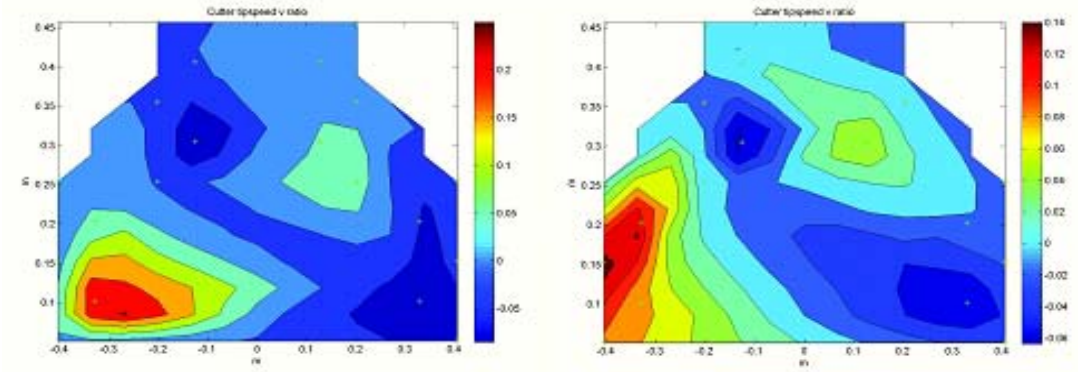

Figure D53. V Cutter Tip Speed Ratio for case 4 (left) and case 4b (right)

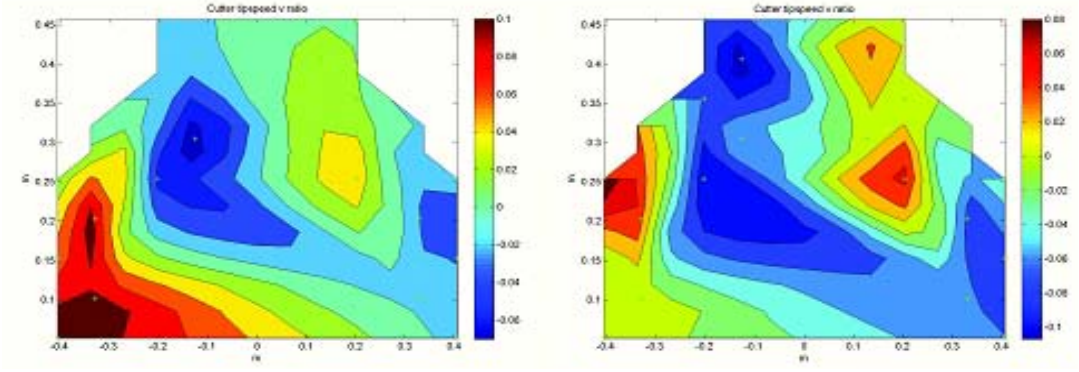

Figure D54. V Cutter Tip Speed Ratio for case 5 (left) and case 5b (right)

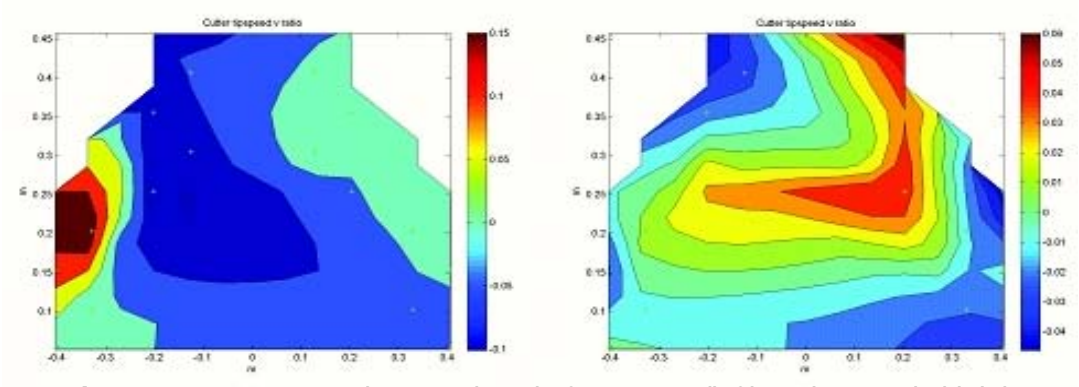

Figure D55. V Cutter Tip Speed Ratio for case 6 (left) and case 6b (right)

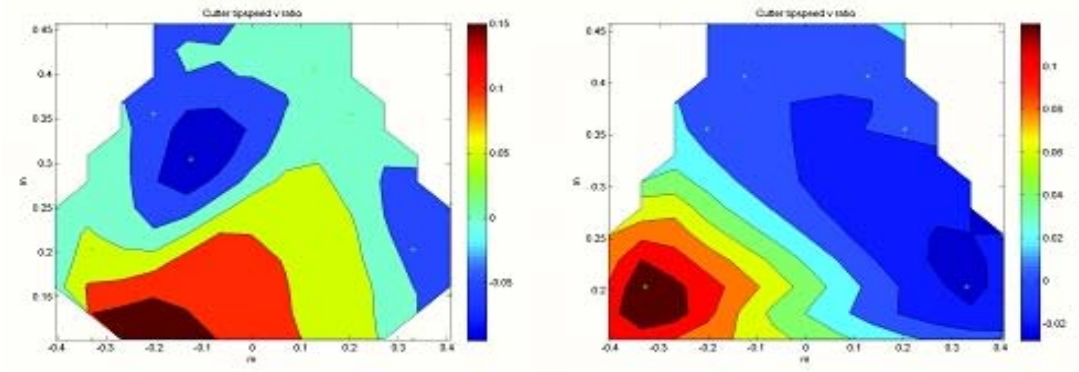

Figure D56. V Cutter Tip Speed Ratio for case 7 (left) and case 7b (right)

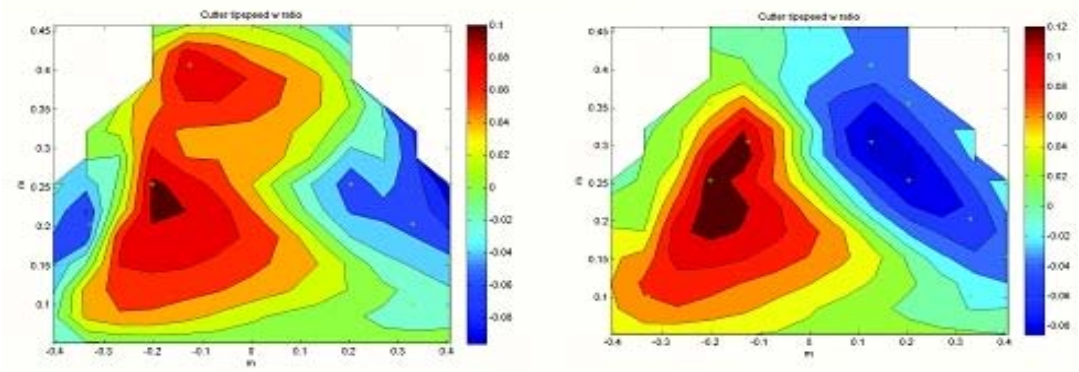

Figure D57. W Cutter Tip Speed Ratio for case 1 (left) and case 1b (right)

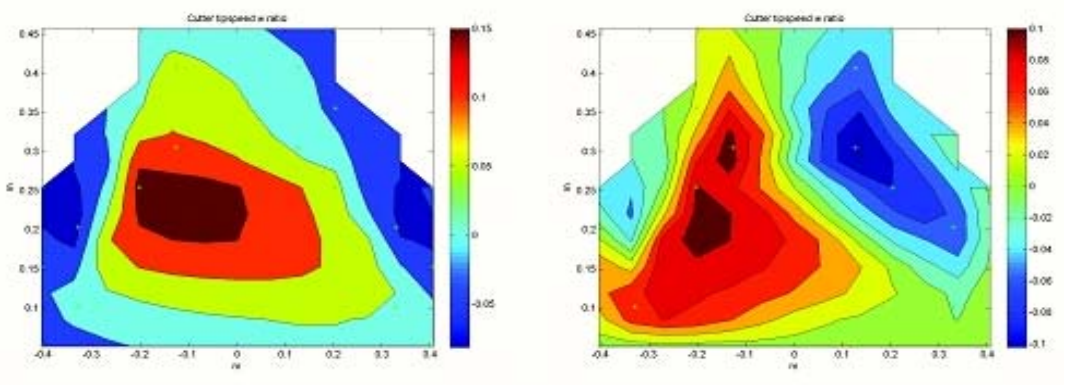

Figure D58. W Cutter Tip Speed Ratio for case 2 (left) and case 2b (right)

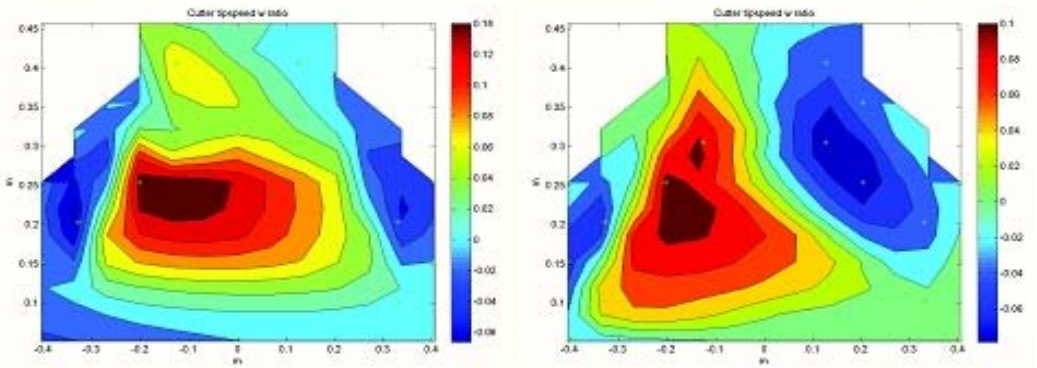

Figure D59. W Cutter Tip Speed Ratio for case 3 (left) and case 3b (right)

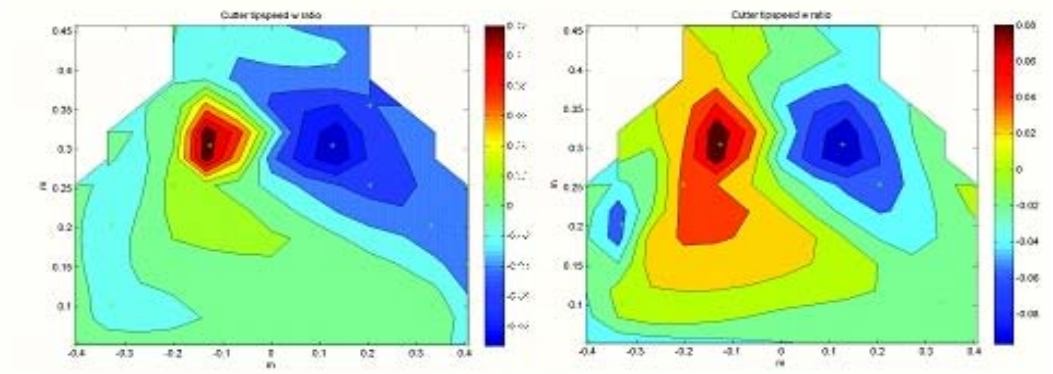

Figure D60. W Cutter Tip Speed Ratio for case 4 (left) and case 4b (right)

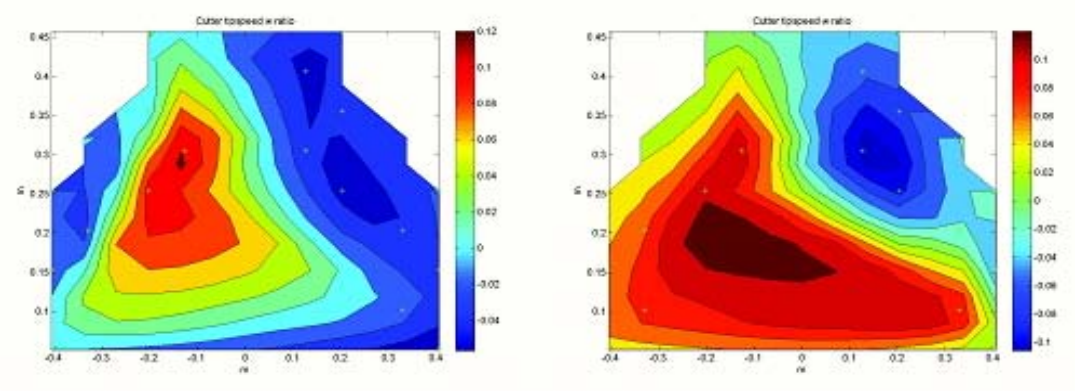

Figure D61. W Cutter Tip Speed Ratio for case 5 (left) and case 5b (right)

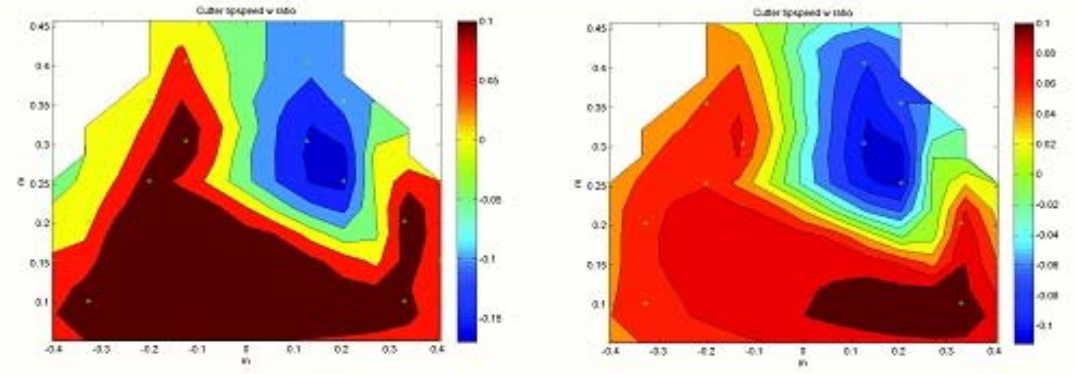

Figure D62. W Cutter Tip Speed Ratio for case 6 (left) and case 6b (right)

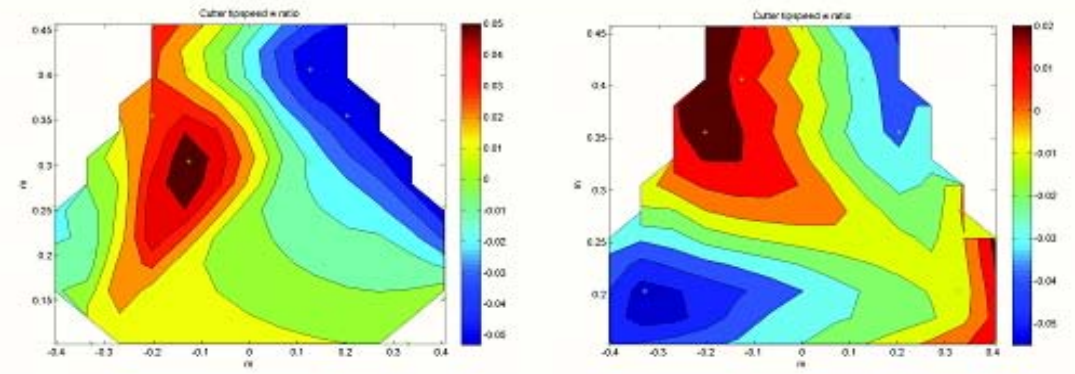

Figure D63. W Cutter Tip Speed Ratio for case 7 (left) and case 7b (right)

APPENDIX E

NUMERICAL MODEL GRAPHICAL RESULTS

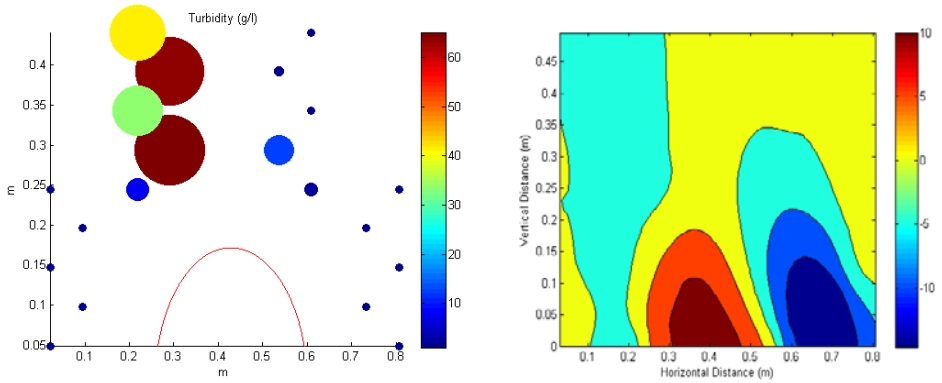

Figure E1. Turbidity and Divergence for NFCRM test case C1A

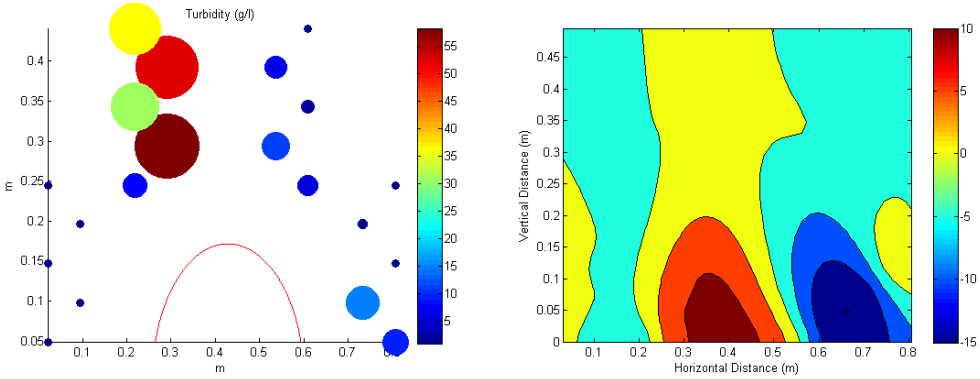

Figure E2. Turbidity and Divergence for NFCRM test case C1B

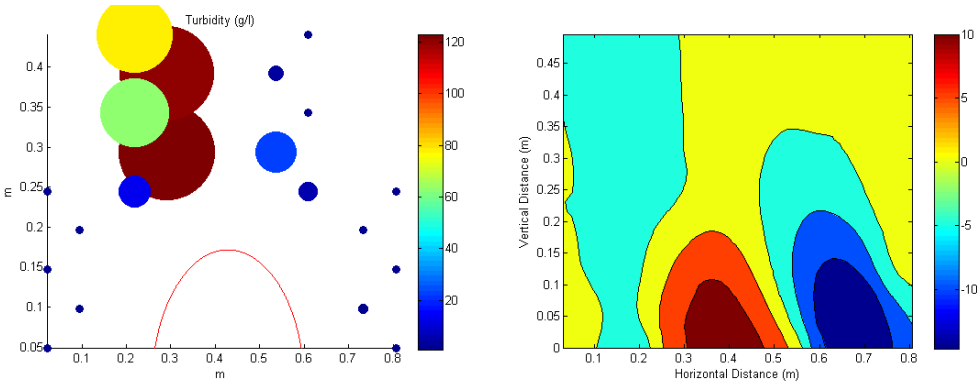

Figure E3. Turbidity and Divergence for NFCRM test case C2A

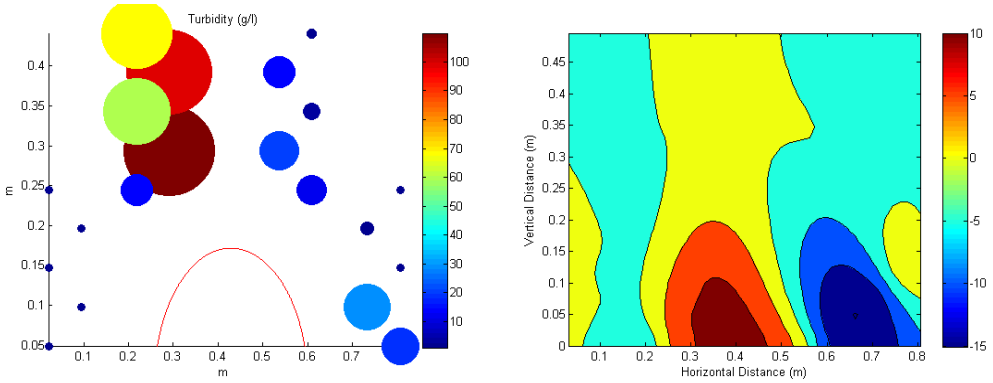

Figure E4. Turbidity and Divergence for NFCRM test case C2B

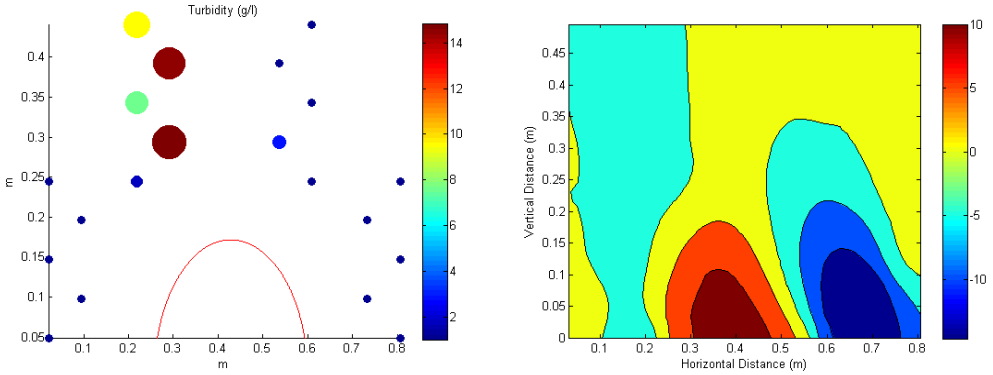

Figure E5. Turbidity and Divergence for NFCRM test case C3A

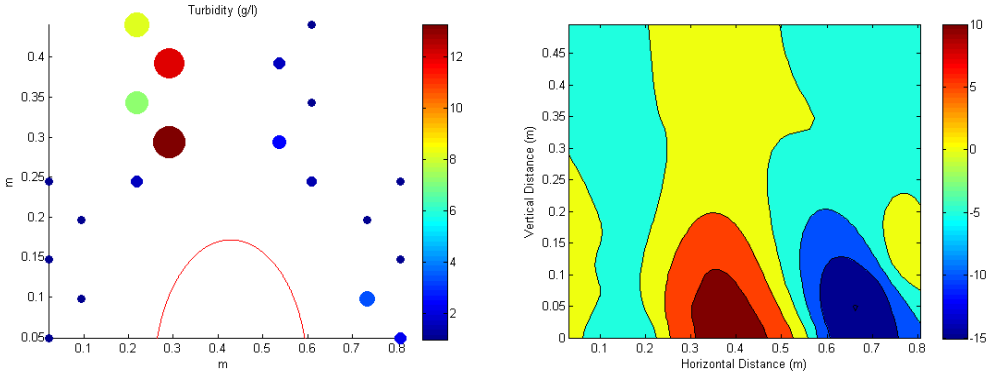

Figure E6. Turbidity and Divergence for NFCRM test case C3B.

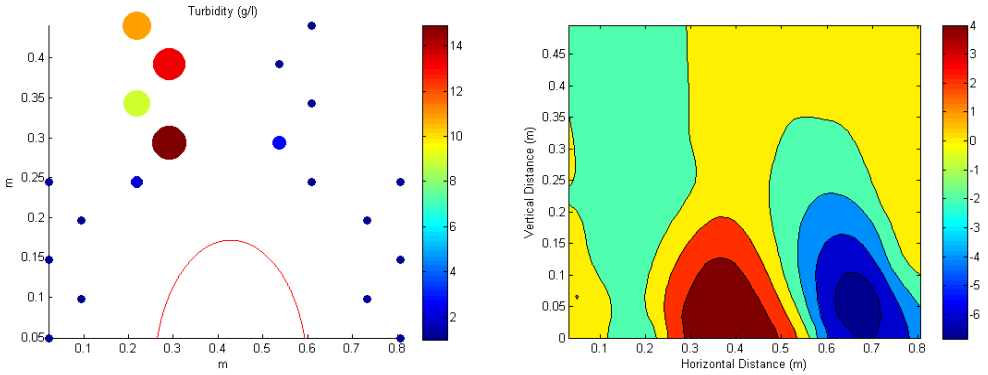

Figure E7. Turbidity and Divergence for NFCRM test case C4A.

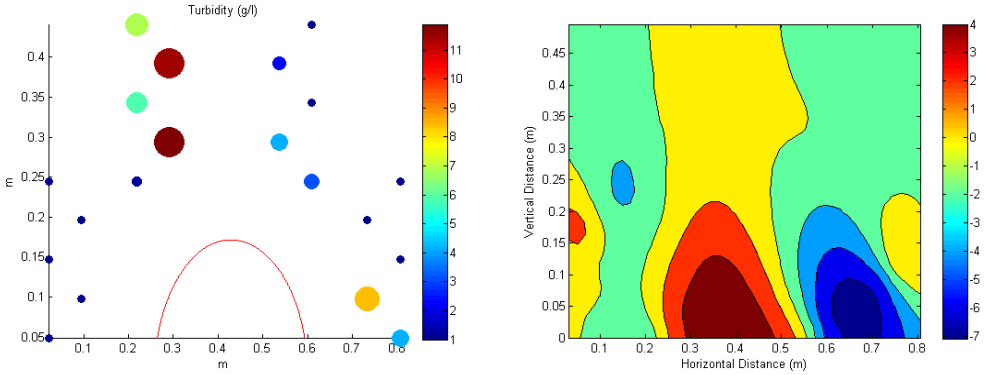

Figure E8. Turbidity and Divergence for NFCRM test case C4B.

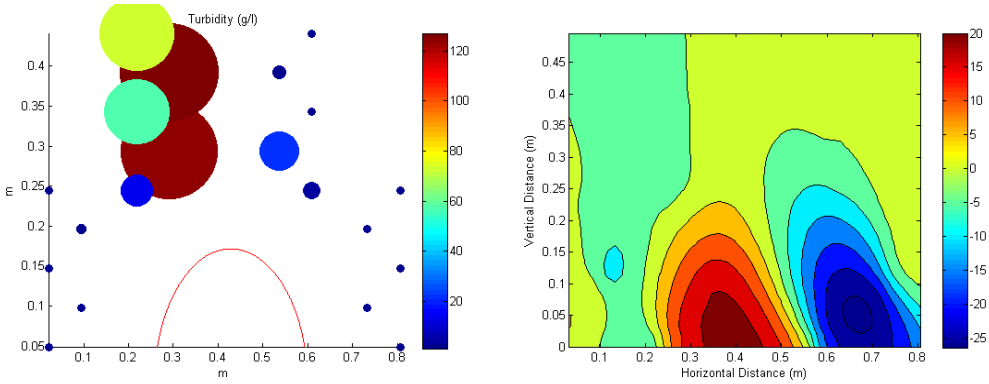

Figure E9. Turbidity and Divergence for NFCRM test case C5A.

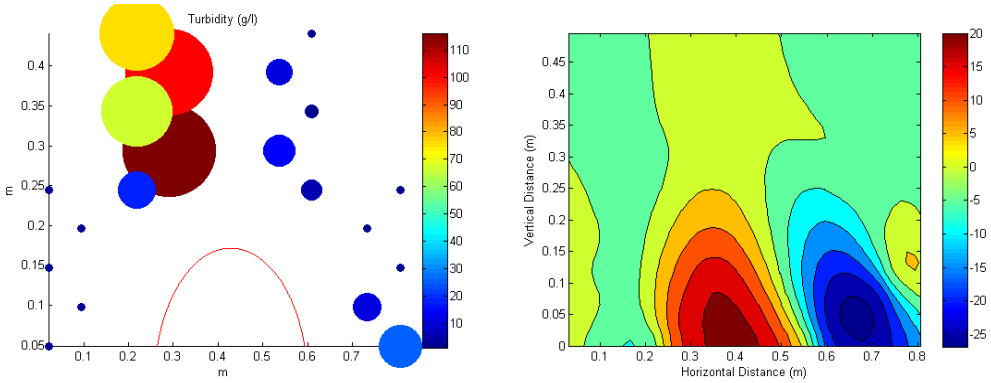

Figure E10. Turbidity and Divergence for NFCRM test case C5B.

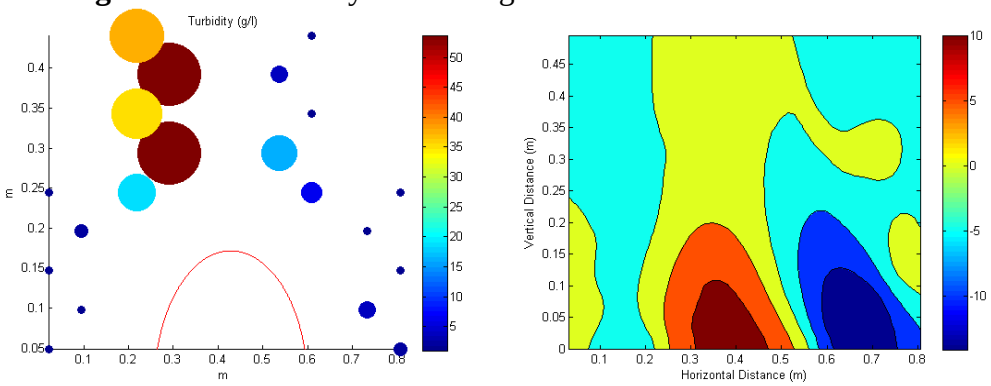

Figure E11. Turbidity and Divergence for NFCRM test case C6A.

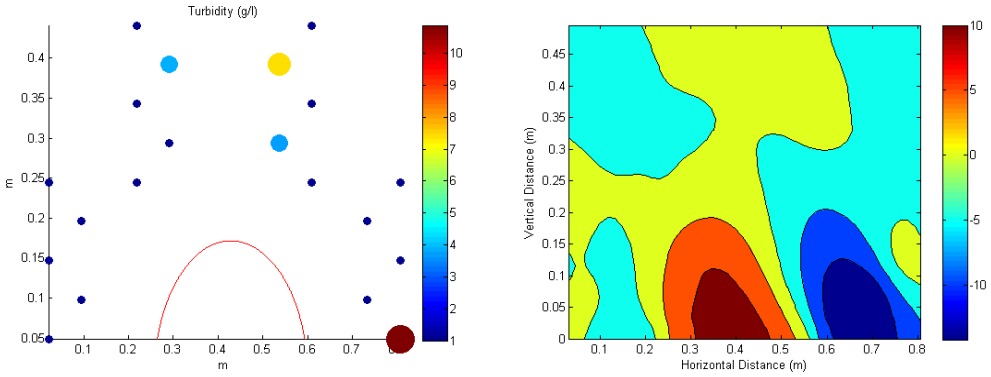

Figure E12. Turbidity and Divergence for NFCRM test case C6B.

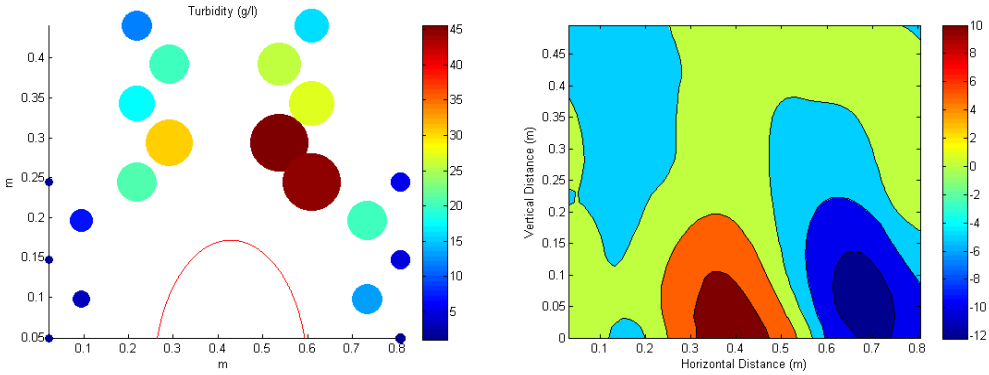

Figure E13. Turbidity and Divergence for NFCRM test case C7A.

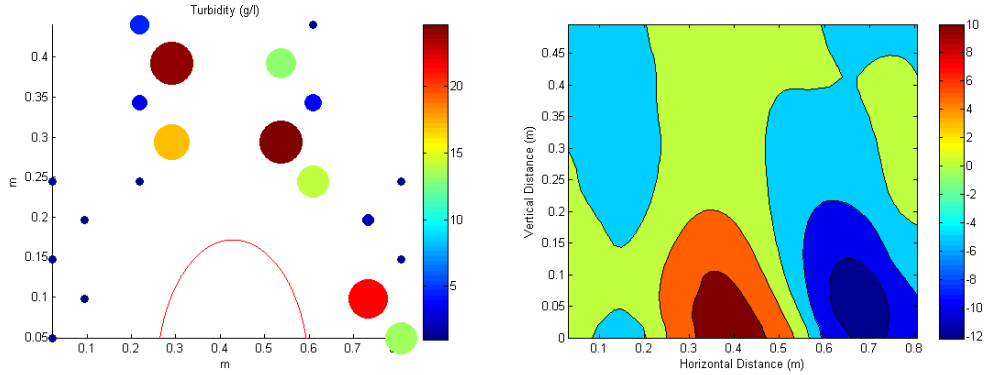

Figure E14. Turbidity and Divergence for NFCRM test case C7B.

APPENDIX F

NUMERICAL MATLAB CODE FOR NFCRM

```
 function varargout = NFCSDRM(varargin)

gui_Singleton = 1;
gui_State = struct('gui_Name',       mfilename, ...
                   'gui_Singleton',  gui_Singleton, ...
                   'gui_OpeningFcn', @NFCSDRM_OpeningFcn, ...
                   'gui_OutputFcn',  @NFCSDRM_OutputFcn, ...
                   'gui_LayoutFcn',  [] , ...
                   'gui_Callback',   []);
if nargin && ischar(varargin{1})
    gui_State.gui_Callback = str2func(varargin{1});
end

if nargout
    [varargout{1:nargout}] = gui_mainfcn(gui_State, varargin{:});
else
    gui_mainfcn(gui_State, varargin{:});
end
% End initialization code - DO NOT EDIT
% --- Executes just before NFCSDRM is made visible.
function NFCSDRM_OpeningFcn(hObject, eventdata, handles, varargin)
% Choose default command line output for NFCSDRM
handles.output = hObject;
% Update handles structure
guidata(hObject, handles);
% UIWAIT makes NFCSDRM wait for user response (see UIRESUME)
% uiwait(handles.figure1);
% --- Outputs from this function are returned to the command line.
function varargout = NFCSDRM_OutputFcn(hObject, eventdata, handles)
% varargout  cell array for returning output args (see VARARGOUT);
% hObject    handle to figure
% eventdata  reserved - to be defined in a future version of MATLAB
% handles    structure with handles and user data (see GUIDATA)
% Get default command line output from handles structure
varargout{1} = handles.output;
picA = imread('mansoncutter.tif');
checkim=image(picA);
axis off;

% --- Executes on button press in pushbutton1.
function pushbutton1_Callback(hObject, eventdata, handles)
%CUTTER RESUSPENSION MODEL
%JOHN C.HENRIKSEN
%TEXAS A&M UNIVERSITY
%OCEAN ENGINEERING
%CENTER FOR DREDGING STUDIES
```

```
%ADVISOR: DR. ROBERT RANDALL
%clear all;
set(hObject, ...
    'Visible', 'off');
%ENTER THE NECESSARY USER INPUTS
prompt={'Suction Pipe Diameter (m):','Flowrate (GPM):',...
      'Cutter Mean Diameter(m)','Length of cutter (m)', ...
      'Cutter RPM (revs/min)','Cut Thickness (m)',...
      'Swing Speed (m/s)','Cutter Blade Number',...
      'Angle of cut (degrees from horizontal)','Sediment Diameter
(um)', ...
      'Sediment Concentration (kg/m3)','Undercutting=1
Overcutting=2',...
      'Time of Simulation(s)'};
dlg_title ='Near-Field Model Input';
num_lines = 1;
def =
{'0.0762','200','0.3308','0.3308','86','0.2032','0.0173','5','24','260'
,'2650','1','20','3'};
answer = inputdlg(prompt,dlg_title,num_lines,def);
answer_str(1,:) = char(answer(1,:));
answer_str2(1,:) = char(answer(2,:));
answer_str3(1,:) = char(answer(3,:));
answer_str4(1,:) = char(answer(4,:));
answer_str5(1,:) = char(answer(5,:));
answer_str6(1,:) = char(answer(6,:));
answer_str7(1,:) = char(answer(7,:));
answer_str8(1,:) = char(answer(8,:));
answer_str9(1,:) = char(answer(9,:));
answer_str10(1,:) = char(answer(10,:));
answer_str11(1,:) = char(answer(11,:));
answer_str12(1,:) = char(answer(12,:));
answer_str13(1,:) = char(answer(13,:));
%%%%%%%%%%%%%%%
piped = (str2num(answer_str(1,:)));
flowrate = str2num(answer_str2(1,:));
cdiam = str2num(answer_str3(1,:));
clen = str2num(answer_str4(1,:));
crpm = str2num(answer_str5(1,:));
cthick = (str2num(answer_str6(1,:)));
swing = str2num(answer_str7(1,:));
bladenum = str2num(answer_str8(1,:));
cangle = str2num(answer_str9(1,:));
sediam = str2num(answer_str10(1,:));
sedconc = str2num(answer_str11(1,:));
cuttype = str2num(answer_str12(1,:));
endt = str2num(answer_str13(1,:));
%%%%%%%%%%%%%%%%
prompt2={'Current Flowrate(m/s)','Water depth (m)',...
      'Horizontal Diffusion (m2/s)','Lateral Diffusion (m2/s)',...
      'Vertical Diffusion (m2/s)'};
dlg_title ='Far-Field Model Input';
num_lines = 1;
def = {'0.1','3','5','5','5'};
```

```
answer = inputdlg(prompt2,dlg_title,num_lines,def);
answer_str14(1,:) = char(answer(1,:));
answer_str15(1,:) = char(answer(2,:));
answer_str16(1,:) = char(answer(3,:));
answer_str17(1,:) = char(answer(4,:));
answer_str18(1,:) = char(answer(5,:));
%%%%%%%%%%%%%%%%%%%%%%
farflow = (str2num(answer_str14(1,:)));
fardepth= str2num(answer_str15(1,:));
kx = str2num(answer_str16(1,:));
ky = str2num(answer_str17(1,:));
kz = str2num(answer_str18(1,:));

picA = imread('mansoncutter.tif');
image(picA,'Visible','off');
axis off;
%WE WILL START WITH THE EMPIRICAL SECTION CALCULATIONS
%CONVERT EVERYTHING TO METERS AND KILOGRAMS
%GPM TO CUBIC METERS
flowrate=flowrate*(6.309e-5);
%COMPUTE RADIUS of specific variables
piperad=piped/2;
cradius=cdiam/2;
%OTHER CONSTANTS
%DENSITY and KINEMATIC VISCOCITY OF WATER
rhow=1000;
kvisw=1.12*(10^-6);
%GRAVITY
grav=9.8;
%%%%%%%%%%%%%%%%%%%%%%%%%%%%%%%%%%%%%%%%%%%%%%%%%%%%%%%%
%USER INPUT
RPM=crpm;cutter_D=cdiam;thickcut=cthick;
sediment_diam=sediam;swingspeed=swing;
%%%%%%%%%%%%%%%%%%%%%%%%%%%%%%%%%%%%%%%%%%%%%%%%%%%%%%%%
%STANDARDS AND RATIOS
cutter_ModelD=((13.5*2.54)/100);cutter_ModelR=cutter_ModelD*0.5;
swing_Model=(0.6*2.54)/100;cutter_R=cutter_D/2;
lengthscale=cutter_D/cutter_ModelD;tipspeed=RPM*(6.28318/60)*cutter_R;
tipstandard=86*(6.28318/60)*cutter_ModelR;tipratio=tipspeed/tipstandard
;
cutratio=thickcut/cutter_D;
%%%%%%%%%%%%%%%%%%%%%%%%%%%%%%%%%%%%%%%%%%%%%%%%%%%%%%%%
%%%%%%%%%%%%%%%%%%%%%%%%%%%%%%%%%%%%%%%%%%%%%%%%%%%%%%%%
%sediment particle characteristics
%CONVERT MICROMETERS TO METERS
sediam=(sediam)*(10^-6);dvolume=(4/3)*pi*(sediam/2)^3;
dsarea=4*pi*(sediam/2)^2;sg=sedconc/1000;
smass=sg*1000*dvolume;sgpar=2.6;sgfl=1.0;
%DETERMINE SETTLING VELOCITY OF PARTICLE
%USE DIETRICH (1982)
%ASSUME SPHERICAL PARTICLES
CSF=1.0;M=6;Dstar=(sgpar-sgfl)*grav*(sediam^3);
Dstar=Dstar/(rhow*kvisw^2);R1coef=log10(Dstar);
R1=-3.76715+(1.92944*R1coef)-(0.09815*R1coef^2)...
```

```
    -(0.00575*R1coef^3)+(0.00056*R1coef^4);
R2coef=1-CSF;R2coef2=0.5-CSF;
R2=log10(1-(R2coef/0.85))-((R2coef^2.3)*tanh(R1coef-4.6))...
    +(0.3*R2coef2*(R2coef^2)*(R1coef-4.6));
R3coef=(1+(3.5-M)/2.5);R3=(0.65-((CSF/2.83)*tanh(R1coef-4.6)))^R3coef;
Wstar=R3*(10^(R1+R2));wsettle=(Wstar*grav*(sgpar-sgfl)*kvisw)/rhow;
wsettle=wsettle^(1/3);

%ANGULAR VELOCITY of CUTTER
omega=(crpm/60)*2*pi;
%PIPE SUCTION VELOCITY
pipevelocity=flowrate/(pi*piperad^2);
%NOW COMPUTE THICKNESS OF EACH CUT hprime
hprime=((swing*60)/(crpm*bladenum));
%The center of the suction pipe for this model is located one third or
the
%distance or the cutter radius below the center of the cutter
pipeheight=-(cradius/1.5);
if cuttype==1
    %Undercutting
    rnot=(0.4*pipevelocity)/omega;
else
    %Overcutting
    rnot=(0.4*pipevelocity)/omega;
end

%HERE IS WHERE I PUT FIGURE OUT THE LENGTH OF THE release along the
blade
%Calculate the length of the material
lprime=cradius-rnot;
if rnot>=cradius
   lprime=0.05*cradius;
end
%Check to see if the thickness of cut is greater than this
%This covers a shallow cut scenario
if cthick<lprime
   lprime=cthick;
end
%Calculate volume of material for each cut (cubic meters)
%HERE WE HAVE INCORPORATED THE LADDER ANGLE
cvolm3=hprime*lprime*clen*cosd(cangle);
%Calculate kg of material per cut
cmass=cvolm3*sedconc;
%%%%%%%%%%%%%%%%%%%%%%%%%%%%%%%%%%%%%%%%%%%%%%%%%%%%%%%%%%%%%%%%%%%%
%DOMAIN BOUNDARIES
endy=2.5*cutter_D;endz=2.5*cutter_D;
%%%%%%%%%%%%%%%%%%%%%%%%%%%%%%%%%%%%%%%%%%%%%%%%%%%%%%%%%%%%%%%%%%%%
%DISCRETIZATION AND INITALIZATION
dy=0.05*cutter_D;dz=0.05*cutter_D;y=[0:dy:endy];z=[0:dz:endz];
ny=length(y);nz=length(z);C=zeros(ny,nz,2);Cadd=zeros(ny,nz,1);
Coefm=zeros(ny,nz,1);mc=zeros(ny,nz,1);bottom_C=zeros(ny,nz,1);
v=zeros(ny,nz);w=zeros(ny,nz);
DZ=zeros(ny,nz);DY=zeros(ny,nz);
yb_n_l=(ny*dy/2)-cutter_R;yb_n_r=(ny*dy/2)+cutter_R;
```

```
%%%%%%%%%%%%%%%%%%%%%%%%%%%%%%%%%%%%%%%%%%%%%%%
max_vel=(tipspeed+swingspeed);
%COURANT NUMBER
Cr=0.5;
%HERE IS Dt based on the courant number and the Maximum Diffusion
dt=(dy/max_vel)*Cr;dt=dt/10000;time=[0:dt:endt];nt=length(time);
% %Now that we have the mass for each cut we have to calculate what it
would be for
% %each time step
ncutps=((crpm/60)*(bladenum));ncutpdelt=ncutps*dt;totmassdt=cmass*ncutp
delt
%%%%%%%%%%%%%%%%%%%%%%%%%%%%%%%%%%%%%%%
totmass=totmassdt;
%LETS GRAPH THIS DISPLAY
hdist=[cdiam*-1.5:0.001:cdiam*1.5];
hsize=length(hdist);
if cuttype==1
   %UNDERCUTTING DISPLAY
   for i=1:hsize
      cutthick(i)=-cradius+cthick;
      if hdist(i)< -cradius
         cutthick(i)= -cradius;
      elseif hdist(i)> cradius
         cutthick(i)= -cradius +cthick;
      else
         cutthick(i)=-cradius;
      end
   end
else
   %OVERCUTTING DISPLAY
   for i=1:hsize
      cutthick(i)=-cradius+cthick;
      if hdist(i)< -cradius
         cutthick(i)= -cradius + cthick;
      elseif hdist(i)> cradius
         cutthick(i)= -cradius;
      else
         cutthick(i)=-cradius;
      end
   end
end
ypipe=[-piperad:0.0001:piperad];
sizeyp=length(ypipe);
ycutter=[-cradius:0.0001:cradius];
sizeycutter=length(ycutter);
ylengcut=[0:0.0001:cradius];
sizeylengcut=length(ylengcut);
zlengcut=zeros(1,sizeylengcut);
for i=1:sizeyp
   zpipe(i)=sqrt(piperad^2-(ypipe(i)^2));
   zpipeneg(i)=zpipe(i)*(-1);
   zpipeneg(i)=zpipeneg(i)+pipeheight;
   zpipe(i)=zpipe(i)+pipeheight;
end
```

```
for i=1:sizeycutter
   zcutter(i)=sqrt(cradius^2-(ycutter(i)^2));
   zcutterneg(i)=zcutter(i)*(-1);
end
ysand=[cradius-lprime:0.0001:cradius];
lysand=length(ysand);
zsand=zeros(1,lysand);
if cuttype==1
   %UNDERCUTTING DISPLAY

   axes(handles.axes3)
   axis([-cdiam*1.5 cdiam*1.5 -cdiam*1.5 cdiam*1.5]);hold on
   plot(ypipe,zpipe)
   title('Setup for Dredging')
   xlabel('Horizontal Distance (m)')
   ylabel('Vertical Distance (m)')
   plot(ycutter,zcutter,'r')
   plot(ypipe,zpipeneg)
   plot(ycutter,zcutterneg,'r')
   plot(hdist,cutthick,'k')
   plot(ylengcut,zlengcut,'m')
   plot(ysand,zsand,'g','MarkerSize',30)
   yarrow=0;
   zarrow=cdiam;
   zarrowmag=cdiam;
   quiver(yarrow,zarrow/1.5,zarrowmag,0,'k')
   text(-cdiam/2,zarrow,'Undercut Swing Direction')


else
   %OVERCUTTING DISPLAY
   axes(handles.axes3)
   axis([-cdiam*1.5 cdiam*1.5 -cdiam*1.5 cdiam*1.5]);hold on
   plot(ypipe,zpipe)
   plot(ycutter,zcutter,'r')
   plot(ypipe,zpipeneg)
   plot(ycutter,zcutterneg,'r')
   plot(hdist,cutthick,'k')
   plot(-ylengcut,zlengcut,'m')
   plot(-ysand,zsand,'g')
   title('Setup for Dredging');xlabel('m');ylabel('m')
   yarrow=0;zarrow=cdiam;zarrowmag=-cdiam;
   quiver(yarrow,zarrow/1.5,zarrowmag,0,'k')
   text(-cdiam/2,zarrow,'Overcut Swing Direction')
end
% %NOW THAT WE HAVE THE FLUX WE CAN PROGRAM THE ADVECTION DIFFUSION
MODEL
%HERE IS WHERE I AM ADDING INFO ON SAMPLING POINTS AROUND CUTTER
%%%%%%%%%%%%%%%%%%%%%%%%%%%%%%%%%%%%%%%%%%%%%%%%%%%%%%%%%%%%%%%%%%
%INCHES TO METERS
ydiam=[5 5 8 8 8 13 13 16 16 16 -5 -5 -8 -8 -8 -13 -13 -16 -16 -16 ];
zdiam=[12 16 10 14 18 4 8  2 6 10 12 16 10 14 18 4 8 2 6 10];
ydiamv=[5 5 8 8 8 13 13 16 16 16 -5 -5 -8 -8 -8 -13 -13 -16 -16 ...
```

```
    -16 -13.5/2 -13.5/4 0 13.5/4 13.5/2];
zdiamv=[12 16 10 14 18 4 8  2 6 10 12 16 10 14 18 4 8 2 6 10 0 13.5/4
...
    13.5/2 13.5/4 0];
ydiam7b=[ 5  8 8  13  16 16  -5  -8 -8  -13 -16 -16];
zdiam7b=[ 16  14 18  8   6 10  16  14 18  8  6 10];
ydiam7bv=[ 5  8 8  13  16 16  -5  -8 -8  -13 -16 -16 -13.5/2 -13.5/4
...
    0 13.5/4 13.5/2];
zdiam7bv=[ 16  14 18  8   6 10  16  14 18  8  6 10  0 13.5/4 ...
    13.5/2 13.5/4 0];
%%%%%%%%%%%%%%%%%%%%%%%%%%%%%%%%%%%%%%%%%%%%%%%%%%%%%%%%%%%%%%%%%%%%%%%%%%%%
%%
ydiam=ydiam*2.54;zdiam=zdiam*2.54;ydiam=ydiam/100;zdiam=zdiam/100;
ydiamv=ydiamv*2.54;zdiamv=zdiamv*2.54;ydiamv=ydiamv/100;zdiamv=zdiamv/1
00;
ydiam7b=ydiam7b*2.54;zdiam7b=zdiam7b*2.54;ydiam7b=ydiam7b/100;zdiam7b=z
diam7b/100;
ydiam7=ydiam7b;zdiam7=zdiam7b;
ydiam7bv=ydiam7bv*2.54;zdiam7bv=zdiam7bv*2.54;ydiam7bv=ydiam7bv/100;
zdiam7bv=zdiam7bv/100;ydiam7v=ydiam7bv;zdiam7v=zdiam7bv;
%%%%%%%%%%%%%%%%%%%%%%%%%%%%%%%%%%%%%%%%%%%%%%%%%%%%%%%%%%%%%%%%%%%%%%%%%%%%
%%%%
%%%%%%%%%%%%%%%%%%%%%%%%%%%%%%%%%%%%%%%%%%%%%%%%%%%%%%%%%%%%%%%%%%%%%%%%%%%%
%
ydiamstore=ydiam;zdiamstore=zdiam;
%%%%%%%%%%%%%%%%%%%%%%%%%%%%%%%%%%%%%%%%%%%%%%%%%%%%%%%%%%%%%%%%%%%%%%%%%%%%
%%
%%%%%%%%%%%%%%%%%%%%%%%%%%%%%%%%%%%%%%%%%%%%%%%%%%%%%%%%%%%%%%%%%%%%%%%%%%%%
%%%%%
%THE FOLLOWING IS THE RAW DATA FROM THE LAB TESTS CONDUCTED
%THE DATA IS GROUPED IN TO OVERCUTTING DATA AND UNDERCUTTING DATA
%THIS DATA IS THEN INTERPOLATED BASED ON THE CUTTING DEPTH
%Turbidity is in Grams/Liter=kg/m3
%Velocity is in M/s;
%%%%%%%%%%%%%%%%%%%%%%%%%%%%%%%%%%%%%%%%%%%%%%%%%%%%%%%%%%%%%%%%%%%%%%%%%%%%
%%%%
%CASE1
meant1 = [62.4165   62.2970   41.4646   40.3067   14.3757   0.0605 ...
      0.0649 27.3469   12.4578   25.6414   28.3090   16.8343   10.6452
...
      6.7748 3.8656   52.6104   27.0483   17.5387   17.5112    9.3660];

meanv1 = [0.0426   -0.0358    0.0656    0.0174    0.0432   -0.0998  ...
      -0.2069 -0.0666   -0.1436   -0.0375   -0.2372   -0.1463   -0.0350
...
      -0.0265 -0.0075    0.2803    0.2520    0.1358    0.2269    0.0937
...
      -tipspeed -0.5*tipspeed 0 0.5*tipspeed tipspeed];
meanw1 =[0.0364    0.0567   -0.0754    0.0289   -0.0604   -0.0088   ...
      -0.0644 0.0084   -0.0495   -0.1433    0.0795    0.1447    0.1541
...
      0.0772 0.0117    0.0812   -0.0899   -0.0083   -0.0619   -0.0220
...
```

```
      0 0.5*tipspeed tipspeed 0.5*tipspeed 0];
cfv1 =[ -0.3053    0.4551    0.4353   -0.0937    0.1141    0.0139   ...
      0.0010 -0.1197    0.3727    0.9792   -0.7246   -0.3328   -0.4828
...
      -0.2287 -0.0047    0.4507    0.6550    0.9320    0.4461
0.4855];
cfw1 =[1.9172   -0.2812    0.8340    0.3148    0.2185    0.0078
0.0023 ...
      -2.7023   -0.2909   -0.5706   -0.6246   -0.1261    0.4662
0.0532 ...
      0.0258    0.3424   -0.0001   -0.0926    0.0514   -0.0414];
%convert to g/m3
meant1=meant1/1000;meant1=abs(meant1);cfv1=cfv1/1000;cfw1=cfw1/1000;
%%%%%%%%%%%%%%%%%%%%%%%%%%%%%%%%%%%%%%%%%%%%%%%%%%%%%%%%%%%%%%%%%%%%%%%%
%%%%
%CASE1B
meant1b=[9.7999 5.0016 9.3956 5.0731 3.7149 1.0000 2.0000 6.4203 6.2708
...
      4.4786 8.0628 5.7220 7.4243 6.1116 4.7558 6.8687 8.0198 6.4971
4.7757 ...
      5.8203];
meanv1b=[0.0629    0.0433    0.0865    0.0403    0.0029   -0.1506 ...
      -0.0219   -0.0995   -0.0271   -0.0088 -0.1989   -0.0976   -0.1972
...
      -0.1294   -0.0623    0.0121    0.2166    0.0181    0.0080
0.1698 ...
      -tipspeed -0.5*tipspeed 0 0.5*tipspeed tipspeed];
meanw1b=[  -0.1299   -0.0410   -0.1236   -0.0506   -0.0457   -0.0051...
      -0.0911    0.0301   -0.0508    0.0006 0.1944    0.0276
0.1963...
      0.0651    0.0221    0.1232    0.0509    0.0756    0.0841
0.0195 ...
      0 0.5*tipspeed tipspeed 0.5*tipspeed 0];
cfv1b = [ -0.0317    0.0780    0.0448    0.0071    0.0001   -0.0020
...
      -0.0006   -0.0229   -0.0197   -0.0088 -0.0696   -0.1413   -0.0186
...
      -0.0099   -0.0429    0.0359    0.0802    0.0032    0.0063
0.0283];
cfw1b=[0.0717    0.0555    0.0379    0.0240    0.0023   -0.0042   -
0.0037 ...
      -0.2510   -0.1978   -0.0683 0.0007   -0.0211   -0.0125   -
0.0056...
      -0.0210    0.0086   -0.0743   -0.0024    0.0030   -0.0007];
meant1b=meant1b/1000;meant1b=abs(meant1b);cfv1b=cfv1b/1000;cfw1b=cfw1b/
1000;
%%%%%%%%%%%%%%%%%%%%%%%%%%%%%%%%%%%%%%%%%%%%%%%%%%%%%%%%%%%%%%%%%%%%%%%%
%%%%
%%%%%%%%%%%%%%%%%%%%%%%%%%%%%%%%%%%%%%%%%%%%%%%%%%%%%%%%%%%%%%%%%%%%%%%%
%%%
%CASE6
meant6=[26.4698   33.2572   27.0204   26.8330   25.5333    1.0000 ...
      2.0000   10.0417   29.5900   29.6219 16.3390   11.7578
12.6172...
```

```
      13.7081    9.2517    8.3184   18.2521    8.3573   12.1194
12.2845];
meanv6=[ 0.0313    0.0129   -0.0074    0.0179    0.0049   -0.0170  ...
      0.0254   -0.0429    0.0094    0.0014 -0.1106   -0.0670   -0.1432
...
      -0.1173   -0.0750    0.0242    0.2770    0.0287    0.1922
0.2630 ...
      -tipspeed -0.5*tipspeed 0 0.5*tipspeed tipspeed];
meanw6=[-0.2336   -0.1298   -0.2521   -0.1275   -0.1072    0.1577 ...
      0.2112    0.1211    0.0942    0.0746 0.2039    0.0872    0.1817
...
      0.0601    0.0472    0.1742    0.0463    0.1447    0.0866   -
0.0233 ...
       0 0.5*tipspeed tipspeed 0.5*tipspeed 0];
cfv6=[ 0.2367   -0.0373  0.0039   -0.0730    0.0270    0.0036
0.0003...
      -0.3910   -0.0679   -0.0261 -0.1573   -0.2391   -0.1240   -
0.0700...
      -0.0656    0.0523    0.1331    0.0660    0.1573    0.1588];
cfw6=[ -0.0218    0.1869    0.3017    0.1157    0.1419    0.0005 ...
      -0.0003   -0.5983   -0.2160   -0.1512 0.0644    0.0808
0.0311...
      0.0171   -0.0485    0.0684   -0.0089   -0.0330   -0.0157   -
0.0438];
meant6=meant6/1000;meant6=abs(meant6);cfv6=cfv6/1000;cfw6=cfw6/1000;
%%%%%%%%%%%%%%%%%%%%%%%%%%%%%%%%%%%%%%%%%%%%%%%%%%%%%%%%%%%%%%%%%%%%%%%%
%%%
%CASE6B
meant6b=[5.3698    6.4763    6.2157    6.4222    6.7987    1.0000...
      2.0000    2.3206    4.7051    5.7820 3.9640    5.2585    4.0602
...
      4.4973    5.1638    3.6342    3.8046    4.1785    3.8191
4.2231];
meanv6b=[ 0.0241    0.0467    0.0706    0.0585    0.1013   -0.0282  ...
      -0.0117   -0.0425   -0.0112   -0.0687 0.0148   -0.0367
0.0475...
      -0.0236   -0.0592   -0.0049    0.0207    0.0045   -0.0326   -
0.0028 ...
      -tipspeed -0.5*tipspeed 0 0.5*tipspeed tipspeed];
meanw6b=[-0.1534   -0.1172   -0.1593   -0.0984   -0.0389    0.1638 ...
      0.1327    0.1416    0.0897    0.0269 0.1224    0.0857
0.1154...
      0.0911    0.0645    0.1074    0.1066    0.0823    0.0785
0.0756 ...
       0 0.5*tipspeed tipspeed 0.5*tipspeed 0];
cfv6b=[ 0.0202   -0.0178    0.0091    0.0039    0.0023   -0.0002 ...
      -0.0001   -0.0241   -0.0105   -0.0157  0.0019   -0.0045
0.0029...
      -0.0008    0.0000    0.0004   -0.0003   -0.0001    0.0009
0.0093];
cfw6b=[ -0.0106   -0.0151   -0.0036   -0.0001    0.0000    0.0010 ...
      0.0011   -0.0137   -0.0139   -0.0362 -0.0001   -0.0116    0.0035
...
```

```
      0.0016   -0.0021   -0.0001    0.0023   -0.0002    0.0005
0.0014];
meant6b=meant6b/1000;meant6b=abs(meant6b);cfv6b=cfv6b/1000;cfw6b=cfw6b/
1000;
%%%%%%%%%%%%%%%%%%%%%%%%%%%%%%%%%%%%%%%%%%%%%%%%%%%%%%%%%%%%%%%%%%%%%%%
%
%%%%%%%%%%%%%%%%%%%%
%CASE7
meant7=[  0.0035    0.0040    0.0053        0.0023...
         0.0013    0.0167        0.0037  0.0041    0.0038 ...
          0.005    0.0058    0.0056];
meanv7=[ 0.0293   0.0248    0.0352       -0.0325   ...
      -0.0237   -0.0108       0.0057    -0.0147   -0.0218     ...
      0.0945      0.0461    0.0484 ...
      -tipspeed -0.5*tipspeed 0 0.5*tipspeed tipspeed];
meanw7=[    -0.0725   -0.0630   -0.0644       -0.0137   ...
      0.0127   -0.0721      0.0255   0.0449    0.0570     ...
      -0.0096    0.0005   -0.0177 ...
      0 0.5*tipspeed tipspeed 0.5*tipspeed 0];
cfv7=[   -0.0001   -0.0006  0.0629      0.0001    0.0134  ...
      0.7564        0.0003  -0.0301   -0.0330        0.2181 ...
       0.1910    0.4040];
cfw7=[   -0.0005     0.0001  0.1032     -0.0013    0.0087 ...
      -1.5978       0.0014   -0.0052   -0.0042     -0.0819 ...
       -0.0576   -0.1919];
meant7=meant7/1000;meant7=abs(meant7);cfv7=cfv7/1000;cfw7=cfw7/1000;
%%%%%%%%%%%%%%%%%%%%%%%%%%%%%%%%%%%%%%%%%%%%%%%%%%%%%%%%%%%%%%%%%%%%%%%
%%%%%%%%
%CASE7B
meant7b=[3.9541  4.2216  3.5725   1.0000    7.0231  3.8449 ...
      4.1114    4.3755  3.5269   25.6463  10.3855   13.1438];
meanv7b=[ 0.0026    0.0022  0.0371   -0.0401    0.0059   -0.0098
0.0242...
       0.0176    0.0122    0.2031  0.1756  0.1172 ...
       -tipspeed -0.5*tipspeed 0 0.5*tipspeed tipspeed];
meanw7b=[ -0.0368    -0.0482   -0.0615   -0.0090    0.0247    0.0352
...
      0.0223    0.0393   0.0415   -0.0807  -0.0617   -0.0379 ...
       0 0.5*tipspeed tipspeed 0.5*tipspeed 0];
cfv7b=[ 0.0111    0.0041  -0.0001   -0.0005    0.1200  0.0087 ...
       -0.0197   -0.0142   -0.0002   -0.1489  0.1350    0.2145];
cfw7b=[  -0.0073    0.0027   -0.0001   -0.0057   -0.1799 0.0017 ...
       0.0093  0.0199  0.0008   -0.1783  -0.0496   -0.0071];
meant7b=meant7b/1000;meant7b=abs(meant7b);cfv7b=cfv7b/1000;cfw7b=cfw7b/
1000;
%NOW LINEARLY INTERPOLATE BASED ON THE DEPTH OF CUT
%THIS IS DONE FOR BOTH VELOCITY AND DIFFUSION
%Create the ratio array  for depth of cut
thickratio=[4/12 8/12 12/12];
%%%%%%%%%%%%%%%%%%%%%%%%%%%%%%%%%%%%%%%%%%%%%%%%%%%%%%%%%%%%%%%%%%%%%%%
%%%%%%%%%%%%%%%%%%%%%%%%%%%%%%%%%%%%%%%%%%%%%%%%%%%%%%%%%%%%%%%%%%%%%%%
lengthconv=1/lengthscale;
lyold=y*lengthconv;lzold=z*lengthconv;ystop=(max(lyold))/2;
[Yold,Zold] = meshgrid(lyold,lzold);
```

```
%DIFFUSION MATRIX CALCULATIONS
%DONE FOR EACH TEST CASE THEN INTERPOLATED
%%%%%%%%%%%%%%%%%%%%%%%%%%%%%%%%%%%%%%%%%%%%%%%%%%%%%%%%%%%%%%%%%%%%%%%%%%%%%%%
%Case1
ydiamd=ydiam+ystop;ydiamd7=ydiam7+ystop;ydiamd7b=ydiam7b+ystop;
ydiamv=ydiamv+ystop;ydiamd7v=ydiam7v+ystop;ydiamd7bv=ydiam7bv+ystop;
ex_st='linear';
cw1 = griddata(ydiamd,zdiam,cfw1,Yold,Zold,ex_st);
cv1 = griddata(ydiamd,zdiam,cfv1,Yold,Zold,ex_st);
t1 = griddata(ydiamd,zdiam,meant1,Yold,Zold,ex_st);
v1 = griddata(ydiamv,zdiamv,meanv1,Yold,Zold,'v4');
w1 = griddata(ydiamv,zdiamv,meanw1,Yold,Zold,'v4');
[DCDY1,DCDZ1]=gradient(t1,dy*lengthconv);
[m,n]=size(DCDZ1);Diffy1=-1*cv1./DCDY1;Diffz1=-1*cw1./DCDZ1;
for i=1:m
   for j=1:n
      if isnan(Diffy1(i,j))==1
         Diffy1(i,j)=0.;
      end

      if Diffy1(i,j)<0
         Diffy1(i,j)=0;
      end

      if isnan(Diffz1(i,j))==1
         Diffz1(i,j)=0.;
      end

      if Diffz1(i,j)<0
         Diffz1(i,j)=0;
      end
       if isnan(v1(i,j))==1
         v1(i,j)=0.;
       end
        if isnan(w1(i,j))==1
         w1(i,j)=0.;
        end
   end
end


Dz1=Diffz1;Dy1=Diffy1;
%%%%%%%%%%%%%%%%%%%%%%%%%%%%%%%%%%%%%%%%%%%%%%%%%%%%%%%%%%%%%%%%%%%%%%%%%%%%%%%
%Case1b
ex_st='linear';
cw1b = griddata(ydiamd,zdiam,cfw1b,Yold,Zold,ex_st);
cv1b = griddata(ydiamd,zdiam,cfv1b,Yold,Zold,ex_st);
t1b = griddata(ydiamd,zdiam,meant1b,Yold,Zold,ex_st);
v1b = griddata(ydiamv,zdiamv,meanv1b,Yold,Zold,'v4');
w1b = griddata(ydiamv,zdiamv,meanw1b,Yold,Zold,'v4');
[DCDY1b,DCDZ1b]=gradient(t1b,dy*lengthconv);
[m,n]=size(DCDZ1b);
Diffy1b=-1*cv1b./DCDY1b;
Diffz1b=-1*cw1b./DCDZ1b;
```

```
for i=1:m
   for j=1:n
      if isnan(Diffy1b(i,j))==1
         Diffy1b(i,j)=0.;
      end

      if Diffy1b(i,j)<0
         Diffy1b(i,j)=0;
      end

      if isnan(Diffz1b(i,j))==1
         Diffz1b(i,j)=0.;
      end

      if Diffz1b(i,j)<0
         Diffz1b(i,j)=0.;
      end
        if isnan(v1b(i,j))==1
         v1b(i,j)=0.;
       end
        if isnan(w1b(i,j))==1
         w1b(i,j)=0.;
        end

   end
end

Dz1b=Diffz1b;Dy1b=Diffy1b;
%%%%%%%%%%%%%%%%%%%%%%%%%%%%%%%%%%%%%%%%%%%%%%%%%%%%%%%%%%%%%%%%%%%%%%%
%%%%%%%%%%%%%%%%%%%
%Case6
ex_st='linear';
cw6 = griddata(ydiamd,zdiam,cfw6,Yold,Zold,ex_st);
cv6 = griddata(ydiamd,zdiam,cfv6,Yold,Zold,ex_st);
t6 = griddata(ydiamd,zdiam,meant6,Yold,Zold,ex_st);
v6 = griddata(ydiamv,zdiamv,meanv6,Yold,Zold,'v4');
w6 = griddata(ydiamv,zdiamv,meanw6,Yold,Zold,'v4');
[DCDY6,DCDZ6]=gradient(t6,dy*lengthconv);
[m,n]=size(DCDZ6);Diffy6=-1*cv6./DCDY6;Diffz6=-1*cw6./DCDZ6;
for i=1:m
   for j=1:n
      if isnan(Diffy6(i,j))==1
         Diffy6(i,j)=0.;
      end

      if Diffy6(i,j)<0
         Diffy6(i,j)=0;
      end

      if isnan(Diffz6(i,j))==1
         Diffz6(i,j)=0.;
      end

      if Diffz6(i,j)<0
```

```
         Diffz6(i,j)=0;
      end
       if isnan(v6(i,j))==1
         v6(i,j)=0.;
       end
        if isnan(w6(i,j))==1
         w6(i,j)=0.;
        end
   end
end
Dz6=Diffz6;Dy6=Diffy6;
%%%%%%%%%%%%%%%%%%%%%%%%%%%%%%%%%%%%%%%%%%%%%%%%%%%%%%%%%%%%%%%%%%%%%%%%%%%%%%%%%%%%%%%%%%%%%%%%
%%%%%%%%%%%%%%%%%%%
%Case6b

ex_st='linear';
cw6b = griddata(ydiamd,zdiam,cfw6b,Yold,Zold,ex_st);
cv6b = griddata(ydiamd,zdiam,cfv6b,Yold,Zold,ex_st);
t6b = griddata(ydiamd,zdiam,meant6b,Yold,Zold,ex_st);
v6b = griddata(ydiamv,zdiamv,meanv6b,Yold,Zold,'v4');
w6b = griddata(ydiamv,zdiamv,meanw6b,Yold,Zold,'v4');
[DCDY6b,DCDZ6b]=gradient(t6b,dy*lengthconv);
[m,n]=size(DCDZ6b);Diffy6b=-1*cv6b./DCDY6b;Diffz6b=-1*cw6b./DCDZ6b;
for i=1:m
   for j=1:n
      if isnan(Diffy6b(i,j))==1
         Diffy6b(i,j)=0.;
      end

      if Diffy6b(i,j)<0
         Diffy6b(i,j)=0;
      end

      if isnan(Diffz6b(i,j))==1
         Diffz6b(i,j)=0.;
      end

      if Diffz6b(i,j)<0
         Diffz6b(i,j)=0;
      end
        if isnan(v6b(i,j))==1
         v6b(i,j)=0.;
       end
        if isnan(w6b(i,j))==1
         w6b(i,j)=0.;
        end
   end
end

Dz6b=Diffz6b;Dy6b=Diffy6b;
%%%%%%%%%%%%%%%%%%%%%%%%%%%%%%%%%%%%%%%%%%%%%%%%%%%%%%%%%%%%%%%%%%%%%%%%%%%%%%%%%%%%%%%%%%%%%%%%
%%%%%%%%%%%%%%%%%%%
%Case7
ydiamd=ydiam+ystop;
```

```
ex_st='linear';
cw7 = griddata(ydiamd7,zdiam7,cfw7,Yold,Zold,ex_st);
cv7 = griddata(ydiamd7,zdiam7,cfv7,Yold,Zold,ex_st);
t7 = griddata(ydiamd7,zdiam7,meant7,Yold,Zold,ex_st);
v7 = griddata(ydiamd7bv,zdiam7bv,meanv7,Yold,Zold,'v4');
w7 = griddata(ydiamd7bv,zdiam7bv,meanw7,Yold,Zold,'v4');
[DCDY7,DCDZ7]=gradient(t7,dy*lengthconv);
[m,n]=size(DCDZ7);Diffy7=-1*cv7./DCDY7;Diffz7=-1*cw7./DCDZ7;
for i=1:m
   for j=1:n
      if isnan(Diffy7(i,j))==1
         Diffy7(i,j)=0.;
      end

      if Diffy7(i,j)<0
         Diffy7(i,j)=0;
      end

      if isnan(Diffz7(i,j))==1
         Diffz7(i,j)=0.;
      end

      if Diffz7(i,j)<0
         Diffz7(i,j)=0;
      end

      if isnan(v7(i,j))==1
         v7(i,j)=0.;
       end
        if isnan(w7(i,j))==1
         w7(i,j)=0.;
        end

   end
end
Dz7=Diffz7;Dy7=Diffy7;
%%%%%%%%%%%%%%%%%%%%%%%%%%%%%%%%%%%%%%%%%%%%%%%%%%%%%%%%%%%%%%%%%%%%%%%%
%%%%
%Case7b
ex_st='linear';
cw7b = griddata(ydiamd7b,zdiam7b,cfw7b,Yold,Zold,ex_st);
cv7b = griddata(ydiamd7b,zdiam7b,cfv7b,Yold,Zold,ex_st);
t7b = griddata(ydiamd7b,zdiam7b,meant7b,Yold,Zold,ex_st);
v7b = griddata(ydiamd7bv,zdiam7bv,meanv7b,Yold,Zold,'v4');
w7b = griddata(ydiamd7bv,zdiam7bv,meanw7b,Yold,Zold,'v4');
[DCDY7b,DCDZ7b]=gradient(t7b,dy*lengthconv);
[m,n]=size(DCDZ7b);
Diffy7b=-1*cv7b./DCDY7b;
Diffz7b=-1*cw7./DCDZ7b;
for i=1:m
   for j=1:n
      if isnan(Diffy7b(i,j))==1
         Diffy7b(i,j)=0.;
      end
```

```
      if Diffy7b(i,j)<0
         Diffy7b(i,j)=0;
      end
      if isnan(Diffz7b(i,j))==1
         Diffz7b(i,j)=0.;
      end
      if Diffz7b(i,j)<0
         Diffz7b(i,j)=0;
      end
        if isnan(v7b(i,j))==1
         v7b(i,j)=0.;
       end
        if isnan(w7b(i,j))==1
         w7b(i,j)=0.;
        end

   end
end

Dz7b=Diffz7b;Dy7b=Diffy7b;
%%%%%%%%%%%%%%%%%%%%%%%%%%%%%%%%%%%%%%%%%%%%%%%%%%%%%%%%%%%%%%%%%%%%%%%
%%
% %CREATE ADVECTION DIFFUSION TERMS
% %%%%%%%%%%%%%%%%%%%%%%%%%%%%%%%%%%%%%%%%%%
% %ADVECTION
% %NOW SCALE THE LOCATION OF THE POINTS BY THE LENGTHSCALE
ydiam=ydiam*lengthscale;ydiamstore=ydiam;zdiam=zdiam*lengthscale;
%SHIFT THE Y DIMENSION TO THE CENTER OF THE DOMAIN
ydiam=ydiam + endy/2;
%CREATE BOTH MATRIXES FOR V AND W
[Ynew,Znew] = meshgrid(y,z);
%%%%%%%%%%%%%%%%%%%%%%%%%%%%%%%%%%%%%%%%%%%%%%%%%%%%%%%%%%%%%%%
%%%%%%%%%%%%%%%%%%%SCALE ADVECTION AND DIFFUSION
%FIRST SCALE ACCORDING TO CUTTER DEPTH
% % %%%%%%%%%%%%%%%%%%%%%%%%%%%%%%%%%%%%%%%%%%%%%%%%%%%%%%%%%%%%%%%%%%%
%%HERE IS UNDERCUTTING VS OVERCUTTING
%UNDERCUTTING
if cuttype==1
   for i=1:ny
      for j=1:nz
         pv=[v6(i,j) v1(i,j) v7(i,j)];
         pw=[w6(i,j) w1(i,j) w7(i,j)];
         v(i,j)=interp1(thickratio,pv,cutratio);
         w(i,j)=interp1(thickratio,pw,cutratio);
         pdy=[Dy6(i,j) Dy1(i,j) Dy7(i,j)];
         pdz=[Dz6(i,j) Dz1(i,j) Dz7(i,j)];
         DY(i,j)=interp1(thickratio,pdy,cutratio);
         DZ(i,j)=interp1(thickratio,pdz,cutratio);
      end
   end
   %%%%%%%%%%%%%%%%%%%%%%%%%%%%%%%%%%%%%%%%%%%%%%
   %OVERCUTTING
else
   for i=1:ny
```

```
      for j=1:nz
         pv=[v6b(i,j) v1b(i,j) v7b(i,j)];
         pw=[w6b(i,j) w1b(i,j) w7b(i,j)];
         v(i,j)=interp1(thickratio,pv,cutratio);
         w(i,j)=interp1(thickratio,pw,cutratio);
         pdy=[Dy6b(i,j) Dy1b(i,j) Dy7b(i,j)];
         pdz=[Dz6b(i,j) Dz1b(i,j) Dz7b(i,j)];
         DY(i,j)=interp1(thickratio,pdy,cutratio);
         DZ(i,j)=interp1(thickratio,pdz,cutratio);
      end
   end
end
%%%%%%%%%%%%%%%%%%%%%%%%%%%%%%%%%%%%%%%%%%%%%%%%%%%
%SUBTRACT THE MODEL SWING SPEED VELOCITY FROM THE V VELOCITY
if cuttype==1
    v=v+swing_Model;
else
    v=v-swing_Model;
end
%SCALE V and W according to cutter tip speed ratio
v=v*tipratio;w=w*tipratio;
%LETS PLOT THE DIVERGENCE
[VY,VZ]=gradient(v,dy,dz);
[WY,WZ]=gradient(w,dy,dz);
divergence=VY+VZ;
figure(3000)
contourf(y,z,divergence)
axis([1.5*min(ydiam) 1*max(ydiam) 0 1.5*cutter_D])
colorbar;
xlabel('Horizontal Distance (m)');ylabel('Vertical Distance (m)')
%NOW SCALE DIFFUSION ACCORDING TO THE PECLET NUMBER LV/D
DY=DY*tipratio;DY=DY*lengthscale;DZ=DZ*tipratio;DZ=DZ*lengthscale;
%GOING TO USE MEAN HERE OF DY AND DZ
DYcoef1=mean(mean(DY));DZcoef1=mean(mean(DZ));
for i=1:ny
    for j=1:nz
        DZ(i,j)=DYcoef1;
        DY(i,j)=DZcoef1;
    end
end
%SUBTRACT NUMERICAL DIFFUSION FROM DZ and DY
Dn=0.5*max_vel*(dy-max_vel*(dt*100));
for i=1:ny
    for j=1:nz
        DZ(i,j)=DZcoef1-Dn;
        if DZ(i,j) <= 0
            DZ(i,j)=DZcoef1;
        end
          DY(i,j)=DYcoef1-Dn;
          if DY(i,j) <= 0
            DY(i,j)=DYcoef1;
        end

    end
```

```
end
%%%%%%%%%%%%%%%%%%%%%%%%%%%%%%%%%%%%%%%%%%%%%%%%%%%%%
%%%%%%%%%%%%%%%%%%%%%%%%%%%%
ycircle=[-cutter_R:dy:cutter_R];
sizec=length(ycircle);
leftint=int8(yb_n_l/dy);
rightint=int8(yb_n_r/dy);
midcirc=round(sizec/2);
%THESE TWO LOOPS CALCULATES THE TANGENTIAL VELOCITIES AROUND THE
%CUTTER DIAMETER
for i=1:midcirc
   zangle(i)=90*((i-1)/midcirc);
   tipcompz(i)=tipspeed*(sind(zangle(i)));
   tipcompy(i)=-tipspeed*(cos(zangle(i)));
    zcircle(i)=((cutter_R^2-ycircle(i)^2))^.5;
   %ratiozy=zcircle(i)/cutter_R;
   %tipcompz(i)= tipspeed*ratiozy;
   %tipcompy(i)=-tipspeed*(1-ratiozy);
end
for i=midcirc+1:sizec
   zangle(i)=90-zangle(i-midcirc);
   tipcompz(i)=tipspeed*(sind(zangle(i)));
   tipcompy(i)=tipspeed*(cos(zangle(i)));
    zcircle(i)=((cutter_R^2-ycircle(i)^2))^.5;
   %ratiozy=zcircle(i)/cutter_R;
   %tipcompz(i)= tipspeed*ratiozy;
   %tipcompy(i)=tipspeed*(1-ratiozy);
end
ycircle=ycircle+endy/2;
%CALCULATE HOW FAR THE CIRCLE actually goes based on cutter height
%WE KNOW THE CUT RATIO
if cutratio>0.5
   heightcut=thickcut-cutter_R;
   lengthy=(cutter_R^2-heightcut^2)^0.5;
   sizey=floor((lengthy)/dy)-1;
else
   sizey=midcirc-1
end
%UNDERCUTTING DISTRIBUTION
%USING LINEAR DISTRIBUTION (TRIANGLE) VERSION OF FLUX
%FIRST CALCULATE SURFACE AREA OVER WHICH FLUX IS DISTRIBUTED
surfaceareacutter=clen*cosd(cangle)*pi*cdiam*(0.5+cutratio);
if cuttype==1
   underend=midcirc+sizey;
   for i=1:underend
      ycount(i)=round(ycircle(i)/dy)+1;
      zcount(i)=round(zcircle(i)/dz);
      zcount(i)=zcount(i)+1;
      v(zcount(i),ycount(i))=tipcompy(i);
      w(zcount(i),ycount(i))=tipcompz(i);
   end
   massheightmax=totmass/(0.5*(underend-1));
   spready=1/(underend-1);
   massp=[0:spready:1];
```

```
   massh=massheightmax*massp;
   lmass=length(massp);
   masstriangle(1)=0;
   massh(underend+1)=0;
   for i=2:lmass+1
    base=i-1;
    base2=i-2;
    area=0.5*base*massh(i);
    area2=0.5*base2*massh(i-1);
    masstriangle(i)=area-area2;
   end
   for i=1:underend

bottom_C(zcount(i),ycount(i))=masstriangle(i)/(tipspeed*surfaceareacutt
er);
   end
   %%%%%%OVERCUTTING DISTRIBUTION
else
   overend=midcirc-sizey;
   sizeunder=sizec-overend+1;
   for i=sizec:-1:overend
      ycount(i)=round(ycircle(i)/dy)+1;
      zcount(i)=round(zcircle(i)/dz);
      zcount(i)=zcount(i)+1;
      v(zcount(i),ycount(i))=tipcompy(i);
      w(zcount(i),ycount(i))=tipcompz(i);
   end
   massheightmax=totmass/(0.5*(sizeunder-1));
   spready=1/(sizeunder-1);massp=[0:spready:1];
   massh=massheightmax*massp;lmass=length(massp);
   masstriangle(1)=0;massh(sizeunder+1)=0;
   for i=2:lmass+1
    base=i-1;
    base2=i-2;
    area=0.5*base*massh(i);
    area2=0.5*base2*massh(i-1);
    masstriangle(i)=area-area2;
   end
    overj=0;
   for i=overend:sizec
       overj=overj+1;

bottom_C(zcount(i),ycount(i))=masstriangle(overj)/(tipspeed*surfacearea
cutter);
   end
end
% %%%%%%%%%%%%%%%%%%%%%%%%%%%%%%%%%%%%%%%%%%%%%%%%%%%%%%%%%%%%%%%%%%%%%%%
%ADJUST THE V COMPONENT FOR THE ACTUAL SWING SPEED
%UNDERCUTTING
if cuttype==1
   v=v-swingspeed;
   %OVERCUTTING
else
   v=v+swingspeed;
```

```
end
%%%%%%%%%%%%%%%%%%%%%%%%%%%%%%%%%%%%%%%%%%%
%HERE IS WHERE THE INITIAL BOUNDARY CONDITION EXISTS
for i=1:ny
   for j=1:nz
      if y(i)>yb_n_l & y(i)<yb_n_r
         bottom_C(i,j)=0;
      else
         bottom_C(i,j)=0;
      end

   end
end
% %%%%%%%%%%%%%%%%%%%%%%%%%%%%%%%%%%%%%%%%%%%%%%%%%%%%%%%%
% %%%%%%%%%%%%%%%%%%%%%%%%%%%%%%%%%%%%%%%%%%%%%%%%%%%%%%
%STORE THE ORIGINAL W THAT IS NOT AFFECTED BY SETTLING
wstore=w;
%NEED SETTLING EQUATION HERE
settlespeed=wsettle;
settleconc=10^(-6);
%%%%%%%%%%%%%%%%%%%%%%%%%%%%%%%%%%%%%%%%%%%%%%%%%%%%%%%%%%%%%
%%%%%%%%%%%%%%%%%%%%%%%%%%%%%%%%%%%%%%%%%%%%%%%%%%%%%%%%%%%
%%%%%%%%%%%%%%%%%%%%%%%%%%%%%%%%%%%%%%%%%%%%%%%%%%%%%%%%%%%
%TIME STEPPING BEGINS HERE!!!!!!
% start time-stepping
for n=1:nt
   %ADD SETTLING EFFECT FIRST
   for i=1:ny
      for j=1:nz
         if C(i,j,1)>=settleconc
            w(i,j)=w(i,j)-settlespeed;
         else
            w(i,j)=w(i,j);
         end
      end
   end
   %%%%%%%%%%%%%%%%%%%%%%%%%%%%%%%%%%%%%%%%%%%%%%%%%%%%%%%%%%%%%%%%%%%%
   %REFRESH VELOCITIES OF CUTTER TIP

   %UNDERCUTTING
   if cuttype==1
      for i=1:underend
         w(zcount(i),ycount(i))=tipcompz(i);
      end
      %OVERCUTTING
   else
      for i=sizec:-1:overend
         w(zcount(i),ycount(i))=tipcompz(i);
      end
   end
   %%%FIRST PREDICTOR
   E_predictor=E_calc_upwind(C(:,:,1),v,w,DY,DZ,dy,dz,ny,nz);

%    %%%%%%%%%%%%%%%%%%%%%%%%%%%%%%%%%%%%%%%%%%%%%%%%%%%%%%%%%%%%%%%%%%%%%
```

```
%%%BOTTOM BOUNDARY CONDITION
for i=1:ny
   for j=1:nz
      if j==1 & (y(i)<yb_n_l & y(i)>yb_n_r)
         C(i,j,2)=bottom_C(i,j);
      else
         C(i,j,2)=C(i,j,1)+dt*E_predictor(i,j);
      end
   end
end
%%%%%%%%%%%%%%%%%%%%%%%%%%%%%%%%%%%%%%%%%%%%%%%%%%%%%%%%%%%%%%%%%%%%%%%
% HERE IS WHERE I ADD THE OTHER BOUNDARY AROUND THE DIAMETER
% UNDERCUTTING
if cuttype==1
   sizeunder=length(underend);
   for i=1:underend
     C(ycount(i),zcount(i),2)=C(ycount(i),zcount(i))+...
          0.5*masstriangle(i)/(tipspeed*surfaceareacutter);
   end
   %OVERCUTTING
else
   overj=0;
for i=overend:sizec
    overj=overj+1;
     C(ycount(i),zcount(i),2)=C(ycount(i),zcount(i))+...
        0.5*masstriangle(overj)/(tipspeed*surfaceareacutter);
end
end
%%%%%%%%%%%%%%%%%%%%%%%%%%%%%%%%%%%%%%%%%%%%%%%%%%%%%%%%%%%%%%%%%%%%%%%
%%%%%%%% SECOND PREDICTOR
E_corrector=E_calc_upwind(C(:,:,2),v,w,DY,DZ,dy,dz,ny,nz);

%%%%%%%%%%%%%%%%%%%%%%%%%%%%%%%%%%%%%%%%%%%%%%%%%%%%%%%%%%%%%%%%%%%%%%%
for i=1:ny
   for j=1:nz
      if j==1 & (y(i)>yb_n_l & y(i)<yb_n_r)
         C(i,j,2)=bottom_C(i,j);
      else
         C(i,j,2)=C(i,j,1)+dt/2*(E_predictor(i,j)+E_corrector(i,j));
      end
   end
end
%%%%%%%%%%%%%%%%%%%%%%%%%%%%%%%%%%%%%%%%%%%%%%%%%%%%%%%%%%%%%%%%%%%%%%%
%UNDERCUTTING
if cuttype==1
   for i=1:underend
      C(ycount(i),zcount(i),2)=C(ycount(i),zcount(i))+...
         0.5*masstriangle(i)/(tipspeed*surfaceareacutter);
   end

 %  OVERCUTTING
else
  overj=0;
 for i=overend:sizec
```

```
        overj=overj+1;
        C(ycount(i),zcount(i),2)=C(ycount(i),zcount(i))+...
           0.5*masstriangle(overj)/(tipspeed*surfaceareacutter);
     end
    end
    %%%%%%%%%%%%%%%%%%%%%%%%%%%%%%%%%%%%%%%%%%%%%%%%%%%%%%%%%%%%%%%%%%%%
    %PRINT OUT FIGURES FOR UNDERCUTTING OR OVERCUTTING
    if mod(n,1000000)==0
        count=n*dt
         if cuttype==1
          axes(handles.axes1); surf(y,z,C(:,:,2)')
          axis([1.5*min(ydiam) 1*max(ydiam) 0 1.5*cutter_D])
          view(0,90);shading interp
          colorbar;title('Near-Field Model');
         xlabel('Horizontal Distance (m)');ylabel('Vertical Distance
(m)')
        else
          axes(handles.axes1)
          surf(y,z,C(:,:,2)')
          axis([1.5*min(ydiam) 1*max(ydiam) 0 1.5*cutter_D])
          view(0,90); shading interp
          colorbar;title('Near-Field Model')
          xlabel('Horizontal Distance (m)')
          ylabel('Vertical Distance (m)')
         end
%%%%%%%%%%%%%%%%%%%%%%%%%%%%%%%%%%%%%%%%%%%%%%%%%%%%%%%%%%%%%%%%%%%%%%%
%%%%%
%%%%%%%%%%%%%%%%%%%%%%%%%%KUO'S FAR-FIELD
OUTPOUT%%%%%%%%%%%%%%%%%%%%%%%
% % %%%%%%%%%%%%%%%%%%%%%%%%%%%%%%%%%%%%%%%%%%%%%%%%%%%%%
%OBTAIN Qfar 1 cutter diameter above cutter and in center of cutter
cypoint=(endy*0.5)/dy;czpoint=(cdiam*1.5)/dz;
sourctermc=C(cypoint,czpoint,1);sourcterm=sourctermc*2*cdiam*clen*swing
;
Qfar=sourcterm;
% %Current Velocity U
Ufar=farflow;
%Settling Speed w
wfar=wsettle;nfar=30;
rfar=fardepth;
 [xfar,yfar,zfar] = meshgrid(1:nfar,-nfar:1:nfar,1:nfar);
 coef1far=4000*pi*((kx*ky)^.5);
 coef2far=4*ky/Ufar;
 coef3far=4*kz/Ufar;
 coef4far=wfar/Ufar;
 coef5far=Qfar/coef1far;
 for i=1:(2*nfar)+1
for j=1:nfar
    for k=1:nfar
        if i==nfar+1
            afar=xfar(i+1,j,k);
            bfar=yfar(i,j,k);
            cfar=zfar(i,j,k);
        else
```

```
        afar=xfar(i,j,k);
        bfar=yfar(i,j,k);
        cfar=zfar(i,j,k);
        end
        coefafar=coef5far/abs(afar);
        coefbfar=(bfar^2)/(coef2far*afar);
        coefcfar=(cfar+coef4far*afar)^2;
        coefdfar=coef3far*afar;
        concfar(i,j,k)=coefafar*exp(-coefbfar-(coefcfar/coefdfar));
    end
end
end
 axes(handles.axes2)
 xarray=xfar(:,:,rfar);
 yarray=yfar(:,:,rfar);
 carray=concfar(:,:,rfar);
 contourf(xarray,yarray,carray)
 title('Far-Field Model g/l')
 xlabel('Horizontal Distance (m)')
 ylabel('Lateral Distance (m)')
 colorbar
%%%%%%%%%%%%%%%%%%%%%%%%%%%%%%%%%%%%%%%%%%%%%%%%%%%%%%%%%%%%%%%%%%%%%%%%%%%%

   end
   %%%%%%%%%%%%%%%%%%%%%%%%%%%%%%%%%%%%%%%%%%%%%%%%%%%%%%%%%%%%%%%%%%%%%%%%%%%
   % RENEW OF C AND W
   C(:,:,1)=C(:,:,2);
   %ADD EFFECT OF MASS LOSS DUE TO DIVERGENT FLOW FIELD
  for i=1:ny
      for j=1:nz
            mc(i,j,1)=C(i,j,1)*dy*dz;
        end
   end
  totmasscheck=totmass*n;summassc=sum(sum(mc(:,:,1)));
  masslost=abs(totmasscheck-summassc);
   for i=1:ny
      for j=1:nz

Coefm(i,j,1)=mc(i,j,1)/(summassc);Cadd(i,j,1)=Coefm(i,j,1)*masslost;
         C(i,j,1)=C(i,j,1)+Cadd(i,j,1);
        end
   end
w=wstore;

end
cyds=round((ystop-cradius)/dy);
cyde=round((ystop+cradius)/dy);
turbline=cyds:cyde
for i=1:length(turbline)
cypoint2=turbline(i);
czpoint2=round((3*cradius)/dy);
sourctermc=C(cypoint2,czpoint2,1)/1000;
sourcterm(i)=1000*sourctermc*2*cdiam*clen*swing;
end
```

```
%THIS IS THE FINAL OUTPUT
source=mean(sourcterm)
%WE HAVE COORDINATES FOR XDIAM and YDIAM

%TEST1
for i=1:length(ydiam)
    cyp(i)=round(ydiam(i)/dy);
    czp(i)=round(zdiam(i)/dz);
    tcheckspat(i)=C(cyp(i),czp(i),1);
end
tcheckspat

%LETS PLOT THE TWO TURBIDITY PLOTS
%LETS MAKE A CIRCLE TO REPRESENT THE CUTTER RADIUS
  cirrad=(6.75*2.54)/100;
  xcircle=[-cirrad:.0005:cirrad];
  sizecirc=size(xcircle);
  sizec=sizecirc(1,2);
  for i=1:sizec
      ycircle(i)=((cirrad^2-xcircle(i)^2))^.5;
  end
xcircle=xcircle+ystop;
  meant1=meant1*1000
  figure(20)
      scatter(ydiam,zdiam,meant1*50,meant1,'filled')
      axis tight; hold on;
      plot(xcircle,ycircle,'r')
    colorbar
    title('Turbidity (g/l)')
    xlabel('m')
    ylabel('m')
    %print -dtiff 'PIANCcase1bturb.tiff'

for i=1:20
    if tcheckspat(i)<=1
        tcheckspat(i)=1;
    end
end
 figure(21)
      scatter(ydiam,zdiam,tcheckspat*50,tcheckspat,'filled')
      axis tight; hold on;
      plot(xcircle,ycircle,'r')
    colorbar
    title('Turbidity (g/l)')
    xlabel('m')
    ylabel('m')
print -dbitmap  'guipicnew.bmp'

%%%%%%%%%%%%%%%%%%%%%%%%%%%%%%%%%%%%%%%%%%%%%%%%%%%%%%%%%%%%%%%%%%%%%%%%%%
%%%%%%
%%%%%%%%%%%%%%%%%%%%%%%%%%%END OF
PROGRAM%%%%%%%%%%%%%%%%%%%%%%%%%%%%%%%%%%%%%
```

VITA

Name: John Christopher Henriksen

Address: 4309 Pablo Oaks Court Suite One Jacksonville, FL 32224

Email Address: jhenriksen@mansonconstruction.com

Education: B.A., Neuroscience, The University of Delaware, 2001
B.S., Environmental Science, The University of Delaware, 2001
M.S., Engineering, Dartmouth College, 2003
Ph.D., Ocean Engineering, Texas A&M University, 2009